# INVESTIGATING ASSOCIATIONS BETWEEN ELECTROPHYSIOLOGICAL AND PATHOLOGICAL CHANGES IN THE TgF344-AD RAT MODEL FOR ALZHEIMER'S DISEASE

A thesis submitted to the University of Manchester for the degree of Doctor of Philosophy in the Faculty of Biology, Medicine and Health

**2023**

**YUHONG SUN**

**SCHOOL OF HEALTH SCIENCE, DIVISION OF PHAMACY AND OPTOMETRY**

## Contents

Word Count: 61,192

## List of Figures

## List of Tables

## List of Abbreviations

ABC: avidin-biotin complexes

ACh: acetylcholine

AChE: acetylcholinesterase

AD: Alzheimer's disease

ADDL: Aβ-derived diffusible ligands

$\alpha_5$IA: inverse agonist of $GABA_A$ receptors $\alpha_5$ subunit

aMCI: amnestic mild cognitive impairment

AMPAR: α-amino-3-hydroxy-5-methyl-4-isoxazolepropionic acid receptor

ApoE: Apolipoprotein E

APP: amyloid precursor protein

ASC: apoptosis-associated speck-like protein containing a C-terminal caspase-recruitment domain

$A\beta_{1-40}$ or $A\beta_{40}$: β-amyloid peptide 1-40

$A\beta_{1-42}$ or $A\beta_{42}$: β-amyloid peptide 1-42

BSA: bovine serum albumin

CA1: *Cornu Ammonis* 1

CA2: *Cornu Ammonis* 2

CA3: *Cornu Ammonis* 3

CCK: cholecystokinin

CNS: central nervous system

CSD: current source density

CSF: cerebrospinal fluid

DAB: 3,3'-Diaminobenzidine

DAMP: danger associated molecular pattern

TBOA: dl-threo-β-benzyloxyaspartic acid

DG: Dentate gyrus

DH: dorsal hippocampus

E/I: excitation/inhibition

EAAT: excitatory amino acid transporter

EEG: electroencephalogram

EDTA: ethylenediaminetetraacetic acid

ELISA: enzyme-linked immunosorbent assay

EMA: European Medicines Agency

EOAD: early-onset Alzheimer's disease

ER: endoplasmic reticulum

ERK: extracellular signal-regulated kinase

FAD: familial AD

FCx: frontal cortex

FDA: the U.S. Food and Drug Administration

fEPSP: field excitatory post-synaptic potential

fMRI: functional magnetic resonance imaging

GABA: γ-Aminobutyric acid

$GABA_{\alpha5}$: α5-containing $GABA_A$ receptor

GAD: glutamic acid decarboxylase

GSK-3β: glycogen synthase kinase-3 beta

HFS: high frequency stimulation

HRP: horseradish peroxidase

I/O: input/output

IF: immunofluorescence

IHC: immunohistochemistry

IL-1β: interleukin-1β

$IP_3R$: inositol trisphosphate receptor

LFS: low frequency stimulation

LOAD: late-onset Alzheimer's disease

LTD: long-term depression

LTP: long-term potentiation

MAPT: microtubule-associated protein tau

MCI: mild cognitive impairment

mGluR: metabotropic glutamate receptor

NAM: negative allosteric modulator

NFT: neurofibrillary tangle

NHS: normal horse serum

NMDAR: N-methyl-D-aspartate receptor

NPY: neuropeptide Y

NR2A: NMDA receptor 2A subunit

NR2B: NMDA receptor 2B subunit

NSAID: non-steroidal anti-inflammatory drug

P1: pulse 1

P2: pulse 2

PAMP: pathogen associated molecular pattern

PBS: phosphate-buffered saline

PET: positron emission tomography

PFC: prefrontal cortex

PPF: paired pulse facilitation

PPI: paired pulse index

PS: population spike

PS1: presenilin 1

PS2: presenilin 2

PSD-95: post-synaptic density 95

PV: parvalbumin

RYR: ryanodine receptor

sAD: sporadic Alzheimer's disease

sAPPα: soluble APP-α

SERCA: sarco/endoplasmic reticulum $Ca^{2+}$-ATPase

SHR: spontaneously hypertensive rat

SNAP-25: synaptosomal-associated protein 25kDa

SOM: somatostatin

SV2A: synaptic vesicle glycoprotein 2A

t-SNARE: target - Soluble NSF (N-ethylmaleimide-sensitive factor) Attachment Receptor

VAMP: vesicle associated membrane protein

VGLUT: vesicular glutamate transporter

VH: ventral hippocampus

VIP: vasoactive intestinal peptide

## Abstract

Hippocampal hyperexcitability and disinhibition have been implicated in cognitive deficits at early stages of Alzheimer's disease. Using the TgF344-AD transgenic rat model expressing APPsw and PS1ΔE9 genes, early changes in hippocampal synaptic plasticity and changes in synaptic transmission and neuroinflammation were investigated.

Evoked responses in dorsal hippocampal CA1 were recorded following CA3 Schaffer stimulation in urethane-anaesthetised 6- and 9-month-old male TgF344-AD (TG) and wild-type (WT) rats, to determine the induction properties for synaptic plasticity, baseline connectivity. Levels of proteins related to synaptic transmission and excitatory/inhibitory function were measured with capillary electrophoresis immunoblotting (Wes) and immunohistochemistry in the dorsal hippocampus. Both microglia activation and levels of the proinflammatory cytokine interleukin-1β (IL-1β) were determined with immunofluorescence in the CA1.

9-month-old TG rats showed significantly lower paired-pulse facilitation at short interpulse intervals, increased baseline input/output, and a higher probability of having population spikes at Pulse2 after high frequency stimulation, indicating increased hippocampal output excitability in the CA1 region at this age. HFS induced long-term potentiation was significantly reduced in CA1 of 6- and 9-month-old TG rats. Additionally, the 6-month-old TG showed enhanced depotentiation.

Density of PV-positive interneurons were significantly lower in hippocampal CA2/3 (but not CA1 or dentate gyrus) in 9-month-old TG rats only. We observed a higher percentage of IL-1β-expressing microglia in CA1 of both 6- and 9-month-old TG rats.

Collectively, these results indicate synaptic deficits in TG rats at 9 months that were accompanied with CA1 hyperexcitability and a reduction of PV inhibition upstream of the CA3-CA1 circuity, with progressively increasing hippocampal neuroinflammation.

In conclusion, investigating changes in 6- and 9-month-old TG rats present an interesting window for investigating electrophysiological and pathological changes in this model related to the early stages and subsequent progression of Alzheimer's disease.

## Declaration

No portion of the work referred to in the thesis has been submitted in support of an application for another degree or qualification of this or any other university or other institute of learning.

## Copyright Statement

i. The author of this thesis (including any appendices and/or schedules to this thesis) owns certain copyright or related rights in it (the "Copyright") and they have given the University of Manchester certain rights to use such Copyright, including for administrative purposes.

ii. Copies of this thesis, either in full or in extracts and whether in hard or electronic copy, may be made only in accordance with the Copyright, Designs and Patents Act 1988 (as amended) and regulations issued under it or, where appropriate, in accordance with licensing agreements which the University has from time to time. This page must form part of any such copies made.

iii. The ownership of certain Copyright, patents, designs, trademarks and other intellectual property (the "Intellectual Property") and any reproductions of copyright works in the thesis, for example graphs and tables ("Reproductions"), which may be described in this thesis, may not be owned by the author and may be owned by third parties. Such Intellectual Property and Reproductions cannot and must not be made available for use without the prior written permission of the owner(s) of the relevant Intellectual Property and/or Reproductions.

iv. Further information on the conditions under which disclosure, publication and commercialisation of this thesis, the Copyright and any Intellectual Property

and/or Reproductions described in it may take place is available in the University IP Policy (see http://documents.manchester.ac.uk/DocuInfo.aspx?DocID=24420), in any relevant Thesis restriction declarations deposited in the University Library, the University Library's regulations (see http://www.library.manchester.ac.uk/about/regulations/) and in the University's policy on Presentation of Theses.

## Contributions from collaborators

All experiments and analyses were performed by Yuhong Sun other than:

Chapter 4:

- 6-month-old Wes experiment and analyses were performed by Yuhong Sun, and 9-month-old Wes experiment and analyses were performed by Lauren Rimmer.
- 6-month-old parvalbumin (PV) density experiment and analysis were performed by Yuhong Sun, and 6-month-old parvalbumin (PV) density experiment and analysis were performed by Lauren Rimmer.

# Chapter 1. General Introduction

## 1.1. Alzheimer's disease - symptoms, aetiologies & current treatments

Comprising 60% to 70% of dementia cases and 5% of deaths in the elderly, Alzheimer's disease (AD) is one of the most dreadful neurodegenerative diseases without any cure to date (Rizzi et al., 2014, Ganguli et al., 2005). The prevalence and incidence of AD varies around the globe (Rizzi et al., 2014). In the UK and high-income Western countries, there is a decrease in the incidence of dementia in the last 25 years (Matthews et al., 2016). However, clinical AD cases are still high, because of the increasing number of elderly people. About 13.9 million US population over 65 years old are estimated to be diagnosed with clinical AD by 2060 from the 'baby bloom' generation (Rajan et al., 2021). In low-income countries in Latin America, Middle East and Africa, AD prevalence is estimated to be higher than what is expected for the level of population aging due to more associative risks to AD, including low educational background, poor diet and lack of physical activities that could cause comorbidities including hypertension (Rizzi et al., 2014). The prevalence and death rate could also be affected by the impact of the COVID-19 pandemic (de Erausquin et al., 2021). Together this high number of clinical AD cases and long average duration to death (5.9±3.7 years) lead to dramatic socioeconomic burdens, resulting in a $321 billion total payment in the Year 2022, plus more than 80% of unpaid caregivers (Ganguli et al., 2005, Friedman et al., 2015, Alzheimer'sAssociation, 2022). Therefore, being one of the costliest diseases, effective diagnosis, treatments, and a cure for AD needs to be addressed quickly. To help with this, a deeper understanding of the neurobiological mechanisms involved in the progression of the disease will help with early prevention.

### 1.1.1. Risk factors

Age is one of the most important risk factors of AD, about 95% AD patients develop sporadic AD with unknown cause when they are above 65 years old (Querfurth and Laferla, 2010). This is known as late-onset AD (LOAD) (Bekris et al., 2010, Querfurth and Laferla, 2010). In contrast, 5% of AD patients inherit genetic mutations to develop familial AD (FAD) and have an early onset, thus known as early-onset AD (EOAD) (Zhu et al., 2015, Cope et al., 2022). The crucial genes involved in developing AD are the ones encoding amyloid precursor protein (APP) and presenilin 1 or 2 (PS1 or PS2) (Benilova et al., 2012, Shen and Kelleher, 2007). Meanwhile, expression of a pair of Apolipoprotein E (ApoE) ε4 alleles showed high risk of developing sporadic AD (Liu et al., 2013). These mutations promote an increased Aβ concentration by increasing secretion from APP processing, or reducing Aβ clearance, providing sufficient Aβ species for disease progression (Benilova et al., 2012). Additionally, factors ranging from lifestyle to environment, from comorbidities to educational levels, are also risk factors that could advance AD onset time and aggravate disease development and progression (Oudin, 2020, Javanshiri et al., 2018, Paradise et al., 2009).

### 1.1.2. Symptoms and underlying pathology

In the brains of AD patients, neurodegeneration in the hippocampal formation leads to a progressive loss of episodic memory and cognitive impairment, causing patients to be unable to remember places or events (Selkoe, 1991, Tulving, 2002). Later, patients may experience sleep disruption, and further may develop non-cognitive symptoms, alterations in mood and behaviour such as depression (Li et al., 2014). However, about 20 years before the diagnostic cognitive symptoms, pathologies already exist in the patients' brain, when it is known as the

preclinical stage (Gordon et al., 2018). These pathological biomarkers can be visualised using positron emission tomography (PET) or detected in the cerebrospinal fluid (CSF) or plasma (Sperling et al., 2020, Olsson et al., 2016).

There are two recognised biological hallmarks in AD brains, one is the extracellular amyloid plaques produced from aggregation of β-amyloid peptide 1-42 ($A\beta_{1-42}$ or $A\beta_{42}$) and the other being intracellular neurofibrillary tangles (NFTs) formed with hyper-phosphorylated tau protein (Hardy and Higgins, 1992). Other physiological changes, including production of neuroinflammatory markers, synaptic dysfunction and shrinkage of brain structures exacerbate as AD progresses (Hardy and Higgins, 1992, Sisodia and St George-Hyslop, 2002, Leclerc and Abulrob, 2013).

### 1.1.3. Hypothesised aetiologies

In the year 1906, the first case of Alzheimer's disease was diagnosed (Katzman, 2008). However, it was not identified as an important research field until recent decades, and the direct cause leading to the disease progression remains unknown (Katzman, 2008). Based on the pathologies observed in the post-mortem human brains, several hypotheses have come out throughout the years, with the involvement of misfolded proteins and neuroinflammation as driving factors (Querfurth and Laferla, 2010). This section will focus on the hypothesised aetiologies including the famous amyloid cascade hypothesis, tauopathy, neuroinflammation factors, $Ca^{2+}$ hypothesis and cholinergic hypothesis for the development of AD.

#### *1.1.3.1. Amyloid Cascade Hypothesis*

One of the major pathologies of AD is the Aβ plaques that are aggregates of $A\beta_{42}$ peptides, which were found in the CSF of patients without any cognitive symptoms at early stage of AD (Katzman, 2008, Olsson et al., 2016). These Aβ-containing species might have been accumulating for at least 20 years in the brain regions important for memory, becoming the earliest detectable biomarker for the development of AD (Jack et al., 2010, Gordon et al., 2018, Jack et al., 2013). Therefore, over-expression of Aβ, either due to overproduction or reduced clearance, is believed to play a causative role for AD progression (Leclerc and Abulrob, 2013, Benilova et al., 2012). As a consequence, it was firstly hypothesised that the imbalance between production and clearance causes accumulation of Aβ to initiate AD progression, which is known as the amyloid cascade hypothesis (Hardy and Higgins, 1992; Querfurth and LaFerla, 2010).

The Aβ monomer (~4kDa) is a product of the cleavage of the transmembrane polypeptide APP (Sisodia and St George-Hyslop, 2002). Despite limited knowledge on its function, APP seems to play a role in initiating the transport of the cleavage enzymes for Aβ production (Adeela et al., 2001, Sisodia and St George-Hyslop, 2002). In the brain, one of the three isoforms of APP, $APP_{695}$, can be cleaved in two distinct pathways **(Figure 1.1)** (Sisodia and St George-Hyslop, 2002). In the non-amyloidogenic pathway, APP is cleaved by α-secretase between residues 16 and 17 of Aβ, producing the neurotrophic soluble APP-α (sAPPα) that has neuroprotective functions (Morris et al., 2014). The remaining transmembrane peptide is then cleaved by γ-secretase, inhibiting the production of Aβ species (Morris et al., 2014).

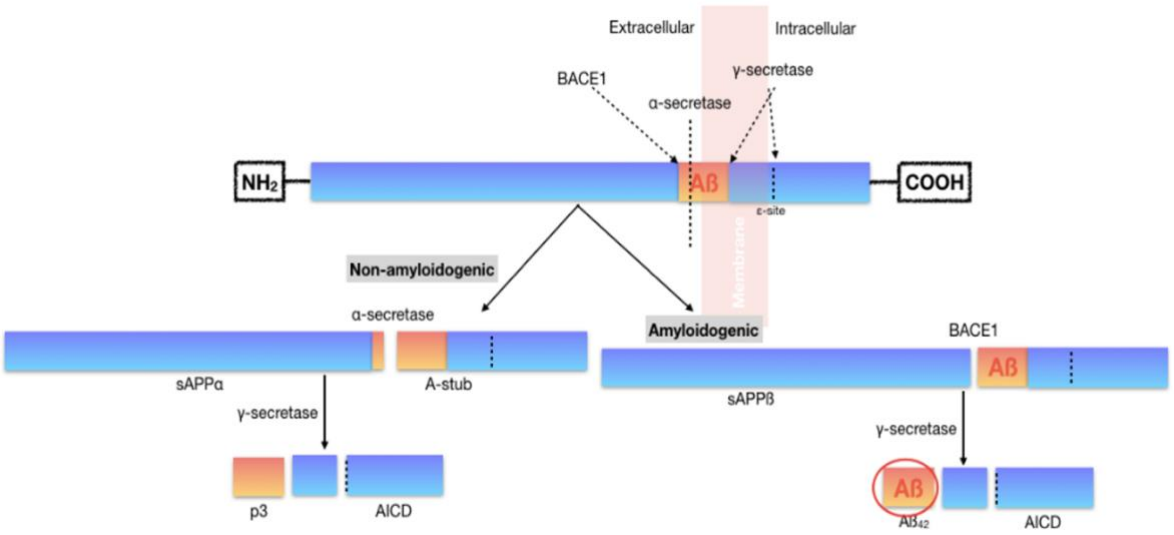


***Figure 1.1. Two ways to cleave amyloid precursor protein (APP).***

*In the non-amyloidogenic pathway, APP is cleaved by α-secretase followed by γ-secretase, resulting in sAPPα and amyloid intracellular domain (AICD). In AD, α-secretase is replaced by β-site APP cleaving enzyme 1 (BACE1), which cleaves at a different binding site, resulting in the production of Aβ peptides of different lengths (Querfurth and LaFerla, 2010; Morris et al., 2014).*

Pathologically, however, β-site APP cleaving enzyme 1 (BACE1) is the first enzyme to cleave APP instead of α-secretase (Sisodia and St George-Hyslop, 2002). The cleavage by BACE1 leads to the production of intact and active Aβ of different lengths, including $Aβ_{1-40}$ and $Aβ_{1-42}$ (**Figure 1.1**) (Sisodia and St George-Hyslop, 2002). The $Aβ_{42}$ isoform has many deteriorating functions including disturbing $Ca^{2+}$ homeostasis, causing the formation of NFTs and neuroinflammation (Hardy and Higgins, 1992, Heneka, 2017). Also, $Aβ_{42}$ isoform tends to aggregate more easily, producing different types of soluble oligomers, highly-sheeted protofibrils and, finally, insoluble fibrils and plaques (**Figure 1.2**) (Benilova et al., 2012). In the amyloid cascade hypothesis, the products from BACE1 cleavage and $Aβ_{42}$ aggregation can cause synaptic dysfunction, production of NFTs and neuroinflammation, triggering global

neuronal dysfunction and degeneration, and eventually leading to cognitive symptoms seen in the patients (**Figure 1.2**) (Hardy and Higgins, 1992, Goure et al., 2014, Ballard et al., 2011).

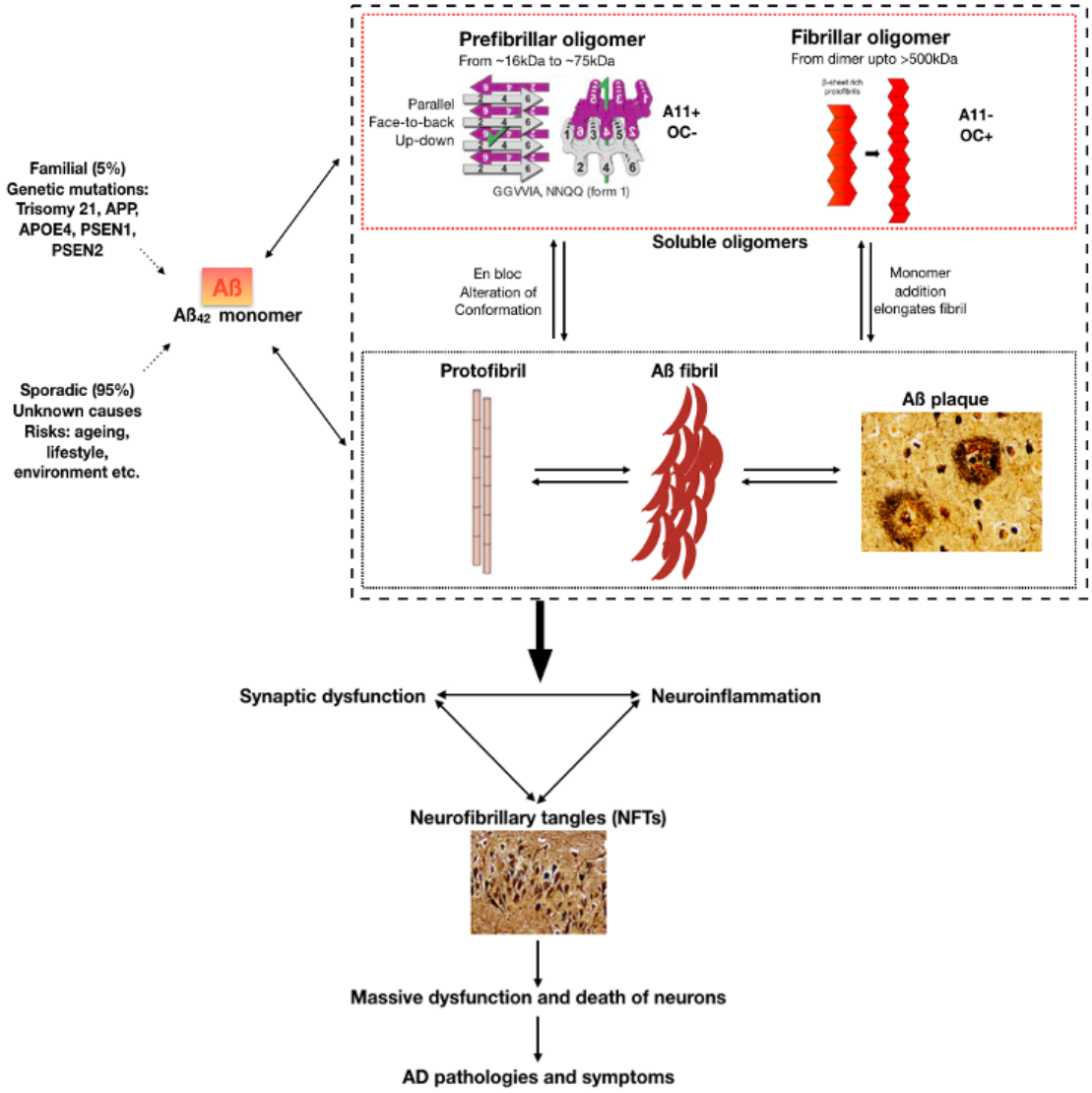


***Figure 1.2. Amyloid cascade hypothesis.***

*Amyloid cascade hypothesis suggests that AD is caused by aggregation of Aβ$_{42}$ that can trigger a cascade of events leading to massive neurodegeneration. Aβ$_{42}$ is more prone to aggregate and cause the formation of soluble oligomers with different configurations. The resulting soluble oligomers form insoluble fibrils via different pathways. This extracellular Aβ accumulation leads to synaptic dysfunction, neuroinflammation and production of NFTs, eventually causing widespread neuronal injuries in the brains of AD patients. (Morris et al., 2014, Glabe, 2008)*

It was originally believed that neurodegeneration was originated from and caused by insoluble Aβ plaques (Pozueta et al., 2013), because unusually distorted and twisted dendrites were found close to the vicinity of Aβ plaques that could potentially make neurotransmission more difficult (Hyman and Gomez-Isla, 1994). However, soluble Aβ oligomers are now believed to be neurotoxic and do more harm to the synapse, whereas insoluble aggregates and Aβ monomers may be in fact involved in removing the toxicity of oligomers *in vivo* (Palop and Mucke, 2010, Goure et al., 2014).

Notably, different configurations were found in soluble Aβ oligomers of the same size, and they exhibit different toxicity strength (Glabe, 2008, Deshpande et al., 2006). Soluble Aβ oligomers with a low molecular weight (LMW) of less than 75kD are composed of 15-20 monomers and can be recognised by the conformational antibody A11 for prefibrillar oligomers that are rarely associated with plaques (**Figure 1.2**) (Kayed et al., 2003, Glabe, 2008). Interestingly, the prefibrillar oligomers could not be recognised by the OC antibody which is a conformational antibody specifically for the fibrillar oligomers whose molecular weight can go up to 500kDa (**Figure 1.2**) (Kayed et al., 2007, Glabe, 2008). However, the small LMW oligomers are thought to be easier to diffuse and contribute more to the progression of AD because they provide more growing ends of the β-sheets per unit mass of peptides for pathogenesis (Glabe, 2008).

Occurring in human brains, the LMW soluble Aβ oligomers have a high affinity to the synapse and cell membrane, and 5nM soluble Aβ oligomers was sufficient to trigger rapid neuronal death in human cortical neurons in culture (Glabe, 2008, Deshpande et al., 2006). Aβ-derived diffusible ligands (ADDLs) are also soluble Aβ species but represent the fibrillary type of oligomers (Glabe, 2008). ADDLs induce similar toxicity as the LMW soluble Aβ oligomers but

require a 5-fold longer timescale for a comparable toxicity (Deshpande et al., 2006). In contrast, fibrillar Aβ, derived from these soluble Aβ species requires an even higher concentration and longer time to generate a modest neuronal death, suggesting a weaker toxicity than the soluble ones (Deshpande et al., 2006).

The soluble Aβ oligomers can damage cells in the hippocampal formation and cortical regions that potentially leads to a deficit in memory and cognition in AD patients (Pozueta et al., 2013, Robert et al., 2013, Giuffrida et al., 2009, Goure et al., 2014). In experimental models, memory impairment and cognitive deficits have also been observed in mice and rats treated acutely with micromolar concentration of LMW soluble Aβ oligomers (Benilova et al., 2012, Walsh et al., 2002). Therefore, soluble Aβ oligomers with a low molecular weight have aroused more attention for the mechanism of AD development, especially for investigating their effects in the early stage of AD.

#### *1.1.3.2. Tauopathy*

Tau is normally an abundant soluble protein in the axon of a neuron to promote assembly and stability of microtubules and assist vesicle transport (Querfurth and LaFerla, 2010). NFTs are formed from tau filaments as a result of aggregation of pathological insoluble tau protein (Benilova et al., 2012, Querfurth and Laferla, 2010). Similar to Aβ, the nonpathological helical filament form of tau proteins might be inert and protective (Andorfer et al., 2003, Lee et al., 2005). However, the intermediate tau proteins (like Aβ oligomers) produced by hyperphosphorylation are toxic, which could cause the death of neurons and cognitive deficits (Santacruz et al., 2005, Iqbal et al., 2005, Benilova et al., 2012, Querfurth and Laferla, 2010).

Augmentation of hyperphosphorylated and total tau proteins in the cerebrospinal fluid was found to be associated with the reduction of scores in cognitive tests in AD patients (Wallin et al., 2006). Recently, it was found that tau phosphorylation played a role in the cognitive impairment induced by high dietary salt (Faraco et al., 2019). Mice treated with a high-salt diet for 12 weeks exhibited difficulties in recognising novel objects and exhibited deficits in spatial memory using the Barnes maze (Faraco et al., 2019). However, in tau-knock-out mice and mice treated with anti-tau antibodies, salt-induced cognitive impairment was inhibited, suggesting that tauopathy could be, to some extent, involved in the mechanism of AD development and progression (Faraco et al., 2019).

#### *1.1.3.3. Neuroinflammation in Alzheimer's disease*

Evidence suggests that neuroinflammation plays a key role in the early stage of AD, becoming a third biological hallmark for the disease. Recent studies have showed the role of chronic neuroinflammation in AD aetiology, which may link Aβ and tau-pathology together (Daniels et al., 2016, Heppner et al., 2015, Morris et al., 2014).

AD has recently been recognised as an autoimmune disease governed by the sterile inflammation in the brain (Meier-Stephenson et al., 2022, Weaver, 2021). Inflammation can be induced by bacterial or viral infections that are known as pathogen associated molecular patterns (PAMPs) (Lenart et al., 2016). In this case, the immune cells and anti-inflammatory cytokines and chemokines will be recruited to relief the immune response (Lenart et al., 2016). However, sterile inflammation is elicited by intracellular molecules coming out of the cell, which is defined as danger associated molecular patterns (DAMPs) (Lenart et al., 2016). Systemic sterile inflammation in the brain is dangerous, because instead of clearing infections,

it targets healthy cells and contribute to damage and cell death (Lenart et al., 2016). In the case of AD, the pathogens Aβ and tau could act as DAMPs and chronically exacerbate the damage of healthy neurons (White et al., 2017).

The inflammatory response in the central nervous system (CNS) (aka. Neuroinflammation) is regulated by cytokines, chemokines, reactive oxygen species and second messengers (DiSabato et al., 2016). In fact, neuroinflammation is a coin of two sides. In response to transient and low neuroinflammation, it is helpful for neuronal remodelling and tissue repair; whereas for some traumatic injury and chronic neuroinflammation like AD, it is harmful as it leads to reduced plasticity and apoptosis (DiSabato et al., 2016). Also, the induction of neuroinflammation involves the production of both anti-inflammatory and pro-inflammatory molecules generated from microglia and astrocytes which are CNS glial cells (DiSabato et al., 2016). For instance, interleukin-4 (IL-4) is beneficial in promoting axonal growth and neuronal recovery (DiSabato et al., 2016, Zhang and An, 2007). In contrast, using AD as an example, the pro-inflammatory cytokines IL-1β, tumour necrosis factor alpha (TNFα) and interferon gamma (IFN-γ) play essential roles in exacerbating the neuronal damage (DiSabato et al., 2016, Belkhelfa et al., 2014).

Importantly, the clustering of activated microglia around plaques is one important characteristic of AD (Hansen et al., 2018). Microglia are innate CNS immune cells having the phagocytic property to attack pathogens and respond to neural injury (Hansen et al., 2018). Once activated, microglia are damaging in AD as they secrete pro-inflammatory factors mediating synaptic engulfment (Hansen et al., 2018). The microglial cell surface receptor triggering receptor expressed in myeloid cells 2 (TREM2) was found to be mutated in AD and increase the risk of the disease (Jonsson et al., 2013). Aβ functions as a DAMP to induce an

immune response in the brain, and the clearance requires forming complexes with lipoproteins (Takahashi et al., 2005). TREM2 is necessary for the phagocytotic function of microglia, whereas loss of TREM2 function by a mutation related to AD (R47H) impairs the uptake and clearance of Aβ (Takahashi et al., 2005). Microglia with mutated TREM2 also show a reduced ability to engulf debris from damaged neurons, unable to provide a healthy environment for normal neuronal and synaptic function (Hansen et al., 2018).

Apart from reducing Aβ clearance, microglia also respond to Aβ as a DAMP and activate the NLRP3 inflammasome leading to the release of the pro-inflammatory cytokine IL-1β (Heneka, 2017, Dansokho and Heneka, 2017). This then triggers caspase-1 dependent cell death or pyroptosis, which could further cause more neurodegeneration (Bergsbaken et al., 2009).

Other than microglia, astrocytes are the other major cellular component of the innate immune system in CNS (Gonzalez-Reyes et al., 2017). Playing an essential role in the tripartite synapse for glutamatergic and GABAergic transmission in the brain (details see **Chapter 4, Section 4.1.3 and 4.1.4**), astrocytes are glial cells that can remove debris and toxins in the CSF (Gonzalez-Reyes et al., 2017). Proliferation of astrocytes have also been observed at the close vicinity of Aβ plaques and NFTs (Serrano-Pozo et al., 2011). However, this study will focus on the changes in microglia density and activation as a measure of neuroinflammation.

#### *1.1.3.4. $Ca^{2+}$ Hypothesis of Alzheimer's disease*

In late-onset sporadic AD (sAD), more than 120 types of PS1 mutations are inherited (McBrayer and Nixon, 2013, Ryan and Rossor, 2010, Campion et al., 1995). PS1 is a 65kDa holoprotein serving a proteolytic function in the γ-secretase complex (Honarnejad et al., 2013). Cleavage of PS1 results in the catalytic subunit of the γ-secretase complex, which is

involved in cleavage of type 1 intramembrane substrates, including APP (Honarnejad et al., 2013). Mutations in PS1 was shown to cleave APP in favour of producing neurotoxic $A\beta_{42}$ (Honarnejad et al., 2013, De Strooper et al., 1998). In fact, the PS1ΔE9 mutation was found to attenuate the activity of γ-secretase in human neurons by increasing the $A\beta_{42}$/ $A\beta_{40}$ ratio, instead of losing the function independent to γ-secretase (Woodruff et al., 2013).

However, it is still worth noticing that the PS1 holoprotein can control lysosomal acidification and $Ca^{2+}$ homeostasis in lysosomes and the endoplasmic reticulum (ER), which leads to the $Ca^{2+}$ hypothesis for AD (**Figure 1.3**) (McBrayer and Nixon, 2013, Berridge, 2010). Dysregulation of $Ca^{2+}$ homeostasis in lysosome and ER contributes to disruption of synaptic plasticity that can be triggered by PS1 mutation, which is observed in FAD patients and a number of transgenic animal models for AD (McBrayer and Nixon, 2013, Berridge, 2010).

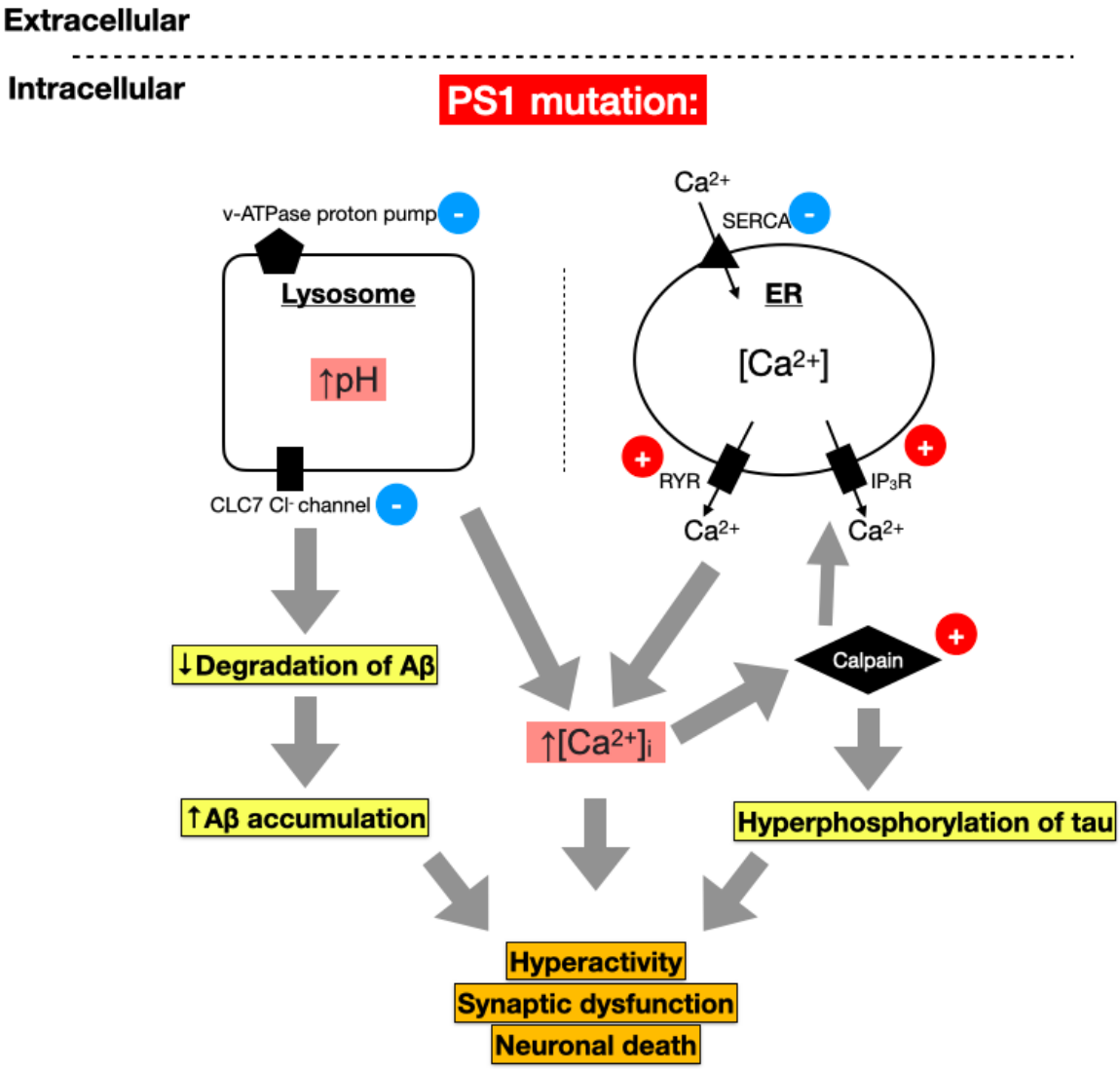


***Figure 1.3. A schematic of calcium hypothesis for Alzheimer's disease.***

*PS1 mutation leads to increase of intracellular calcium concentration by its action on lysosome and endoplasmic reticulum. ER: endoplasmic reticulum; $IP_3R$: inositol trisphosphate receptor; RYR: ryanodine receptor; SERCA: sarco/endoplasmic reticulum $Ca^{2+}$-ATPase; v-ATPase: vacuolar-ATPase.*

The loss of PS1 function could lead to a reduction of assembly and proton-pumping activities of the vacuolar-ATPase on lysosomes, causing less acidification and increased lysosomal pH level (McBrayer and Nixon, 2013). Deacidification in the lysosome results in impairment of autophagy function, which is an essential step to clear faulty misfolded and aggregated

proteins including the sticky $A\beta_{42}$, which is poorly eliminated by normal protein degradation via the ubiquitin-proteasome system (McBrayer and Nixon, 2013). Additionally, the incomplete acidification of the lysosome is also mediated by the dysfunction of the chloride channel CLC7 expressed on the lysosome of microglia (McBrayer and Nixon, 2013, Majumdar et al., 2011). Therefore, impaired lysosomal autophagy leads to diminished Aβ metabolism, with uncleared Aβ exacerbating the level of Aβ species.

Failure of lysosomal acidification also impairs $Ca^{2+}$ efflux from the lysosome, contributing to the elevation of cytosolic $Ca^{2+}$ concentration (McBrayer and Nixon, 2013). However, this is a minor by-product of mal-acidification (Berridge, 2011). One of the major ways to pathologically increase intracellular $Ca^{2+}$ concentration is via the ER where the PS1 mutation also plays a vital role (Berridge, 2011). PS1 could over activate the ryanodine receptor (RYR) and inositol trisphosphate receptor ($IP_3R$) on the ER, to increase efflux of $Ca^{2+}$ (Berridge, 2011). RYR in turn modulates the $IP_3R$ function to exacerbate its activation (Berridge, 2011). The influx of ER $Ca^{2+}$ is via the sarco/endoplasmic reticulum $Ca^{2+}$-ATPase (SERCA) channel, yet in PS1 mutated mice or PS1 knock-out mice/cells, the SERCA channel activity is diminished, leading to less $Ca^{2+}$ reuptake, and further contributes to the increased intracellular $Ca^{2+}$concentration (Berridge, 2011).

In the case of AD, increases in neuronal $Ca^{2+}$ concentration that results from altered ER and lysosomal $Ca^{2+}$ homeostasis will pathologically activate calpain activity (McBrayer and Nixon, 2013). Calpain is a protease that is mostly present in the CNS. Calpain-1 is concentrated at the synapse, while calpain-2 is bound to the NFTs that result from hyperphosphorylation of tau (McBrayer and Nixon, 2013). Calpain activation could enhance cleavage of $IP_3R$ that in turn contributes to changes in ER $Ca^{2+}$efflux (McBrayer and Nixon, 2013). Additionally, in the AD

brain, there is a decrease of an endogenous inhibitor of calpain, calpastatin (McBrayer and Nixon, 2013, Rao et al., 2008). This enhances the calpain activity to activate the downstream molecular cascade including CDK5, ERK1/2, GSK3β, which then contributes to the hyperphosphorylation of tau that is a common pathway that is also seen in sporadic AD (McBrayer and Nixon, 2013, Rao et al., 2008). Therefore, $Ca^{2+}$ elevation not only affects the production of NFTs, but the elevated intraneuronal $Ca^{2+}$ concentration *per se* is sufficient to cause synaptic dysfunction by enhancing long-term depression as well as impairing short-term plasticity (Berridge, 2011). Therefore, the disturbed $Ca^{2+}$ homeostasis might equally play a critical role in the pathophysiology of AD progression.

#### *1.1.3.5. Cholinergic Hypothesis*

Memory and cognitive difficulties seen in AD patients are also believed to be associated with degeneration of cholinergic neurones in the basal forebrain, which is known as the cholinergic hypothesis of AD (Newman et al., 2012). Generally, there is a decrease of choline acetyltransferase, the enzyme producing acetylcholine (ACh), thus, affecting ACh synthesis; the binding between ACh and its receptors is not as efficient as in normal individuals, leading to cognitive impairment of the patients (Francis et al., 1999). Indeed, blockade of cholinergic receptors and lesions of cholinergic neurones affect working and episodic memory as well as attention, whereas administration of ACh improves working memory and enhances LTP in rats (Newman et al., 2012). In contrast, activation of cholinergic receptors with nicotine can boost attention and slow AD progression in humans (Newman et al., 2012, van Duijn and Hofman, 1991).

### 1.1.4. Current pharmacological treatments for AD

The U.S. Food and Drug Administration (FDA) has currently approved seven pharmacological treatments for AD. Five of them are for alleviating AD symptoms, namely donepezil (Aricept), rivastigmine (Exelon), galantamine (Reminyl), memantine (Namenda), and memantine combined with donepezil (Alzheimer'sAssociation, 2022). Memantine blocks the activity of glutamatergic N-methyl-d-aspartate (NMDA) receptors to prevent over stimulation by the neurotransmitter glutamate, while the others are selective reversible inhibitors of acetylcholinesterase (AChE) (Razay and Wilcock, 2008, Polinsky, 1998, Wilkinson, 1999, Johnson and Kotermanski, 2006). In the UK, the three AChE inhibitors are used to treat mild to moderate AD, while Memantine is for moderate to severe AD (National Health Service, 2023). However, all these current medications are unable to slow down the disease progression or cure the disease and have mild side effects like nausea and headache (Yiannopoulou and Papageorgiou, 2013, Alzheimer'sAssociation, 2022).

On the 7$^{th}$ June, 2021 the FDA gave an accelerated approval to the drug Aducanumab (Aduhelm), which is currently the sixth approved drug for AD in the US (Yang and Sun, 2021). Unlike the others, Aducanumab targets an underlying mechanism in relation to the progression of AD. It is a human monoclonal antibody that binds to Aβ aggregates and recognises plaques, and can dose-dependently remove Aβ pathologies (Yang and Sun, 2021). The appearance of Aducanumab brings hope to millions of AD patients and their caregivers because of its target, although is not approved and unavailable in Europe and the UK due to the decision of the European Medicines Agency (EMA) (Yang and Sun, 2021, Lythgoe et al., 2022). FDA normally has a very high degree of concordance with the EMA in approving novel medications, yet the disagreement on Aducanumab is of surprise and controversial (Lythgoe et al., 2022). Aducanumab was said to have unreliable clinical evidence of cognitive

improvement and was claimed unsafe, with severe side effect including brain swelling and bleeding (Lythgoe et al., 2022, Ackley et al., 2021).

Luckily, the most recent (January 2023) FDA approved drug Lecanemab (Leqembi) was shown to significantly reduce Aβ plaques, slowing the disease progress by elongating the duration between MCI to mild AD and shortening the time from moderate to severe AD (van Dyck et al., 2023, McDade et al., 2022, Tahami Monfared et al., 2022). Lecanemab is also a humanised monoclonal antibody but targeting Aβ soluble protofibrils – a type of soluble Aβ oligomer in the early stage of AD (van Dyck et al., 2023). Although the administration of Lecanemab also results in side effects like oedema in about 13% of participants, this current success in the clinical trial definitely brings hopes for AD prevention, and further shows that the role of neurotoxic soluble Aβ oligomers in the early stage of the disease (van Dyck et al., 2023).

Nevertheless, it should be noted that AD is still an unmet clinical need, despite the recent novel treatments. It is crucial and valuable to deepen the understanding of the neurochemical mechanisms of AD to develop more effective pharmaceutical compounds or strategies to early AD diagnosis, intervention, treatment, and a final control of disease progression (Kazim et al., 2021).

## 1.2. Animal models for AD research

To study the fundamental mechanism and screen promising pharmacological targets for the treatment of AD, a number of preclinical animal models have been developed. They can be generally divided into two groups, the acute and the transgenic models, but most of them are built based on the amyloid cascade hypothesis (**Figure 1.2**). The acute model mainly studies the transient action of soluble Aβ monomers and/or oligomers following direct cranial

injection of either synthetic, brain-isolated or cell-derived soluble Aβ oligomers, *in vitro* or *in vivo* (Palop and Mucke, 2010, Watremez et al., 2018, Lesné et al., 2006, Podlisny et al., 1995), whereas the majority of the studies carried out in the transgenic models transfect single or multiple human genes related with AD into mice or rats.

### 1.2.1. Non-transgenic Models

In this model, a single dose of Aβ is directly administrated *in vivo* or *ex vivo* in rodents and the behaviour and synaptic function are tested several hours to days after administration. There is gathering evidence that Aβ can cause memory impairments and alter synaptic functions using the acute model.

The source of Aβ can be synthetic soluble Aβ oligomers, be extracted from human AD brains, or derived from cells. For example, amyloid-β-derived diffusible ligands (ADDLs) is one of the commonly used synthetic Aβ for the acute models (Lambert et al., 1998). They can also be produced from Chinese hamster ovary (CHO) cells transfected with human mutated APP genes where the Valine at residue 717 is substituted with Phenylalanine, and these modified CHO cells are referred to as 7PA2 (Podlisny et al., 1995). The 7PA2 cell medium (CM) contains a mixture of soluble Aβ oligomers species, whereas the CHO CM acts as vehicle control (Cleary et al., 2004, Walsh et al., 2002, Podlisny et al., 1995). With different preparation procedures, other types of Aβ oligomers such as prefibrillar Aβ oligomers that are either OC-positive or OC-negative and the fibrillar oligomers, can also be made (Kayed et al., 2007).

Several studies using the acute model for AD have been summarised in **Table 1.1** with their behavioural and synaptic effects concluded.

***Table 1.1. Non-transgenic models in Alzheimer's disease research***

| Animal | Injection | Behaviour | Synaptic function |
|---|---|---|---|
| Rat - P21 brain slices. (Lambert et al., 1998) | *In vitro application of* synthetic ADDLs | | ADDLs rapidly inhibited *in vitro* LTP at the medial perforant path-dentate gyrus granule cell circuit. |
| Adult male Sprague-Dawley rats (O'Hare et al., 1999) | Bilateral injection of 5.0 µl of aggregated $A\beta_{42}$ suspension into dorsal hippocampal CA3. | Cognitive deficits seen as significantly higher numbers of incorrect lever perseverations in the alternating lever cyclic ratio (ALCR) test from day 50 to 90 after administration. | |
| Adult male Wistar rats (Walsh et al., 2002) | *In vivo* microinjection of 7PA2 CM (1.5 µl intracerebroventricular i.c.v.) | | • *In vivo* LTP was completely blocked in hippocampal CA1 region at 3 h post-stimulation with the 7PA2 CM.<br>• LTP was selectively blocked by Aβ oligomers in the absence of monomers, protofibrils or fibrils |
| Adult female Lister Hooded rats (Watremez et al., 2018) | *In vivo* i.c.v. injection of 5 nmol of synthetic Aβ oligomers (10µl) | Cognitive deficits in the novel object recognition task. | A decrease of synaptic markers (SNAP-25 and PSD-95) in the frontal cortex. |

In summary, it is difficult to study the underlying mechanism of pathogenic effects of oligomeric Aβ with acute injection of synthetic Aβ peptides, because it is simply not capable to reproduce APP processing in human brains, and further, synthetic Aβ oligomers can become insoluble and crystallised before the injection (Kayed et al., 2007, Lambert et al., 1998, Morris et al., 2014). Nevertheless, albeit the acute models are limited in relation to modelling

disease pathologies to investigate the progression of the disease, they are still useful in investigating the transient effect of Aβ species.

### 1.2.2. Transgenic Models

Thanks to the discovery of genetic mutations linked with AD, many animal models of AD have been developed, which is essential to study the process of early pathology, as patients show histopathological alterations in their brains prior to clinical symptoms (Bilkei-Gorzo, 2014). There are so far 214 transgenic models for AD that mimic the disease through elevation of aberrant $A\beta_{42}$ and/or NFTs without changing the normal physiology in other parts of the body (Alzforum, 2023). Among these transgenic models for AD, the APP23 mice, APP/PS1 mice, 5xFAD mice, and 3xTg mice are the most commonly used mutations of the models.

#### *1.2.2.1. Transgenic Mouse Models*

APP23 line overexpresses human APP by a single Swedish mutation, causing extensive $A\beta_{42}$ deposition detectable at 6 months of age (Bilkei-Gorzo, 2014). Addition of a mutation in the PSEN1 gene gives rise to the APP/PS1 model. Although substantial NFT load and brain atrophy are not present in this model, pathologies involved in early stage of the disease are present, especially in the hippocampus (Bilkei-Gorzo, 2014).

The 5xFAD mice have five mutations, three of which are human APP genes with Swedish, Florida and London mutations, and the other two are presenilin mutations. They express age-dependent memory deficits and produce extracellular plaques by two months of age, but they do not show NFTs (Oakley et al., 2006). The 5xFAD mouse model is one of the most common preclinical models used in AD research, but it has poor construct validity. For example, it

displays excessive amount of Aβ compared to what is observed in AD patients (Drummond and Wisniewski, 2017) .

However, although transgenic rodent models express AD-like behavioural symptoms, some of them could not entirely represent AD pathologies such as the failure to express massive loss of hippocampal neurons or tauopathy (Bilkei-Gorzo, 2014). In both APP23 and APP/PS1 line, hyperphosphorylated tau can be detected close to the plaques but NFTs are barely observable (Bilkei-Gorzo, 2014). These transgenic animals only show other AD-like pathologies when additional transgenes are added which are not expressed in familial AD (Oddo et al., 2003, Cohen et al., 2013). Therefore, the 3xTgAD model was developed to show both amyloid plaques and NFTs by adding one more mutation in MAPT gene to the APP/PS1 line (Alzforum, 2023).

In the 3xTg mouse model of AD, $A\beta_{42}$ and NTFs appear progressively dependent on age (Mastrangelo and Bowers, 2008). The immunoactivity of intracellular $A\beta_{42}$ can be detected at three to four months of age, with extracellular $A\beta_{42}$ present at 6 months and strong expression of $A\beta_{42}$ by the twelfth month (Billings et al., 2005). Cognitive and synaptic plasticity deficits for this model appear early at 4 months old, whereas aggregation of hyperphosphorylated tau can be detected later at 12 to 15 months, but synaptic deficit as measured by paired-pulse facilitation was impaired in the young 3xTg rats (4-6mo) in CA1 and dentate gyrus *in vivo* (Mastrangelo and Bowers, 2008, Davis et al., 2014). They also show impaired baseline transmission and severely reduced long-term potentiation at 6 months of age before the formation of tangles or plaques (Oddo et al., 2003). The 3xTg model shares the most similarities in pathological and behavioural symptoms with AD patients compared to APP/PS1 and APP23 models.

#### *1.2.2.2. Transgenic Rat Models*

Evolutionally, rats are 4 to 5 million years closer to human compared to mice, and hence they are believed to provide a more reliable model to study AD than transgenic mice (Cohen et al., 2013, Yang et al., 2004). There are currently 17 AD models using rats (Alzforum, 2023). For example, there are previous ones like the APP21, and McGill-R-Thy1-APP models carry human APP695 transgene in Fisher 344 rats and APP751 transgenes in Wistar rats (Chan Anthony et al., 2008, Leon et al., 2010). In the APP21 model, amyloid plaques do not appear until 18 months of age, whereas in the McGill-R-Thy1-APP model, the plaques appear in hippocampus starting from 6 months old (Chan Anthony et al., 2008, Leon et al., 2010). In both models, cognitive deficits indicated by deficits in the Morris water maze showed at 3 months of age (Chan Anthony et al., 2008, Leon et al., 2010). Newer ones use Crispr/Cas9 gene editing technology to knock in humanised APP gene into rats with Long Evans or Sprague Dawley background (Serneels et al., 2020, Pang et al., 2022). For example, the homozygous APP Swe-Arc-Ibe knock-in rats showed spatial memory deficits in the Morris water maze at 5 months old and a loss of synaptic proteins at the age of 9 months in the hippocampus, but showed rapid Aβ aggregation as early as 1 month (Pang et al., 2022).

Some rat models carry both APP and PS1 mutations. For example, a rat model with a Fischer 344 background, which displays a complete range of age-dependent AD pathologies and cognitive impairment (known as TgF344-AD rats) (Cohen et al., 2013). This model contains "Swedish" mutant human APP (APPsw) and delta exon 9 mutant human presenilin-1 (PS1ΔE9) (Cohen et al., 2013). Noted that there are many mutations of APP and PS1, for example, the G384A mutation seen in the APP23xPS45 mice can specifically destroy $Ca^{2+}$ leak function (Nelson et al., 2007). In this animal model, the APPsw mutation generally augments the production of Aβ species, with $Aβ_{42}/Aβ_{40}$ ratio unaffected (Citron et al., 1994, Citron et al.,

1992). In contrast, the PS1ΔE9 mutation impairs APP processing, resulting in increased $A\beta_{42}$ and $A\beta_{42}/A\beta_{40}$ ratio (Woodruff et al., 2013, Dumanchin et al., 2006, Cacquevel et al., 2012). It also disrupts a range of intracellular functions including causing defected mitochondrial and autophagic function, astrocytic response to inflammatory triggers and calcium homeostasis without Aβ pathology (Rojas-Charry et al., 2020, Oksanen et al., 2020).

The TgF344-AD rats have a high concentration of soluble Aβ at 6 months of age before the formation of amyloid deposition and neurodegeneration. At 9 months old, these animals have abundant amounts of soluble Aβ before other pathologies become obvious (Cohen et al., 2013). The TgF344-AD rats express 2.6 times more human APP proteins than endogenous rat APP and 6.2 times more human PS1ΔE9 protein compared to endogenous rat N-terminal PS1 fragment in the wildtype controls quantified by Western blot (Cohen et al., 2013). They show age-dependent increases in levels of detergent-soluble and detergent-insoluble $A\beta_{40}$ and $A\beta_{42}$ between 6 and 26 months; the $A\beta_{42}/A\beta_{40}$ ratio increases with age in the soluble fraction but decreases in the insoluble fraction (Cohen et al., 2013).

There are also some rat models that only express mutations in tau but not Aβ genes using the spontaneously hypertensive rat (SHR) strain. These animals demonstrate NFTs in the cortex and hippocampus at about 8 to 9 months of age (Valachova et al., 2018, Hrnkova et al., 2007, Koson et al., 2008). But they have a shorter lifespan, as short as 7 to 14 months compared to the wild-type rats (approximately 22 to 24 months), and the SHR24 model do not express neuronal loss in the cortex or hippocampus, which cannot fully mimic AD phenotypes (Filipcik et al., 2012, Valachova et al., 2018).

In conclusion, this section introduced some of the most commonly used transgenic mice models such as the 5xFAD and 3xTg mice, and novel transgenic rat models such as the TgF344-

AD rats. Evidenced from human genetic mutations, alterations in APP genes and presenilin 1 and 2 (PS1/PS2) trigger deposition of Aβ, which is one of the major causes of early-onset AD (Selkoe, 2001, Cohen et al., 2013). Using the animal models developed based on the human familial AD, different pharmacological components could be tested on to screen possible therapies for AD patients. However, some models do not fully match and sometimes exaggerate the physiological symptoms in patients. It is still controversial whether Aβ itself is required and sufficient to trigger the cascade of AD pathologies (Cohen et al., 2013). Although these transgenic models are useful and an advantage to study the relationship of genotype to phenotype in familial AD (Selkoe, 2001), more reliable preclinical models that can model sporadic AD should be developed to fully understand the mechanism of the progression of this disease and for successful drug screening.

### 1.3. The association between memory and hippocampus

The structures for memory functions include hippocampus, entorhinal, perirhinal cortices, as well as postrhinal cortex (parahippocampus in human) (Squire and Zola-Morgan, 1991, Cherubini and Miles, 2015). Place cells and grid cells that are important for episodic and spatial memory are found in the hippocampus (Moser et al., 2015). Located at the temporal lobe and being a part of the limbic system, the hippocampus can be roughly separated into the dorsal and ventral parts, and they generally have different functions (Anand and Dhikav, 2012). Essentially, the dorsal hippocampus primarily performs cognitive functions for learning and memory, whereas the ventral hippocampus is more associated with stress and emotions (Fanselow and Dong, 2010, Lee et al., 2019).

In rodents, dorsal hippocampus could be further segregated into *Cornu Ammonis* 1, 2 and 3 (CA1, CA2 and CA3) and dentate gyrus (DG) (Clark and Squire, 2013) (**Figure 1.3**). Subiculum (S) also makes up an important part of the hippocampus, but it is more visible in the ventral hippocampal sections (Clark and Squire, 2013, Paxinos and Watson, 2007). The hippocampus receives sensory information form layer II of the entorhinal cortex (EC) to DG via the perforant path, and the excitatory input from DG proceeds to CA3 through mossy fibres (Clark and Squire, 2013). CA3 inputs synapses on the CA1 pyramidal cells, known as the Schaffer collateral pathway, but CA3 also receives recurrent input (Clark and Squire, 2013). CA1 also receives monosynaptic inputs from layer III of the EC as well as receiving CA2 input to its superficial layer (Clark and Squire, 2013, Kohara et al., 2014). Lastly, CA1 outputs project to the subiculum and layer V of the EC (Clark and Squire, 2013).

EC being an input to the hippocampus, is one of the first affected regions in AD patients (Kazim et al., 2021, Braak and Braak, 1996, Braak and Braak, 1991). Also, the NFTs firstly attack CA1, followed by subiculum, and then CA2 and CA3 (Braak and Braak, 1991, Braak et al., 1993). Since the hippocampus is involved in learning and memory, it is very plastic but vulnerable to different external stimuli (Anand and Dhikav, 2012). In this section, the way that the hippocampus encodes memory will be briefly introduced, as well as how this is affected in the early stage of AD.

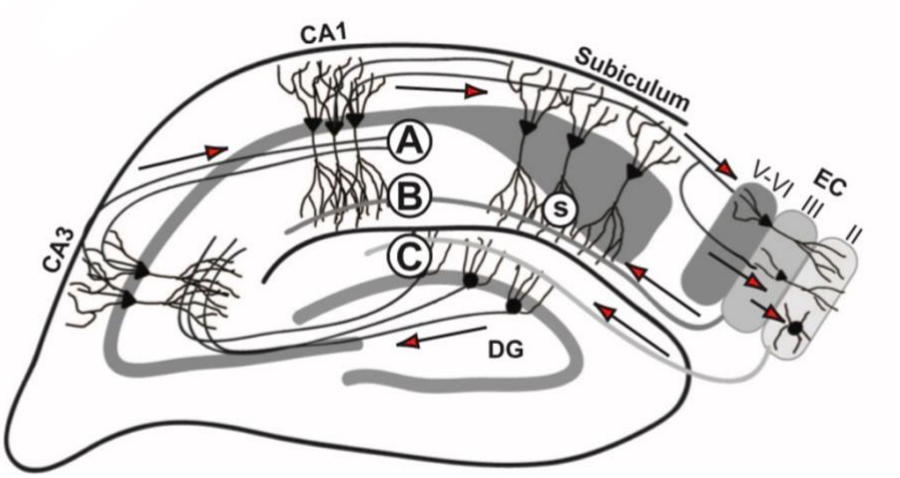


***Figure 1.4. Hippocampal circuits of rodents.***

*There are three major glutamatergic (excitatory) pathways in the rodent hippocampus. A. Schaffer collateral pathway from CA3 pyramidal cells to CA1 pyramidal cells. B. Tempero-ammonic path from entorhinal cortex (EC) layer III to the apical dendrites of CA1 and subiculum. C. Perforant path from EC layer II to the dentate gyrus. (Davis et al., 2014)*

### 1.3.1. Hippocampal oscillations and memory

The hippocampal functions of spatial navigation and memory processing are controlled by synchronous firing of neurons, which is known as rhythmic oscillations (Lopez-Madrona et al., 2020, Pastalkova et al., 2008, Passingham, 1979). Oscillations at multiple frequencies can generate simultaneously in the hippocampus, where theta (4-8Hz) and gamma (30-100Hz) oscillations are important for memory and cognition (Lopez-Madrona et al., 2020, Lisman, 2010). Sharp wave ripple (SWR) oscillation which is a brief high-frequency oscillation (140–240Hz) in the hippocampus is associated with social and episodic memory consolidation (Wiegand et al., 2016).

The activity of theta rhythm is generated from layer II and III of the EC and travels the pathway of the hippocampal trisynaptic circuits **(Figure 1.3)** (Buzsaki, 2002, Lopez-Madrona et al., 2020). Using a lot of animal and computational models of different species, a number of roles

of theta oscillation have been hypothesised since the middle of the 20th century, including arousal signals in rapid-eye movement sleep, information processing, decision making, and memory consolidation (Buzsáki, 2005). In theory, memory encoding is processed by input from EC into the CA1 at a specific theta phase, while memory retrieval happens when CA3 input arrives CA1 at various phases of theta waves (Lopez-Madrona et al., 2020, Douchamps et al., 2013, Hasselmo et al., 2002, Siegle and Wilson, 2014). Therefore, CA1 is a crucial place to record changes related to memory processing.

Gamma activity is nested within the theta rhythm and provides an organizational substrate for representing serial pieces of information (Colgin and Moser, 2010, Penttonen et al., 1998). Hippocampal gamma oscillations are generated by interneurons, which are crucial for balancing excitatory and inhibitory output. It is also important in selecting the hippocampal input for long-term storage and facilitating memory encoding (Colgin and Moser, 2010). Gamma activity is commonly observed in many cortical regions during sleep and wake stages, but in neurological diseases, including schizophrenia, autism and dementia, changes in gamma oscillations have been observed (Tukker et al., 2007, Uhlhaas and Singer, 2006, Buzsaki and Wang, 2012).

Clinical studies found impaired theta and gamma oscillations. Using resting-state electroencephalogram (EEG), AD patients showed increased slow oscillation power (delta 1-3Hz and theta 3-7Hz) as well as enhanced coherence compared to age-matched controls (Meghdadi et al., 2021). MCI patients also showed increased slow wave power in the temporal lobe (Meghdadi et al., 2021). Notably, normal ageing showed decreased slow wave power (Meghdadi et al., 2021), suggesting the route of AD brains is pathological.

Theta-gamma coupling (TGC) is an emerging biological feature that is related to AD (Kitchigina, 2018). Gamma activity can be nested into the peak of theta oscillation, representing cortical excitability and interactions among networks, and is considered as a process of memory encoding (Cope et al., 2022, Goodman et al., 2018, Kitchigina, 2018). TGC provides sufficient space to store combined and versatile memory information, becoming an early marker of neuronal circuit dysfunction relevant for AD (Lopez-Madrona et al., 2020, Joo et al., 2016). The strength of TGC in the hippocampus directly correlates with cognitive function during spatial learning (Kitchigina, 2018; Tort et al., 2009). Impaired TGC has been observed in patients with schizophrenia and other neurological disorders, as well as patients at early stages of AD (Lopez-Madrona et al., 2020). In patients with AD, their TGC is reduced compared to the age-matched controls (Goodman et al., 2018). In transgenic animals, theta-gamma modulation is present both in the low gamma (35-60 Hz) and in the high gamma (100-120Hz) bands, and much attenuated in the TgF344-AD littermates (Joo et al., 2016).

### 1.3.2. Impaired long-term plasticity in models for Alzheimer's disease

Long-term synaptic plasticity can be studied with an evoked phenomenon called long-term potentiation (LTP), which is a cellular model for learning and memory. The establishment of LTP suggests the synapse is strengthened. One of the classic protocols for LTP induction is activating the Schaffer collateral pathway from CA3 region of hippocampus to CA1 pyramidal cells (O'Hare et al., 2013, Buzsáki, 1980).

There is gathering evidence that Aβ can alter LTP induction and cause memory defects. Treatment with soluble Aβ oligomers extracted from human AD brains inhibits LTP in mouse

hippocampal slices and disrupt the ability for mice to learn (Ganesh et al., 2008). Synthetic ADDL also inhibit LTP both *in vitro* and *in vivo* in ADDL-treated mice (Lambert et al., 1998).

Acute application of cell derived soluble Aβ oligomers on cognition and synaptic plasticity have been extensively studied *in vitro* and *in vivo* (Walsh et al., 2005, Klyubin et al., 2005, Walsh et al., 2002). For example, Aβ oligomers produced from the 7PA2 cell line (Chinese hamster ovary cells affected with human APP) could acutely inhibit LTP induction at the CA1 region of the Schaffer collateral pathway when the cell medium was injected to the ventricles in the rat brains, while the LTP could be rescued if Aβ was blocked by antibodies (Walsh et al., 2002). Administration of 7PA2 cell medium in the ventricles could also rapidly inhibit hippocampal LTP induction *in vitro* and *in vivo*, with the complex learning ability of these animals transiently impaired (O'Hare et al., 2013, Townsend et al., 2006).

In transgenic models, the loss of LTP establishment is also strongly linked with deposition of soluble Aβ (Palop and Mucke, 2010). For example, the 7-month-old Tg2576 mice with APP transgenes showed attenuated LTP in hippocampal CA1 (Townsend et al., 2010). Deficits in synaptic transmission observed in these middle-aged mice was not seen in younger or older animals, suggesting that the damaged effect of Aβ is mainly due to the soluble form but not the insoluble plaques (Townsend et al., 2010).

### 1.3.3. Hippocampal hyperexcitability in Alzheimer's disease

Hyperexcitability means the threshold or probability to activate a neuron by a stimulus is reduced (Targa Dias Anastacio et al., 2022). Enhanced hippocampal activation was observed in patients with mild cognitive impairment (MCI) when performing memory tasks using imaging methods like functional magnetic resonance imaging (fMRI) (Dickerson et al., 2005,

Hamalainen et al., 2007). Interestingly, this hyperactivity was not seen in normal ageing or AD patients, and AD patients in fact had hypoactivation in the hippocampus and entorhinal cortex, suggesting that the hippocampal hyperactivity could be a phenomenon related to the early stage of the disease (Dickerson et al., 2005, Hamalainen et al., 2007). Moreover, enhanced brain activity in neocortex and hippocampus was also frequently found in LOAD patients who carry the ApoE ε4 alleles at the pre-symptomatic stage (Bookheimer et al., 2000).

In animal models and cell models for AD, hippocampal synaptic hyperexcitability was also shown as increased burst firing or reduced threshold of neurons (McGarrity et al., 2017, Ghatak et al., 2019, Kazim et al., 2017). Young APP23xPS45 mice at about 2 months of age showed an increased number of hyperactive pyramidal neurons at hippocampal CA1 region (Busche et al., 2008). Also, enhanced synchronising network activity has been suggested in the development of AD, where patients co-expressing epileptiform activity exhibit higher rate of disease progression (Vossel et al., 2017, Das et al., 2021). Additionally, there is evidence that blocking hyperexcitability in a mouse model of AD (5xFAD model) could reduce Aβ deposition (Gail Canter et al., 2019). Thus, hippocampal hyperexcitability occurs at different levels in the early stage of AD and could have therapeutic benefit for halting the disease progression (Targa Dias Anastacio et al., 2022).

There are several potential causes for increased neuronal excitability, including synaptic disinhibition, dysregulated $Ca^{2+}$ homeostasis, the role of glial cells and neuroinflammation, higher activity of glutamatergic neurotransmission, as well as the direct effect of AD pathologies Aβ and tau (Targa Dias Anastacio et al., 2022). Aβ could induce release of glutamate and D-serine from astrocytes and microglia to overactivate the glutamatergic N-methyl-D-aspartate (NMDA) receptor (Talantova et al., 2013, Wu et al., 2004). Glutamate

reuptake, found to be diminished after administration of soluble Aβ, increased the neuronal activity in hippocampal CA1 region (Zott et al., 2019). Moreover, Aβ is directly linked with increased neuronal activity via enhancing $Ca^{2+}$ influx through L-type voltage-sensitive calcium channels (Ho et al., 2001).

Interestingly, a study suggested that the origin of the hyperexcitability could be related to relatively reduced synapse inhibition rather than overflow of intracellular $Ca^{2+}$ (Busche et al., 2008). The direct evidence came from a set of experiments using two-photon $Ca^{2+}$ imaging in the APP23xPS45 mice, where the frequency of neuronal activity increased near the proximity to the Aβ deposition (Busche et al., 2008). This spontaneous $Ca^{2+}$ activity could be completely and reversibly silenced by the sodium channel blocker, tetrodotoxin (TTX), suggesting the $Ca^{2+}$ response was fully generated by the firing of action potential rather than background $Ca^{2+}$ (Busche et al., 2008). Additionally, the activity of the hyperactivated neuron could be reduced by diazepam, the agonist of γ-aminobutyric acid type A ($GABA_A$) receptor, whereas their activity was increased with the $GABA_A$ receptor antagonist, gabazine (Busche et al., 2008).

### 1.3.4. Synaptic E/I balance and Alzheimer's disease

The balance of excitatory/inhibitory (E/I) input is essential for normal brain function and maintaining the homeostasis of synaptic plasticity (Bi et al., 2020). E/I balance is modulated by the fine tuning in weighing out excitatory and inhibitory neurotransmission in response to external stimuli (Bi et al., 2020). Significantly increased synaptic E/I ratio was shown in the post-mortem parietal cortex of AD patients (Lauterborn et al., 2021).

Importantly, epileptiform activity in the brain can also be manifested as a type of hyperactivity by shifting the E/I balance towards excitation (Targa Dias Anastacio et al., 2022). Many studies

have shown the increased prevalence of developing seizures and epilepsy in patients with mild dementia (Pandis and Scarmeas, 2012, Cuesta et al., 2022, Bi et al., 2020). In patients with the epileptiform activities, the gamma frequency power generated by GABAergic interneurons was significantly reduced, suggesting that the loss of interneuron inhibition might contribute to the hyperexcitability (Cuesta et al., 2022). Also, in experimental models for epilepsy, reduced hippocampal inhibition and selective loss of interneurons was reported (Sloviter, 1987). Therefore, there might be a possible loss of E/I balance and a potential disinhibition in the brain regions that are hyperexcitable.

In fact, seizure and AD share many pathologies, seizure worsens the cognitive decline of the patients (Vossel et al., 2017). Low dose of antiepileptic drugs such as levetiracetam were shown to be beneficial to AD patients with improved hippocampal-based memory tasks, and they were efficacious in reducing neuronal hyperexcitability in AD mice models (Vossel et al., 2017, Bakker et al., 2015). Also interestingly, in a study using brain tissue from patients with temporal lobe epilepsy but without cognitive deficits, Aβ plaques were found in the temporal lobectomy samples in about 10% of the patients (Vossel et al., 2017).

Thus, in the early stage of AD, a similar underlying mechanism could be involved as it is in seizures. Re-balancing the E/I input in patients with mild cognitive decline might be of pharmacological benefit to target.

## 1.4. Hypothesis and Aims

Hippocampal circuitry dysfunction has already been observed in AD patients at the presymptomatic stage of the disease. Since AD is still uncured and the underlying mechanism that drives the disease progression remains unclear, it is important to investigate this

question further. The TgF344 transgenic rat model for AD is a well-characterised model with age-dependent accumulation of Aβ, as well as tauopathy and neuroinflammation phenotypes without expression of genes for hyperphosphorylated tau. Therefore, TgF344-AD rats could be a useful model to study the mechanism associated with the prodromal stage of AD, such as synaptic functions, pathologies and changes in E/I balance.

In this project, the association between electrophysiological and pathological changes were investigated in adult TgF344-AD and age-matched wildtype rats at the ages when the amount of soluble Aβ oligomers but not plaques was found to be abundant. Specifically, using the 6- and 9-month-old male TgF344-AD rats and age-matched wildtype controls, changes in synaptic strength and short- and long-term plasticity were measured for CA3 evoked CA1 responses in the dorsal hippocampus using *in vivo* electrophysiology. Next, pilot analysis for synaptic plasticity was carried out in the DG from the same recording electrode for the CA3→DG circuit. Lastly, markers for synaptic function, GABAergic inhibition and glutamatergic transmission were studied using automated capillary-based immunoblotting method as well as immunostaining using the post-mortem brain tissues of 6- and 9-month-old rats.

From this set of studies, we aim to get a better understanding of the pathogenesis to synaptic dysfunction that might lead to cognitive impairment, at the pre-symptomatic stage of AD. It will also help provide more information about this preclinical model to examine its validity for future drug screening.

# Chapter 2. *In vivo* electrophysiology – evoked responses in CA1 in dorsal hippocampus

## 2.1. Introduction

The hippocampal formation is crucial for encoding and retrieving declarative memory. This includes episodic memory, which represents personal experiences or places and associated events (Buzsáki, 2005, Cohen, 1993, Eichenbaum, 2000). Whilst episodic memory is claimed to be unique to human (Tulving, 2002), many researchers have claimed to show episodic-like memory in bird and rodent species (Clayton and Dickinson, 1998, Eacott and Norman, 2004, Davis et al., 2013). The storage of information as memory has been suggested to require strengthening of synaptic weights between activated neurones both within and between different regions of the hippocampal formation (Eichenbaum, 2000, Chapman et al., 1999). This region was found to be one of those most affected in AD, as validated by imaging technologies like functional magnetic nuclear imaging (fMRI) in AD patients (Seab et al., 1988). Therefore, AD is identified as a synaptic disease because synaptic dysfunction is highly associated with memory loss in the patients (Chakroborty et al., 2012, Scheff et al., 2006). In animals such as rats and monkeys, the damage of regions in the hippocampal formation (including the dentate gyrus, the hippocampus proper and the subiculum) could lead to deficits in memory capacity without affecting sensory or motor functions (Squire, 1992, Eichenbaum, 2000, Martin, 2003). Common models of these storage mechanisms rely on short- and long-term synaptic plasticity (Eichenbaum, 2000).

Paired-pulse facilitation (PPF) is one of the important features to test short-term plasticity at the cellular level. PPF is a phenomenon where the neuronal response to the second stimulus of a paired electrical pulse sequence is relatively larger compared to that generated by the first stimulus, particularly if the time between the two stimuli is short, commonly less than 200ms (Commins et al., 1998b). This is because in response to the first stimulation, the concentration of $Ca^{2+}$ increases in pre-synaptic terminals, leading to neurotransmitter release;

when the second stimulus arrives, this builds further upon the raised $Ca^{2+}$ concentration from the first stimulus, thereby increasing synaptic release and the subsequent postsynaptic response compared to that generated by the first stimulus. This is the residual calcium hypothesis, where the rise in presynaptic $Ca^{2+}$ level to the second stimulus is augmented by the residual $Ca^{2+}$ from the first stimulus, facilitating a larger postsynaptic response to the second pulse (Zucker and Regehr, 2002). PPF is an important feature of short-term synaptic memory. The strength of facilitation depends on the time interval between two pulses relative to the presynaptic buffering dynamics in the presynaptic terminal (Zucker and Regehr, 2002).

Synaptic long-term potentiation (LTP), on the other hand, is a well-established and crucial model of long-term learning and memory consolidation in preclinical research (Bliss and Collingridge, 1993). It has been promoted as a putative neural mechanism of associative memory formation or storage in the mammalian brain (Ashok, 2011). In normally functioning synapses, a brief train of high-frequency stimuli (HFS) can rapidly evoke strengthening of excitatory synaptic transmission that can persist for hours to weeks (Ashok, 2011, Bliss and Collingridge, 1993, Grover and Teyler, 1990, Malenka and Bear, 2004, Pozueta et al., 2013). The counterpart of LTP is known as long-term depression (LTD), which also involves prolonged modifications of the synapse to reduce synaptic efficacy triggered by low-frequency stimulation (LFS) (Ashok, 2011, Malenka and Bear, 2004). This transmission at the excitatory synapse is accurately modulated by the number of working glutamatergic N-methyl-D-aspartate receptors (NMDARs) and α-amino-3-hydroxy-5-methyl-4-isoxazolepropionic acid receptors (AMPARs) located at the synapse (Palop and Mucke, 2010).

Depending on the induced change in intraneuronal $Ca^{2+}$ concentration in the post-synaptic neuron and activation of downstream cascades, either LTP or LTD can be induced (Palop and Mucke, 2010, Malenka and Bear, 2004). LTP requires less than 2-3s of large $Ca^{2+}$ influx, this can be achieved by activation of synaptic NMDARs and maintained by insertion of AMPARs (Malenka and Bear, 2004, Palop and Mucke, 2010), while LTD induction involves activation of perisynaptic glutamate receptors (NMDARs and mGluRs) and internalisation of synaptic NMDARs and AMPARs in response to a small increase in intracellular $Ca^{2+}$ level from the external and internal sources (Palop and Mucke, 2010, Berridge, 2011). There are many ways that the synapse can be modified to facilitate the induction of long-term or short-term synaptic changes, including but not limited to changes in pre-synaptic vesicle trafficking and docking, as well as the number and structure of dendritic spines (Matsuzaki et al., 2004). Induction of LTP leads to expansion of dendritic spine number and volume at the post-synaptic neuron where AMPARs could be inserted; whereas LTD induces shrinking of spines and AMPAR endocytosis (Palop and Mucke, 2010).

Hippocampal hyperexcitability and synaptic disinhibition are associated with cognitive decline in a number of neurological models (McGarrity et al., 2017). Hippocampal neural networks are vulnerable to molecular changes resulting from soluble Aβ that brings the excitatory / inhibitory balance more towards excitation (Palop et al., 2007, Sosulina et al., 2021, Palop and Mucke, 2016, Palop and Mucke, 2010). Experiments have shown decreased glutamate reuptake in the synaptic cleft in acute models of AD with soluble Aβ oligomers from various sources (Li et al., 2009). The augmentation of excitatory glutamate levels, and hence a pathologically increased excitability, could facilitate synaptic depression, causing depressed LTP and enhanced LTD in many AD models (Li et al., 2009, Palop and Mucke, 2010).

Recent studies have found hippocampal synaptic hyperexcitability in several preclinical models for AD research, and overactivity of the hippocampus has been increasingly suggested to be involved in the early stage of AD in patients (Palop et al., 2007, Palop and Mucke, 2010, Davis et al., 2014, Huh et al., 2016). Smith and McMahon (2018) provided the first *ex vivo* study in the TgF344-AD rat, showing that PPF and LTP were not affected in the hippocampal CA3 to CA1 circuit at 6 and 9 months of age (Smith and McMahon, 2018). The *in vivo* synaptic status of this model at this age remained unclear. This study aims to compare short- and long-term synaptic plasticity *in vivo* in the 6- and 9-month-old TgF344-AD rats versus age-matched controls using multi-electrode electrophysiological recordings. In particular, this chapter will focus on the evoked CA1 response to activation of the hippocampal Schaffer collateral pathway for synaptic input/output transmission, PPF, and LTP/LTD. The probability of having population spikes will be studied as an output excitability of CA1 pyramidal cells.

## 2.2. Methods and Materials

### 2.2.1. Animals

Animal procedures for *in vivo* electrophysiology and post-mortem tissue study were carried out under the Animals (Scientific Procedures) Act of 1986 (United Kingdom) and authorised by the UK Home Office and the Animal Welfare and Ethical Review Board (AWERB) of the University of Manchester under Home Office Project License P5F473F4F.

TgF344-AD rats and age-matched F344 wildtype controls were kept under standard housing conditions in the Biological Services Facility of the University of Manchester under a 12h light/dark cycle at a temperature of 20°C (±1°C) and humidity of 40-60% with food and water ad lib (GR1800 double decker cage for rats; 5 rats/cage). Experimental animals were bred in

Manchester by crossing transgenic with wildtype littermates at about 4 months old. The genotype of the breeder was randomised for each gender and breeding cages normally held one male and two female rats. The juvenile offsprings were ear-punched, and the tissues were analysed by TransnetYX® automated genotyping service (TransnetYX, Inc., Cordova, USA) for APPsw and PS1ΔE9 genes. If both genes were detected, the animal was deemed as transgenic (TG); otherwise, if neither gene was detected, the animal was determined as wildtype (WT).

### 2.2.2. *In vivo* electrophysiology

#### *2.2.2.1. Surgery and equipment.*

The rats were anaesthetised with 30%(w/v) urethane (ethyl carbamate, Sigma, UK) in saline (1.4g/kg) by intraperitoneal injection. A top up of 0.1-0.4ml 30%(w/v) urethane was applied if required to obtain surgical anaesthesia. Once achieved, the rat was placed in a stereotaxic apparatus (1430, Kopf, USA) with Bregma and Lambda in the same horizontal plane to match the rat brain atlas (Paxinos and Watson, 2007). Body temperature was kept at 36.4°C during surgery with a homoeothermic blanket (Harvard Apparatus, Edenbridge, UK), and the skull surface was exposed from the midline for craniotomies. The rat's head was immobilised in the stereotaxic frame and the left skull surface was completely exposed. Elliptical holes with major axis of ~1.5mm and minor axis of ~1mm were drilled above CA3 (B=-1.8mm, ML=-2.4mm; $30^{o}$ angle from vertical in the sagittal plane) for the stimulating electrode and above CA1 (B=-4.25mm, ML=-2.6mm; vertical insertion) for the recording electrode.

Two types of 32-channel recording electrodes were used, where these did not have recording differences except the configuration and length. One of the recording electrodes was made with 10mm long linear multi-electrode recording arrays containing 2 parallel shanks of 16

electrode contacts. The electrode contacts were linearly aligned and separated by 100µm centre-to-centre and the shanks were 500µm apart (G446; A2x16; NeuroNexus Technologies, Inc., Ann Arbor, MI, USA). Most of the data reported here was recorded using this electrode type. The other electrode type contained 4 shanks of 8 electrode contacts, with inter-electrode spacing of 50µm and inter-shank spacing of 200µm (A4x8; NeuroNexus Technologies, Inc., Ann Arbor, MI, USA). In all recordings the electrode array was inserted vertically to a depth of 2.6mm (with A2x16) or 2.3mm (with A4x8) from brain surface to span the CA1 region (**Figure 2.1**). The analyses in this study were made from electrodes located within either (a) the dendritic zone receiving the Schaffer collaterals in CA1 *stratum radiatum* or (b) CA1 *stratum pyramidale* in order to record population spikes. In many cases the tips of a 2x16 recording array would also extend into the dentate gyrus (DG). The DG responses were analysed and are presented in **Chapter 3**. The bipolar stimulating electrode (twisted 125µm diameter Teflon-insulated stainless-steel wires; Advent RM, UK) was inserted at an angle of 30$^{o}$ to a depth of 2.6~3.0mm to reach the molecular layer of CA3 and activate the Schaffer collateral pathway. The recording electrodes were coated with fluorescent dye (CM-DiI; Invitrogen, Paisley, UK) for visualizing electrode position *post hoc*. In practice, the location of the recording electrode was ascertained by comparing the field excitatory post-synaptic potential (fEPSP) of each channel using NeuroExplorer software (version 5, Plexon Inc., USA) and comparing this laminar profile to the established pattern (Leung and Péloquin, 2010, Gruart et al., 2015).

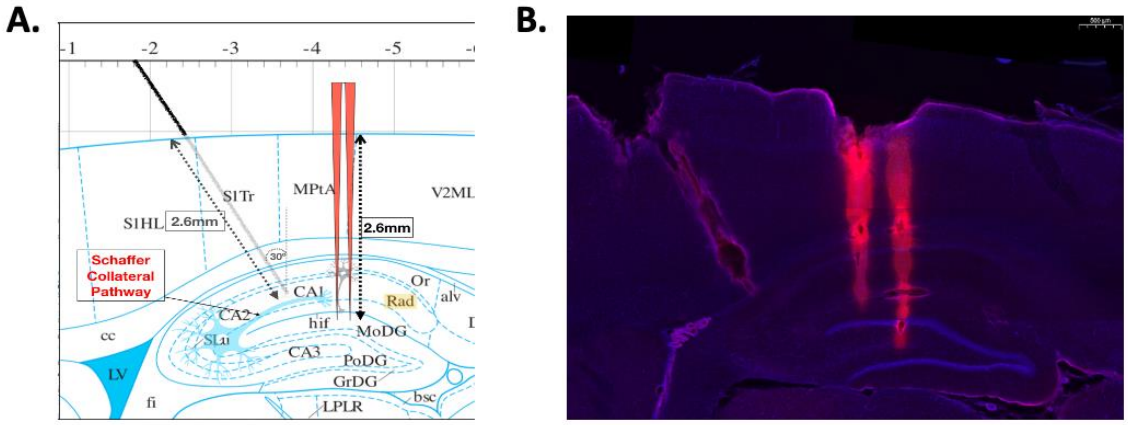


***Figure 2.1. Electrode position and responses for in vivo electrophysiology.***

***(A)*** *Target positions of electrodes as plotted onto the rat brain atlas.* ***(B)*** *A typical example of a reconstruction of electrode position from composite 50μm sagittal sections of the left dorsal hippocampus of a TgF344-AD rat. The pink florescence trace indicates the position of the 2x16 recording electrode. Five consecutive images were used for the 3D reconstruction. The stimulating electrode track can be seen on the left. Images were acquired on a 3D-Histech Pannoramic-250 microscope slide-scanner using a 20x/ 0.80 Plan Apochromat objective (Zeiss) and the DAPI and TRITC filter sets. Snapshots of the slide-scans were taken using the Case Viewer software (3D-Histech) at 2x.*

#### *2.2.2.2. Stimulation Protocols.*

Constant current stimuli (DS3, Digitimer, UK) were triggered by 1ms 5V square wave pulses from a National Instruments card (PCI-6071E, NI, UK) controlled by custom-written scripts (LabView8.2, National Instruments, UK). The duration of each stimulus was fixed at 0.2ms throughout the experiment. The triggering event and neuronal responses to each stimulating or electric condition were recorded using Recorder64 software (10kHz sampling frequency 12-bit A/D, 1kHz low-pass filtering 1-pole Butterworth, x500 Amplification). The evoked responses were recorded as triggered sweeps where each sweep started 50ms before the stimulus and ended 250ms after the stimulus (or stimuli) finished.

After insertion of the recording electrode to target location the stimulating electrode final location was determined by lowering it slowly during stimulation to observe the characteristic CA3-evoked CA1 EPSPs resulting from Schaffer collateral pathway activation. This was done by stimulating with paired pulses (inter-pulse interval (IPI) = 50ms) at 60-200μA every 3s. If a characteristic PPF profile was obtained, the stimulating electrode was then left in place and an input/output (I/O) curve was plotted by measuring the amplitude of the first pulse (P1) when delivering paired pulses over a range of currents (25μA, 50μA, 100μA, 200μA, 300μA, random order) (**Figure 2.2, Step 1**). The current that gave rise to 50% output was determined, which was maintained for the rest of the experiment except for 75% high frequency stimuli (HFS) to induce LTP (HFS: 5 bursts of 20 pulses of 200Hz stimulation, inter-burst interval = 3s). A protocol of baseline PPF contained 20 paired pulses delivered at 6 different IPIs (25ms, 50ms, 100ms, 200ms, 500ms, 1000ms, random order) where the interval between pairs was 3s (**Figure 2.2, Step 2**). The same PPF protocol was also applied directly after HFS (**Figure 2.2, Step 4**). Sequences of paired pulses (IPI = 50ms) were used to measure responses before (**Figure 2.2, Step 3**) and after induction of long-term potentiation (LTP) (**Figure 2.2, Step 5**). Each paired pulse was delivered every 30s for 15min to generate a baseline prior to HFS. After HFS induction the presence of HFS-induced LTP was then examined by again delivering 50ms IPI paired-pulses every 30s for a further 30min (at 50% of I/O curve), about 10min after post-HFS PPF recordings (**Figure 2.2, Step 6**). The effect of low-frequency stimulation (LFS; 900 pulses at 1Hz) on synaptic plasticity was studied after the post-HFS I/O, only in the 6-month-old animals. The post-LFS PPF (**Figure 2.2, Step 7**), long-term depotentiation (**Figure 2.2, Step 8**), and post-LFS I/O (**Figure 2.2, Step 9**) were recorded and analysed.

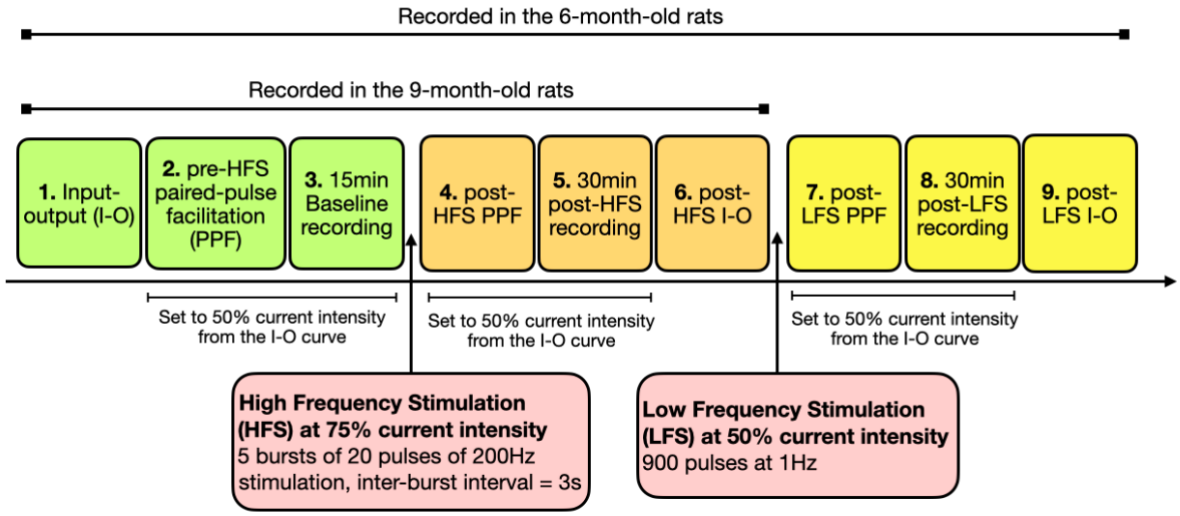


***Figure 2.2. An illustration of electrical recording protocol.***

*In the 6-month-old animals, the evoked response recordings were composed of 9 sets of recordings of ipsilateral CA3-evoked CA1 responses in the Schaffer Collateral pathway (Step 1-9). In the 9-month-old animals, the recordings were from Step 1-6.*

#### *2.2.2.3. Data processing*

Data were extracted and measured using a self-written MATLAB script (version 2019b, the Mathworks, USA). The evoked fEPSP slope was measured as the maximum gradient of the initial descending component of the response and the amplitude was measured as the potential difference between the response trough and the immediate pre-stimulus baseline value. In this chapter, fEPSPs were analysed from CA1 proximal *stratum radiatum* for I/O, PPF and LTP protocols, whereas the identification of population spike was done in the recordings near CA1 *stratum pyramidale* layer.

For LTP, the maximum slope and amplitude of P1 was measured and normalised to the corresponding averaged baseline magnitude for each rat. For PPF, the maximum slope and magnitude of both P1 and P2 were measured to calculate the paired-pulse index (PPI), which

is the percentage ratio of the second response (P2) versus the first response (P1) of a pair of recording:

$$\text{PPI \%} = \frac{P2-P1}{P1} \text{ X } 100\%$$

The size of a response was represented as the maximum slope and amplitude.

### 2.2.3. Statistical Analysis

For all data, GraphPad Prism 8.1 (GraphPad Software, Inc.) was used for statistical analysis and figure generation. Normality was checked with Shapiro-Wilk tests and equal variance with Levene test. Two-way ANOVA or mixed-effect model of two-way ANOVA was used for comparing multiple factors (e.g., pre- and post-HFS vs. genotype, etc.). Violation of sphericity in datasets was corrected with Geisser-Greenhouse method when the data were measured repeatedly from the same subject. If there was a significant ANOVA result then *post hoc* multiple comparisons were performed, for example, in LTP analyses Bonferroni correction multiple comparisons were carried out because it is commonly used for this type of experiment. Specifically, for generating I/O curves, individual Gompertz functions were fit to data using OriginPro 2019b (OriginLab Corporation, USA) in order to minimize the chances of type I or II errors with the usual ANOVA/t-test approach to this data type. To statistically analyse PPF, because there were three factors (genotype, stimulation and IPIs), 3-way ANOVA with a recommended Tukey's *post hoc* comparison test was performed to observe any significant changes in the PPI magnitude. A mixed-effect model of 3-way ANOVA was used if there were missing values in the data for analysis.

## 2.3. Results

Field excitatory post-synaptic potentials (fEPSPs) were recorded and measured at CA1 *stratum radiatum* as a response of triggering upstream CA3 neurons with paired pulses (**Figure 2.3**). Population spikes were identified from the recording channels near CA1 *stratum pyramidale* layer above the sink dipole (**Figure 2.3.C**).

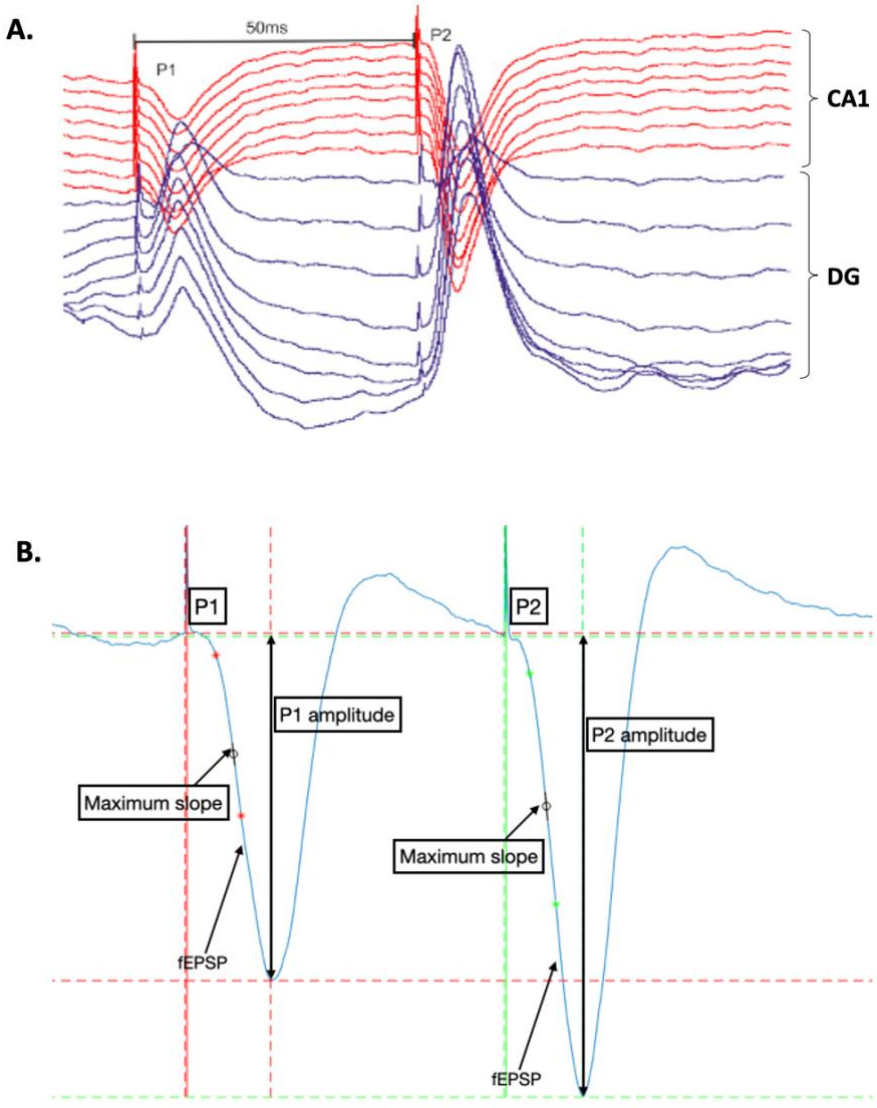

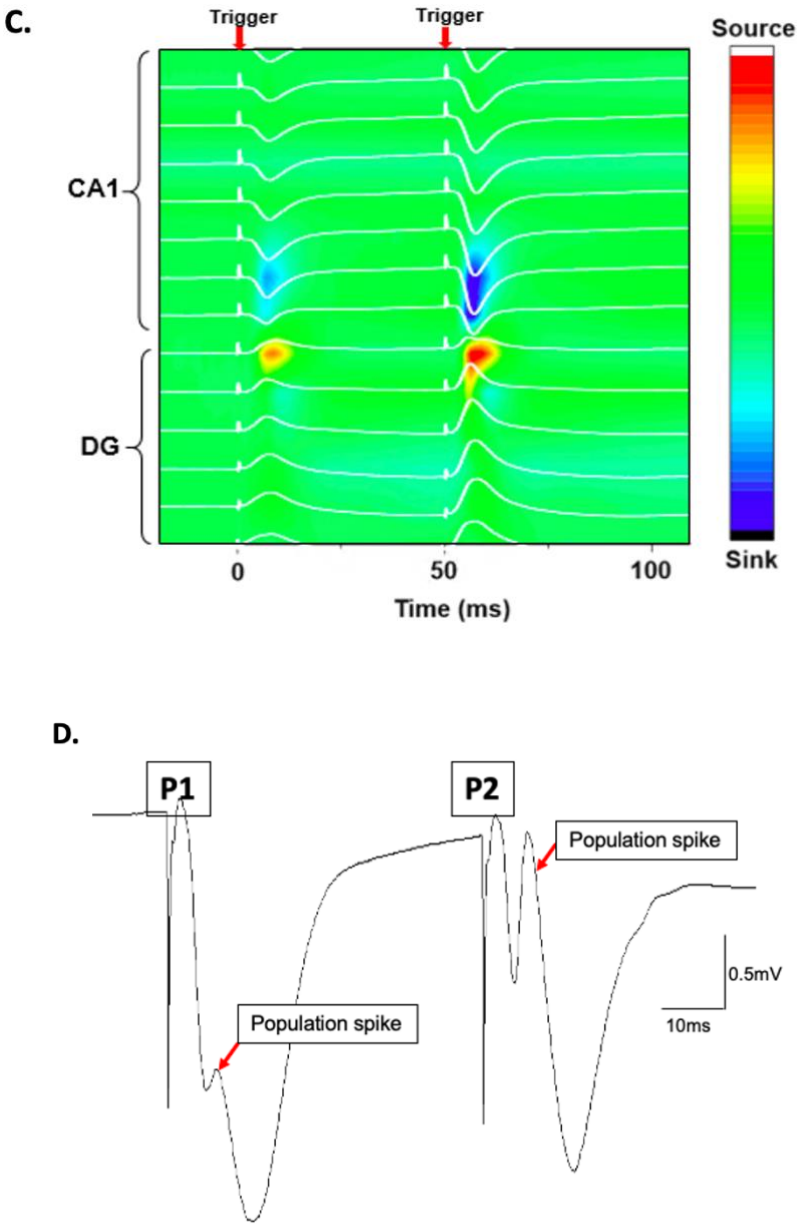


***Figure 2.3. Illustrations of the evoked paired responses in CA1 and DG.***

***(A)*** *Typical paired fEPSPs from the anterior shank of a A2x16 electrode in a randomly selected WT rat pre-HFS. The negative-going responses (red) were recorded from CA1, and the positive-going responses (purple) were from dentate gyrus (DG). All experimental subjects were confirmed to show a similar profile before continuing with the experiment.* ***(B)*** *A typical CA1 paired-pulse response in CA1 from a randomly selected animal. The maximum slope and amplitude were measured for analysis.* ***(C)*** *Example of a WT rat to show current source density analysis of evoked voltages to confirm the current source and sink of Schaffer input to CA1.* ***(D)*** *An illustrative example of population spikes (PS). PS can be seen here as population action potentials embedded in the CA1 EPSP for pulse 1 (P1) and pulse 2 (P2) after CA3-evoked stimulation at 300uA. Inter-pulse interval in all figures is 50ms. Current in* ***A-C*** *was set at 50% of I/O curve for each animal.*

### 2.3.1. Changes of evoked responses in the 6-month-old rats

#### *2.3.1.1. Input/output curves for the 6-month-old WT and TG rats*

An I/O curve was plotted using a Gompertz-fit at the start of the experiment over a range of stimulating currents (input) to determine the current that gave rise to 50% fEPSP (output) potential for each animal, where this 50% values was subsequently used for PPF and LTP/LTD experiments. A similar I/O curve was produced 50min after HFS to measure the maintenance of any HFS-induced response changes. To access baseline connectivity, the shape of I/O curve, the maximum output and the current for generating 50% output were compared between WT and TG groups at the baseline and post-HFS points.

At baseline, there was no difference in terms of the shape of the I/O curve between WT and TG at 6 months of age measured with slope or amplitude (**Figure 2.4, black lines**). Statistical analysis showed significant effect of current but no genotype difference at the baseline when responses were measured either by slope (current: $F(4, 76) = 128.5$, $P<0.0001$; genotype: $F(1, 19) = 0.2003$, $P=0.6595$; current x genotype: $F(4, 76) = 1.200$, $P=0.3176$) or amplitude (current: $F(4, 74) = 133.6$, $P<0.0001$; genotype: $F(1, 19) = 0.1745$, $P=0.6808$; current x genotype: $F(4, 74) = 1.329$, $P=0.2673$) (**Figure 2.4, black lines**) .

The post-HFS I/O was measured after PPF and HFS protocol – about 50mins after HFS delivery. To compare the changes between WT and TG under different current at post-HFS, mixed-effect ANOVA was carried out using the slope measurement. The result showed significant effects of current ($F(4, 75) = 114.1$, $P<0.0001$), genotype ($F(1, 19) = 5.918$, $P=0.0250$) and interaction between these two factors ($F(4, 75) = 7.216$, $P<0.0001$) after HFS delivery (**Figure 2.4.A&B, pink lines**). The *post hoc* Šídák's multiple comparisons test showed that TG had

significantly smaller slope output compared to WT at 200uA (P=0.0035) and 300uA (P=0.0009) (**Figure 2.4, B vs. A**).

To investigate the effect of HFS stimuli on the input/output function for the slope measurements, two-way ANOVA was performed within WT and TG groups respectively. In the WT group, there was a significant effect of HFS ($F(1, 9) = 21.26$, $P=0.0013$), as well as current ($F(4, 36) = 58.25$, $P<0.0001$) with an interaction ($F(4, 35) = 26.77$, $P<0.0001$). *Post hoc* comparison test of Šídák's showed increased post-HFS slope output at 100uA (P=0.0003), 200uA (P<0.0001) and 300uA (P<0.0001) for the WT animals (**Figure 2.4.A**). In contrast, the TG animals did not show significant effect of HFS ($F(1, 10) = 0.6648$, $P=0.4339$) or interaction ($F(4, 40) = 1.281$, $P=0.2934$) on slope output, although current showed marked effect as expected ($F(4, 40) = 93.78$, $P<0.0001$) (**Figure 2.4.B**).

The amplitude measurement was also analysed to compare the changes between WT and TG under different current at post-HFS. The mixed-effect ANOVA showed significant effects of current ($F(4, 74) = 84.74$, $P<0.0001$), genotype ($F(1, 19) = 4.864$, $P=0.0399$) and interaction ($F(4, 74) = 2.741$, $P=0.0348$) after HFS delivery (**Figure 2.4.C&D, pink lines**). Šídák's multiple comparisons showed that TG had significantly smaller voltage output compared to the WT at 200uA (P=0.0293) and 300uA (P=0.0225).

The amplitude output was also compared within each group. For the WT animals, mixed-effect ANOVA showed that there were significant effects of current ($F(4, 36) = 44.10$, $P<0.0001$), HFS ($F(1, 9) = 20.71$, $P=0.0014$) and an interaction between these two factors ($F(4, 32) = 5.156$, $P=0.0025$). Šídák's multiple comparisons showed that WT rats had remarkably higher amplitude output at 50uA (P=0.0070), 100uA (P<0.0001), 200uA (P=0.0001) and 300uA (P=0.0094) compared to baseline (**Figure 2.4.C**). However, for the TG animals, the only

significant effect came from the stimulation intensity (F (4, 40) = 91.47, P<0.0001). There was no effect of HFS (F (1, 10) = 0.0001, P=0.9922) and no interaction (F (4, 40) = 1.064, P=0.3872) (**Figure 2.4.D**). In general, after HFS, the I/O curve of WT animals shifted up (**Figure 2.4.A, 2.4.C**); however, although there was a trend for a small post-HFS increase in TG rats, I/O curves remained similar to baseline in 6-month-old TG rats for both slope and amplitude (**Figure 2.4.B, 2.4.D**).

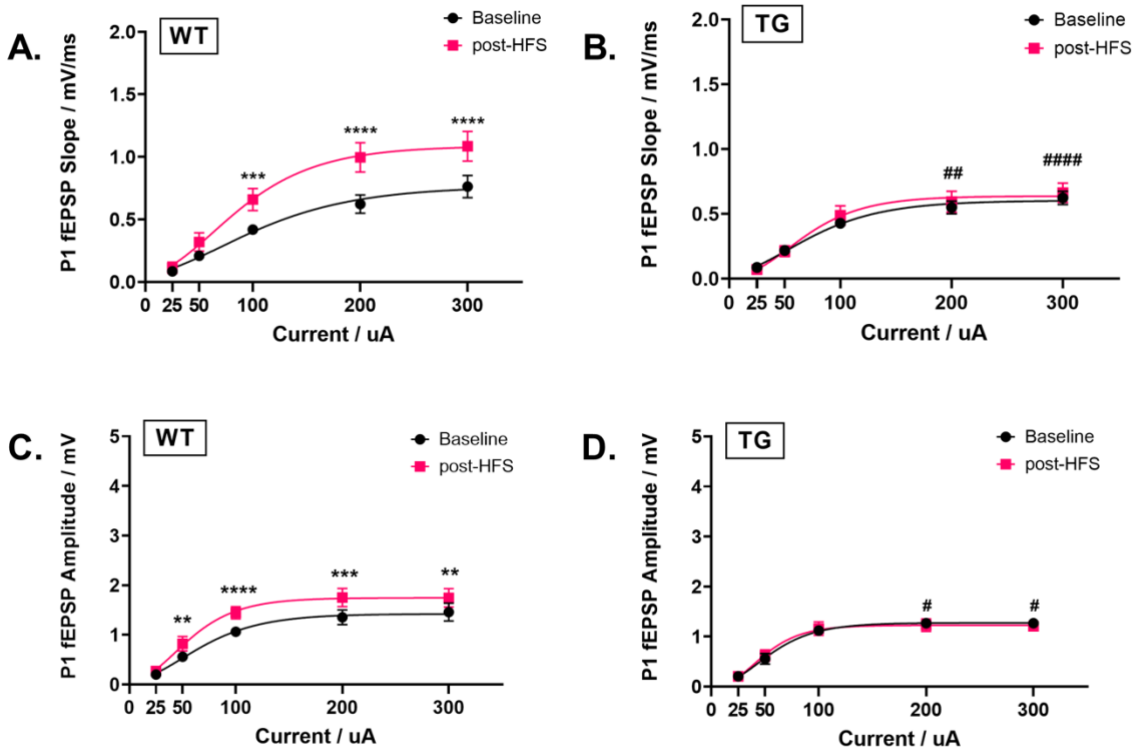


***Figure 2.4. Hippocampal CA3-CA1 input/output (I/O) curves for 6-month-old WT and TG rats at baseline and post-HFS.***

*The pre- and post-HFS I/O curves of 6-month-old WT rats are presented as **(A)** slope and **(C)** amplitude measurements of the P1 fEPSPs, those for TG rats are presented in **(B)** and **(D)**, respectively. The I/O curves of TG rats were not different from that of the WT controls at the baseline. However, after HFS, only the I/O curves of WT rats shifted upwardly. two-way ANOVA was employed with Sidak's multiple comparison. *: compared within the group; #: compared TG versus WT groups at post-HFS. WT: n=10, TG: n=11. Data are presented as mean±SEM. **P<0.01, ***P<0.001, ****P<0.0001; #P<0.05, ##P<0.01, ####P<0.0001.*

The above comparisons on the Gompertz-fit curve itself may result in spurious statistical output due to the high number of comparisons. Therefore, the maximum and 50% output currents were determined using the Gompertz-fit curve for individual animals using the measurement of slope or amplitude (**Figure 2.5**). Two-way ANOVA with Šídák's multiple comparisons was used to determine any statistical differences for the maximum output.

To compare the maximum response output using slope measurement, two-way ANOVA showed significant effects of HFS ($F(1, 19) = 23.68$, $P=0.0001$) and genotype ($F(1, 19) = 6.287$, $P=0.0214$), as well as a significant interaction between these two factors ($F(1, 19) = 15.20$, $P=0.0010$). Within genotype groups, the Šídák's *post hoc* test showed that the maximum output of WT animals was significantly increased after HFS ($P <0.0001$), but the maximum post-HFS output of the TG animals was not different from baseline ($P=0.7418$) (**Figure 2.5.A**). Between the genotypes, there was no difference for maximum slope output between WT and TG groups at the baseline ($P=0.4577$), but the maximum slope output of TG animals was significantly smaller than the WT rats during the post-HFS period ($P=0.0017$) (**Figure 2.5.A**).

To compare the maximum response output using amplitude measurement, two-way ANOVA showed that there was a significant effect of HFS ($F(1, 19) = 4.492$, $P=0.0475$) and significant interaction between stimulation and genotype ($F(1, 19) = 8.300$, $P=0.0096$). However, the effect of genotype was not statistically significant ($F(1, 19) = 2.689$, $P=0.1175$). Within each genotype group, WT animals showed significantly increased maximum amplitude after HFS delivery ($P=0.0053$), but the maximum amplitude remained similar for TG animals before and after HFS ($P=0.8298$; *post-hoc* Šídák) (**Figure 2.5.B**). Between genotypes, there was no difference in maximum amplitude produced by WT or TG animals at baseline ($P= 0.7058$), but

TG animals showed markedly smaller maximum output compared to the WT rat after HFS (P= 0.0430) (**Figure 2.5.B**).

To further access the changes in baseline connectivity, the current for generating 50% output was determined and compared between WT and TG groups before and after HFS (**Figure 2.5.C-E**). As a result of two-way ANOVA, there was no statistical effect of HFS, genotype or interaction for the 50% output current as calculated using slope (HFS: F (1, 19) = 1.260, P=0.2756; genotype: F (1, 19) = 2.966, P=0.1013; HFS x genotype: F (1, 19) = 0.3469, P=0.5628) (**Figure 2.5.C**). No statistical effect was found for amplitude measurements as a result of mixed-effect ANOVA (stimulation: F (1, 18) = 3.126, P=0.0940; genotype: F (1, 19) = 0.6585, P=0.4271; stimulation x genotype: F (1, 18) = 0.3631, P=0.5543) (**Figure 2.5.D**).

The 50% output current of each animal was also determined with an oscilloscope during the experiment to compare changes in two groups before and after HFS. However, from the experimentally recorded data, two-way ANOVA showed significant effect of HFS (F (1, 19) = 8.340, P=0.0094), but no effect of genotype (F (1, 19) = 0.2666, P=0.6116) or interaction between these factors (F (1, 19) = 1.454, P=0.2427). A *post hoc* test of Šídák's multiple comparisons found the stimulation effect came from the WT group whose voltage output was significantly higher after HFS than at the baseline (P=0.0214) (**Figure 2.5.E**).

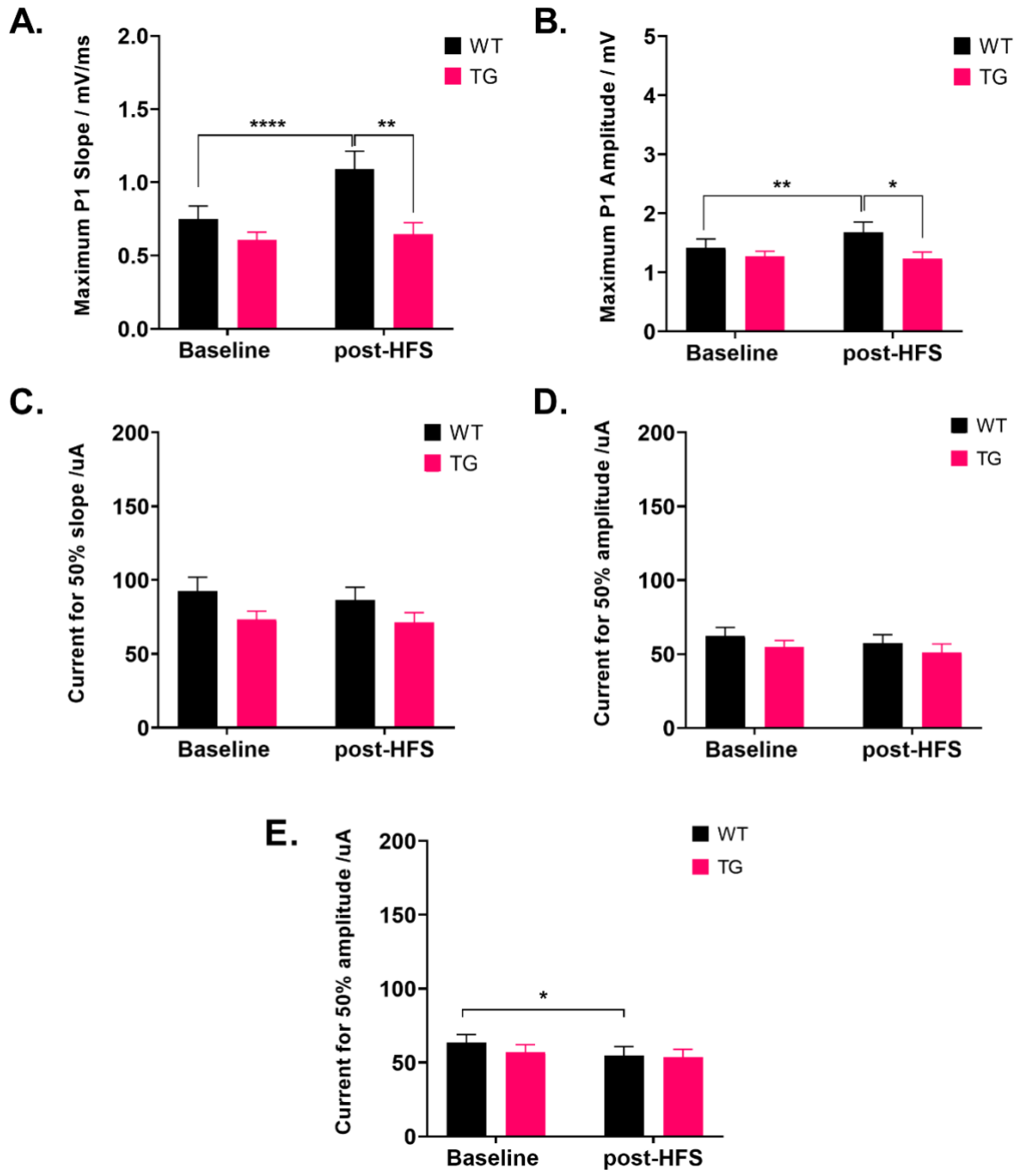


***Figure 2.5. Comparison of hippocampal CA3-CA1 input/output function of the 6-month-old WT and TG rats pre- and post-HFS.***

*The maximum output was presented for WT and TG groups at 6 months of age as a measure of **(A)** slope and **(B)** amplitude of P1 fEPSP. The current required for 50% output was calculated using Gompertz fit for each animal with the measure of **(C)** slope, **(D)** amplitude, and **(E)** from the experimental measures on the oscilloscope. WT: n=10, TG: n=11, Data were presented as mean±SEM. *P<0.05, **P<0.01, ****P<0.0001.*

In conclusion, the I/O of 6-month-old TG rats was not different from WT at baseline. However, the HFS-induced increased response in TG rats (see next section) was not maintained to the same extent when compared to WT. Thus, the TG I/O returned to near baseline levels at the point where the second I/O was measured. WT rats showed LTP maintenance following HFS stimulation when the I/O was measured 50min after HFS, consistent with their upward shift in I/O curve compared to pre-HFS levels.

#### *2.3.1.2. Paired pulse facilitation in the 6-month-old WT and TG rats*

To assess changes in short-term plasticity at the age of 6 months in hippocampal CA1 region between baseline and immediate post-HFS periods, 20 paired pulses were delivered at range of inter-pulse intervals (IPIs), and facilitation was calculated by the formula shown in **Section 2.2.2.3**. as the paired-pulse index (PPI), a measure of the maximum initial slope and amplitude. A three-way ANOVA was applied to statistically compare the factors of genotype, HFS and IPIs in 6-month-old WT and TG rats' hippocampal CA1.

As a measure of slope, there was a significant effect of HFS ($F(1, 19) = 91.99$, $P<0.0001$) and IPI ($F(5, 95) = 520.7$, $P<0.0001$), but no statistical effect of genotype ($F(1, 19) = 0.2040$, $P=0.6567$). The interaction between IPI and stimulation was significant ($F(5, 95) = 39.61$, $P<0.0001$), but no significance was found for IPI x genotype ($F(5, 95) = 1.151$, $P=0.3392$) or stimulation x genotype ($F(1, 19) = 3.474$, $P=0.0779$). There was no significant interaction between the three factors ($F(5, 95) = 2.438$, $P=0.0400$).

For slope measurements, the *post hoc* test of Tukey's multiple comparison showed that significant differences appeared at shorter IPIs, namely 25ms, 50ms and 100ms. At IPI of 25ms, the PPI was significantly smaller, indicating a reduction of facilitation at CA1, after delivery of

HFS for both WT (P<0.0001) and TG (P<0.0001) at 6 months of age (**Figure 2.6.B**). The reduction of PPI after HFS was also seen at 50ms and 100ms IPIs for both WT (50ms: P<0.0001; 100ms: P<0.0001) and TG (50ms: P<0.0001; 100ms: P=0.0040) (**Figure 2.6.B**). However, no PPI difference was found between WT and TG baseline or after HFS at any IPI. There was no statistical difference between genotype or stimulation at longer IPIs of 200ms, 500ms or 1000ms.

When PPI was calculated by amplitude, a similar statistical difference to that seen for slope was found at 6 months old in CA1. The three-way ANOVA showed significant effects of IPIs ($F(5, 95) = 155.7$, $P<0.0001$) and HFS ($F(1, 19) = 143.2$, $P<0.0001$), but no statistical effect of genotype ($F(1, 19) = 0.5903$, $P=0.4518$). The interaction between IPI and HFS was significant ($F(5, 95) = 96.94$, $P<0.0001$) but no effect was seen for IPI x genotype ($F(5, 95) = 2.018$, $P=0.0829$) or HFS x genotype ($F(1, 19) = 1.148$, $P=0.2973$). There was no interaction between these three factors ($F(5, 95) = 0.7517$, $P=0.5869$) for amplitude at 6 months.

The Tukey's *post hoc* multiple comparison revealed amplitude differences that were again similar to those seen for slope measures. Statistical differences were shown at shorter IPIs where at IPIs of 25ms, 50ms and 100ms there was a remarkable PPI reduction and, hence, a reduction of facilitation at CA1, as the effect of HFS was found in both WT (25ms: P<0.0001; 50ms: P<0.0001; 100ms: P<0.0001) and TG (25ms: P<0.0001; 50ms: P<0.0001; 100ms: P<0.0001) animals at the age of 6 months (**Figure 2.6.C**). No significant differences were found between genotypes at the baseline or post-HFS at 25ms, 50ms or 100ms IPIs. There was also no difference at longer IPIs of 200ms, 500ms or 1000ms for genotype or stimulations.

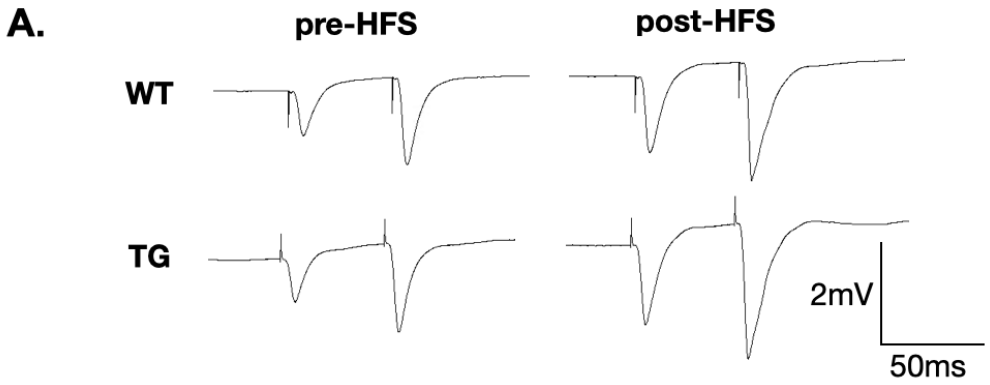
A.
pre-HFS
post-HFS
WT
TG
2mV
50ms

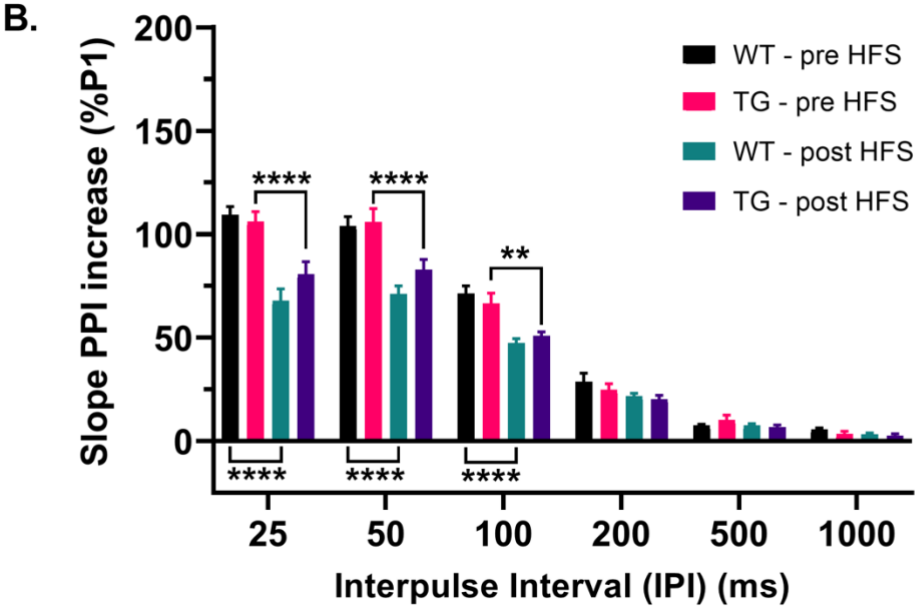
B.
Slope PPI increase (%P1)
200
150
100
50
0
****
****
**
****
****
****
25
50
100
200
500
1000
Interpulse Interval (IPI) (ms)
WT - pre HFS
TG - pre HFS
WT - post HFS
TG - post HFS

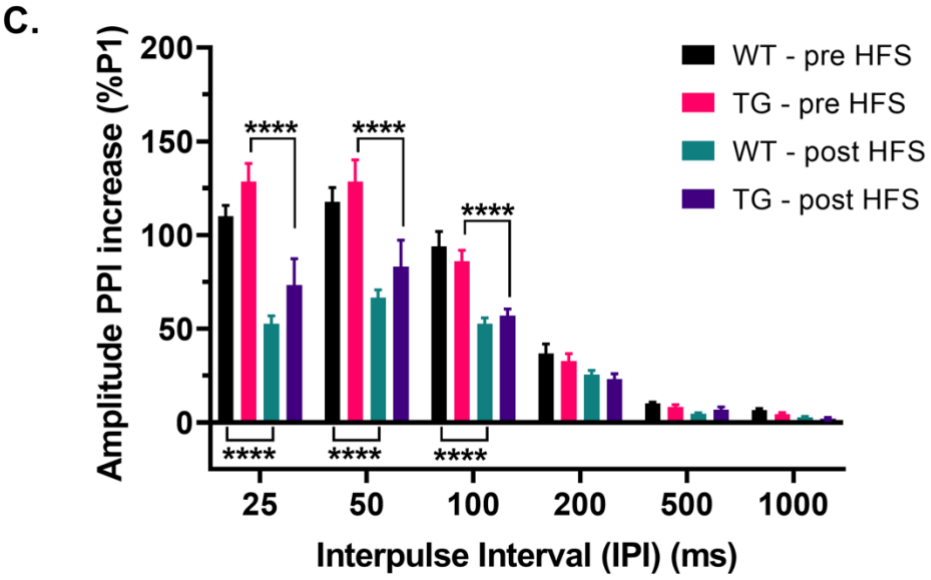
C.
Amplitude PPI increase (%P1)
200
150
100
50
0
****
****
****
****
****
****
25
50
100
200
500
1000
Interpulse Interval (IPI) (ms)
WT - pre HFS
TG - pre HFS
WT - post HFS
TG - post HFS

***Figure 2.6. No genotype difference in paired-pulse facilitation in 6-month-old TgF344-AD model.***

*Paired pulses were delivered at a current that gives 50% output. fEPSPs were recorded at CA1 of hippocampus by the stimulation of Schaffer collateral pathway.* ***(A)*** *Examples of fEPSP traces before and after HFS of a randomly selected rat from each group in CA1.* ***(B)*** *Slope and* ***(C)*** *amplitude of the fEPSPs were measured. Three-way ANOVA of mixed-effect model was carried out, followed by Tukey's multiple comparisons test. WT: n=10, TG: n=11. Data were presented as mean ± SEM. **P<0.01, ****P<0.0001.*

In general, the short-term plasticity as a representation of PPF remained intact at CA3→CA1 synapse for the TG model animals at 6 months of age before and after HFS with no statistical differences compared to the WT controls.

#### *2.3.1.3. Long-term potentiation and depotentiation in the 6-month-old WT and TG rats*

To assess long-term plasticity at CA3-CA1 synapse of the 6-month-old WT and TG rats, a classic protocol for long-term potentiation (LTP) was applied by delivering high-frequency stimulations (HFS, 5 bursts of 20 pulses at 200Hz, inter-burst interval = 3s) after a stable recording of baseline was reached. Long-term depression (LTD; depotentiation) was achieved by applying low-frequency stimulation (LFS, 900 pulses at 1Hz) after the 30-minute recording period to measure post-HFS LTP. The analysis was taken using the measurements of slope and amplitude of the P1 response. To compare the effects of stimulation and genotype on the size of evoked fEPSP responses, two-way ANOVA with Bonferroni's *post hoc* test was applied.

With slope measurements, two-way ANOVA showed significant effects of genotype ($F(1, 19) = 7.556$, $P=0.0128$) and stimulations (HFS or LFS) ($F(2, 38) = 22.87$, $P<0.0001$) at the age of 6 months in CA1. There was also a significant interaction between genotype and stimulations (HFS or LFS) ($F(2, 38) = 4.677$, $P=0.0153$). Similar significant effects were also found if

calculated by amplitude as shown by two-way ANOVA (genotype: F (1, 19) = 5.435, P=0.0309; stimulations: F (2, 38) = 39.51, P<0.0001; stimulating conditions x genotype: F (2, 38) = 4.057, P=0.0253).

Bonferroni's multiple comparisons showed that both WT (slope: P<0.0001; amplitude: P<0.0001) and TG (slope: P=0.0091; amplitude: P<0.0001) rats could successfully establish HFS-induced LTP at age of 6 months at CA3-CA1 synapse (**Figure 2.7**). The 30-minute post-HFS response size of the TG was significantly smaller compared to the WT as a measure by the slope (P= 0.0373), although amplitude measurements were generally smaller in TG compared to WT, these were not statistically different (P=0.1065).

For LFS-induced depotentiation, Bonferroni's multiple comparisons showed a significant reduction of magnitude of the post-LFS responses compared to the post-HFS in both WT (slope: P=0.0290; amplitude: P=0.0012) and TG (slope: P=0.0010; amplitude: P=<0.0001). Moreover, in the 6-month-old WT rats, the post-LFS magnitude was significantly greater than that at the baseline (slope: P=0.0059; amplitude: P=0.0062), but the post-LFS response size did not differ from the baseline in the TG rats (slope & amplitude: P>0.9999).

To further analyse the strength of depotentiation as the effects of genotype and LFS, a statistical comparison of the response size during the last 5-minute of post-HFS recording and the first 5-min of post-LFS recording was made using two-way ANOVA (**figure 2.7.E&F**). As a result, both genotype (slope: F (1, 19) = 7.170, P=0.0149; magnitude: F (1, 19) = 5.222, P=0.0340) and LFS (slope: F (1, 19) = 12.77; P=0.0020; magnitude: F (1, 19) = 39.14, P<0.0001) contributed to the significant differences seen in the post-LFS magnitude, whereas there was no interaction between genotype and LFS (slope: F (1, 19) = 0.8775, P=0.3607; amplitude: F (1, 19) = 2.026, P=0.1708) if comparing the response size during these 5-minute segments.

Bonferroni's multiple comparison revealed that the response magnitude of the TG rats was not significantly different from that of the WT rats in the last 5-minute post-HFS recording (slope: P=0.0846, amplitude: P=0.1745), but the response of TG rats was markedly reduced compared to the WT controls in the first 5-minute of the post-LFS recording (slope: P=0.0148; amplitude: P=0.0260). Within the 6-month-old WT controls, the response magnitude during the first 5-minute post-LFS recording was not significantly different from that of the last 5-minute post-HFS recording as a measure of slope (P=0.1686), although it was statistically smaller as a measure of amplitude (P= 0.0069). However, within the 6-month-old TG animals, the response size during the first 5-minute post-LFS recording was remarkably smaller than that during the last 5-minute post-HFS recording as calculated from both slope (P= 0.0081) and amplitude (P<0.0001), with greater effect size.

To assess whether the depotentiation by LFS was strong enough to drop below the baseline, paired t-test was then performed on the averaged 30-minute post-LFS response size to the 15-minute baseline for the WT and TG groups respectively. As a result, the post-LFS size was not different from that of the baseline in either of the groups as calculated by slope (WT: P=0.0667; TG: P=0.2901) or amplitude (WT: P=0.0520; TG: P= 0.5309).

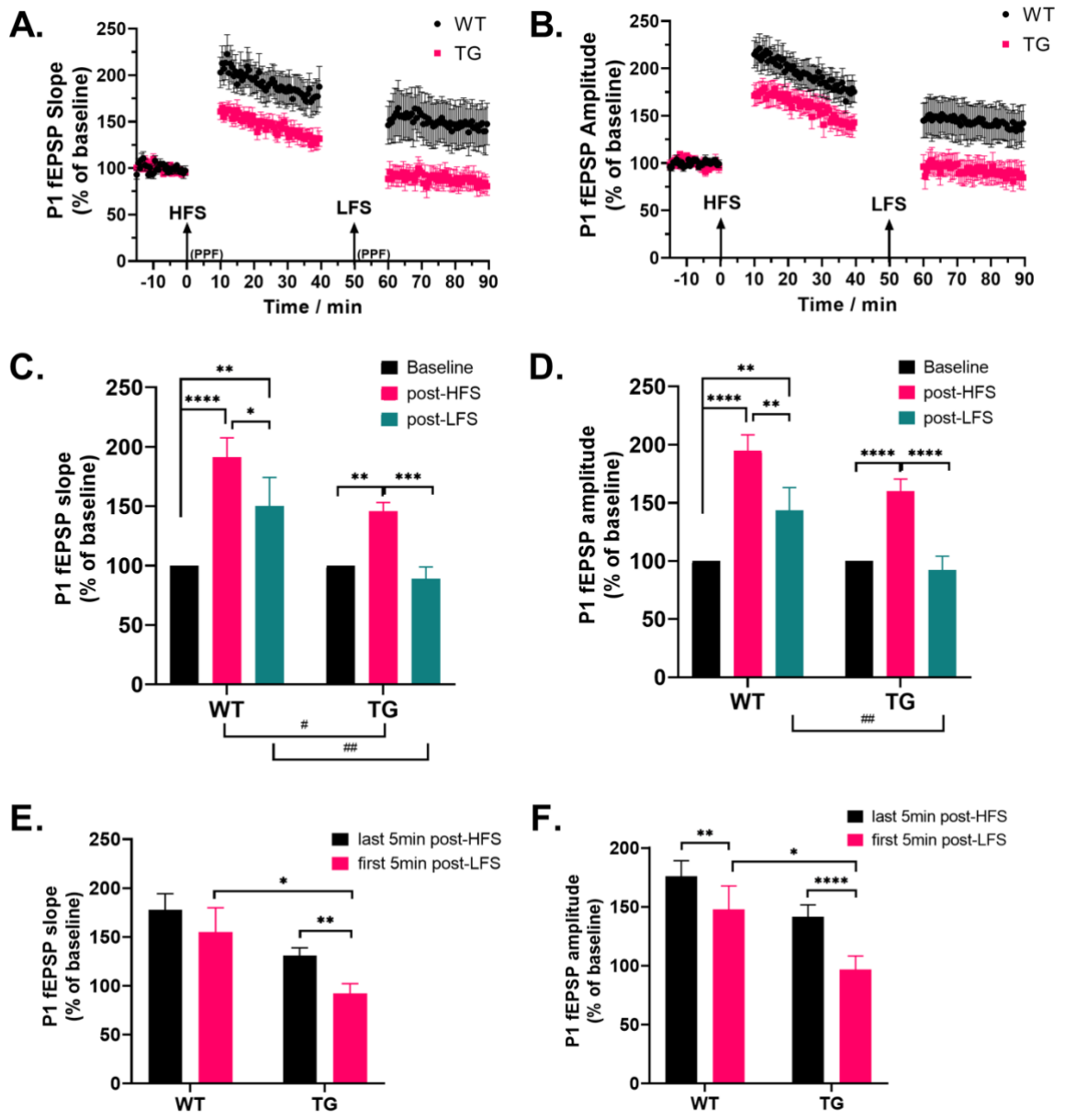


***Figure 2.7. High-frequency stimulation (HFS) induced long-term potentiation (LTP) followed by low-frequency stimulation (LFS) induced depotentiation in CA1 of 6-month-old male TgF344-AD rats.***

*Scatter plots of CA1 evoked-excitatory post-synaptic potential (fEPSP) for **(A)** slope and **(B)** amplitude during experimental time course. Comparisons were made for the averaged fEPSP at the baseline, post-HFS and post-LFS for **(C)** slope and **(D)** amplitude. The response size during the last 5min post-HFS recording and first 5min post-LFS recording were plotted for **(E)** slope and **(F)** amplitude measurements. WT: n=10, TG: n=11. Data presented as mean ± SEM. *P<0.05, **P<0.01, ***P<0.001, ****P<0.0001, #P<0.05, ##P<0.01.*

In summary, for long-term plasticity of the CA3-CA1 circuit in the 6-month-old animals, both groups of animals could establish LTP, and TG animals exhibited reduced LTP and increased LFS-induced depotentiation compared to WT controls.

#### *2.3.1.4. Hippocampal CA1 output excitability in the 6-month-old WT and TG rats*

To assess the hippocampal CA1 *output* excitability in 6-month-old animals, the probability of producing population spikes was calculated from the CA3-evoked CA1 responses when the stimulation current was 100uA, 200uA and 300uA, in both pulses of the paired stimulations. Specifically, during the I/O protocol, 20 paired pulse responses were recorded in CA1 region at each stimulus intensity. The appearance of a population spike was identified in these 20 pairs of responses for each pulse and the probability of a population spike component occurring for each pulse was calculated under each condition, i.e., at the baseline, post-HFS and post-LFS. Two-way repeated measures ANOVA was performed to statistically determine whether genotype and/or current intensity had significant effects in all three conditions for P1 and P2 with Geisser-Greenhouse correction to maintain dataset sphericity.

As a result, no effect of genotype or interaction of genotype and current intensity were found when the rats were at 6 months of age for either P1 or P2 (**Table 2.1**). However, there was significant effect of current intensity for P1 post-HFS ($F(1.488, 28.28) = 4.818$, $P=0.0239$, $\varepsilon=0.7441$), P1 post-LFS ($F(1.235, 23.46) = 4.212$, $P=0.0440$, $\varepsilon=0.6175$), P2 post-HFS ($F(1.377, 26.16) = 14.08$, $P=0.0003$, $\varepsilon=0.6885$), and P2 post-LFS ($F(1.852, 35.18) = 18.18$, $P<0.0001$, $\varepsilon=0.9259$), as shown by two-way ANOVA.

***Table 2.1. Summary of two-way ANOVA results for comparing the effect of genotype and current intensity for probability to generate population spikes***.

| | Pulse 1 (P1) | | Pulse 2 (P2) | |
|---|---|---|---|---|
| **pre-HFS (baseline)** | Current x Genotype | F (2, 38) = 2.181, P=0.1268 | Current x Genotype | F (2, 38) = 1.048, P=0.3606 |
| | Current | F (1.203, 22.85) = 2.735, P=0.1064, ε=0.6014 | Current | F (1.820, 34.59) = 1.431, P=0.2525, ε=0.9102 |
| | Genotype | F (1, 19) = 1.771, P=0.1990 | Genotype | F (1, 19) = 0.1997, P=0.6600 |
| | | | | |
| **post-HFS** | Current x Genotype | F (2, 38) = 0.03554, P=0.9651 | Current x Genotype | F (2, 38) = 1.875, P=0.1673 |
| | Current * | F (1.488, 28.28) = 4.818, P=0.0239, ε=0.7441 | Current *** | F (1.377, 26.16) = 14.08, P=0.0003, ε=0.6885 |
| | Genotype | F (1, 19) = 0.7835, P=0.3871 | Genotype | F (1, 19) = 1.545, P=0.2290 |
| | | | | |
| **post-LFS** | Current x Genotype | F (2, 38) = 0.4269, P=0.6556 | Current x Genotype | F (2, 38) = 1.064, P=0.3550 |
| | Current * | F (1.235, 23.46) = 4.212, P=0.0440, ε=0.6175 | Current **** | F (1.852, 35.18) = 18.18, P<0.0001, ε=0.9259 |
| | Genotype | F (1, 19) = 0.9160, P=0.3506 | Genotype | F (1, 19) = 1.206, P=0.2858 |

To further investigate the origin of the significant effects, Šídák's multiple comparisons test was carried out to compare differences of probability to generate a population spike under different current intensities within each genotype group. For P2 post-HFS in the 6-month-old TG group, it was significantly more likely to have a population spike if the stimulation intensity was 200uA (P=0.0305) and 300uA (P=0.0103) compared to 100uA respectively (**Figure 2.8.E**), whereas there was no difference for the same current intensity in the age-matched WT controls (100uA vs 200uA: P=0.3600; 100uA vs 300uA: P=0.0887). For P2 post-LFS, there was a significantly higher chance to get population spikes at 300uA than at 100uA in the WT animals (P=0.0311), whereas in the TG rats, at both 200uA (P=0.0320) and 300uA (P=0.0032), the probabilities were significantly higher than at 100uA (**Figure 2.8.F**).

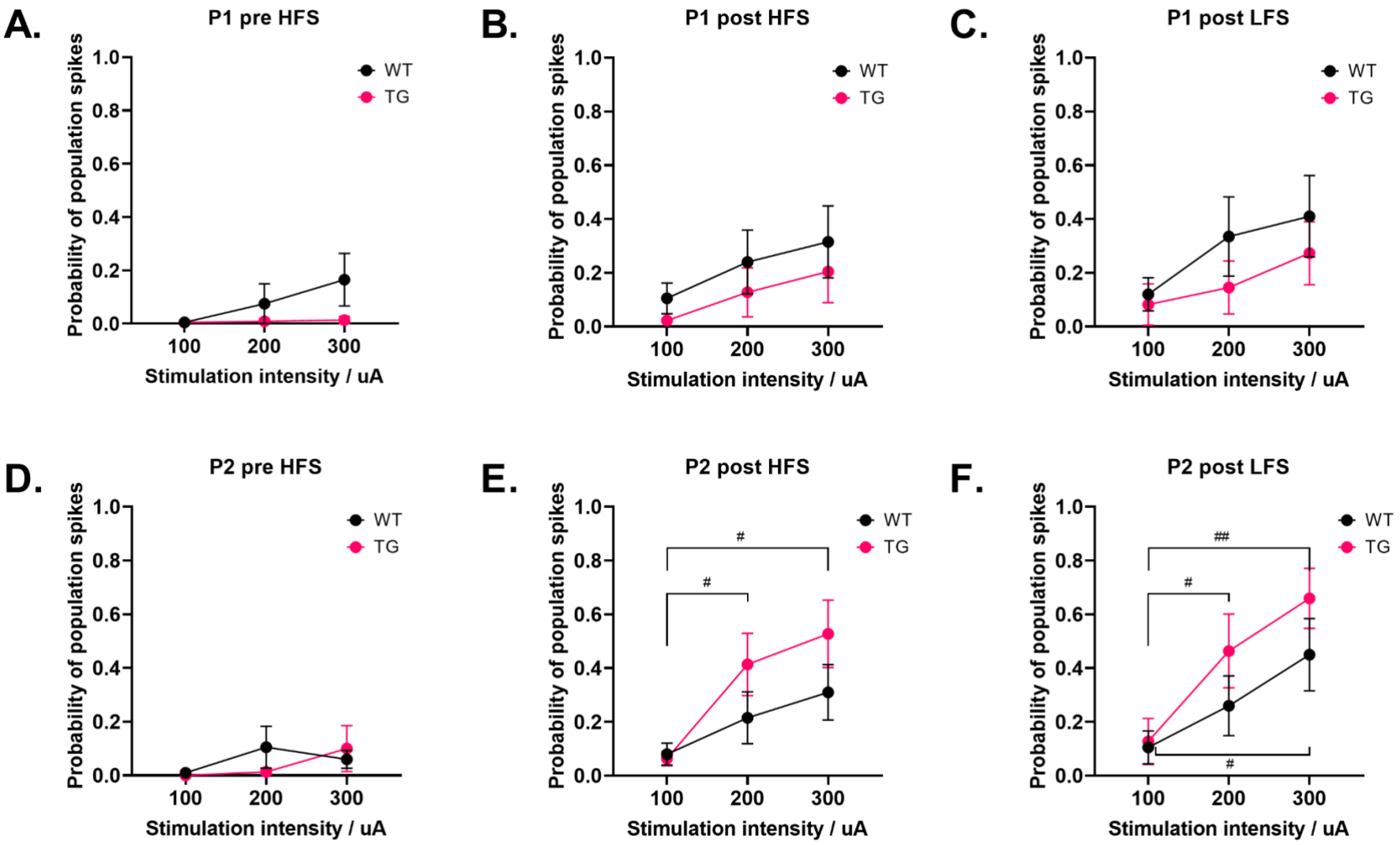
A.
P1 pre HFS
B.
P1 post HFS
C.
P1 post LFS
D.
P2 pre HFS
E.
P2 post HFS
F.
P2 post LFS
Probability of population spikes
Stimulation intensity / uA
WT
TG
1.0
0.8
0.6
0.4
0.2
0.0
100
200
300
#
##

***Figure 2.8. Probability of having population spike (PS) in CA1 region of dorsal hippocampus at the age of 6 months.***

*Probability of PS was calculated at high stimulating intensities for 6-month-old WT and TG for pulse 1 (P1) and pulse 2 (P2) at **(A)** & **(D)** the baseline, **(B)** & **(E)** after high frequency stimulation (post HFS) and **(C)** & **(F)** after low frequency stimulation (post LFS). two-way ANOVA with post hoc test was performed for P1 and P2 separately under each stimulating period. WT: n=10, TG: n=11; Data presented as mean ± SEM. Comparison within groups: #p<0.05, ##p<0.01.*

There was no *post hoc* significant difference within a group under other stimulating conditions, nor *post hoc* significant difference between WT and TG groups, at other stimulating conditions, where the statistical data were summarised in **Table 2.2**.

***Table 2.2. Adjusted p-value of probability to generate population spikes in CA1 region of 6-month-old rats at different stimulation intensities.***

| | | Pulse 1 (P1) | | | Pulse 2 (P2) | | |
|---|---|---|---|---|---|---|---|
| | | pre HFS (baseline) | post-HFS | post-LFS | pre HFS (baseline) | post-HFS | post-LFS |
| Šídák's | Between groups | | | | | | |
| | WT-TG | | | | | | |
| | 100uA | P=0.9999 | P=0.4629 | P=0.9738 | P=0.4238 | P=0.9826 | P=0.9955 |
| | 200uA | P=0.7894 | P=0.8428 | P=0.657 | P=0.6141 | P=0.4934 | P=0.6007 |
| | 300uA | P=0.4082 | P=0.9029 | P=0.8618 | P=0.9641 | P=0.4821 | P=0.5726 |
| Tukey's | Within groups | | | | | | |
| | WT | | | | | | |
| | 100uA vs 200uA | P=0.6394 | P=0.4177 | P=0.2458 | P=0.4842 | P=0.36 | P=0.1866 |
| | 100uA vs 300uA | P=0.2836 | P=0.1382 | P=0.1411 | P=0.3816 | P=0.0887 | * P=0.0311 |
| | 200uA vs 300uA | P=0.0884 | P=0.3155 | P=0.5206 | P=0.7643 | P=0.0933 | P=0.1208 |
| | | | | | | | |
| | TG | | | | | | |
| | 100uA vs 200uA | P=0.5934 | P=0.4883 | P=0.8848 | P=0.3779 | * P=0.0305 | * P=0.032 |
| | 100uA vs 300uA | P=0.8157 | P=0.2969 | P=0.4525 | P=0.4967 | * P=0.0103 | ** P=0.0032 |
| | 200uA vs 300uA | P=0.9621 | P=0.5137 | P=0.0571 | P=0.5199 | P=0.2298 | P=0.1595 |

In summary, these data suggested that, although 6-month-old TG group tended to have more chance to get population spikes in CA1 region, hence being more excitable, at high current intensities in P2 after HFS and LFS, no statistical genotype differences were found in terms of hippocampal CA1 output excitability.

### 2.3.2. Changes of evoked responses in the 9-month-old rats

The same protocol for evoked responses for I/O, PPF and LTP was applied to WT and TG rats at 9 months of age to assess any changes of synaptic connectivity and plasticity that could be different from at 6 months old.

#### *2.3.2.1. Input/output curves for the 9-month-old WT and TG rats*

Similar to the 6-month-old protocol, an I/O curve was first generated to determine the 50% output current for each animal at 9 months of age for subsequently use during the PPF and LTP experiments. A similar I/O curve was produced after HFS to examine changes in synaptic connectivity. Two-way ANOVA or mixed effect model was used to statically compare the changes of the output between TG and WT groups for the I/O curve under different stimulating intensities.

Firstly, under baseline I/O conditions between TG and WT groups, two-way ANOVA showed that the significant effects of current (slope: $F(4, 56) = 39.78$, $P<0.0001$; amplitude: $F(4, 56) = 50.94$, $P<0.0001$) and interaction between current and genotype (slope: $F(4, 56) = 2.953$, $P=0.0277$; amplitude: $F(4, 56) = 6.698$, $P=0.0002$) at baseline, but no genotype effect was detected (slope: $F(1, 14) = 0.7303$, $P=0.4072$; amplitude: $F(1, 14) = 3.444$, $P=0.0847$). Šídák multiple comparisons showed that TG had significantly raised amplitude values compared to WT controls at 200uA ($P=0.0130$) and 300uA ($P=0.0033$) (**Figure 2.9.D vs. 2.9.C, black lines**).

After HFS, two-way ANOVA showed that there were significant effects of current ($F(4, 52) = 55.20$, $P<0.0001$) and interaction between current and genotype ($F(4, 52) = 4.299$, $P=0.0044$), but no genotype effect ($F(1, 13) = 1.810$, $P=0.2015$) for slope. Similar results were found using the mixed-effect ANOVA with the amplitude measurements at post-HFS (current: $F(4, 51) = 53.00$, $P<0.0001$; genotype: $F(1, 13) = 2.888$, $P=0.1131$; current x genotype: $F(4, 51) = 4.485$,

P=0.0035). However, Šídák multiple comparisons test showed that at 300uA TG had significantly higher output for slope (P=0.0104) (**Figure 2.9.B vs. 2.9.A**) and amplitude (P=0.0095) (**Figure 2.9.D vs. 2.9.C**) measurements. Therefore, between WT and TG groups, the I/O curve in 9-month-old TG rats tended to shift upwardly compared to the WT controls at both baseline and after HFS **(Figure 2.9)**.

Two-way ANOVA or mixed-effect model was employed to study the I/O difference within each genotype group at baseline and post-HFS periods. For WT animals, mixed-effects analysis revealed no effect of HFS (slope: F (1, 7) = 0.3744, P=0.5600; amplitude: F (1, 7) = 1.616, P=0.2442) or interaction between HFS and current (slope: F (4, 23) = 0.5307, 0.7144; amplitude: F (4, 22) = 1.170, P=0.3509) on the output pre- and post-HFS, although there was the expected effect of current (slope: F (4, 28) = 15.81, P<0.0001; amplitude: F (4, 28) = 17.26, P<0.0001) (slope: **Figure 2.9.A**; amplitude: **Figure 2.9.C**). For TG animals, there were significant differences for the slope output caused by current (F (4, 28) = 40.93, P<0.0001), HFS stimuli (F (1, 7) = 16.99, P=0.0045) and their interaction (F (4, 28) = 11.28, P<0.0001). Additionally, Šídák's multiple comparisons test showed significant increases of slope output after HFS in the 9-month-old TG animals at 200uA (P<0.0001) and 300uA (P<0.0001) (**Figure 2.9.B**). However, for amplitude, two-way ANOVA showed no effect of the HFS stimuli (F (1, 7) = 0.7194, P=0.4244) or interaction between current and HFS stimuli (F (4, 28) = 0.7104, P=0.5917) on the post-HFS output in the TG animals, although current was again a significant factor, as expected (F (4, 28) = 41.29, P<0.0001) (**Figure 2.9.D**). Therefore, for the WT groups, there were no statistical changes of the output as a result of HFS, although their post-HFS I/O seemed to locate above the baseline I/O. And for the TG group, statistical changes of the output pre- and post-HFS were found in the slope but not amplitude measurement.

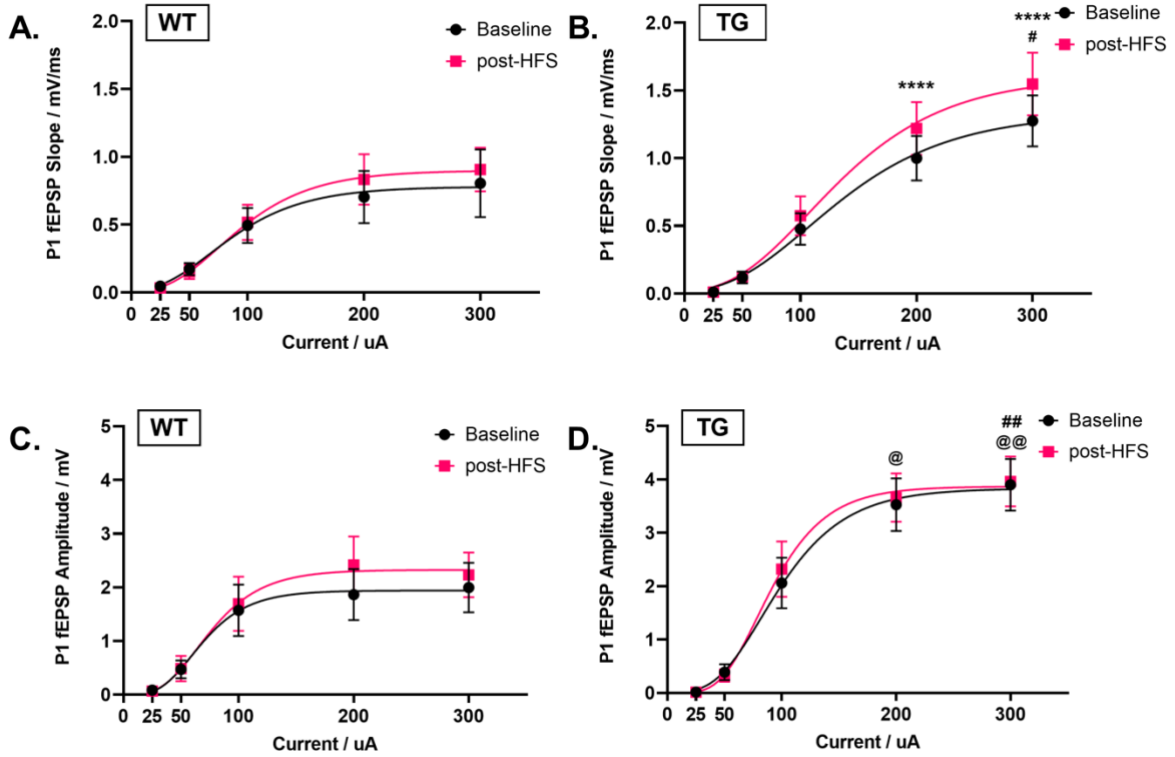


***Figure 2.9. Hippocampal CA3-CA1 input/output (I/O) curves for 9-month-old WT and TG rats at the baseline and post-HFS.***

*The pre- and post-HFS I/O curves of 9-month-old WT rats were presented as **(A)** slope and **(C)** amplitude measurements of the P1 fEPSPs, whereas the I/O curves of the 9-month-old TG rats were presented in **(B)** slope and **(D)** amplitude of P1 fEPSP. At the baseline, the I/O curves of the TG shifted upwardly compared to the WT controls. two-way or mixed model ANOVA was used with Sidak's multiple comparison. *: compared within the group; @: compared between TG versus WT groups at the baseline; #: compared between TG versus WT groups at post-HFS. ****P<0.0001, @P<0.05, @@P<0.01, ##P<0.01. Data were presented as mean±SEM. Baseline: n=8 per group, post-HFS: WT: n=7, TG: n=8.*

The Gompertz fit was used to calculate the maximum output as measured with slope and amplitude for individual subjects. Comparisons were made between and within groups by ANOVA to further analyse the difference in I/O maximum output.

With the slope measurement, mixed-effect ANOVA showed significant effect of stimulation by HFS ($F(1, 13) = 5.279$, $P=0.0388$). No statistical effect was found that was caused by

genotype (F (1, 14) = 3.548, P=0.0806) or interaction (F (1, 13) = 0.02058, P=0.8881). The *post hoc* Šídák multiple comparisons did not detect any significant changes between or within WT and TG groups (**Figure 2.10.A**).

However, using the amplitude measurement, a significant effect was found for genotype using the mixed-effect analysis (F (1, 14) = 7.138, P=0.0182); whereas stimulation did not cause significant effect (F (1, 13) = 0.9565, 0.3459), nor was interaction significant (F (1, 13) = 0.5232, 0.4823). The Šídák's multiple comparisons showed that TG had remarkably larger maximum output compared to the WT controls at both the baseline (P= 0.0203) and post-HFS (P=0.0370) (**Figure 2.10.B**). Nevertheless, the maximum voltage output was not statistically different before or after HFS within the WT (P=0.4593) or the TG (P=0.9790) group.

The current for providing 50% output under slope and amplitude measurement were determined using Gompertz fit for each subject, and statistical comparisons were made between and within WT and TG groups by ANOVA. The mixed-effect analysis showed no significant effect of any of the factors for slope (stimulation: F (1, 13) = 0.05314, P=0.8213; genotype: F (1, 14) = 2.889, P= 0.1113) (**Figure 2.10.C**) or amplitude (stimulation: F (1, 13) = 4.144, P=0.0627; genotype: F (1, 14) = 0.7077, P=0.4143) (**Figure 2.10.D**) with no significant interaction (slope: F (1, 13) = 1.123, P= 0.3086; amplitude: F (1, 13) = 0.1366, P= 0.7176). With mixed-effect analysis, there was no statistical difference of the experimentally determined current for 50% output (stimulation: F (1, 13) = 4.314, P=0.0582; genotype: F (1, 14) = 0.1078, P=0.7476; stimulation x genotype: F (1, 13) = 0.05673, P=0.8155) (**Figure 2.10.E**).

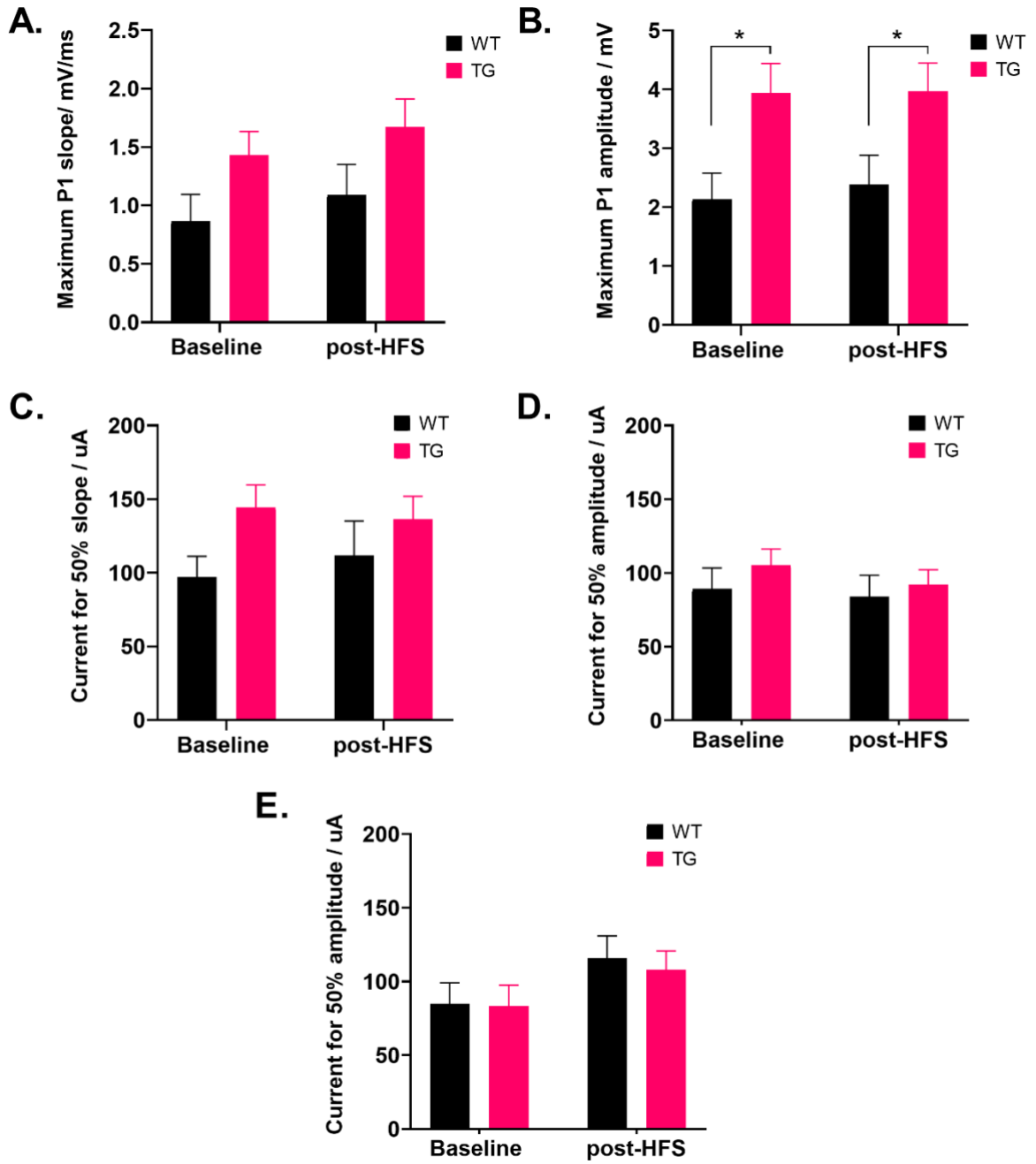


***Figure 2.10. Comparison of hippocampal CA3-CA1 input/output function of the 9-month-old WT and TG rats pre- and post-HFS.***

*The maximum output was presented for WT and TG groups at 9 months of age as a measure of **(A)** slope and **(B)** amplitude of P1 fEPSP. The current required for 50% output was calculated using Gompertz fit for each animal with the measure of **(C)** slope, **(D)** amplitude, and **(E)** from the experimental measures on the oscilloscope. Baseline: n=8 per group, post-HFS: WT: n=7, TG: n=8.Data were presented as mean±SEM. *P<0.05.*

In conclusion, there was no difference in terms of the current for 50% output between WT and TG animals at the baseline or after HFS. However, the maximum output tended to increase in the TG animals compared to the controls, with TG group showed a surprisingly upwardly-shifted I/O curve.

#### *2.3.2.2. Paired pulse facilitation in the 9-month-old WT and TG rats*

To study short-term plasticity of the CA3-CA1 synapse, PPF was tested at baseline and directly after HFS over a range of different paired-pulse intervals (IPIs). **Figure 2.11** shows the amount of synaptic facilitation to the second response in a paired pulse, as calculated by either slope or amplitude. As IPI increased, there was a decreasing pattern of the degree of synaptic facilitation represented by paired-pulse index (PPI), especially at short IPIs (25ms, 50ms and 100ms). No paired-pulse depression was observed.

Three-way ANOVA was performed to determine statistical differences for the three factors, namely genotype, stimulation and IPI, singly or interacting with one another to generate effects. For slope measures a mixed-effect model of three-way ANOVA showed that genotype ($P=0.0062$, $F(1, 14) = 10.35$), IPI ($P<0.0001$, $F(5, 70) = 46.82$) and stimulation ($P=0.0002$, $F(1, 14) = 24.65$) all significantly affected synaptic facilitation. The HFS stimulation interacted with genotype ($P=0.0055$, $F(1, 14) = 10.75$) and IPI ($P=0.0002$, $F(5, 64) = 5.737$), respectively, to cause these changes. The interaction between IPI and genotype was also significant ($P<0.0001$, $F(5, 70) = 9.042$). However, triple interaction within these three factors was not significant ($P=0.0595$, $F(5, 64) = 2.254$). A *post hoc* Tukey's multiple comparison showed that TG rats had significantly smaller PPI at baseline and, therefore, less facilitation compared to WT when IPI was 25ms ($P<0.0001$) and 50ms ($P<0.0001$) **(Figure 2.11.B)**. After HFS, synaptic facilitation was

also observed to be smaller in the TG animals at IPIs less than 200ms, with a significant reduction of PPI was found at 25ms IPI (P=0.0243) **(Figure 2.11.B)**. Within the same genotype, the post-HFS PPI was markedly reduced in the WT animals at 25ms (P=0.0016), 50ms (P<0.0001) and 100ms (P=0.0008) IPIs. However, although PPI of TG animals tended to reduce after HFS at all the IPIs tested here, no statistical difference was found **(Figure 2.11.B)**.

The general pattern of PPI throughout different IPIs tended to be similar when calculated using amplitude **(Figure 2.11.C)**. A mixed-effect model of three-way ANOVA showed that genotype (P=0.0013, F (1, 14) = 16.11), stimulation (P=0.0002, F (1, 14) = 25.83) and IPIs (P<0.0001, F (5, 70) = 69.44) could on their own caused significant changes in the magnitude of paired-pulse facilitation. Genotype could interact with HFS (P=0.0117, F (1, 14) = 8.393) and IPIs (P<0.0001, F (5, 70) = 14.01), respectively, to cause a significant effect. HFS and IPIs also interacted with each other (P<0.0001, F (5, 64) = 13.53). Additionally, these three factors interacted (P=0.0017, F (5, 64) = 4.401). Tukey's multiple comparison test further showed that, at 25ms and 50ms, TG animals had significantly smaller PPI and less facilitation compared to WT controls, before (25ms: P<0.0001; 50ms: P<0.0001) and after HFS (25ms: P=0.0148; 50ms: P=0.0234). When IPI was 100ms, significant PPI reduction was observed in TG rats before HFS (P=0.0009) but not after (P=0.8035). Similar to the slope results, amplitude measurements also showed significantly decreased PPI magnitude to HFS only in the WT animals at short IPIs **(Figure 2.11.C)**. The marked differences were observed at 25ms (P<0.0001), 50ms (P<0.0001) and 100ms (P<0.0001) for the WT. No significant reduction was found for the TG animals as an effect of HFS.

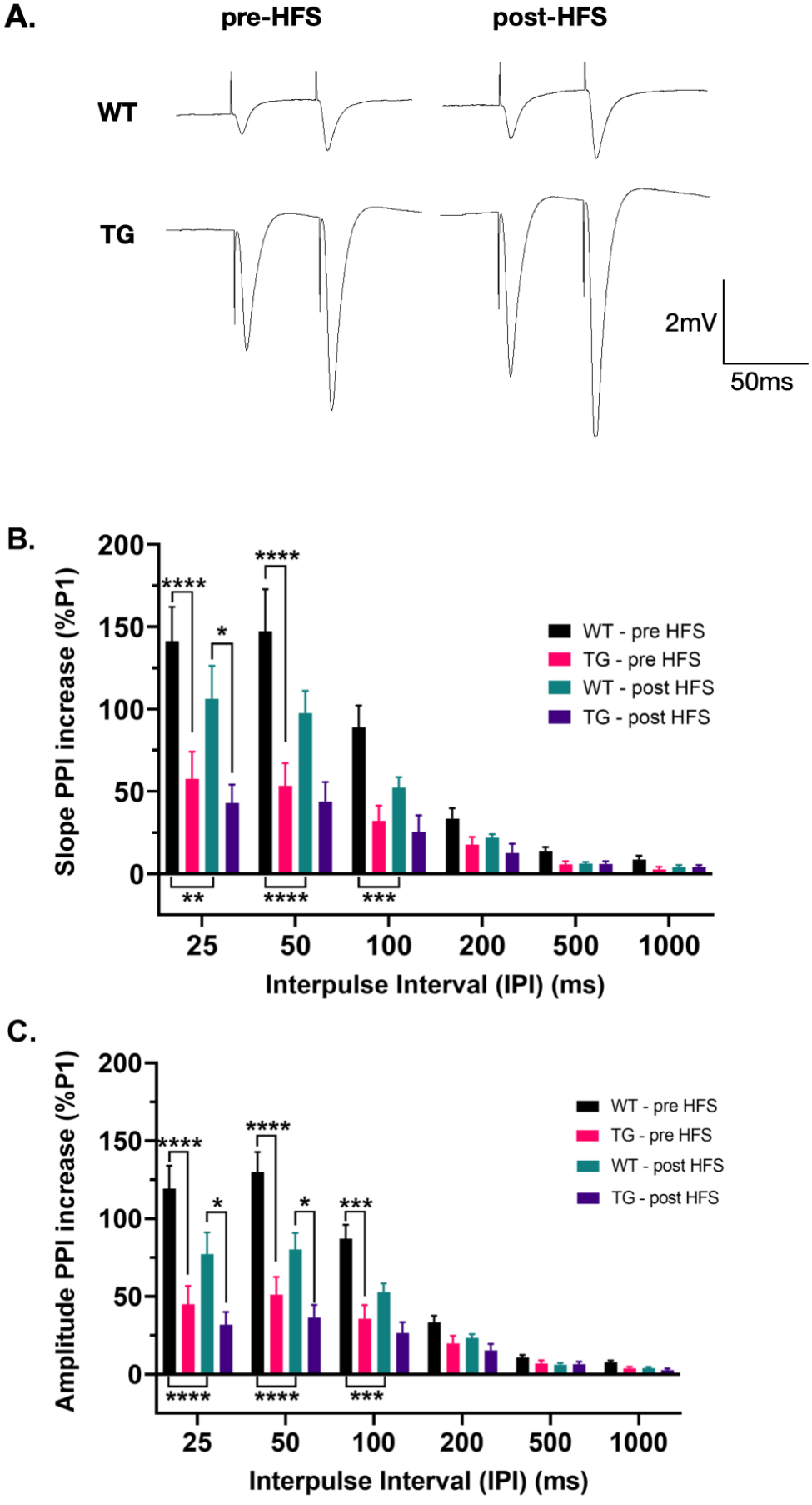
A.
pre-HFS
post-HFS
WT
TG
2mV
50ms
B.
Slope PPI increase (%P1)
200
150
100
50
0
****
*
****
**
****
***
WT - pre HFS
TG - pre HFS
WT - post HFS
TG - post HFS
25
50
100
200
500
1000
Interpulse Interval (IPI) (ms)
C.
Amplitude PPI increase (%P1)
200
150
100
50
0
****
*
****
*
***
****
****
***
WT - pre HFS
TG - pre HFS
WT - post HFS
TG - post HFS
25
50
100
200
500
1000
Interpulse Interval (IPI) (ms)

***Figure 2.11. 9-month-old male TgF344-AD rats showed smaller paired-pulse facilitation.***

*Paired pulses were delivered at a current that gives 50% output. fEPSPs were recorded at CA1 of hippocampus by the stimulation of Schaffer collateral pathway.* ***(A)*** *Examples of fEPSP traces before and after HFS of a randomly selected rat from each group in CA1 at 9 months of age.* ***(B)*** *Slope and* ***(C)*** *amplitude of the fEPSPs were measured. Three-way ANOVA of mixed-effect model was carried out, followed by Tukey's multiple comparisons test. pre-HFS: n=8 per group; post-HFS: WT: n=8, TG: n=7. Data were presented as mean ± SEM. *P<0.05, **P<0.01, ***P<0.001, ****P<0.0001.*

#### *2.3.2.3. Long-term potentiation and depotentiation in the 9-month-old WT and TG rats*

Long-term synaptic plasticity of CA3-CA1 circuit was measured in the 9-month-old animals. HFS containing 5 bursts of 20 pulses at 200Hz (3s inter-burst interval) was delivered after a stable 15min baseline was obtained. The CA3-evoked fEPSPs were recorded approximately 10mins after HFS (after PP stimulation) for 30mins to observe LTP establishment.

Two-way ANOVA showed that HFS caused significant increase of response size in both genotype groups (slope: $F(1, 14) = 37.13$, $P<0.0001$; amplitude: $F(1, 14) = 25.32$, $P=0.0002$). There was also a significant genotype effect (slope: $F(1, 14) = 6.810$, $P=0.0206$; amplitude: $F(1, 14) = 6.201$, $P=0.0260$). A significant interaction was found between stimulation and genotype (slope: $F(1, 14) = 6.810$, $P=0.0206$; amplitude: $F(1, 14) = 6.201$, $P=0.0260$).

Bonferroni multiple comparisons showed that within WT animals, the LTP response was convincingly established after HFS (slope: $P<0.0001$; amplitude: $P=0.0002$); however, within the TG animals, the increase of post-HFS response magnitude was not significantly different to the baseline if the responses were averaged for the entire 30mins post-HFS, either measured as slope ($P=0.0547$) or amplitude ($P=0.1877$). The comparison of post-HFS response between WT and TG groups further revealed a significant reduction of LTP magnitude in the TG animals at the age of 9 months (slope: $P=0.0019$; amplitude: $P=0.0030$) **(Figure 2.12)**.

To analyse and determine any nuanced change of evoked responses after HFS in the TG rats, post-HFS responses were averaged for every 10min segment. Interestingly, the statistical results suggested that LTP could be induced in the TG animals, but it had a late establishment: although the initial increase of magnitude was small, it gradually increased over time and then became stabilized (**Figure 2.12.F**). Contrarily, the magnitude of the LTP response was reduced throughout the recording time in the WT littermates, although it was still significantly higher throughout.

According to two-way ANOVA, significant factors were genotype (slope: $F(1, 14) = 6.810$, $P=0.0206$; amplitude: $F(1, 14) = 6.201$, $P=0.0260$) and HFS (slope: $F(1.184, 16.58) = 32.99$, $P<0.0001$; amplitude: $F(1.176, 16.46) = 22.83$, $P=0.0001$) and these also interacted (slope: $F(3, 42) = 7.233$, $P=0.0005$; amplitude: $F(3, 42) = 6.642$, $P=0.0009$).

The Bonferroni *post hoc* test showed that during the first 10mins ($t_{10}$-$t_{20}$) after HFS, WT animals had significantly larger values for slope ($P<0.0001$) and amplitude ($P<0.0001$). This was observed in TG animals for slope ($P=0.0448$) but not amplitude ($P=0.2625$) comparing the baseline response with the response during $t_{10}$-$t_{20}$. The increase of slope magnitude in TG rats was more significant during the second ($t_{20}$-$t_{30}$) and the last ($t_{30}$-$t_{40}$) 10mins post-HFS (TG($t_{20}$-$t_{30}$): $P=0.0042$, TG($t_{30}$-$t_{40}$): $P=0.0127$) compared to their respective baseline, although that for amplitude measurement tend to be significant (TG($t_{20}$-$t_{30}$): $P= 0.1048$; TG($t_{30}$-$t_{40}$): $P= 0.0727$).

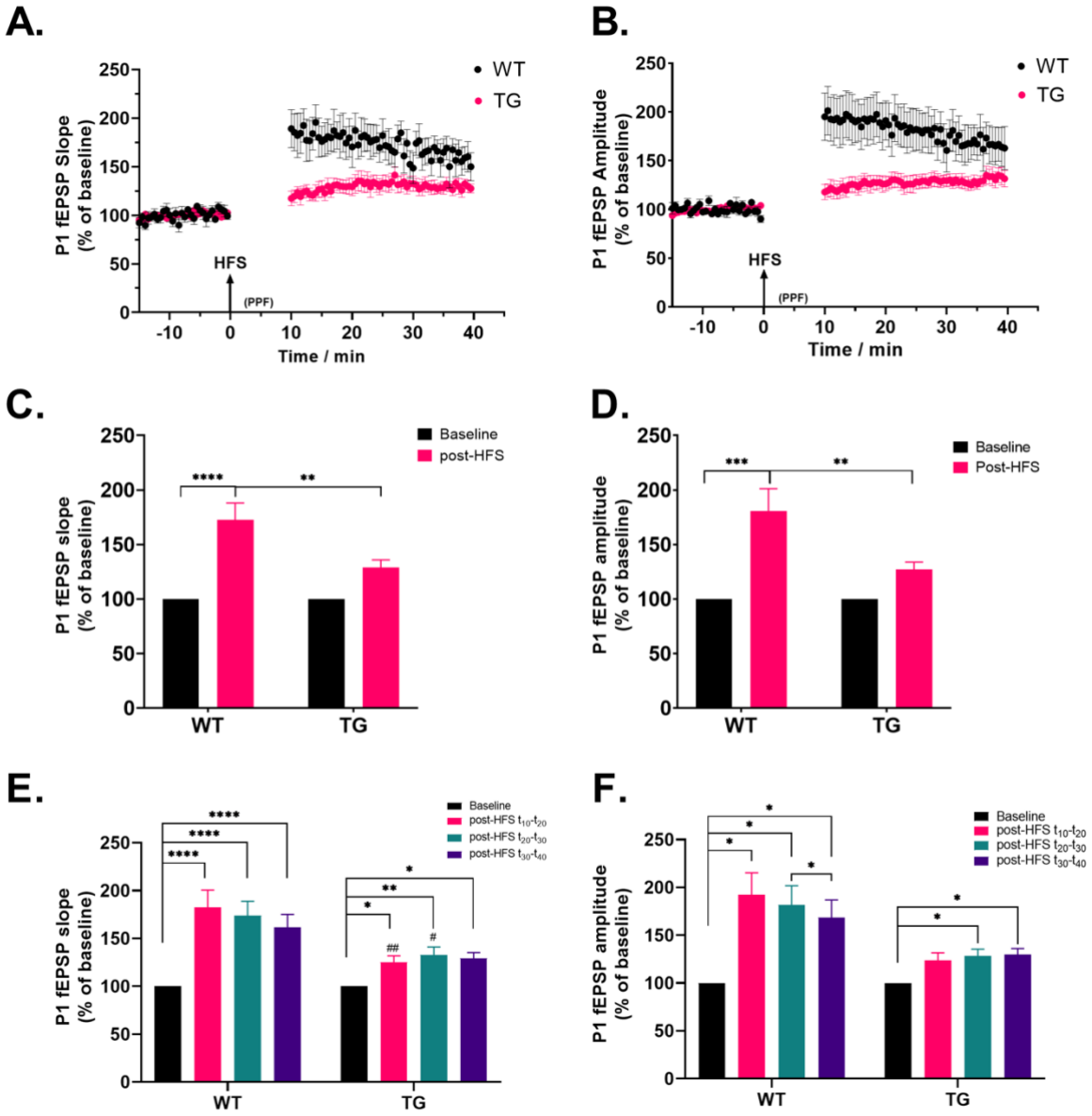


***Figure 2.12. 9-month-old male TgF344-AD rats showed reduced long-term potentiation.***

*Scatter plots of slope for CA1 evoked-excitatory post-synaptic potential during experimental time course as measured with **(A)** slope and **(B)** amplitude. LTP magnitude averaged in the entire 30mins post-HFS recording period measured with **(C)** slope and **(D)** amplitude. Comparison of LTP magnitude averaged in 10mins segments in the post-HFS recording period were made as a measure of **(E)** slope and **(F)** amplitude. The TG rats showed 'late' long-term potentiation. n=8 per group. Data were presented as mean ± SEM. *P<0.05 **P<0.01, ****P<0.0001. #: TG compared to WT during the same time segment. #P<0.05, ##P<0.01.*

Therefore, these results suggest that LTP might be established in the hippocampal CA3-CA1 circuit in the 9-month-old TG rats, but it was a gradual process with largest potentiation later in the post-HFS period, although the magnitude was markedly smaller at all points compared to WT littermates.

#### *2.3.2.4. Hippocampal CA1 output excitability in the 9-month-old WT and TG rats*

The probability of evoking a population spike at high stimulation intensities was calculated as a measure of excitability in the CA1 region of animals at 9 months of age. Similar to the analyses in the 6-month-old rats, population spikes embedded in the fEPSPs at 100uA, 200uA and 300uA were identified during baseline and post-HFS I/O periods. The probability of a population spike during the response to pulse 1 (P1) or pulse 2 (P2) were calculated. Two-way repeated measures (RM) ANOVA was performed for each pulse in each condition in the 9-month-old animals with Geisser-Greenhouse correction to maintain dataset sphericity (**Figure 2.13**) and the results are summarised in **Table 2.3**.

For P1, the current intensity had significant effect on the changes of population spike probability both at baseline ($F(1.623, 27.58) = 3.644$, $P=0.0478$, $\varepsilon= 0.8113$) (**Figure 2.13.A**) and post-HFS ($F(1.443, 24.52) = 6.922$, $P=0.0080$, $\varepsilon= 0.7213$) (**Figure 2.13.B**), but no significant effect for genotype was seen under either pre- or post-HFS. For P1 baseline, there was a significant interaction between genotype and current intensity ($F(2, 34) = 3.766$, $P=0.0333$). Most notably, for P2 post HFS, there was a significant effect of genotype ($F(1, 17) = 6.325$, $P=0.0223$) and current intensity ($F(1.363, 23.18) = 4.831$, $P=0.0284$, $\varepsilon=0.6817$), although their interaction was not significant ($F(2, 34) = 0.5068$, $P=0.6069$) (**Figure 2.13.D**). No ANOVA changes were found for P2 baseline, as shown in **Table 2.3**.

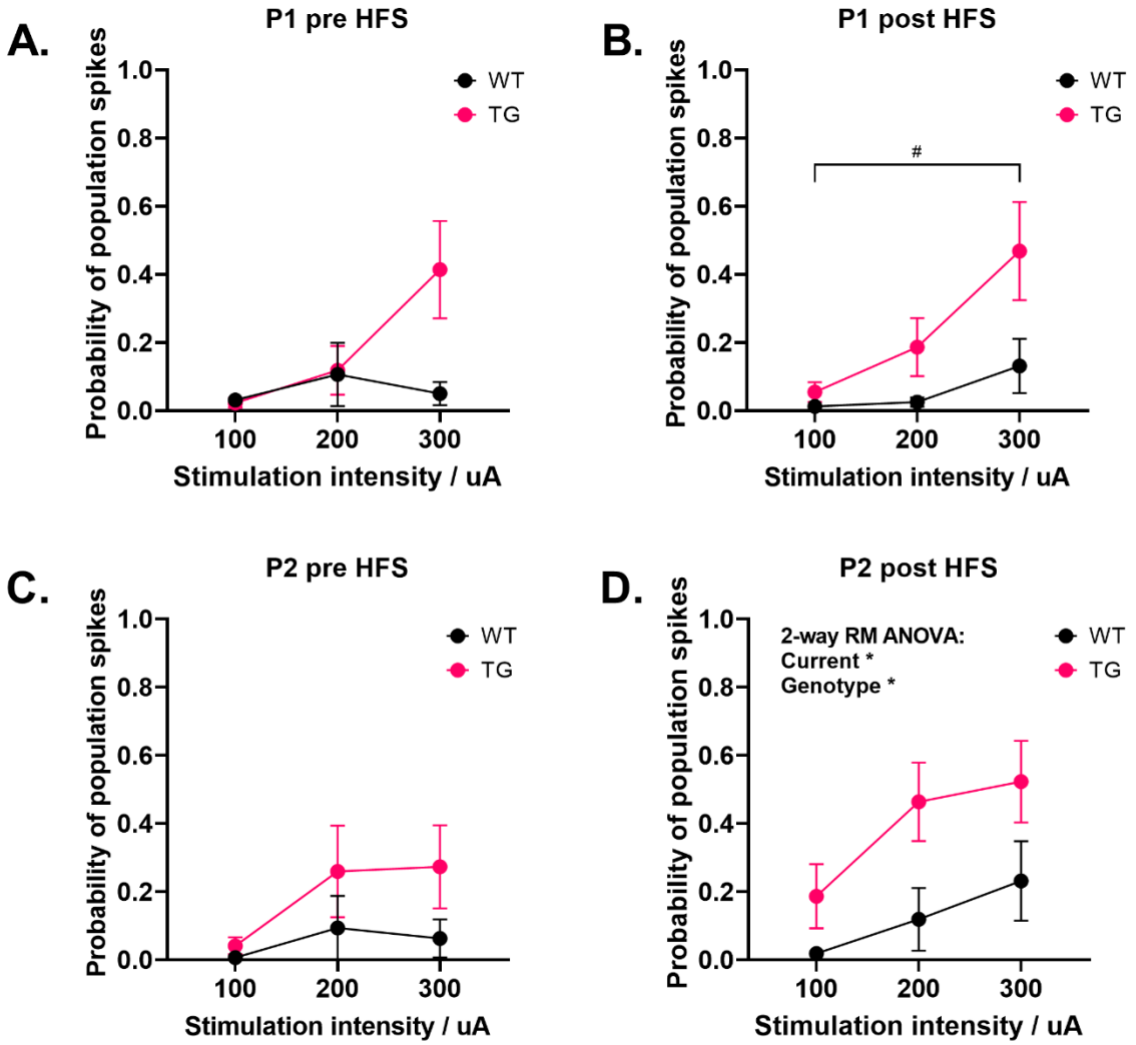


***Figure 2.13. Probability of having population spikes (PS) in CA1 region of dorsal hippocampus at the age of 9 months.***

*Probability of PS was calculated at high stimulating intensities for the 9-month-old WT and TG for **(A)** & **(B)** pulse 1 (P1) and **(C)** & **(D)** pulse 2 (P2) pre- and post- high frequency stimulation (HFS). Two-way ANOVA with Šídák's multiple comparisons test was performed for P1 and P2 separately under each stimulating period. WT: n=8, TG: n=11; Data presented as mean ± SEM. *p<0.05; post hoc comparison within groups: #p<0.05, ##p<0.01.*

***Table 2.3. Two-way repeated-measures ANOVA results testing the effect of genotype and current intensity on the probability of evoked population spikes.***

| | Pulse 1 (P1) | | Pulse 2 (P2) | |
|---|---|---|---|---|
| **pre-HFS (baseline)** | Current x Genotype * | F (2, 34) = 3.766, P=0.0333 | Current x Genotype | F (2, 34) = 0.8454, P=0.4382 |
| | Current * | F (1.623, 27.58) = 3.644, P=0.0478, ε=0.8113 | Current | F (1.280, 21.76) = 2.993, P=0.0895, ε=0.6401 |
| | Genotype | F (1, 17) = 2.273, P=0.1500 | Genotype | F (1, 17) = 1.573, P=0.2268 |
| | | | | |
| **post-HFS** | Current x Genotype | F (2, 34) = 2.009, P=0.1497 | Current x Genotype | F (2, 34) = 0.5068, P=0.6069 |
| | Current ** | F (1.443, 24.52) = 6.922, P=0.0080, ε=0.7213 | Current * | F (1.363, 23.18) = 4.831, P=0.0284, ε=0.6817 |
| | Genotype | F (1, 17) = 4.238, P=0.0552 | Genotype * | F (1, 17) = 6.325, P=0.0223 |

To compare changes of population spike probability within each genotype group as an effect of changing current intensities, Tukey's multiple comparisons test was performed. For P1 post-HFS, the 9-month-old TG rats showed a significantly higher probability of evoking population spikes in CA1 region at 300uA compared to 100uA (P=0.0422) (**Figure 2.13.B**). Although there was a significant ANOVA effect for P2 post-HFS by genotype and current intensity, the *post hoc* results were not statistically different either between two group at each current or within the groups to compare the difference due to the current changes (**Table 2.4**).

***Table 2.4. Post hoc test for statistical differences comparing changes in probability to have population spike between and within genotype groups.***

| | | Pulse 1 (P1) | | Pulse 2 (P2) | |
|---|---|---|---|---|---|
| | | pre HFS (baseline) | post-HFS | pre HFS (baseline) | post-HFS |
| Šídák's | Between groups | | | | |
| | WT-TG | | | | |
| | 100uA | P=0.9784 | P=0.4659 | P=0.4998 | P=0.2867 |
| | 200uA | P=0.9995 | P=0.2438 | P=0.6956 | P=0.0922 |
| | 300uA | P=0.0882 | P=0.1648 | P=0.3632 | P=0.2702 |
| Tukey's | Within groups | | | | |
| | WT | | | | |
| | 100uA vs 200uA | P=0.7091 | P=0.7804 | P=0.6443 | P=0.5786 |
| | 100uA vs 300uA | P=0.8818 | P=0.3461 | P=0.6078 | P=0.2513 |
| | 200uA vs 300uA | P=0.6977 | P=0.365 | P=0.7128 | P=0.3559 |
| | | | | | |
| | TG | | | | |
| | 100uA vs 200uA | P=0.3646 | P=0.3127 | P=0.2606 | P=0.1716 |
| | 100uA vs 300uA | P=0.056 | *P=0.0422 | P=0.1952 | P=0.1692 |
| | 200uA vs 300uA | P=0.1027 | P=0.0723 | P=0.9675 | P=0.7327 |

Taken together, after HFS, these data suggest that 9-month-old TG rats were more likely to exhibit CA1 population spikes, supporting a more excitable state in the CA1 region compared to age-matched WT controls, especially at higher stimulation intensity.

## 2.4. Discussion

Neural synaptic plasticity is one of the major components for hippocampal circuit function and the core to models of memory formation and consolidation that are relevant to AD. The present study investigated synaptic plasticity, as well as baseline connectivity, in the rat hippocampal CA3-CA1 circuit of TG and age-matched WT controls at the ages of 6 or 9 months. The *in vivo* fEPSPs in the Schaffer collateral pathway in the left hemisphere were recorded for I/O, PPF and LTP (and/or depotentiation) in the animals under urethane anaesthesia.

### 2.3.1. Changes in baseline and post-HFS synaptic transmission

For basal synaptic transmission, this study found that genotype differences of the I/O curve appeared at 9 months old at baseline, with TG showing increased responses compared to WT at the same current intensity. The upwardly shifted I/O curve at 9 months but not 6 months old indicates potential hyperexcitability at CA3-CA1 circuit at the later of these two ages in this model. Consistent with an *in vitro* study in the same model, basal synaptic transmission was not affected in the CA3-CA1 circuit at 6 months old (Smith and McMahon, 2018). However, the decrement in maximum slope at 9 months old *in vitro* was not replicated in this *in vivo* study. Moreover, maximum voltage output in our 9-month-old TG animals was significantly *larger* than WT, suggesting an increase of CA3-CA1 baseline synaptic excitability. The increment of maximum output seen in the 9-month-old TG rats is in contrast to several studies in other rodent models for Alzheimer's research that showed reduction of I/O at this age. In 6-month-old 5xFAD mice, there was a reduction of maximum fEPSP slope output in the CA1 *in vitro* (Crouzin et al., 2013). However, in Tg2576 mice with human Aβ mutation, the I/O ratio was found to increase from the age of 6 months in CA1 *in vitro* and a similar increase was still observed in animals aged 14-15 months (Townsend et al., 2010). This inconsistency may be due to different experimental preparation, species and preclinical genetic modifications that could have differentially affected the rate of amyloidosis.

Changes in synaptic transmission/plasticity were also investigated after HFS. At 6 months of age, TG rats exhibited a reduction of maximum output of the response post-HFS compared to WT controls. This finding is in parallel with the result of reduced LTP in the TG rats at this age, where they showed decreased post-HFS response size. Surprisingly, the changes of maximum output upon HFS were not statistically significant in 9-month-old animals, although TG animals showed a similar reduction in LTP compared to WT. However, the mixed-effect

ANOVA results for the effect of HFS was close to 0.05, indicating a potential reduction of maximum output.

Additionally, baseline connectivity was studied as the current for 50% output. The smaller the current required for generating 50% of the maximum slope/voltage output, the stronger the synaptic connectivity should be. In this study, there was no change of the current for 50% output if the data were acquired from MATLAB measurements *post hoc* and fitted to a Gompertz function at 6- or 9- months of age. However, because this value was also used for the PPF and LTP/LTD experiment protocols, it was recorded and tested in the experiment as the voltage output using an oscilloscope. Using this method, the current for 50% output for the 6-month-old WT rats was reduced after HFS, which might be because HFS stimulation increased the synaptic connection. However, the 6-month-old TG rats did not show changes after HFS, although there was no genotype difference detected at baseline or after HFS. Interestingly, in the transgenic Tg4-42 mice that is a model for sporadic AD, the hippocampal hyperexcitability was detected as indicated by changes of I/O as early as 3 months old (Dietrich et al., 2018). Instead of a change in the maximum output, there was a reduction of current required for 50% output in the Tg4-42 model (Dietrich et al., 2018), which was unchanged in the TgF344-AD rats at 6 months. Similarly, at 9 months of age, no genotype difference or effect of HFS was found for the 50% output current, if the experimentally recorded data were used. However, high variance was seen in the calculated data, which increased the uncertainty to some extent. Therefore, the TgF344-AD model showed increased maximum fEPSP output at 9 months of age in the hippocampal Schaffer collateral-CA1 synapse, but the synaptic connectivity strength was not affected.

### 2.3.2. Changes in short-term plasticity

For STP, 9-month-old TG rats showed a significantly lower PPF ratio, whereas, in the 6-month-old animals the PPF ratio of the TG rats was not different from WT controls. These results are contrary to the findings that both adult (4-6mo) and aged (17-18mo) 3xTg mice displayed increased PPF in the CA1 region of the hippocampus (Davis et al., 2014). The results of decreased PPF in the 9-month-old TG also differ to the observation in APP/PS1-21 mice in which their PPF was not affected at 8 months of age (Gengler et al., 2010).

PPF is commonly seen at synapses whose initial release probability is low (Jackman and Regehr, 2017). In PPF, if the interpulse interval (IPI) is within tens to hundreds of milliseconds, the second response of the pair is generally greater than the first one, (McNaughton, 1982, Bliss and Collingridge, 2013, Jackman and Regehr, 2017). According to the residual calcium hypothesis, this is because $Ca^{2+}$ remaining at the synaptic cleft after P1 is added to the pre-synaptic $Ca^{2+}$ signal of P2, causing an increased probability of release of neurotransmitter (McNaughton, 1982). Generally, the PPF ratio has an inversely proportional relationship with synaptic release probability, meaning that the smaller the ratio, the higher the chance of release (Bliss and Collingridge, 2013). The reduction of PPF ratio is commonly seen as a presynaptic effect after LTP induction due to increased glutamate release probability (Bliss and Collingridge, 2013, McNaughton, 1982). In this study of PPF in the TgF344-AD model, the PPF ratio was significantly reduced after HFS in the WT animals at both 6- and 9- months old at short IPIs. The PPF ratio in 6-month-old TG rats also exhibited this property. However, this feature was lost in the 9-month-old TG rats. More interestingly, the PPF ratio of TG rats at 9 months old was even smaller compared to the WT under same IPIs, indicating potential pre-synaptic impairment that leads to an increase of release probability at baseline (Bliss and Collingridge, 2013). In fact, acute administration of Aβ peptide was found to increase the

release probability pre-synaptically in hippocampal slices (Abramov et al., 2009). Levels of synaptic markers in the dorsal hippocampus will be measured in **Chapter 4, Section 4.3**.

Additionally, other explanations of lower PPF are also feasible, for example, a reduced probability of post-synaptic neurotransmitter binding, or reduced $Ca^{2+}$ clearance that could result from complex synaptic mechanisms (Jackman and Regehr, 2017, Zucker and Regehr, 2002). In this study, taking into consideration the large fEPSP response in 9-month-old TG animals, the reduced PPF ratio could also be due to the observation that the P1 response was too big for further facilitation, leading to a possibility of synaptic disinhibition in the CA3→CA1 circuitry (Bartholome et al., 2017, Wojcik et al., 2004).

### 2.3.3. Changes in long-term plasticity

This study also showed that LTP induced by Schaffer-collateral HFS was significantly reduced in the CA1 of TG rats at both 6- and 9- months of age. This is in contrast to the *in vitro* study of this same model where CA1 LTP was unchanged at 6 and 9 months of age (Smith and McMahon, 2018). Nevertheless, the blockade of LTP is consistent in many models involving elevation of Aβ, in acute models of soluble Aβ oligomers (Lambert et al., 1998, Ganesh et al., 2008) as well as *in vivo* models before formation of Aβ plaques (Mucke et al., 2000). Observations in our study are in line with a decreased CA1 LTP reduction in Tg2576 APP mouse model (Chapman et al., 1999, Jung et al., 2011, Huh et al., 2016, Townsend et al., 2010) and a variety of APP/PS1 mouse models at this age *in vivo* (Mango et al., 2019, Richards et al., 2003).

In the Tg2576 mouse with human Aβ expression, LTP *in vitro* was reduced at about 6-7 months of age (Townsend et al., 2010, Huh et al., 2016) and could be rescued with a gamma-secretase

inhibitor (Townsend et al., 2010). 6-month-old 5xFAD mice also exhibited significantly reduced LTP in response to 100Hz tetanus stimuli (Seo et al., 2021). A decay of LTP was also found in APP/PS1-21 mice at 8 months in the CA1 region *in vivo* (Gengler et al., 2010). Interestingly, LTP in Tg2576 mice was abnormally restored at the age of about 14-19 months with elevated I/O ratio, indicating hippocampal hyperexcitability, perhaps due to homoeostatic reductions in synaptic inhibition in response to excitatory synaptic loss (Townsend et al., 2010). However, in the TgF344-AD model, the impaired LTP was continuingly observed to 9-month-old TG animals with I/O elevation, suggesting the age tested here is probably still young to generate abnormal LTP. Although higher LTP was reported in other models, for example, the 3xTg mice showed larger LTP (Zhu, 2019) and the 5xFAD showed increased LTP at 11 months old in response to theta-burst stimulation after application of 100Hz tetani (Seo et al., 2021), the animals used in those studies were older with different stimulation protocols, indicating that aged AD animals might possess different mechanisms for LTP establishment.

The induction of LTP is commonly seen as a post-synaptic process involving the insertion of AMPA or NMDA receptors (Harris et al., 1984). The establishment of LTP requires influx of $Ca^{2+}$ via these excitatory glutamatergic ion channels to trigger cascades of events in the post-synaptic terminal (Lynch et al., 1983, Grover and Teyler, 1990). One of the commonly accepted perspectives is that pathological levels of aberrant Aβ could impair LTP by indirectly blocking NMDARs (Palop and Mucke, 2010). Aβ may also affect the surface expression of NMDARs and their conductance to suppress NMDAR-dependent LTP (Li et al., 2009, Snyder et al., 2005, Raymond et al., 2003).

LTP could also be induced via routes other than glutamatergic receptors, depending on the employment of specific stimulating protocols. For LTP that is induced with intermediate stimulation frequencies (25-100Hz) application of the NMDA receptor antagonist D,L-2-amino-5-phosphonovalerate (D,L-APV) could completely block LTP induction (Grover and Teyler, 1990). However, with a higher frequency of 200Hz, APV-resistant LTP could be induced, which acts independently from NMDA receptors and relies on activation of L-type voltage-gated $Ca^{2+}$channels located on the post-synaptic neuron (Grover and Teyler, 1990, Berridge, 2011). The stimulating protocol of LTP in this study was 5 trains of 20 stimuli at 200Hz, leading to a possibility of an induction of APV-resistant LTP in this experiment. One of the important features of APV-resistant LTP is a slightly depressed post-HFS response before the establishment of LTP (Grover and Teyler, 1990). Intriguingly, the 9-month-old TG rats in this study appeared to display this feature, where at the first 10 mins of post-HFS recording, the LTP magnitude was not significantly different from the baseline, but it increased and stabilised from the second 10min of post-HFS recording. This observation is fascinating because it could suggest the possibility of a compensatory mechanism to support LTP bypassing the NMDA receptors in the 9-month-old TG rats at CA3-CA1 synapse.

One of the routes for generating LTD phenomenon is by endocytosis of post-synaptic AMPA receptors via receptor trafficking and phosphorylation (Malenka and Bear, 2004). The activation of extrasynaptic NMDARs (NR2B-enriched NMDARs) is important for LTD induction (Taylor et al., 2021, Papouin et al., 2012). Levels of NMDAR subunits NR2A and NR2B in the dorsal hippocampus of the 6- and 9-month-old animals in this study will be measured in **Chapter 4 Section 4.3.4**. The changes of post-synaptic receptor function could be a result of Aβ (Palop and Mucke, 2010) as Aβ oligomers increase the probability of neurotransmitter release at the CA3-CA1 synapse (Taylor et al., 2021). LTD induction could also occur via

metabotropic glutamate receptors (mGluRs), depending on the choice of stimulation protocols (Taylor et al., 2021, Malenka and Bear, 2004, Liu et al., 2004, Li et al., 2009).

In the 6-month-old animals in this study, 900 stimuli of 1Hz LFS was delivered to induce NMDAR-dependent LTD (or depotentiation) after the post-HFS recordings, and the TG animals showed a significantly smaller magnitude of post-LFS response than the WT. Although from one-sample t-test, the averaged 30-minute post-LFS response did not significantly differ from baseline in the WT animals, nor did it drop below baseline in the TG animals, the 6-month-old TG rats still exhibited increased LTD response compared to WT. This finding suggests stronger depotentiation in TG animals with elevated pathological Aβ levels and agrees with many other studies (Cohen et al., 2013, Mango et al., 2019). Opposite to LTP that is associated with spine formation and strengthening of learning and memory, LTD is associated with shrinkage of dendritic spines and thus being a model of forgetting (Li et al., 2009). Therefore, stronger depotentiation in TG rats may be consistent with increased forgetting in AD patients.

Electrical-evoked LTD is enhanced in the CA1 region by soluble Aβ oligomers from various sources (Li et al., 2009). In acute hippocampal slices, NMDAR-dependent LTD was enhanced by 50nM Aβ oligomers (Taylor et al., 2021), where the concentration was reported to be sufficient to block CA1 LTP (Rammes et al., 2011). Although many reports claim enhanced LTD in the AD transgenic animals in hippocampal slides (Palop and Mucke, 2010), one report suggested that depotentiation was unchanged in CA1 in 14-month-old APP/PS1 mice (Faldini et al., 2019). However, in the THY-Tau22 model for tauopathy, LTD depotentiation was found to be facilitated in hippocampal slices, suggesting that enhanced NMDAR-dependent depotentiation might be facilitated by hyperphosphorylation of tau (Faldini et al., 2019). Indeed, experiments that induce LTD *in vitro* using chemicals and *in vivo* with optogenetic

method were found to increase hyperphosphorylated tau (Taylor et al., 2021). These findings bring together a possible link between Aβ oligomer and tauopathy via the mechanism underlying enhanced LTD (Taylor et al., 2021). Also, there could be regional differences, as in cerebellar brain slices where LTD failed to induce in 8-month-old APP/PS1 mice but not the wildtype controls (Kuwabara et al., 2014).

Compared to hippocampal slices, LTD or LTD-like depotentiation has not been tested intensively *in vivo*. Yet interestingly, *in vivo* LTD could be robustly induced by a weak LFS protocol (300 pulses at 1 Hz at 95% maximum output) in hippocampal CA1 two weeks after the injection of synthetic soluble Aβ in the ventricle, which was not induced in the vehicle-treated rats (Hu et al., 2022). Aβ was suggested to increase the amount of LTD by blocking synaptic glutamate uptake, leading to an overflow of glutamate and abnormal activation of NMDAR-2B receptors located extrasynaptically, as well as mGluRs (Kazim et al., 2021, Li et al., 2009, Hsieh et al., 2006, Matos et al., 2008, Varga et al., 2014). Notably, the selective mGluR5 antagonist MTEP was found to rescue this pathologically facilitated LTD in the soluble Aβ-injected animals, suggesting that even though LTD can be induced via different routes, their pathological mechanisms could be surprisingly converged (Hu et al., 2022).

### 2.3.4. Calcium hypothesis of Alzheimer's disease

It is worth noticing that, apart from extracellular $Ca^{2+}$ passing through dendritic NMDARs to trigger a serine-threonine protein phosphatase cascade for activating endocytosis of post-synaptic receptors (Mulkey and Malenka, 1992, Malenka and Bear, 2004), intracellular $Ca^{2+}$is also a crucial source for the signalling of LTD induction (Berridge, 2011). Importantly, pathological Aβ, particularly the oligomeric forms, could alter the action of intracellular

$Ca^{2+}$signalling (Berridge, 2011). It is hypothesised that a prolonged increase of intraneuronal resting $Ca^{2+}$ concentration that might result from amyloid pathology could lead to enhancement of LTD, which could negatively affect memory consolidation (Berridge, 2011, Berridge, 2010, Kuchibhotla et al., 2008). Indeed, the intraneuronal $Ca^{2+}$concentration was significantly elevated in the 3xTg-AD mice compared to corresponding wild-type mice (Lopez et al., 2008) in young, adult and old mice along the lifespan (Stutzmann et al., 2006). Also surprisingly, the PS1 mutation, but not mutations in APP or Tau, may augment intracellular $Ca^{2+}$concentration from the ER via the inositol trisphosphate ($IP_3$) and ryanodine receptors (RYR) (Berridge, 2011, Stutzmann et al., 2006). Given that the TgF344-AD model also expresses human PS1 mutations, there might be a potential contribution of PS1 pathology through alteration of calcium homeostasis and failure of lysosomal acidification for synaptic dysfunction (McBrayer and Nixon, 2013, Berridge, 2011). Although from the current set of experiments it is rather difficult to confirm a direct contribution of intracellular $Ca^{2+}$ levels to synaptic function (or direct contribution of Aβ on intracellular calcium), taking into consideration the LTP/LTD deficits and the 9-month-old PPF ratio, dysfunction in intracellular $Ca^{2+}$ signalling may play a role in AD progression as an effect of amyloidosis in the early stage.

### 2.3.5. Hippocampal hyperexcitability and GABAergic disinhibition

Another major perspective to synaptic deficits at the early stage of AD is that of synaptic hyperexcitability and disinhibition of the GABAergic input (Hector and Brouillette, 2020, McGarrity et al., 2017). Rather than hypoactivity, more recent evidence has pointed to neuronal hyperactivity due to less inhibition instead of more glutamatergic excitation due to soluble Aβ oligomers (Hector and Brouillette, 2020, Zott et al., 2018). In the hippocampus,

CA1 pyramidal neurons receive excitatory input from CA3 principal cells via Schaffer collateral pathway and inhibitory modulation by the interneurons in the local microcircuitry in CA3 (Varga et al., 2014).

Direct hippocampal hyperexcitability evidence comes from brain imaging and clinical observations. Patients with amnestic mild cognitive impairment (aMCI), a prodromal stage of AD, frequently show excessive hippocampal DG/CA3 activity during memory tasks imaged by high resolution fMRI scans (Bakker et al., 2012, Setti et al., 2017). Additionally, many studies have suggested a link between AD and epilepsy, the abnormal increase of neuronal firing (Vossel et al., 2017, Friedman et al., 2012). Patients with severe AD appeared to be more vulnerable to epilepsy and more prone to develop epileptic-like symptoms, suggesting aberrant synaptic hyperexcitability in advanced AD brains (Pandis and Scarmeas, 2012). Moreover, AD patients with seizure or subclinical epileptiform activity could accelerate in a decline of memory and cognition (Vossel et al., 2017).

Hippocampal synaptic hyperexcitability has also been observed in a number of preclinical models of AD. For example, both young and old 3xTg mice displayed stronger *in vivo* PPF in the CA1 region of hippocampus (Davis et al., 2014). A significantly larger LTP response was equally observed in 3xTg mice (Zhu, 2019). Moreover, in old cognitively impaired Tg2576 mice aged from 14- to 19-month-old, the previously diminished *in vivo* LTP was found to re-emerge (Huh et al., 2016, Townsend et al., 2010). This observation suggests that abnormally increased LTP in the aged Tg2576 mice might cause a gradual decline of short-term recognition memory, instead of enhancing it. In sum, these findings supported the existence of abnormal hippocampal hyperexcitability in preclinical models for AD research, especially in older individuals, that has a strong concordance with fMRI data in patients.

However, although decreased PPF was found in the 9-month-old TG rats in this experiment, the reduced PPF ratio could be because the P1 response was too big for further facilitation. Considering the large fEPSP in the 9-month-old TG rats with their upwardly-shifted I/O curve, it is possible that there was an enhancement of the neurotransmitter release in these animals, probably via increased number of synaptic vesicles or dysfunction of releasing proteins in the presynaptic neuron (Bartholome et al., 2017, Wojcik et al., 2004). The massively increased fEPSP might also be a consequence of presynaptic disinhibition, where the pre-synaptic neurons could be less inhibited by GABAergic interneurons (McGarrity et al., 2017).

The disinhibition of GABAergic interneurons has gradually become a popular explanation for synaptic dysfunction associated with Aβ-induced cognitive decline (McGarrity et al., 2017). Notably, Huh et al. (2016) suggested that aberrant LTP re-emerged in the aged Tg2576 mice and could be attributed to a loss of parvalbumin (PV) interneurons, which is a type of GABAergic inhibitory neuron preventing over-excitation of pyramidal cells in the hippocampal CA1 region and elsewhere (Huh et al., 2016, Palop and Mucke, 2010). Hence, it is possible that synaptic hyperexcitability in this study was a result of PV interneuron loss. In another study, direct application of Aβ also reduces the synaptic transmission of GABAergic neurons (Ulrich, 2015). These studies support the idea that presynaptic disinhibition would trigger hyperexcitability in the 9-month-old TG rats, perhaps due to loss of PV $GABA_A$ receptors or even the inhibitory interneurons themselves where the proteins and receptors locate. PV protein levels and density in dorsal hippocampus of will be measured in **Chapter 4, Section 4.3.2**.

### 2.3.6. Hippocampal hyperexcitability and population spikes

While fEPSPs are considered as the input to the neural network, the spiking rate are recognised as the output of this network (Varga et al., 2014). To assess the output excitability of hippocampal CA1 pyramidal neurons, the probability of evoked population spikes was calculated under the I/O protocol in the 6- and 9-month-old animals. The more frequent the appearance of a population spike, the more excitable the CA1 neurons would be, due to increasing evoked spiking frequency in the CA3-CA1 circuit (EPSP to spike conversion).

In this study, 6-month-old TG rats showed a tendency to be more likely to produce a population spike, especially to P2 post-HFS and post-LFS, under high current stimulations. The significant two-way RM ANOVA effect on genotype provided further evidence of an augmentation of hippocampal excitability in the 9-month-old TG animals, after HFS in P2. These results concur with those in mouse brain slices incubated with synthetic $A\beta_{42}$ oligomers (BAM10 sequence specific positive and OC conformational specific positive antibodies) which showed increased spontaneous firing rate in hippocampal CA1 (Varga et al., 2014). Also, $A\beta_{42}$ has the effect of increasing neuronal firing rate by inducing *in vitro* and *in vivo* epileptiform activity and seizures in mice (Marc Aurel et al., 2012, Minkeviciene et al., 2009). Additionally, $Ca^{2+}$ imaging revealed increased transient frequency hyperactivity of CA1 pyramidal neurons in McGill-R-Thy1-APP rats with amyloidosis at 6-9 months old (Sosulina et al., 2021). The evoked firing, or CA1 population spikes, involves the fast-actioning AMPARs (Varga et al., 2014, Wood and Tattersall, 2001). It is worth noting that the spontaneous neuronal firing rate in hippocampal CA1 region was not meditated by AMPARs, but rather NMDARs, especially extra-synaptic NR2Bs that has a higher affinity than synaptic NR2As (Varga et al., 2014).

Compared with other studies, it is difficult to confirm the origin of CA1 hyperexcitability observed in this study with a simple calculation of the probability to have population spikes. Whether CA1 hyperexcitability comes from changes in dorsal hippocampal CA1 microcircuitry, or upstream CA3 synaptic disinhibition, or intrinsic alterations of the receptors on CA1 pyramidal cells, needs further investigation. Yet, it is still reasonably clear that the current results indicate hyperexcitable hippocampal CA1 pyramidal cells in 9-month-old TG animals, with enhanced evoked population spike firing at the CA3-CA1 synapse. Further studies could be carried out on the features of these evoked population spikes for their amplitude, size, as well as frequency (whether there are and how many multiple population spikes embedded in one fEPSP).

### 2.3.7. Limitations and improvements

Notably, during the recording time, if the animals were in slow oscillation state, neuronal excitability could vary. Therefore, the depth of anaesthesia could also be monitored throughout the recording process including the usage of oximeter, which was lacking in this set of experiments.

Next, one might notice that the statistical analysis results were varying if calculated with slope or amplitude measurement. For example, it is easily spotted that the maximum output at 6 months of age measured with amplitude and slope gave rise to the same conclusion, whereas at 9-month-old time point, the maximum output was different if measured with slope but not amplitude, thus, giving rise to different conclusions. Similar variation could also be noticed in the current for 50% output (measured with slope or amplitude) that is calculated *post hoc* from Gompertz fit compared to the experimentally determined results. This variation in slope

and amplitude measurement could be one of the biggest sources of uncertainty. Admittedly, the maximum initial slope is usually favoured because it could to a large extent reflect the authentic fEPSP response, whereas the amplitude measurement is thought to be less reliable due to contamination of population spikes and feedforward inhibitory conductance. From the practical experience in this set of experiments, population spikes could be observed more frequently under currents exceeding 200uA and post-HFS. At low current input, especially 25uA, fEPSPs were small as near threshold, making slope measurement less reliable than amplitude. Indeed, the MATLAB script used in this evoked response study displayed the original data from the Plexon software acquisition instead of filtered waveforms that are free from influence of spontaneous oscillations. Practically, if the displayed waveform fluctuated highly, the slope measurement from this MATLAB script could be more varying, potentially causing variations in statistical analysis and further calculations However, averaging across 20 repeats for each measure may mitigate the influence of a few noisy responses.

In terms of the experimental design, the LFS-induced depotentiation was only investigated in the 6-month-old animals. Whether the *in vivo* hippocampal LTD in experimental models could change in an age-dependent manner would be another question to answer. Therefore, investigating LTD-depotentiation in 9-month-old rats is an important next step.

## 2.4. Conclusion

This study has examined the *in vivo* short- and long-term synaptic functions and connectivity at the CA3-CA1 synapse in the dorsal hippocampus of the TgF344-AD model at 6 and 9 months of age. While long-term plasticity in TG was impaired at both ages, deficits of short-term plasticity appeared at 9 months old, with increased baseline connectivity in TG rats at this age.

One of the more important findings emerging from this study is that enhanced LTD appeared in the 6-month-old TG rats. Overall, these findings strongly indicate *in vivo* synaptic dysfunction at the Schaffer collateral in animals at early stage of AD. Not only was the input to CA1 pyramidal neurons impaired with CA3-CA1 synaptic dysfunction, the output from CA1 pyramidal neurons was also hyperexcitable in the TG animals, especially at 9 months of age. Despite a further analysis to clarify whether corresponding LTD deficits also exist in older TG animals, post-mortem tissue analysis on synaptic markers and circuit modulators is required to understand a possible mechanism for the synaptic dysfunction in these TG animals associated with aberrant Aβ accumulation in dorsal hippocampus.

# Chapter 3. *In vivo* electrophysiology – evoked responses in dentate gyrus in dorsal hippocampus

## 3.1. Introduction

Dentate gyrus (DG) can be seen as the entrance to the hippocampus for information from entorhinal cortex (Scharfman, 2007). Thus, DG granule cells receive excitatory inputs from layer II of entorhinal cortex (EC) via the perforant path and DG output then flows to CA3 principal cells via mossy fibres (Clark and Squire, 2013). As the entrance point to hippocampus, DG is important in spatial memory encoding or learning by converting grid-like firing of the EC to place-like firing (Rolls, 2013). DG plays a key role in supporting spatial pattern separation, which is the ability to distinguish two similar experience, which is impaired in patients with mild cognitive impairment (MCI) (Kesner and Rolls, 2015, Rolls, 2013, Yassa et al., 2010). By receiving information from DG, CA3 principal cells are important in pattern completion and rapid learning (Rolls, 2013).

Normally, DG granule cells contact CA3 *stratum lucidum* at their thorny excrescent spines with giant mossy fibre boutons, delivering monosynaptic excitatory postsynaptic inputs (Pan et al., 2022). They also connect with CA3 neurons via a disynaptic inhibitory input by firstly innervating an interneuron with a filopodial extension on the mossy fibre to complete a feedforward inhibitory circuit (Pan et al., 2022, Zucca et al., 2017). However, it is suggested that CA3 principal cells 'back-project' to the DG and that CA3 might be a major gateway to hippocampus (Scharfman, 2007). Anatomically, CA3c cells are closely adjacent to DG, and robust back-projections between ventral hippocampus and CA3c cells have been found in adult rats (Scharfman, 2007). CA3 back-projection was found to innervate hilar neurons, although a direct physiological innervation of CA3 neurons to DG granule cells has not been found yet (Scharfman, 2007).The CA3 back-projection to DG is thought to be primarily inhibitory, which may subserve a key role in prevention of temporal lateral epilepsy where hilar GABAergic inhibitory cells are damaged (Scharfman, 2007).

In Chapter 2, the Schaffer collateral pathway from CA3 was activated and fEPSPs were recorded in the recipient CA1 region with multichannel electrodes. The electrodes used in these experiments were sufficiently long to cover the entire CA1 *stratum radiatum*. In some cases, the electrodes reached the DG, so simultaneous CA1 and DG recordings were possible. The CA3→CA1 responses were negative in CA1, whereas the responses recorded in the DG was positive, which is consistent with the current source of fEPSPs being often the most reliably-encountered response component across the laminar profile of CA1 and DG, for example, following perforant path activation.

Therefore, to study whether changes in short- and long-term plasticity also happened in the CA3→DG circuit in the same TG animals that showed deficits in CA3→CA1 pathway (**Chapter 2**), fEPSPs in DG were measured and analysed. Specifically, the 6-month-old PPF and LTP/LTD, as well as 9-month-old LTP in the TgF344-AD rats and age-matched wildtype animals were analysed for this pilot study.

## 3.2. Methods and Materials

Because the DG response were simultaneously acquired when obtaining the CA1 responses on the same recording electrode, the surgery, recording methods and stimulating protocols were the same as used in **Chapter 2.2**. DG responses had positive waveforms (**Chapter 2, Figure 2.3**), and the DG data were analysed for PPF, LTP/LTD in the 6-month-old rats, and LTP in the 9-month-old rats. Statistical analysis was the same as **Chapter 2.2.3** for PPF and LTP/LTD. Note that the LTD (or depotentiation) was only recorded in the 6-month-old animals due to experimental progresses, and thus in the 9-month-old animals, only LTP data were presented.

## 3.3. Results

The evoked CA3 response was simultaneously recorded in the DG of the same animals **(Chapter 2, Figure 2.1)**. The biggest positive DG responses were selected for each animal for the analysis. Then changes in PPF, LTP/LTD in the 6-month-old rats and LTP in the 9-month-old rats were analysed for this Chapter.

### 3.3.1. No change in PPF in dentate gyrus of the 6-month-old rats

To study short-term plasticity of the CA3→DG back-projection in the DG of 6-month-old WT and TG rats, paired pulses were delivered at 50% maximum output current with a range of inter-pulse intervals (IPIs) before and after HFS. Slope and amplitude of the paired responses were measured. Percentage of facilitation in P2 was calculated under the slope and amplitude measures. As the focus of the work was on CA3→CA1 plasticity, we chose the 50% current value for DG recordings from the CA3→CA1 baseline I/O analysis.

Similar statistical results were found using the slope and amplitude measurements **(Figure 3.1)**. Three-way ANOVA showed no genotype differences (slope: $P=0.4207$; amplitude: $P=0.4237$) or interaction for genotype x HFS (slope: $P=0.6373$; amplitude: $P=0.4171$), or genotype x IPI (slope: $P=0.1955$; amplitude: $P=0.2167$). There were significant differences in the IPI (slope: $P<0.0001$; amplitude: $P<0.0001$) and HFS (slope: $P<0.0001$; amplitude: $P<0.0001$) revealed by three-way ANOVA, but no interaction was found for these three factors together (genotype x IPI x HFS: slope: $P=0.5166$; amplitude: $P=0.2687$). There was a general trend for PPF to be larger in TG rats for both slope and amplitude at short baseline IPIs (**Figure 3.1**).

The *post hoc* Tukey's multiple comparison showed that significant differences within each genotype appeared at short IPIs of 25ms, 50ms and 100ms for both slope and amplitude measures. For both WT and TG rats, the baseline PPF was significantly larger than that after HFS at 25ms (slope: WT: P=0.0003, TG: P<0.0001; amplitude: WT: P<0.0001, TG: P<0.0001), 50ms (slope: WT: P=0.0003, TG: P<0.0001; amplitude: WT: P<0.0001, TG: P<0.0001) and 100ms (slope: WT: P=0.0005, TG: P=0.0012; amplitude: WT: P<0.0001, TG: P<0.0001) (**Figure 3.1**).

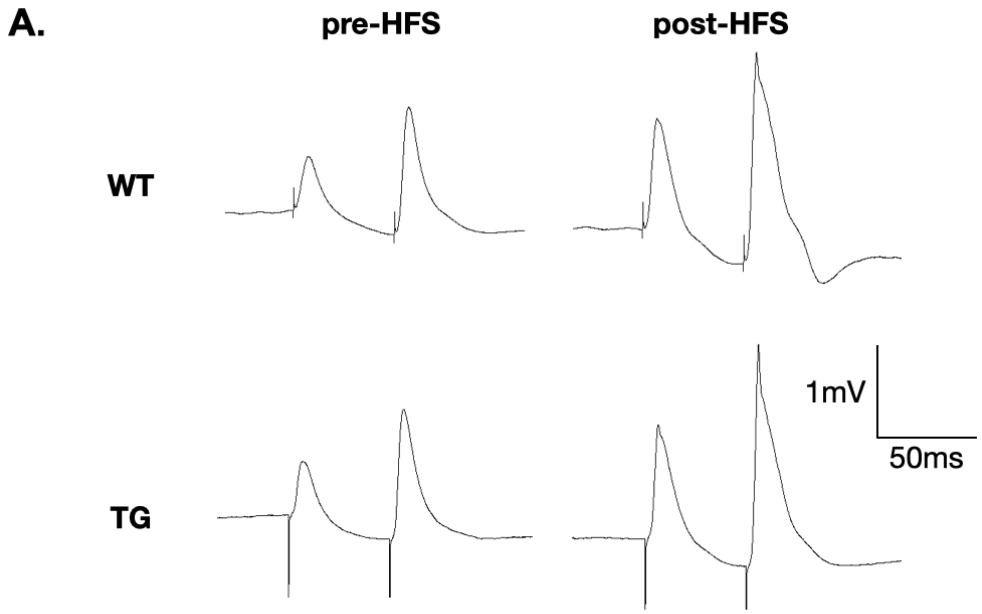

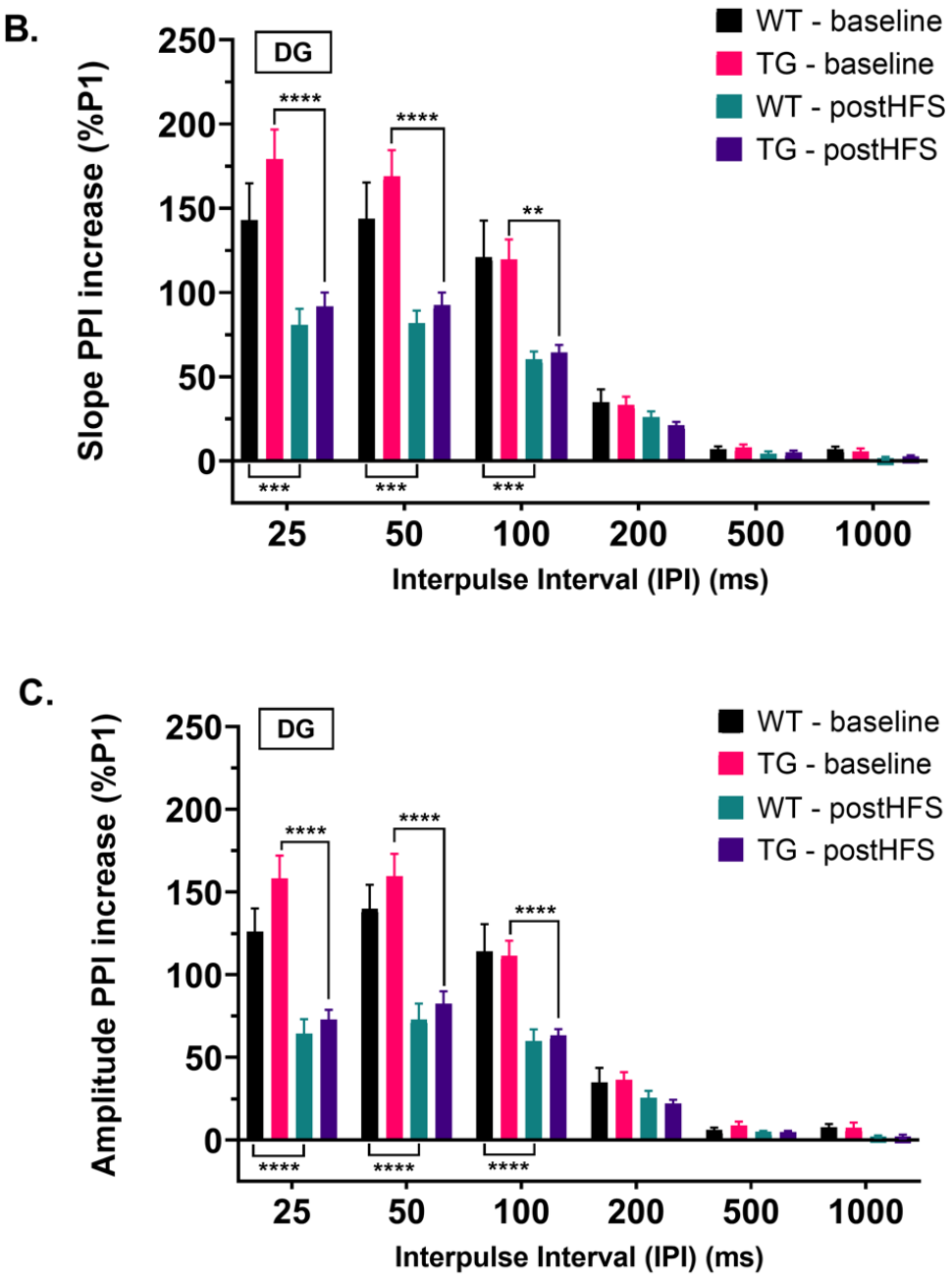


***Figure 3.1. No genotype difference in paired-pulse facilitation in DG in 6-month-old rats.***

*Paired pulses were delivered at a current that gave 50% output. fEPSPs were recorded at DG by the stimulation at CA3.* ***(A)*** *Examples of fEPSP traces before and after HFS of a randomly selected 6-month-old rat from each group in DG.* ***(B)*** *Slope and* ***(C)*** *amplitude of the paired responses were measured. Three-way ANOVA followed by Tukey's multiple comparisons test were carried out. WT: n=10, TG: n=11. Data presented as mean±SEM. **p<0.01, ***p<0.001, ****p<0.0001.*

### 3.3.2. 6-month-old rats showed no genotype difference in LTP/LTD in dentate gyrus

To study the changes in long-term plasticity of the CA3→DG circuit, HFS-induced LTP and LFS-induced depotentiation were recorded and measured in DG when stimulating CA3 neurons in the 6-month-old WT and TG rats **(Figure 3.2.A, 3.2.B)**. Similar results were obtained with slope and amplitude measures. Two-way ANOVA showed significant effect of stimulation (HFS or LFS) (slope & amplitude: $P<0.0001$), but no effect of genotype (slope: $P=0.0964$; amplitude: $P=0.1257$) or interaction (slope: $P=0.0863$; amplitude: $P=0.1314$).

Bonferroni multiple comparison further revealed that, in the 6-month-old WT animals, the post-HFS response was significantly greater compared to baseline (slope: $P<0.0001$; amplitude: $P<0.0001$) and post-LFS (slope: $P=0.0033$; amplitude: $P<0.0001$) **(Figure 3.2)**. Also, the post-LFS response was statistically larger than baseline P1 fEPSPs in WT rats (slope: $P=0.0130$; amplitude: $P=0.0440$) **(Figure 3.2)**. Within the TG group, the post-HFS responses were also significantly greater compared to that of the baseline (slope: $P=0.0002$; amplitude: $P<0.0001$) and post-LFS (slope: $P=0.0002$; amplitude: $P<0.0001$), as shown by the Bonferroni's *post hoc* test **(Figure 3.2)**. However, no difference between P1 fEPSP at post-LFS was found when comparing the P1 fEPSP at baseline ($P>0.9999$) in the TG animals, suggesting complete depotentiation of LTP. Additionally, although in the scatter plots that the post-LFS responses of the TG rats was below that of the WTs, there was no statistical differences between the genotypes, although p-value was close to 0.05 for slope (slope: $P=0.0641$; amplitude: $P=0.0821$).

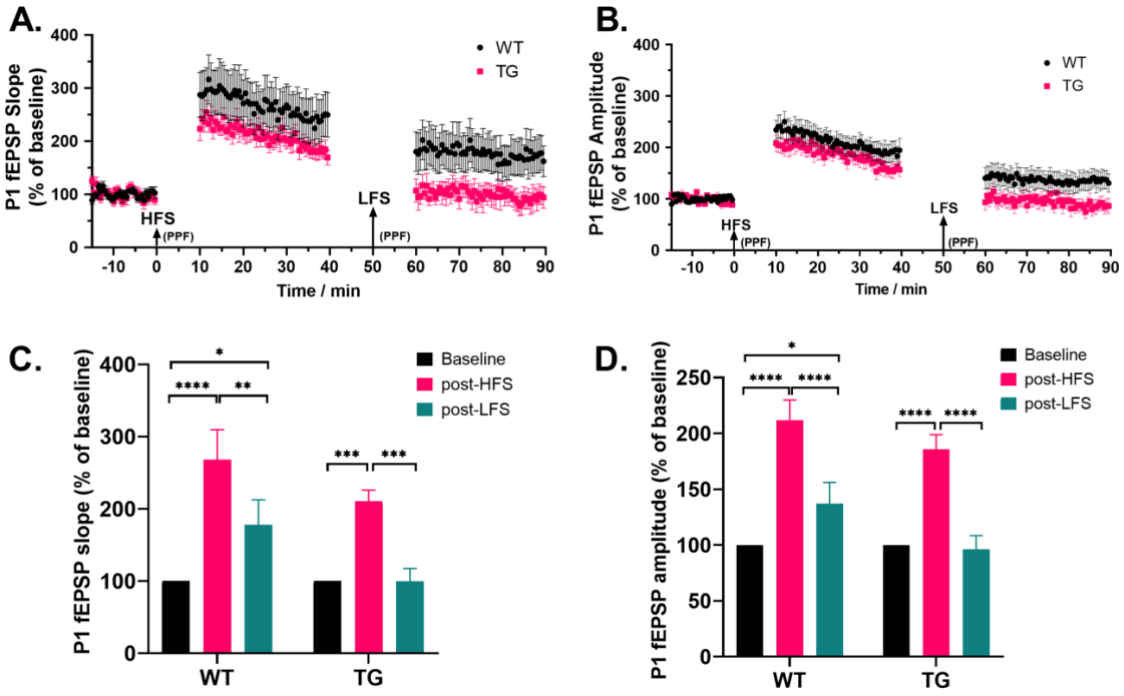


***Figure 3.2. No genotype changes in HFS-induced long-term potentiation or LFS-induced depotentiation in DG of 6-month-old rats.***

*Scatter plots of CA3→DG evoked-excitatory post-synaptic potential (fEPSP) for* ***(A)*** *slope and* ***(B)*** *amplitude during experimental time course. Statistical comparisons were made for the averaged fEPSP at the baseline, after HFS and after LFS for* ***(C)*** *slope and* ***(D)*** *amplitude. WT: n=10, TG: n=11. Data presented as mean±SEM. *p<0.05, **p<0.01, ***p<0.001, ****p<0.0001.*

### 3.3.3. 9-month-old rats showed no genotype difference in LTP at dentate gyrus

To further investigate any age-related changes in long-term plasticity of the CA3→DG circuit, the *in vivo* HFS-induced LTP was recorded in the 9-month-old rats in the DG. The P1 fEPSPs were analysed with the measures of slope and amplitude **(Figure 3.3)**. The results with both slope and amplitude measurements were similar. Shown by two-way repeated-measures ANOVA, there was a significant effect of HFS (slope: P=0.0002; amplitude: P=0.0002), but no effect of genotype (slope: P= 0.8367; amplitude: P=0.9806) and no interaction (genotype x HFS: slope: P= 0.8367; amplitude: P= 0.9806). *Post hoc* Bonferroni's multiple comparison showed that the post-HFS response of both WT (slope: P=0.0070; amplitude: P=0.0050) and

TG (slope: P=0.0041; amplitude: P= 0.0054) rats were significantly higher compared to baseline (**Figure 3.3.C, 3.3.D**). However, there was no difference between genotype post-HFS measured with slope or amplitude (P>0.9999).

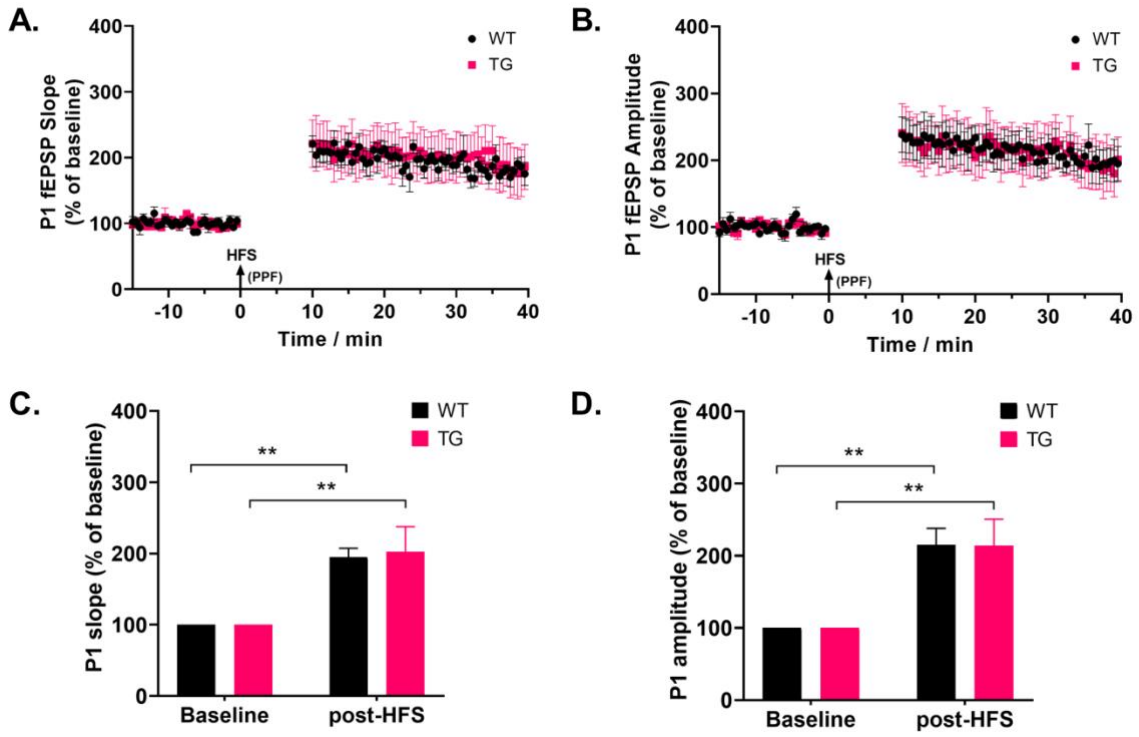


***Figure 3.3. No genotype difference in long-term potentiation in DG of 9-month-old rats.***

*Scatter plots for CA3-evoked DG fEPSPs as measured with **(A)** slope and **(B)** amplitude. LTP magnitude averaged in the entire 30mins post-HFS recording period measured with **(C)** slope and **(D)** amplitude. n=7 per group. Data presented as mean±SEM. **p<0.01.*

## 3.4. Discussion

To study changes in short- and long-term synaptic plasticity in the CA3→DG back-projection at the early-stages of AD-like pathology, DG responses that were simultaneously recorded alongside those in CA1 following CA3 stimulation were analysed. Briefly, there was no effect of genotype for PPF at 6 months of age, and no statistical differences were found in long-term plasticity between WT and TG rats at either 6 or 9 months old. The finding in 6-month-old PPF

was comparable to the observations in the CA1 of the same animals. However, this observation that long-term plasticity was not significantly impaired in the back-projection to DG but was changed in the Schaffer collateral pathway to CA1 at both ages (in the same animals at the same time) suggests that the impact of amyloid might differ across the hippocampus (Hyman et al., 1984, Reilly et al., 2003, Braak and Braak, 1996, Braak and Braak, 1991). However, spontaneous oscillations in CA1 and DG should be analysed for changes to eliminate the effect of multiple connections into CA1 and DG. Nevertheless, the difference in CA1 and DG responses provides a reliable internal control where the changes in CA1 is because of the synaptic deficits instead of non-specific effect such as that of the anaesthesia.

Yet notedly, the 6-month-old TG rats showed greater magnitude of depotentiation from the scatter plot, especially using the slope measurements (**Figure 3.2.A**), although no genotype differences were detected with the *post hoc* multiple comparison. This could suggest a potential enhancement of LTD in the 6-month-old TG rats at the CA3→DG circuit, too.

Equally interestingly, the impaired LTP observed in CA1 of the TG animals at both ages (**Chapter 2**) was not reflected in the DG. Moreover, the magnitude of LTP induction in DG of the 9-month-old TG rats is highly similar to that of the WT, whereas the LTP magnitude of the 6-month-old animals was below that of the WTs at trend level. These observations are in agreement with the findings in Tg2576 mice, where the impaired LTP in the hippocampal Schaffer collateral pathway at 6-7 months old re-emerged when they were aged (14-19mo) (Huh et al., 2016). The re-emerged LTP was not able to be suppressed by inhibitor of ErbB receptor due to loss of PV interneurons, where PV expression was significantly lower in the aged Tg2576 mice in CA1-3 region (Huh et al., 2016). In the TgF344-AD model in this study,

PV interneuron density was reduced in CA2/3 at 9 months of age but not 6 months, suggesting that the unimpaired CA3→DG LTP here might not be a normal one.

As the DG receives direct excitatory input from layer II of EC (Clark and Squire, 2013), the activation of CA1 pyramidal cells by stimulating CA3 could also affect the transfer of synaptic signals to the downstream regions including EC (particularly at current intensities that produce populations spikes in CA1). Also, the CA3 back-projection to DG is more profound in ventral hippocampus (Scharfman, 2007), whereas here the recordings were in the dorsal hippocampus. Therefore, the responses in DG in this experiment could be a complex combination of signals from CA3 and EC when recording the field responses. A direct measure of CA3→DG plasticity should be made with more precise methods such as whole-cell patch clamp or silencing of EC layer II during CA3 stimulation (Tennant et al., 2018).

Despite a limitation of the precision of the recording for a direct measure of CA3→DG circuit, these results provide the first *in vivo* evidence of the CA3→DG plasticity in the AD model at the early stage. More importantly, the DG fEPSPs were recorded in the same animals that have synaptic deficits in the CA3→CA1 circuits as well as the loss of PV interneurons (measured in **Chapter 4, Section 4.3.2**).

## 3.5. Conclusion

In summary, there were no significant changes by genotype in short- and long-term plasticity at the CA3→DG back-projection in the 6-month-old animals, and no alteration of long-term plasticity in the 9-month-old TG animals, which appeared to have synaptic dysfunction in the CA1 region *in vivo*. However, further investigations should be done on the properties of this

circuit with pharmacological blockade using precise recording methods, in order to understand its role and function in early AD.

# Chapter 4. Post-mortem tissue analysis

## 4.1. Introduction

In the previous chapters, the *in vivo* electrophysiological properties were examined in the 6- and 9-month-old TG rats and their age-matched wild-type controls. Changes appeared in the TG animals predominantly at 9 months of age in terms of short- and long-term plasticity and baseline connectivity. Hyperactivation of the hippocampal CA1 was also revealed by the increased population spike probability post-HFS at P2. However, the underlying molecular causes of these observations remain unclear. Also, the levels of AD hallmarks, including soluble Aβ oligomers and neuroinflammation, are also unknown at the age tested here. Therefore, this chapter studies a range of pathologies regarding prodromal stages of AD, investigating changes in levels of synaptic, GABAergic and glutamatergic markers, as well as neuroinflammation.

### 4.1.1. GABAergic inhibition by parvalbumin interneurons

CA1 pyramidal neurons increase their firing rate to encode spatial information depending on the excitatory inputs (Oren and Kullmann, 2012). However, the input/output of hippocampal circuits can also be finely modulated by GABAergic inhibition via more than 20 types of interneurons (Oren and Kullmann, 2012, Nahar et al., 2021). They can be subclassified based on their expression of particular proteins, including parvalbumin (PV), somatostatin (SOM), vasoactive intestinal peptide (VIP), neuropeptide Y (NPY), and cholecystokinin (CCK) (Nahar et al., 2021).

PV is a 12kDa calcium binding protein, also known as a $Ca^{2+}$ buffer, to regulate intracellular $Ca^{2+}$ concentration to protect mitochondria and other cytosolic functions from $Ca^{2+}$ overload (Andrioli et al., 2007, Caccavano et al., 2020, Caillard et al., 2000). Other $Ca^{2+}$ buffers include

calbindin D-28k, and calretinin (Caillard et al., 2000). Within these $Ca^{2+}$ buffers, there is evidence for a loss of parvalbumin in AD (Mahar et al., 2016). Strong synapses, modulated by GABAergic inhibition can be formed between the basket and bistratified PV interneurons and the glutamatergic pyramidal cells via feedforward inhibition to prevent hypersynchronicity and hyperactivity in the hippocampus (Ruden et al., 2021, Keith and El-Husseini, 2008, Ferrante and Ascoli, 2015), whereby this connection could contribute to a variety of cognitive functions, depending on the regions that they are located (Olah et al., 2022, Yao et al., 2020).

PV interneurons are a type of fast-spiking interneuron that are found in multiple regions of the brain, including the hippocampus and cortices (Nahar et al., 2021). In the hippocampus, PV interneurons only comprise a small percentage of the neuronal population, however, they control and maintain the balance of the microcircuitry with the glutamatergic pyramidal cells of hippocampal subregions, by stabilising communication between CA1 neurons, and through lateral inhibition of the granular cells in DG (Nahar et al., 2021). PV interneurons can be classified into basket, bistratified and axo-axonic (chandelier) cells, which are located around the *stratum pyramidale* (s.p) layer of the hippocampus and innervate the local pyramidal cells (Nahar et al., 2021, Pelkey et al., 2017). These subtypes may have different targets and functions and may contribute to events differently. For example, PV basket cells primarily activate the pyramidal neurons at soma and proximal dendrite, whereas chandelier cells innervate postsynaptic pyramidal neurons at the initial segment of axon (Pelkey et al., 2017). Also, in young 5xFAD mice, only basket cells showed a reduction of spike rate during sharp wave ripples (SWRs), with no change in the other PV types (Caccavano et al., 2020).

PV interneurons play a pivotal role in many neurological diseases such as schizophrenia, autism spectrum disorders, epilepsy, and AD (Nahar et al., 2021). Failure in activation of PV

interneurons was found in schizophrenia and autism, leading to a reduction of GABAergic inhibitory function in these diseases (Nahar et al., 2021). Loss of PV interneurons has been observed in epileptic patients in the DG (Andrioli et al., 2007). Interestingly, many patients with AD at the early stage also appear to have epileptic-like activities and a shift of the E/I balance towards excitation. In the 5xFAD model at the early stage (2-3 months), the firing of action potentials in PV interneurons was reduced in both the cortex and in the hippocampal CA1 region prior to plaque formation (Olah et al., 2022, Caccavano et al., 2020). Furthermore, in the aged 3xTg mice, the density of PV interneurons was reduced in the hippocampal CA1 region. The density of cells expressing the $Ca^{2+}$ buffer calretinin was also reduced, indicating an impairment of calcium homeostasis when AD symptomatology progressed in the animals (Zallo et al., 2018).

Because of its fast-spiking property, PV interneurons are known as a generator of gamma oscillations (20-100Hz) that are important for working memory, cognition, and information processing depending on the brain regions where they locate (Ruden et al., 2021). Reduction of slow gamma oscillation (20-50Hz) was found in the 5xFAD model for AD before the formation of plaques. Interestingly, activation of PV interneurons at 40Hz, using optogenetics, could not only diminish the production of $A\beta_{40}$ and $A\beta_{42}$ (12F4 antibody) in hippocampal CA1, but it could also recruit microglia and shift them to an activated phagocytic state (Iaccarino et al., 2016). These observations suggest gamma oscillations generated by PV interneurons could trigger the uptake of Aβ pathogens by recruiting microglia in CA1.

Taken together, these studies highlight the importance of PV interneurons in health and disease.

### 4.1.2. Synaptic markers SNAP-25 and PSD-95

AD is a disease with synaptic dysfunction and a general decrease of synaptic density has been previously reported in AD brains (Noor and Zahid, 2017, Clinton et al., 1994). Genetic transcripts for synaptic proteins are significantly downregulated in the patients in both MCI and AD (Counts et al., 2014). These transcripts include transcripts encoding for vesical trafficking and docking at the presynaptic neurons, and those regulating glutamatergic function post-synaptically (Counts et al., 2014). Therefore, two synaptic markers related to synaptic density, SNAP-25 and PSD-95 were selected to study as potential markers for changes in pre- and post-synaptic function respectively.

Synaptosomal-associated protein 25kDa (SNAP-25) is a soluble t-SNARE (target - Soluble NSF (N-ethylmaleimide-sensitive factor) Attachment Receptor) molecule located in pre-synaptic terminals of neurons on the plasma membrane (Noor and Zahid, 2017, Antonucci et al., 2016). In combination with syntaxin, that is also on the plasma membrane, and vesicle associated membrane proteins (VAMP), on the synaptic vesicle membrane, it is involved in calcium-dependent exocytosis of synaptic vesicles by interacting with regulatory proteins on the vesicle, such as synaptotagmin (Noor and Zahid, 2017, Mohrmann et al., 2013, Karmakar et al., 2019, Antonucci et al., 2016) (**Figure 4.1.A**). There are two SNARE binding sites of SNAP25, and they are responsible for vesicle docking and fusion, as well as triggering the release of neurotransmitters (Noor and Zahid, 2017, Mohrmann et al., 2013). SNAP-25 has the function of supporting memory formation by modifying its expression level at pre-synaptic terminals, where the amount of SNAP-25 was found to be directly proportional to neuronal activity (Noor and Zahid, 2017).

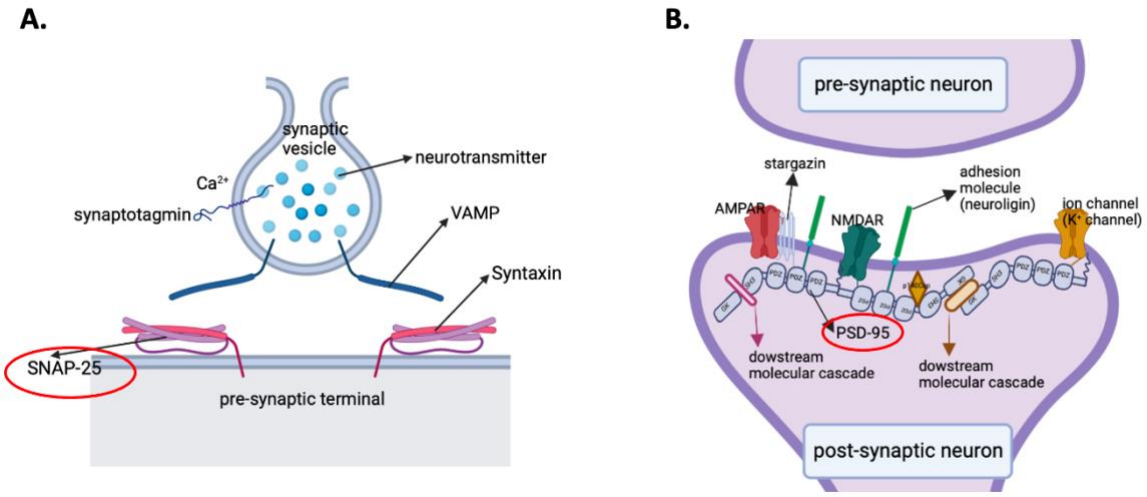


***Figure 4.1. Relative locations and function of synaptic markers SNAP-25 and PSD-95.***

***(A)*** *SNAP-25 is a pre-synaptic marker in the SNARE complex for synaptic vesicle fusion and neurotransmitter release. The SNARE complex is formed among SNAP-25, Syntaxin and VAMP. Synaptobrevin is an example of a VAMP. Membrane fusion will occur, and neurotransmitter will release when regulatory proteins, such as synaptotagmin, on the synaptic vesicle receive Ca2+ signals. VAMP = vesicle associated membrane proteins; SNAP-25 = synaptosomal-associated protein 25kDa; SNARE = soluble NSF (N-ethylmaleimide-sensitive factor) attachment receptor. Figure modified from Karmakar et al. (2019) and created with Biorender* ***(B)*** *Simplified connection of the scaffold protein PSD-95 in relation with receptors, ion channels and adhesion molecules on the post-synaptic compartment. PSD-95 = postsynaptic density protein 95; PDZ = PSD-95/Dlg/ ZO1 protiens; SH3 = Src-homology-3; GK = guanylate kinase; AMPAR = α-amino-3-hydroxy-5-methyl-4-isoxazolepropionic acid receptor; NMDAR = N-methyl-D-aspartate receptor. Figure modified from Keith & El-Husseini (2008) and created with Biorender.*

SNAP-25 plays a role in a variety of neurological disorders, ranging from schizophrenia to AD, bipolar disorder and attention deficit hyperactivity disorder (Karmakar et al., 2019, Thompson et al., 2003). The levels of SNAP-25 in the cerebrospinal fluid (CSF) showed a correlation with synaptic degeneration and the severity of AD in patients, making it a potential biomarker for early AD diagnosis (Brinkmalm et al., 2014). In AD and other dementias, such as vascular and frontal temporal dementia, there is a significant reduction of the pre-synaptic proteins SNAP-25, synaptophysin and synaptotagmin in both cortical and hippocampal tissues (Minger et al., 2001, Sinclair et al., 2015, Furuya et al., 2012). Acute down-regulation of SNAP-25 was found

to impair LTP in the hippocampal CA1 region *in vitro* and *in vivo* by reducing the spine density (Fossati et al., 2015). No change in miniature excitatory post-synaptic currents (mEPSCs) was found in SNAP-25 ablated neurons (Fossati et al., 2015). However, in the CSF of AD patients, there was an increase of SNAP-25 fragments from early-stage to severe AD measured with mass spectrometry (Brinkmalm et al., 2014). Similarly, in MCI patients carrying the AD risk gene ApoE ε4, their SNAP-25 level in the CSF was also significantly higher than non-carriers; whereas in cognitively normal old subjects, the CSF SNAP-25 was not different between ApoE ε4 carriers and non-carriers (Wang et al., 2018). These observations suggest that changes in SNAP-25 could be detected at the prodromal stage of AD as a sign of cognition impairment (Wang et al., 2018).

The post-synaptic marker, post-synaptic density 95 (PSD-95) is a crucial scaffold protein at all excitatory synapses in the brain and is in the downstream cascade after generation of LTP (Beique et al., 2006, Shao et al., 2011, Sultana et al., 2010). The key roles of PSD-95 at the post-synaptic site include regulating neurotransmitter receptors, ion channels and adhesion molecules, helping to maintain the E/I balance in the brain (Keith and El-Husseini, 2008). PSD-95 represents synaptic strength as it is recruited in a use-dependent manner for N-methyl-D-aspartate (NMDA) receptor clustering and manipulation of the amount of α-amino-3-hydroxy-5-methyl-4-isoxazolepropionic acid (AMPA) receptors (Fossati et al., 2015, Ehrlich and Malinow, 2004). The PSD-95 protein binds directly to subunits of NMDA receptors and indirectly to AMPA receptors via Stargazin (**Figure 4.1.B**) (Vickers et al., 2006).

PSD-95 was shown to play a role in regulating the threshold of LTP induction and modulating synaptic spines that are central to synaptic plasticity (Vickers et al., 2006, El-Husseini et al., 2000). Overexpression of PSD-95 in hippocampal neurons led to an increase in both the size

and number of synaptic spines, enhancing clustering and activity of post-synaptic glutamatergic receptors (Vickers et al., 2006, El-Husseini et al., 2000). Also, changes of PSD-95 expression modulate synaptic strength by affecting AMPA receptor recruitment (Keith and El-Husseini, 2008, Schnell et al., 2002). Interestingly, overexpression of PSD-95 completely blocks LTP in hippocampal slices, probably due to receptor saturation, and enhances LTD, because more AMPA receptors are available for internalisation (Keith and El-Husseini, 2008, Stein et al., 2003). On the other hand, PSD-95 knock-out mice showed reduced AMPA receptor current (Beique et al., 2006). Taken together, these studies suggest that PSD-95 is an important post-synaptic protein contributing to synaptic plasticity, synaptic stabilisation and is of importance in learning and memory (El-Husseini et al., 2000, Broadhead et al., 2016).

PSD-95 was found to regulate E/I balance, alteration of which is observed in many psychiatric and neurological diseases, due to synaptic imbalance (Keith and El-Husseini, 2008). For example, in epileptic patients there is an increase of PSD-95-NMDAR complexes in the cortices that lead to more excitation (Ying et al., 2004). However, in the brains of AD patients, reduction of PSD-95 fluorescent immunoreactivity was found in the synaptosomes of the human association neocortex in which the neurons degenerate in AD (Gylys et al., 2004). Another study also found reduction of PSD-95 protein levels in the grey matter of the temporal lobe in AD patients using Western blot (Yuki et al., 2014). In hippocampus of patients with MCI, the level of PSD-95 was significantly reduced, suggesting this protein might have altered function at pre-AD stages (Sultana et al., 2010). However, the level of PSD-95 in CSF was significantly elevated in patients with AD compared to MCI patients and healthy controls (Kivisakk et al., 2022). Interestingly, increased CSF PSD-95 was also found in other neurodegenerative diseases as well as inflammatory conditions such as neurosarcoidosis and meningitis (Kivisakk et al., 2022, Rao et al., 2012, Wippel et al., 2013).

SNAP-25 and PSD-95 can form a molecular complex connected by the adaptor protein p140Cap (**Figure 4.1.B**), indicating that SNAP-25 might control post-synaptic plasticity by reducing stabilisation of PSD-95 (Fossati et al., 2015, Tomasoni et al., 2013, Jaworski et al., 2009). As PSD-95 plays essential roles in clustering NMDA receptors, AMPA receptors, $K^+$ channels and signalling proteins during the formation and maintenance of dendritic spines (Kivisakk et al., 2022), reductions of SNAP-25 could make PSD-95 clustering more mobile to make receptor insertion unstable, impairing the synaptic strength post-synaptically (Fossati et al., 2015). In contrary, overexpression of SNAP-25 could lead to increased number of PSD-95-containing spines (Tomasoni et al., 2013). Therefore, although SNAP-25 is a protein located at the pre-synaptic compartment (Kerti et al., 2012), it still modifies the post-synapse by changing the morphology of the dendritic spine (Antonucci et al., 2016).

In general, for the traditional understanding of their functions, the pre-synaptic marker SNAP-25 is in charge of exocytosis of synaptic vesicles and related more to short-term plasticity (Antonucci et al., 2016), whereas the post-synaptic marker PSD-95 is associated more to long-term synaptic changes via recruitment of receptors (Keith and El-Husseini, 2008). SNAP-25 and PSD-95 have been extensively studied in neurological disorders involving a change of E/I balance, such as schizophrenia and epilepsy. In the early stage of AD, the existence of hyperexcitability and change of E/I balance have been proposed. Therefore, it is undoubtedly important to investigate the levels of SNAP-25 and PSD-95 in the hippocampus of the TgF344-AD rat model to elucidate molecular changes that play a role in synaptic strength and plasticity. Other presynaptic markers, like synaptic vesicle glycoprotein 2A (SV2A) and the vesicular glutamate transporter (VGLUT) are also of value for investigation of synaptic plasticity. These have also been found to be reduced in AD, thus impairing synaptic plasticity (Kong et al., 2021,

Chen et al., 2011). However, due to difficulties in available antibodies, they are not studied in this set of experiments.

### 4.1.3. Glutamatergic dysfunction in Alzheimer's disease via NMDA receptors

Deficits in glutamate homeostasis could promote excitation of the neuronal circuit (Zott et al., 2018). The glutamate tripartite synapse, involving communication between neurons and astrocytes, is essential for excitatory neurotransmission (Zhang et al., 2016). Briefly, the enzyme glutaminase transforms glutamine (Gln) into the neurotransmitter glutamate (Glu) (Zhang et al., 2016). Glutamate is transferred into synaptic vesicles via vesicular glutamate transporters (VGLUTs) and released into the synaptic cleft following $Ca^{2+}$ influx-induced vesicle fusion (Zhang et al., 2016). Some of the released glutamate will bind to NMDARs at the post-synaptic spines and extrasynaptic NMDARs, while some will be transported into astrocytes by the excitatory amino acid transporters 1/2 (EAAT1/2) or back into the presynaptic neuron by EAAT2/5 (Zhang et al., 2016). Inside the astrocyte, glutamine synthetase will transform glutamate to glutamine, which goes to the presynaptic terminal to provide a production pool for the neurotransmitter glutamate (**Figure 4.2**) (Zhang et al., 2016).

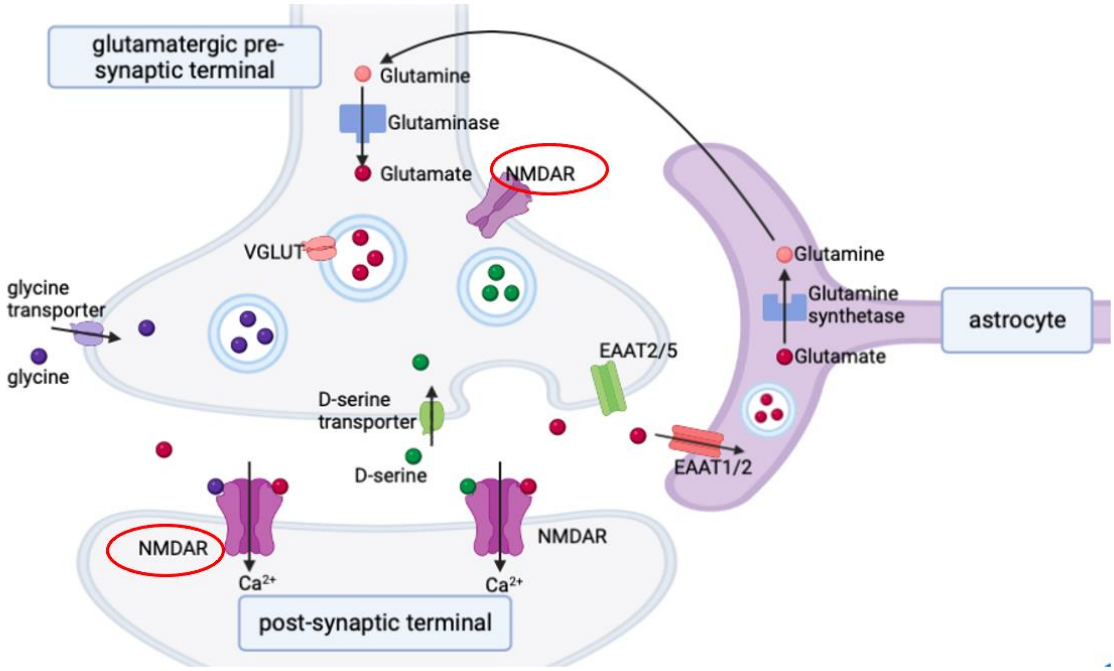


***Figure 4.2. Glutamatergic tripartite synapse.***

*Glutamate is made from glutamine in the presynaptic and packed into vesicles via VGLUT. The excitatory neurotransmitter glutamate will release upon $Ca^{2+}$ influx signaling and bind to activate NMDAR with the co-factor glycine D-serine. The unused glutamate in the synaptic cleft will be recollected by EAATs on the presynaptic terminal and astrocytes. The glutamate in astrocytes will become glutamine under action of the enzyme glutamine synthetase. Astrocytic glutamine is transferred back into the presynaptic terminal, and the tripartite circle starts again. NMDAR=N-methyl-D-aspartate receptor; VLUT=vesicular glutamate transporter; EAAT=excitatory amino acid transporters. Figure modified from Zhang et al. (2016) and created with Biorender.*

To activate NMDARs, glutamate needs to bind to the receptor in combination with the co-factor glycine or D-serine (Zhang et al., 2016). The activated NMDARs will enable $Ca^{2+}$ influx and elicit the downstream cascade, including induction of LTP, a cellular model for learning and memory (Yang et al., 2017, Rammes et al., 2011). Overactivation of NMDARs can cause excitotoxicity and oxidative stress resulting in cell death (Zhang et al., 2016). Aβ has also been shown to elicit excitotoxicity and disturbed $Ca^{2+}$ homeostasis via NMDA-mediated $Ca^{2+}$ influx (Yang et al., 2017, Bezprozvanny and Mattson, 2008, Ferreira et al., 2012). NMDARs in the

hippocampus are therefore essential for excitatory transmission, synaptic plasticity, and learning and memory (Zhang et al., 2016).

NMDARs are composed of a heteromeric congregation of NR1, NR2 (A, B, C and D) and NR3 (A, B) subunits, and the NR2 subunits decide most of the functions of NMDARs (Yang et al., 2017, Zhang et al., 2016). The most common assembly of NMDARs is two NR1 subunits with either two NR2A or NR2B or a mixture of both (Zhang et al., 2016). NR2A increase their expression through development, whereas NR2B are the major subunits in early postnatal brains (Yashiro and Philpot, 2008). In the adult hippocampus, NR2A are predominantly located at the synapse of the membrane, whereas outside the synapse, NR2B are the dominant subtype (Varga et al., 2014, Yang et al., 2017). Both NR2A- and NR2B- containing NMDARs play an important role in LTP, with NR2A more related to LTP induction whereas activation of NR2B enhance LTD (Varga et al., 2014, Kazim et al., 2021, Palop et al., 2007, Palop and Mucke, 2010).

In addition, soluble Aβ oligomers were found to act at extra-synaptic NR2B-containing NMDARs, increasing extra-synaptic NR2B-mediated NMDAR current (Li et al., 2011). Similar effects could be achieved following the administration of the glutamate reuptake inhibitor dl-threo-β-benzyloxyaspartic acid (TBOA) (Li et al., 2011). The Aβ-induced increase of intracellular $Ca^{2+}$ was also shown to be through the activation of NMDARs containing NR2B subunits, whereas blocking NR2A-containing NMDARs showed similar effects (Ferreira et al., 2012). Moreover, NR2B-, but not NR2A-containing NMDARs, are linked with triggering apoptotic signals via the GSK-3β pathway (Varga et al., 2014). These studies would suggest the ratio of NR2A to NR2B plays a crucial role in regulating synaptic function.

### 4.1.4. GABAergic dysfunction in Alzheimer's disease

γ-Aminobutyric acid (GABA) is the major inhibitory neurotransmitter in the central nervous system (Govindpani et al., 2017). GABAergic inhibition plays an important role in preventing hyperactivity in AD. Reductions of GABAergic inhibition has been found in severe AD cases and was associated with cognitive symptoms seen in the patients (Solas et al., 2015). While the majority of excitatory glutamatergic synapses are located on spines, the inhibitory GABAergic synapses are found on the soma, dendritic shaft and proximal axons (Keith and El-Husseini, 2008, Knott et al., 2002, Fujiyama et al., 2002).

GABA is synthesised from a single irreversible enzyme reaction from L-glutamate in the cytoplasm of the pre-synaptic neuron (**Figure 4.3**) (Govindpani et al., 2017). The enzyme involved in this reaction is glutamic acid decarboxylase (GAD), which has two isoforms of 65kDa (GAD65) and 67kDa (GAD67) (Govindpani et al., 2017). Although both isoforms of GAD are expressed in the neuronal cell body and terminal in many brain regions including the cerebral cortex and hippocampus, GAD67 immunoreactivity is more abundant in the cell body whereas immunoreactivity for GAD65 is found to be dominant at the axon terminal (Martin et al., 1991, Esclapez et al., 1994, Tavazzani et al., 2014). In patients with schizophrenia, reductions of GAD67 protein levels were found in the dorsolateral prefrontal cortex and in PV interneurons of the superior frontal gyrus, alongside cognitive symptoms in these patients (Curley et al., 2011, Nahar et al., 2021). In the case of AD, one study found that GAD65-immunoreactive neurons were lost in the hippocampus and medial temporal gyrus of AD patients, and a similar reduction of GAD65 protein level was also found in the temporal gyrus using Western blot (Schwab et al., 2013). However, these changes were not found with GAD67 (Schwab et al., 2013). Nevertheless, in the mouse tissue inoculated with extracellular vesicles isolated from the brains of AD patients, the density of c-fos+/GAD67+ neurons and

the number of GAD67-immunoreactive puncta was reduced around the CA1 pyramidal cells where decreased spontaneous inhibitory current was recorded (Ruan et al., 2021). In sum, these observations suggest that deficits in GABA synthetisation might lead to AD progression.

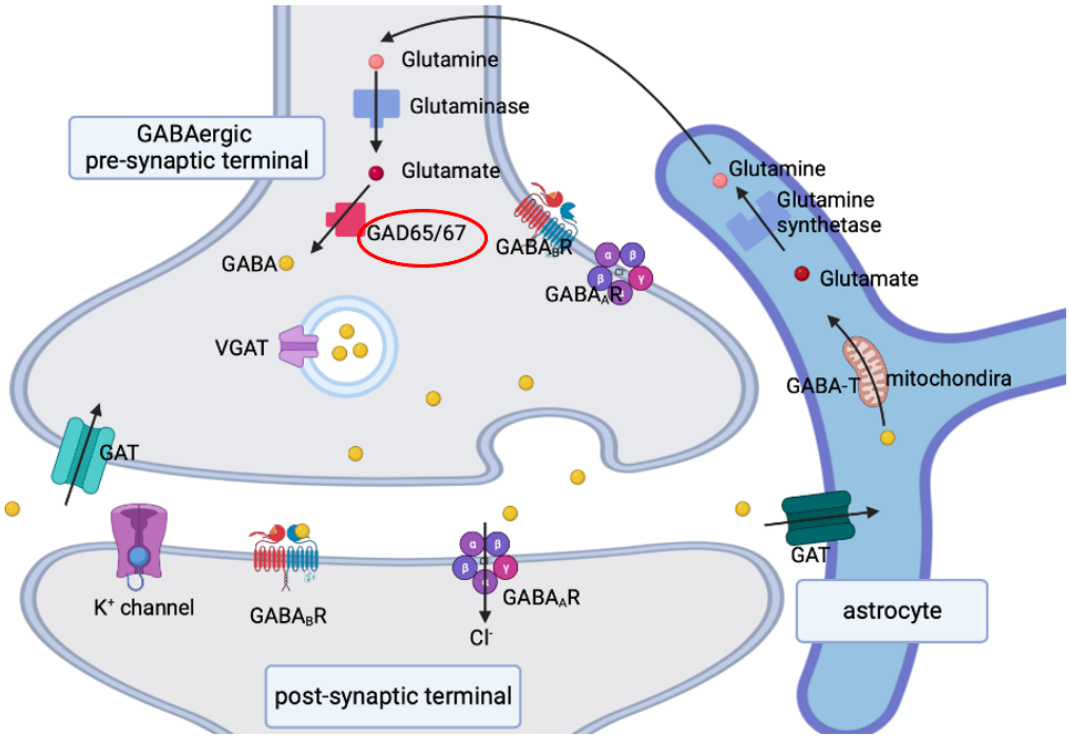


***Figure 4.3. GABAergic tripartite synapse.***

*GABAergic inhibitory neurotransmission also follows the tripartite circle. The inhibitory neurotransmitter GABA is made from glutamate with the enzyme GAD65 or GAD67. GABA molecules are packed into vesicles via VGAT and released upon $Ca^{2+}$ influx signaling. GABA can bind to ionotropic $GABA_AR$ and/or metabotropic $GABA_BR$ located on the post-synaptic terminal for downstream events and bind to extra synaptic GABA receptors. GABA at the synaptic cleft will be recollected via GAT, into the presynaptic neuron or astrocytes. The astrocytic GABA will become glutamate in mitochondria via metabolism (tricarboxylic acid cycle, or TCA cycle), and the tripartite circle starts over again when glutamine is transferred into the presynaptic terminal. GABA=γ-aminobutyric acid; GAD=glutamic acid decarboxylase; GAT=GABA transporter; VGAT= vesicular GABA transporter; GABA-T=GABA transaminase. Figure modified from Govindpani et al. (2017) and created with Biorender.*

Once GABA is synthetised, it is transferred into synaptic vesicles and released to the synaptic cleft (**Figure 4.3**) (Govindpani et al., 2017). GABA can bind to three types of GABA receptors

and activate them for the downstream events (Govindpani et al., 2017). $GABA_{A/C}$ receptors are ionotropic and $GABA_B$ receptors are metabotropic (Govindpani et al., 2017). The $GABA_A$ receptors have a pentameric structure with five subunits from eight subunit families surrounding a central $Cl^-$ channel (Govindpani et al., 2017, Nayeem et al., 1994). The most common form of $GABA_A$ receptors comprise of two α subunits, two β subunits and a γ subunit, although other combinations from other subunit families are also available (Govindpani et al., 2017). It is also the case that many subunits have different subtypes, for example, the α subunit has 6 subtypes 1-6 (Govindpani et al., 2017). While $\alpha_1$ is the most expressed subunit of the $GABA_A$ receptors at the synapse, the $\alpha_5$ subunit is less common but abundant extrasynaptically in the hippocampus (Sieghart and Sperk, 2002, Govindpani et al., 2017, Glykys et al., 2008, Crestani et al., 2002). Due to the heterogenicity of $GABA_A$ receptors, the function, pharmacological properties, and sensitivities of different subunit composition may vary (Govindpani et al., 2017).

Unlike $GABA_A$ receptors, $GABA_B$ receptors are G-protein coupled receptors with two subunits, GB1 and GB2, that possess distinct functionalities (Govindpani et al., 2017, Galvez et al., 2001). Because their activation involves recruitment of second messenger downstream, $GABA_B$ receptors can provide slow and prolonged inhibition, in contrary to the fast and transient action of $GABA_A$ receptors (Terunuma, 2018). $GABA_B$ receptors are also thought to influence synaptic plasticity and memory (Terunuma, 2018). However, augmentation of post-synaptic $GABA_B$ receptor activity impaired spatial memory consolidation, suggesting that in order to rescue memory deficits, $GABA_B$ receptor activity might need to be blocked (Terunuma et al., 2014). $GABA_c$ receptors are highly expressed in retina and are considered a minor subgroup of $GABA_c$ receptors and less involved in cognitive function (Li et al., 2016).

There is growing evidence that normal GABAergic inhibition is affected in AD and as such could provide a promising approach for therapeutic intervention (Govindpani et al., 2017, Li et al., 2016). Decreased GABA protein levels was observed in the temporal cortex in AD patients (Li et al., 2016, Gueli and Taibi, 2013, Bareggi et al., 1982). In patients with AD and AD-like pathologies, a moderate reduction of GABA levels was indicated among many cortical areas, indicating a shift of E/I balance to excitation in the patients (Govindpani et al., 2017, Lowe et al., 1988, Rossor et al., 1984). An age-dependent decrease of GABA current was found in Xenopus oocytes that were transplanted with brains from AD patients (Limon et al., 2012). In the same study, GABA receptors were also found to be significantly less sensitive to GABA compared to Xenopus oocytes transplanted with brains from the control non-AD brains (Limon et al., 2012). If hyperactivation is happening in AD brains, enhancing inhibition could be of benefit for the prevention of AD progression. Indeed, pharmacological application of benzodiazepines, the positive allosteric GABAergic modulator, was shown to prevent hyperactivity, restore slow-wave oscillations, and restore E/I balance in both the APP23 x PS45 and APP23 AD mouse models (Zott et al., 2018, Busche et al., 2015, Griffin et al., 2013).

Different subunits of $GABA_A$ receptors are also subjected to relatively diverse functions. While $\alpha_1$ accounts for sedative effect of diazepam, $\alpha_2$ is generally known to prevent anxiolytic-like behaviour and is also involved in cognition and working memory by manipulating the GABA function in the cortex (Gabriella and Giovanna, 2010, Xu and Wong, 2018). For example, mice with downregulation of $\alpha_2$ subunit in the frontal cortex showed behavioural deficits in prepulse inhibition and impairments in working memory (Hines et al., 2013). Also, clinical trials showed that a selective $GABA_A$ $\alpha_{2/3}$ receptor agonist could improve cognition in schizophrenic patients (Lewis et al., 2008, Xu and Wong, 2018).

Importantly, the $\alpha_5$ subunit of the $GABA_A$ receptor is strongly associated with learning and memory (Li et al., 2016, Gabriella and Giovanna, 2010). Unlike most of the $GABA_A$ receptors expressed at the synapse, $\alpha_5$-containing $GABA_A$ ($GABA\alpha_5$) receptors are largely located extrasynaptically in brain regions including hippocampal CA fields (Crestani et al., 2002, Brunig et al., 2002, June et al., 2001). Extrasynaptically located $GABA\alpha_5$ receptors could modulate tonic inhibition of pyramidal cells in the hippocampus (Koh et al., 2020).

Interestingly, it has been found that selective blockade of $GABA\alpha_5$ receptors using negative allosteric modulators (NAMs) could improve hippocampal dependent cognitive performance in young adult rodents (Koh et al., 2020, Koh et al., 2013). For example, $\alpha_5$ knock-out mice showed facilitated associative learning and trace fear conditioning behaviours that are dependent on the hippocampus (Crestani et al., 2002). The double $\alpha_5$ knock-out mice also showed significantly improved memory in the water maze (Collinson et al., 2002). Upregulation of $\alpha_5$ subunit containing $GABA_A$ receptors was observed alongside cognitive deficits in the 5xFAD mouse model (Li et al., 2016). This evidence strongly supports that inhibition of or a reduction in $\alpha_5$ subunit containing $GABA_A$ receptors could rescue memory, making it a potential therapeutic target for diseases associated with cognitive impairment such as AD (Petrache et al., 2020).

Importantly, $GABA\alpha_5$ receptors were also found to be upregulated by soluble Aβ in mouse hippocampal cultures, which could be prevented by treatment of the inverse agonist of $GABA_A$ receptors $\alpha_5$ subunit ($\alpha_5$IA), a memory enhancer that selectively attenuates the effect of GABA (Vinnakota et al., 2020, Atack, 2010). In the same study, $\alpha_5$IA was also found to reduce Aβ-induced cell death in mouse hippocampal cultures (Vinnakota et al., 2020). Although the action of $\alpha_5$IA is paradoxically via disinhibition that causes hyperactivity which

would be thought to impair memory, oral administration of $\alpha_5$IA was found to increase cell firing rate of CA1 pyramidal cells during foraging behaviour and increase ripple size during wakeful movement in young adult wildtype rats (F344 strain) (Ratner et al., 2021). Nevertheless, the $\alpha_5$IA drug was stopped from clinical development due to renal toxicity in preclinical models and poor tolerability in elderly patients (Hipp et al., 2021). Meanwhile, other novel selective NAMs at $GABA_A$-$\alpha_5$ (basmisanil) are ongoing in clinical trials with preclinical benefits for spatial learning and executive functions, suggesting the $\alpha_5$ subunit could still be an important target to improve cognitive functions (Hipp et al., 2021).

In conclusion, maintaining a suitable dynamic E/I balance is essential and critical to normal function of the CNS (Li et al., 2016). Since altered synaptic balance is implicated in AD, it is necessary to also study the changes of GABAergic inhibition. In this study, GABA synthetisation and receptor function were investigated by measuring levels of GAD67 and GABA$\alpha_5$ in the dorsal hippocampal in post-mortem tissue homogenates.

### 4.1.5. Neuroinflammation: microglia and interleukin-1β

Neuroinflammation and microglial dysfunction has been implied in AD pathogenesis (Das et al., 2021). In this study, microglia and the proinflammatory cytokine interleukin-1β were specifically studied to investigate the neuroinflammatory involvement in early AD.

Microglia activation is considered another important feature or biomarker of AD, alongside Aβ plaques and neurofibrillary tangles (NFTs) (Guo et al., 2022). Under physiological conditions, microglia in the resting state are continuously surveying the surrounding environment looking for potential dangers such as damage associated molecular patterns (DAMPs) (Guo et al., 2022). Resting microglia have a small cell body and long projections with

fine branches (Leyh et al., 2021, Daniels et al., 2016). However, once microglia detect DAMPs or changes of brain homeostasis (Guo et al., 2022), they will become activated with enlarged or rod-like cell body and shorter and thicker projections with fewer branches (Leyh et al., 2021, Daniels et al., 2016). The fully activated microglia display a round shape cell body without projection and can phagocytose neurotoxic debris (Leyh et al., 2021).

The activated microglia can polarise into two phenotypes, the neurotoxic M1 and neuroprotective M2 (Guo et al., 2022, Colonna and Butovsky, 2017). M1 microglia are the classic type which induce neuroinflammation with the production of pro-inflammatory cytokines such as interleukin-1β (IL-1β), tumour necrosis factor α (TNF-α), and chemokine (C-C motif) ligand 2 (CCL-2); whereas M2 microglia are neuroprotective, and able to produce anti-inflammatory cytokines such as IL-10 and transforming growth factor β (TGF-β) (Guo et al., 2022, Colonna and Butovsky, 2017). M2 microglia could also promote phagocytosis of, for example, Aβ deposits (Guo et al., 2022, Colonna and Butovsky, 2017). Therefore, the balance between M1 and M2 types of activated microglia is crucial for understanding damaging and protective effect of neuroinflammation (Guo et al., 2022). Inhibiting M1 and elevating M2 microglia could be beneficial in treating neurodegenerative diseases like AD (Guo et al., 2022).

Moreover, the disease-associated microglia (DAM) are a novel type of activated microglia with the protective effects by enhancing phagocytosis (Keren-Shaul et al., 2017, Guo et al., 2022). The activation of DAM involves two steps: firstly, a triggering receptor expressed on myeloid cells 2 (TREM2)-independent pathway leads the resting microglia to an intermediate state with a reduction of homeostatic microglia checkpoint genes (e.g. *Cx3cr1*) and an increase of TREM2 adapter gene (*Tyrobp*); secondly, a TREM2-dependent mechanism causes the microglia at intermediate state to become phagocytic (Keren-Shaul et al., 2017, Guo et al.,

2022). Interestingly, DAM are located at the close vicinity of Aβ plaques, suggesting their role in clearance of Aβ deposit (Keren-Shaul et al., 2017)

In AD, Aβ acts as a DAMP that results in the activation of microglia, regulating the immune response in the brain by producing one of the most important cytokines, IL-1β (Lenart et al., 2016). Utilising both positron emission tomography (PET) imaging and histological studies, it was demonstrated that activated microglia and astrocytes with high IL-1β expression are concentrated in sites near to $A\beta_{42}$ plaques (White et al., 2017). Moreover, imaging studies showed the presence of inflammation in patients with MCI, suggesting that inflammation occurs early in the disorder and contributes to the clinical symptoms of AD (White et al., 2017, Yasuno et al., 2012). The APP/PS1 mouse model of AD also showed high expression of IL-1β in microglia surrounding $A\beta_{42}$ plaques; whereas mice lacking the IL-1 receptor showed microglia activation when injected with $A\beta_{42}$ into the brain (White et al., 2017). IL-1β also contributes to the production of $A\beta_{42}$ and APP when combined with another cytokine, interferon-γ (Blasko et al., 2000), and it can initiate phosphorylation of tau protein in astrocytes (**Figure 4.4**) (Liu et al., 2006, White et al., 2017). Therefore, $A\beta_{42}$ could prolong the activation of immune cells by continuously recruiting inflammatory mediators, exacerbating the disease (Heppner et al., 2015).

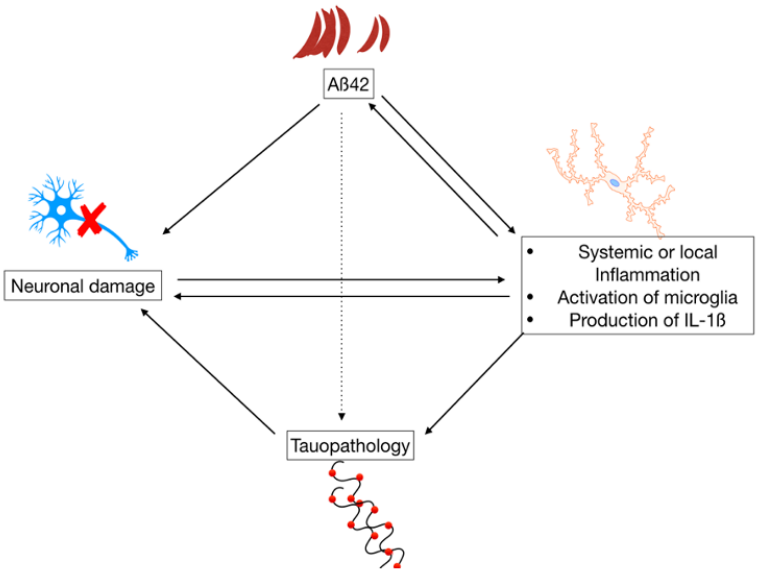


***Figure 4.4. Inflammatory contribution to Alzheimer's disease.***

*$A\beta_{42}$ is pro-inflammatory and will induce an inflammatory response. Both $A\beta_{42}$ and inflammation cause damage to neurones, whereas neuronal damage, in turn, leads to more inflammation via the production of cytokines such as IL-1ß from microglia. $A\beta_{42}$ is known to promote the production of hyperphosphorylated tau protein that form the neurofibrillary tangles (dotted line). Figure modified from White et al. (2017).*

$A\beta_{42}$ activates inflammasomes that are upstream of IL-1β production in immune cells and neurones (White et al., 2017). Inflammasomes are large multi-protein complexes that activate caspase-1, which cleaves inactive pro-IL-1β to form IL-1β (White et al., 2017, Daniels et al., 2016) (Daniels et al., 2016; White et al., 2017). Most of the inflammasomes currently being studied, namely NLRP3, NLRP1 (NLR family, pyrin domain containing 1 and 3), and NLRC4 inflammasomes, respectively, comprise of three parts, an inflammatory sensor that recognises intracellular pathogen associated molecular patterns (PAMPs) and DAMPs, an adaptor protein called Apoptosis-associated Speck-like protein containing a C-terminal caspase-recruitment domain (ASC), and caspase-1 (White et al., 2017).

$A\beta_{42}$ can directly activate the sensor molecule of the NLRP3 inflammasome (Annett et al., 2008). Full knockdown of the NLRP3 gene in APP/PS1 mice ameliorates inflammation in the brain by reducing amyloid plaques (Heneka et al., 2013). *Nlrp3-/-* and *caspase-1-/-* APP/PS1 mice had a reduced formation of IL-1β and had enhanced clearance of $A\beta_{42}$. Memory deficits were also prevented in the mice (Heneka et al., 2013). NLRP1 inflammasomes are commonly expressed in neurones and associated with pyroptotic cell death (White et al., 2017). They can be up-regulated by $A\beta_{42}$ *in vitro*, whereas an *in vivo* study suggested that in APP/PS1/NLRP1-/- mice, pyroptosis of neurones was down-regulated in the hippocampus and the cognitive ability of these animals were better than the controls (Tan et al., 2014, White et al., 2017). This evidence suggests that $A\beta_{42}$ and chronic inflammation are interconnected; it also implies that inhibition of the molecular pathways involved in the formation of IL-1β is a potential therapeutic target to treat AD more effectively (White et al., 2017).

Drugs inhibiting the NLRP3 inflammasome can reduce IL-1β and down-regulate caspase-1 activation, and were shown to be beneficial and protective to cognitive deficits in the 3xTgAD mouse model (Daniels et al., 2016). Reduction of IL-1β in the AD brain could lower the formation of amyloid plaques and the subsequent inflammatory response, preventing neuronal death in affected regions. Daniels et al. firstly showed *in vitro* that the fenamate subclass of non-steroidal anti-inflammatory drugs (NSAIDs) can effectively and selectively inhibit the NLRP3 inflammasome (Daniels et al., 2016, White et al., 2017). *In vitro* studies showed that the fenamate NSAIDs such as flufenamic acid and mefenamic acid specifically reduced IL-1β, indicating that they could also reduce the inflammatory response seen in AD (Daniels et al., 2016). Daniels et al. then provided *in vivo* evidence that chronic administration of mefenamic acid could preserve memory in both an $A\beta_{42}$-injection rat model and in the 3xTg mouse model for AD (Daniels et al., 2016). Mefenamic acid was also effective in completely

abolishing IL-1β expression in the 3xTg transgenic mice that had over-activation of microglia expressing IL-1β (Daniels et al., 2016). Those 3xTg mice treated with mefenamic acid with a constant amount over 28 days had completely reversed memory deficits as compared to the wild-type controls (Daniels et al., 2016).

Therefore, in this study, microglia activation and presence of IL-1β were analysed in the 6- and 9-month-old TG rats and WT controls to investigate early-stage pathologies in the TG rat model for AD.

### 4.1.6. Aim and hypothesis

The aim of this chapter is to study Aβ-related early changes on biomarkers for synaptic, GABAergic and glutamatergic transmission as well as neuroinflammation in the dorsal hippocampus of the TgF344-AD model. Specifically, the levels of SNAP-25, PSD-95, PV, GABA$\alpha_5$, GAD67, NR2A and NR2B were measured using simple Wes analysis in the dorsal hippocampus of the 6- and 9-month-old TG and age-matched WT rats. The PV+ cells were also investigated using immunohistochemistry and cell density was calculated in total dorsal hippocampus and its subregions (CA1, CA2/3, and DG) in rats at 6 and 9 months of age. Neuroinflammation was quantified using microglia activation and co-expression with IL-1β. Briefly, in the dorsal hippocampal CA1 region, the activation states of microglia were determined with calculations of activation scores in 6- and 9-month-old WT and TG rats. In the same animals, the percentage of IL-1β-expressing microglia was investigated in the CA1 region of the hippocampus by co-staining microglia and IL-1β using an immunofluorescent method.

## 4.2. Methods and Materials

### 4.2.1. Simple Western analysis

#### *4.2.1.1. Homogenisation*

Whole brain of the animal cohort from the behavioural tasks and electrophysiology recordings were taken and dissected for frontal cortex (FCx), prefrontal cortex (PFC), dorsal hippocampus (DH) and ventral hippocampus (VH) according to the Paxinos and Watson rat atlas (Paxinos and Watson, 2007). In line with the electrophysiological studies the DH tissue was studied for protein analysis in this thesis. Homogenization buffer (1.21mg/ml Trizma base, 0.11 mg/ml sucrose, and 0.74 mg/ml EDTA) was activated with 0.1M PMSF, 0.1M sodium orthovanadate and protease inhibitor and added to each sample for homogenisation at a concentration of 100mg/ml. Tissue samples were fully homogenised into solution, and then was centrifuged at 800g at 4°C for 15min. The resultant supernatant (S1) was centrifuged at 11,700g at 4°C for 20min to obtain the S2 supernatant which is made up of most of the soluble proteins. The pellet after the second centrifugation was labelled as P2 which includes receptors on lipid membrane.

#### *4.2.1.2. Bradford Assay*

Total bovine serum albumin (BSA) concentration in supernatant two (S2, cytosolic fraction) or pellet two (P2, synaptic fraction) was determined using a Bradford Assay, which is a spectroscopic procedure to measure total protein concentration in a solution. This step was used for the dilution of samples to the same concentration of total soluble proteins for the western analysis. A small portion of the original S2 solution was taken and diluted fivefold with the homogenisation buffer. For P2 samples, 100ul 1X PBS was added for pellet

resuspension before the Bradford assay. Triplicates of 10ul samples were pipetted into a 96-well plate. 200ul dye reagent (1X) was added into each sample and the plate was gently mixed and incubated for 5min in the dark. The absorbance reading at 595±5nm was taken from the spectrophotometer (Hidex Sense version 0.5.64.0, Finland) and blank reading correction was made with this software. A standard curve was plotted using the absorbance from known BSA concentrations, and the concentration of total soluble proteins in each of the homogenised samples were interpolated and calculated with the third order polynomial regression curve (GraphPad PRISM 9.3.1., GraphPad Software, Inc.).

#### *4.2.1.3. Protein level analysis by Wes*

Protein levels in the DH were analysed using the Wes system (ProteinSimple, Bio-Techne, USA), which is an automated Western blot with a capillary system separating proteins based on size. Levels of SNAP-25, PSD-95, PV, GAD67, and GABA$\alpha_5$ were measured in animals at 6 and 9 months old in dorsal hippocampus S2. NR2A and NR2B levels were measured in 6-month-old animals in P2. The protein level analysis was carried out using the process outlined below for each antibody - (1) optimisation of antibody and sample concentrations, (2) measure levels of protein of interest, and (3) measure total protein in each sample on Wes for normalisation of data.

Samples and reagents for Wes analysis were prepared as per the manufactures protocol. Briefly, a biotinylated ladder was prepared with deionised water from the EZ Standard pack (ProteinSimple, Bio-Techne, USA). Samples were added with 1:5 fluorescent master mix (200mM dithiothreitol and 5X sample buffer) from the EZ Standard pack (ProteinSimple, Bio-Techne, USA) before vortex mixing and denaturation. Specifically, S2 samples were denatured

at 95°C for 5mins, while P2 samples at 40°C for 30mins. Samples and reagents were kept on ice whenever needed. The ladder, denatured samples and reagents were loaded into a 25-cartridge Wes well plate (12-230kDa) based on whether it was a total protein analysis or a protein level analysis (**Figure 4.5**) and then centrifuged for 5mins at 2500 rpm to ensure all liquids were at the bottom of each well. Compass software for Simple Western (version 6.1.0) was used alongside the Wes machine to control the incubation timing and reading of chemiluminescence values. The default settings were used to run the total protein plate and all antibodies, apart from for SNAP-25 and GAD67 whose blocking time was increased from 5 to 30 minutes. Compass software (version 6.1.0) was used for acquisition of protein levels as a reading of area under the curve and chemiluminescence value at the peak of proteins of interest.

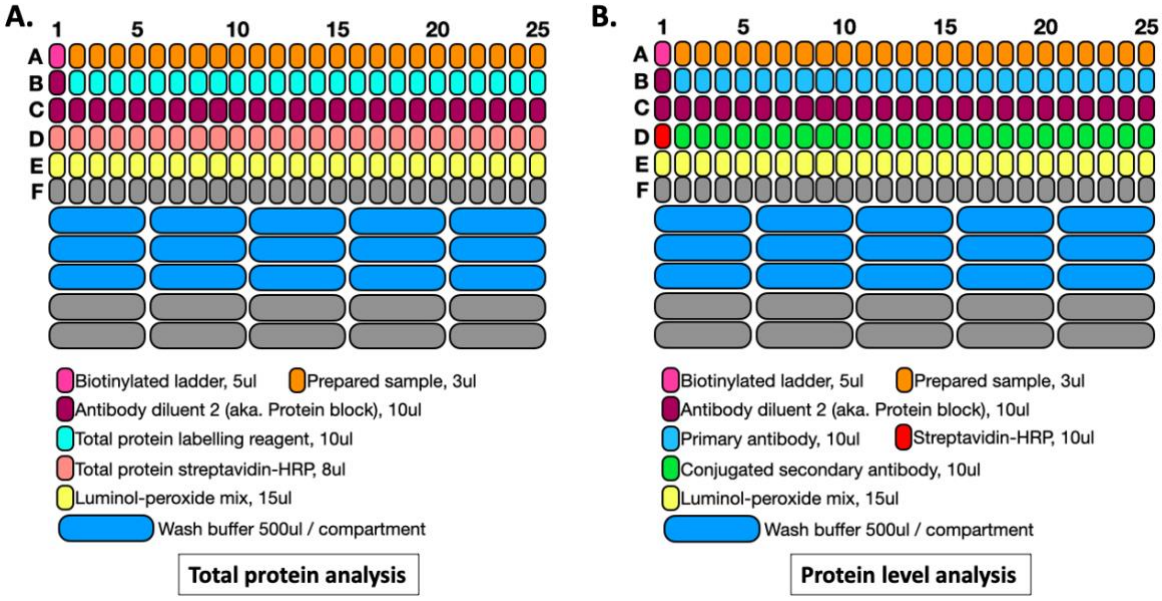


***Figure 4.5. 25-sized Wes well plate and loading instructions of samples and reagents.***

***(A)*** *Plate to load for total protein (TP) analysis. Total protein labelling reagent is made by mixing 150ul TP reagent 1 and 2 with silver lidded tube.* ***(B)*** *Plate to load for optimisation and samples. The sample preparation was the same for TP analysis and protein level analysis. 4ul*

*samples at specific BSA concentration were mixed and vortexed with 1ul Wes fluorescent mix. The mixture was denatured at 95°C for 5min for S2 samples or 40°C for 30min for P2 samples. The resulting mixture was vortexed and flash spin, and then loaded into the plate. Luminol-peroxide was used for chemiluminescence detection. Luminol and peroxide solutions were mixed at a ratio of 1:1.*

To optimise antibody and sample loading concentrations, the antibody of interest was diluted and S2 or P2 of each sample was lowered to the appropriate BSA concentration range. The chemiluminescence value and area under the curve for the protein of interest was extracted at the optimal exposure (64 seconds) in the Compass software (version 6.1.0). The saturation of luminescence signal was checked prior to any data extraction. A best-fit curve was plotted for the chemiluminescence value of the peak (protein of interest) against antibody dilution. The optimal antibody concentration was reached when it was saturated at the lowest background noise, i.e., at the beginning at the plateau of the best-fit curve as highlighted in **Figure 4.6**. At the optimal sample concentration, the plot of area under the curve against sample dilution should be linear (**Figure 4.6.D**).

**A.**

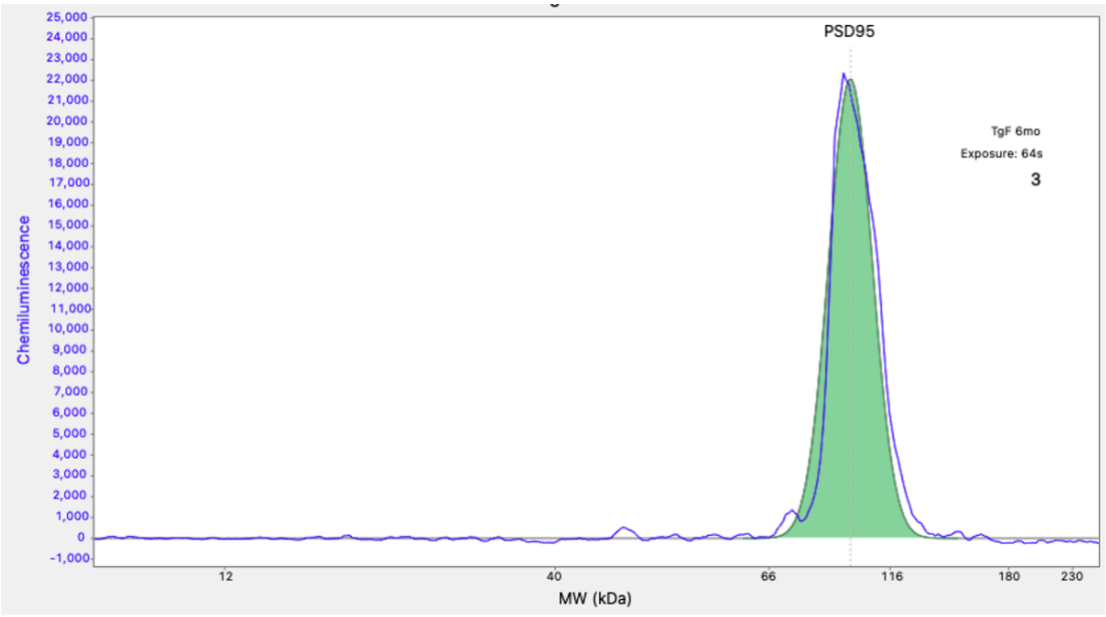

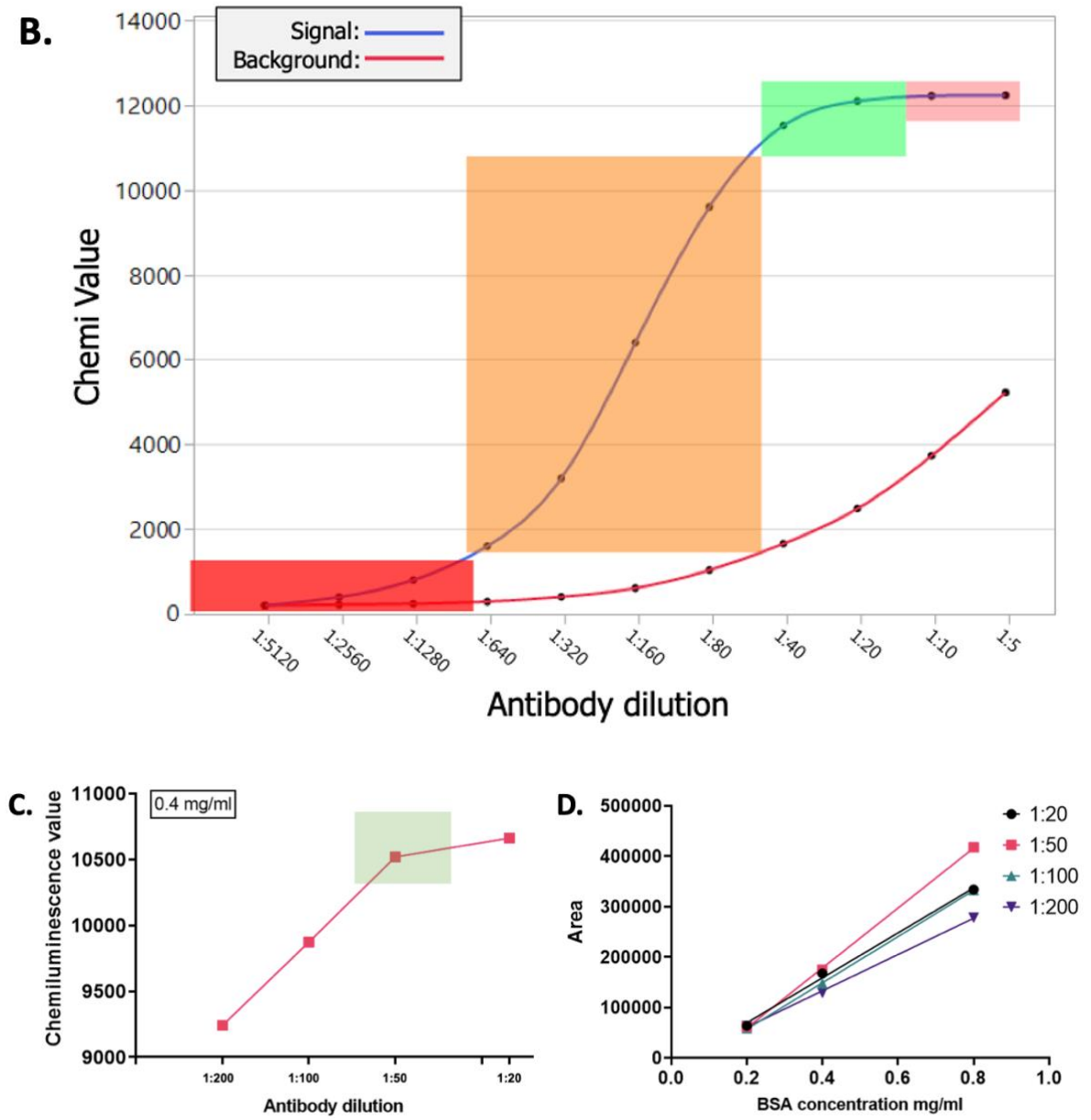


***Figure 4.6. Optimisation of an antibody for Wes.***

***(A)*** *An example of the chemiluminescence curve as detected by the Wes machine. The chemiluminescence value represents the detection signal strength. The area under the curve that is fitted automatically with a Gaussian function represents the level of protein of interest.* ***(B)*** *For optimisation, chemiluminescence value is plotted against the antibody dilution (log 2 scale). The best concentration of antibody is the one at the beginning of the plateau (green), for the highest antibody binding and the lowest background. Red box: antibody binding is too low so that these dilution levels should be avoided; Orange box: antibody binding is increasing but should still be avoided because not all available sites are bound; Green box: optimal antibody dilution level; Pink box: antibody dilution at this level should be avoided due to high background noise (ref: ProteinSimple)* ***(C)*** *An example of the optimum antibody concentration in this study. When sample BSA concentration was 0.4mg/ml, the plot met the optimal at 1:50 dilution for the optimal results.* ***(D)*** *The area under the curve was plotted against the sample*

*BSA concentration to optimise for the antibody dilution. At an appropriate antibody dilution, the area should grow linearly with the increase of sample BSA concentration. Optimisation of other antibodies tested in Wes studies was done with the same method.*

The optimal primary antibody and sample concentrations are summarised in **Table 4.1**. The data for protein levels in samples were extracted in Compass software (version 6.1.0) at the high dynamic range (HDR) exposure of each well plate.

***Table 4.1. Information of primary antibodies used in simple Wes analysis.***

| Primary antibody | Product code & supplier | Secondary | Fraction | Sample BSA concentration (mg/ml) | Antibody dilution |
|---|---|---|---|---|---|
| PV | LS-B14122; LSBio | Anti-rabbit | S2 | 0.2 | 1:50 |
| PSD-95 | AB2723; Abcam | Anti-mouse | S2 | 0.4 | 1:50 |
| SNAP-25 | ab5666; Abcam | Anti-rabbit | S2 | 0.4 | 1:50 |
| GABA$\alpha_5$ | ab10098; Abcam | Anti-rabbit | S2 | 0.8 | 1:50 |
| GAD67 | MAB5406; Millipore | Anti-mouse | S2 | 0.8 | 1:50 |
| NR2A | PPS012; R&D Systems | Anti-rabbit | P2 | 0.02 | 1:100 |
| NR2B | PPS013; R&D Systems | Anti-rabbit | P2 | 0.2 | 1:50 |

The amount of target protein in each sample was normalised to its corresponding total protein levels measured with Wes, and then normalised to the average of that protein in the WT group, for data analysis.

### 4.2.2. Immunostaining

#### *4.2.2.1. Intracardiac perfusion and brain extraction*

Each animal was intracardiacally perfused with 200ml ice-cold 0.1M phosphate-buffered saline (PBS) and brains were collected and post-fixed in 4% paraformaldehyde for two days before being transferred to 30% sucrose. Once the brain fully sunk to the bottom of the vial containing 30% sucrose, it was washed with 0.1M PBS and flash frozen in isopentane on dry ice before being stored at -80°C. Brains were sectioned on a cryostat and dorsal hippocampal sections (30µm) were collected and stored as free-floating sections in a cryoprotectant (30% v/v ethylene glycol, 30% v/v glycerol, 10% v/v 0.2M PBS) at -20°C.

PV interneurons and microglia were stained using immunohistochemistry, and IL-1β expressing microglia were co-stained using immunofluorescence. Optimisations of primary antibodies were carried out at a range of dilutions. Positive controls (sections with only secondary antibody or no primary antibody) were used to check for background staining.

#### *4.2.2.2. Immunohistological staining*

For immunohistochemistry, dorsal hippocampal sections were washed 3 times in 0.1M PBS for 5 minutes. Antigen retrieval was conducted using sodium citrate buffer (10mM sodium citrate, 0.05% Tween 20, pH 6.0) for 30mins at 80°C and then sections were washed 3 times for 5mins. Sections were treated with hydrogen peroxide (1.5% $H_2O_2$, 10% methanol, 0.4% Triton x-100) to remove endogenous peroxidase activity and washed twice for 5mins. Sections were incubated in 5% normal horse serum (NHS, S-2000, Vector Laboratories, USA) with 0.4% Triton x-100 to inhibit non-specific binding following which they were incubated in primary antibody (PV: 1:5000, 235, Swant, Switzerland; Iba-1: 1:2000, ab5076, Abcam) with 5% NHS

overnight at 4°C. Sections were washed twice in 0.1M PBS and incubated for 2h in secondary antibody (1:200; PV: anti-mouse; Iba-1: anti-goat) in 5% NHS at room temperature. Samples were then treated with VECTASTAIN® ABC Kit for 45mins, followed by DAB Substrate treatment (peroxide HRP with Nickel) for about 15mins. Sections were washed in distilled water and stored in 0.1M PBS before being mounted on SuperFrost® Plus slides. Sections were then dehydrated in increasing concentrations of ethanol (70%, 90% and 100%). The dehydrated slides were immersed in Histo-Clear for 5mins and then covered with DPX Mountant (Sigma-Aldrich).

#### *4.2.2.3. Immunofluorescent staining*

To further assess neuroinflammation, the co-localisation of microglia and the proinflammatory cytokine IL-1β was studied in the hippocampal CA1 region with immunofluorescence. Briefly, dorsal hippocampal sections were washed 3 times in 0.1M PBS for 5mins. Antigen retrieval was conducted using sodium citrate buffer (10mM sodium citrate, 0.05% Tween 20, pH 6.0) for 30mins at 80°C. After being washed 3 times for 5mins, sections were incubated in 5% normal chicken serum (NCS; S-3000-20, Vector) with 0.3% Triton x-100 in 0.1M PBS for 90mins to inhibit non-specific binding. Sections were then incubated with Iba-1 (1:500; ab5076, Abcam) and IL-1β (1:200; MAB501, R&D Systems) primary antibodies in 5% NCS in 0.3% PBST overnight at 4°C. Sections were then washed 3 times in 0.1M PBS and incubated with secondary antibodies conjugated with Alexa-488 (A21467, Thermo Fisher Invitrogen) for Iba-1 and Alexa-594 (A21201, Thermo Fisher Invitrogen) for IL-1β at 1:500 in 5% NCS in 0.3% PBST for 2 hours. Sections were washed twice in PBS and rinsed in distilled water for less than 2mins before mounting. Stained free-floating sections were transferred

onto SuperFrost® Plus slides, left dry and mounted using DAPI-containing mounting media (florescent imaging: fluoroshield mounding medium with DAPI, ab104139, Abcam; confocal imaging: ProLong Gold Antifade Mountant with DAPI, Thermo Fisher). Mounted slides were kept at 4°C before being imaged.

#### *4.2.2.4. Image acquisition and analysis*

Images were obtained on a 3D-Histech Pannoramic-250 microscope slide-scanner using a 20x/0.8 Plan-Apochromat objective lens (Zeiss) for immunohistology slides, and acquired in combination with DAPI, FITC and Texas Red filter sets for immunofluorescent slides. Snapshots of the slide-scans were taken and analysed using Case Viewer software (3D-Histech).

Cell counting was performed with genotypes being blinded. The PV- positive stained cells for immunohistochemistry studies were manually counted in CA1, CA2/3, and DG of dorsal hippocampus from at least 6 sections per animal (**Figure 4.7**). The number of Iba-1-positive cells (**Figure 4.8**) in each subregion of dorsal hippocampus was counted using automatic cell detector with QuPath software (version 0.3.2) (Bankhead et al., 2017) from 6 sections per animal. Parameters for the recognition of the cell body were set as: detection image = optical density sum; maximum area = 100-150 $um^2$; minimum area = 20-30$um^2$ and threshold = 0.6-1.1. Cell density was calculated as number of cells per unit $mm^2$ of the dorsal hippocampus or dorsal hippocampal subregions.

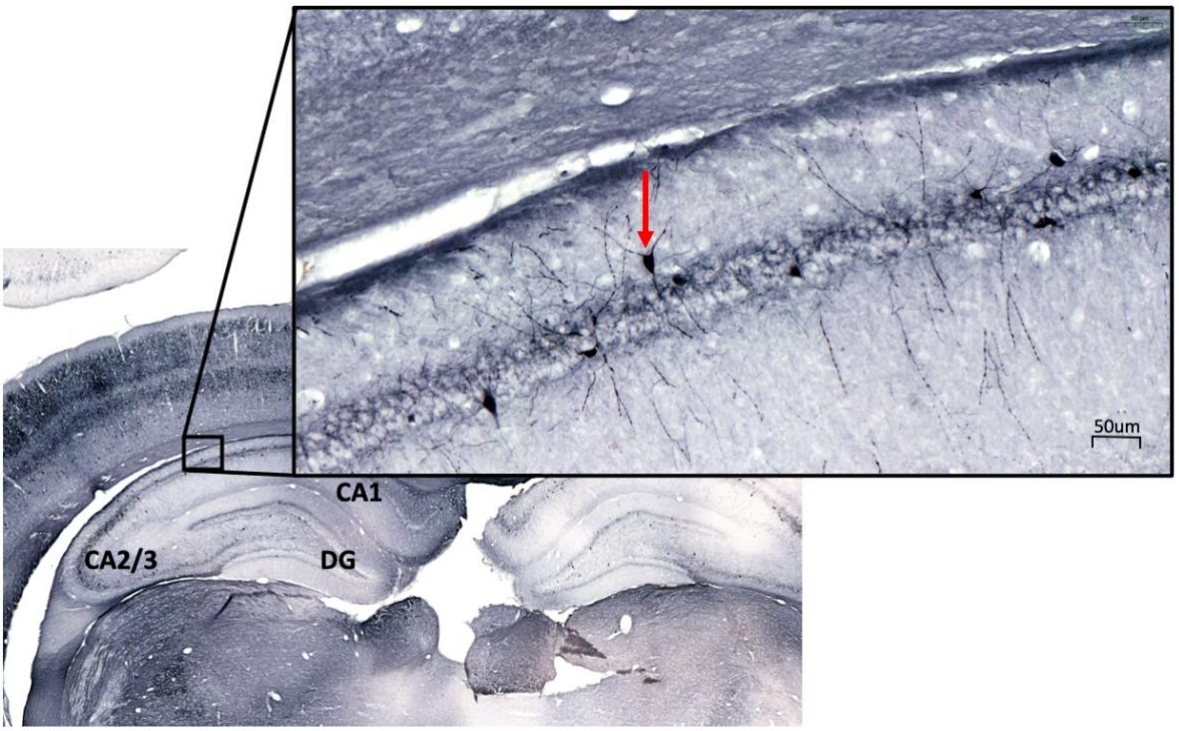


***Figure 4.7. An example of parvalbumin stain in the brain of a randomly selected animal.***

*The red arrow is pointing to a PV positive stain. Number of PV+ interneurons were counted in the dorsal hippocampal subregions CA1, CA2/3 and DG.*

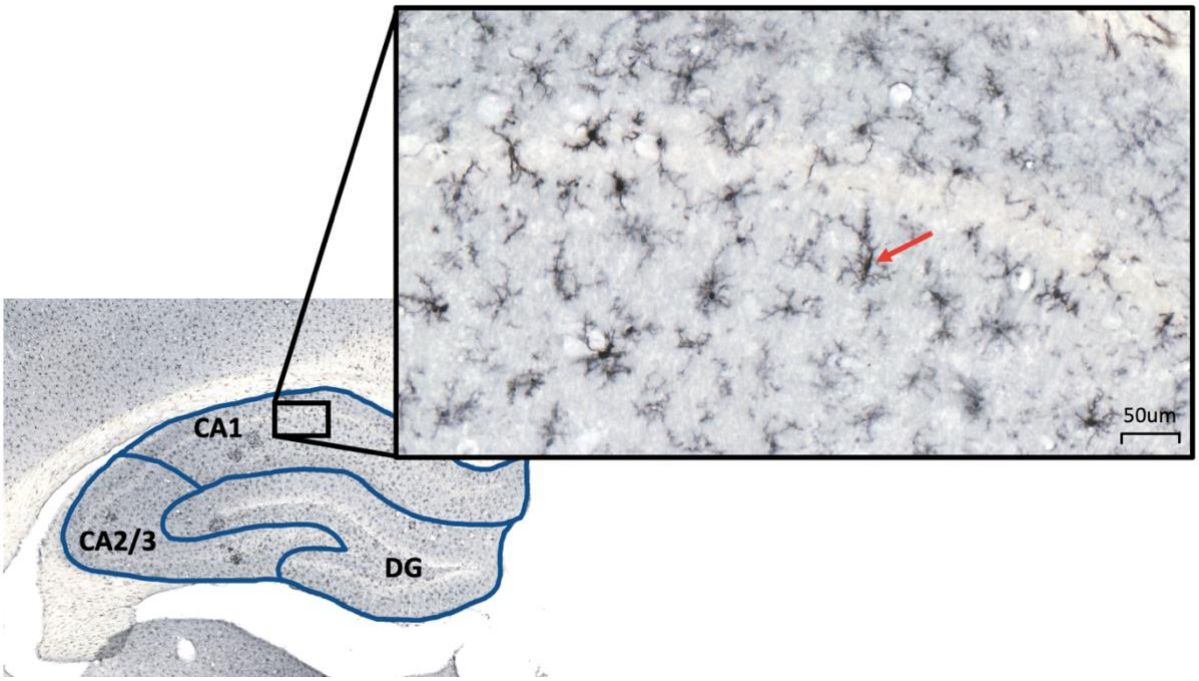


***Figure 4.8. An example of Iba1 stain in the brain of a randomly selected animal.***

*The red arrow is pointing to the cell body of a microglia that is positively stained to Iba1. Number of Iba1+ microglia were counted in the dorsal hippocampal subregions CA1, CA2/3 and DG, outlined in blue.*

For fluorescent co-staining, a minimum of 100 Iba-1-positive cells were labelled in the CA1 region of dorsal hippocampus, the microglial morphology was scored (Cotel et al., 2015), and then the presence of IL-1β was determined on the labelled microglial cells to calculate the percentage of IL-1β-expressing microglia (Daniels et al., 2016). Briefly, the microglia at resting, intermediate, or activated state were identified and were given the score 0, 1 or 2 respectively for the numerical analysis (Daniels et al., 2016) (**Figure 4.9.A**). The scoring of microglia activation state was performed twice by a single examiner, who was blinded to the age and genotype of the animals. The selection of CA1 region was based on Daniels et al. (2016), where a random counting frame (about 0.6mm x 0.3mm) was drawn between the *stratum radiatum* (Rad) layer of CA1 region (**Figure 4.9.B**). Multiple dorsal hippocampal sections were employed to reach at least 100 microglia per animal.

The snapshot widefield microscopes was used to visualise immunofluorescent slides for optimisation before going onto the slide scanner. Images were collected on a Zeiss Axioimager.D2 upright microscope using a 40x/0.75 Plan-neofluar objective (Zeiss) and captured using a Coolsnap HQ2 camera (Photometrics) through Micromanager software v1.4.23. Specific band pass filter sets for DAPI, FITC and Texas red were used to prevent bleed through from one channel to the next. Images were then processed using Fiji ImageJ (http://imagej.net/Fiji/Downloads).

Co-localisation images were collected on a Leica TCS SP8 AOBS inverted confocal using a 63x /1.4 Plan Fluotar oil lens with 2x confocal zoom. The confocal was set as 1 airy unit pinhole, 1000Hz unidirectional scan speed at 1024 x 1024 resolution. Images were collected using

hybrid detectors with the following detection mirror settings; FITC 504-554nm; Texas red 602-691nm by the white light laser with 488nm (10%) and 594nm (10%) laser lines respectively. The 3D Z-stacked images were collected sequentially to eliminate crosstalk between channels. 3D confocal images were stacked using Fiji ImageJ.

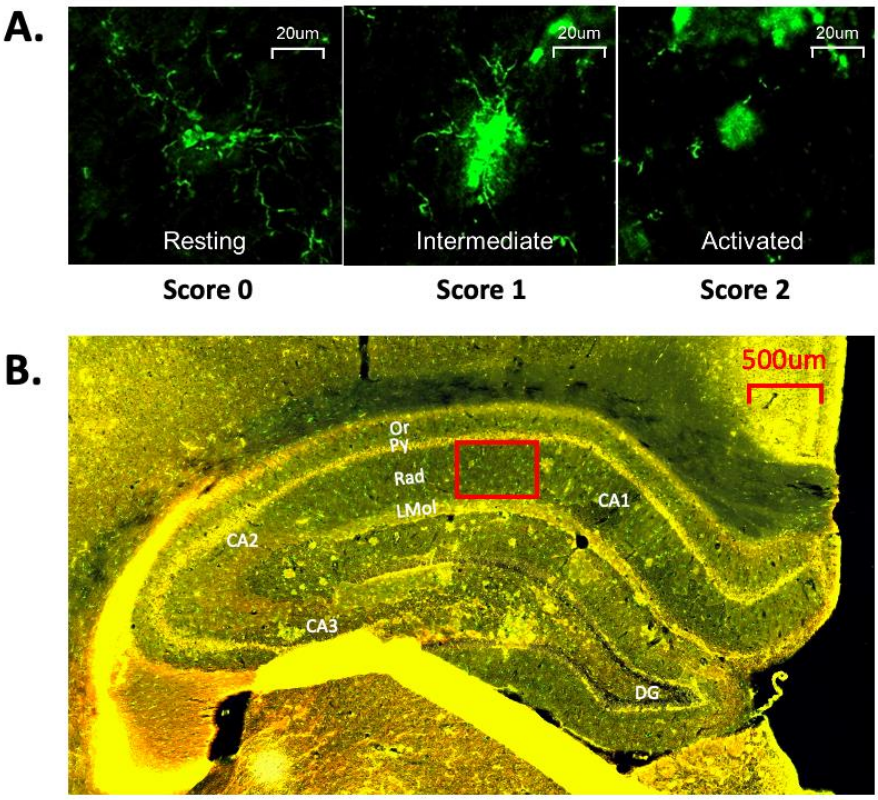


***Figure 4.9. Dorsal hippocampal CA1 region for analysis of immunofluorescence studies.***

***(A)*** *The activation states of each labelled microglia were scored. Microglia at different activation states in immunofluorescent sections. Images were 40x. Resting, intermediate and activated states were scored as 0,1 or 2 respectively.* ***(B)*** *A counting frame of about 0.6mm x 0.3mm was placed in the stratum radiatum of CA1 region in dorsal hippocampus. Microglia were labelled in this frame with a mark when only the green channel was on. Picture shown here is a merge of green (microglia) and red (IL-1β) channels. Or=stratum oriens; Py=Stratum pyramicale; Rad=Stratum radiatum; Lmol=lacunosum moleculare layer of the hippocampus. CA=Cornu Ammonis; DG=dentate gyrus; (Paxinos & Watson, 2007)*

### 4.2.3. Statistical analysis

Clear outliers that were due to Wes machine artefact were excluded, and all data analyses were carried out using GraphPad PRISM 9.3.1, apart from tests for equal variance. Normality was checked with the D'Agostino & Pearson test and Shapiro-Wilk test. Fisher's F test was performed to test for equal variance of two groups of data (GraphPad PRISM 9.3.1) while Levene's test was used when there were more than two groups (Excel, GraphPad PRISM 9.3.1). Unpaired t-test was performed to compare between the two genotypes for the change of a single factor. Mann-Whitney test instead of unpaired t-test was carried out if the data was non-parametrically distributed. To compare difference between two factors (e.g., hippocampal subregions & genotype; genotype & age), two-way ANOVA or mixed-effect model of two-way ANOVA was used depending on data parametricity. If two-way ANOVA results appeared significant, then *post hoc* multiple comparisons were performed, including Tukey's and Šídák's tests, based on recommendation.

## 4.3. Results

For all Wes analysis, the total protein did not differ between genotype at the same age.

### 4.3.1. Simple Wes analysis for the levels of synaptic markers (SNAP-25 & PSD-95)

Simple Wes analysis was applied to compare the amount of a pre-synaptic protein SNAP-25 and a post-synaptic protein PSD-95 to assess synaptic function in the DH. The levels of each protein were expressed as a percentage of control (i.e., WT). All data passed D'Agostino & Pearson test for normality. Unpaired t-test was performed to compare the statistical differences.

At 6 months of age, we found no significant difference in the levels of SNAP-25 between WT and TG (108.3±15.77% of WT; P=0.6723, WT: n=10, TG: n=11) (**Figure 4.10.A)**. At 6 months of age, we found a non-significant increase in the levels of PSD-95 between WT and TG (144.9±24.48% of WT; P=0.1157, WT & TG, n=10 per group) (**Figure 4.10.B)**.

At 9 months of age, we found no significant difference in the levels of SNAP-25 between WT and TG (95.50±8.14% of WT; P=0.6862, WT & TG, n=10 per group) (**Figure 4.10.C)**. At 9 months of age, we found a non-significant increase in the levels of PSD-95 between WT and TG (90.65±4.74% of WT; P=0.2060, WT & TG, n=10 per group) (**Figure 4.10.D)**.

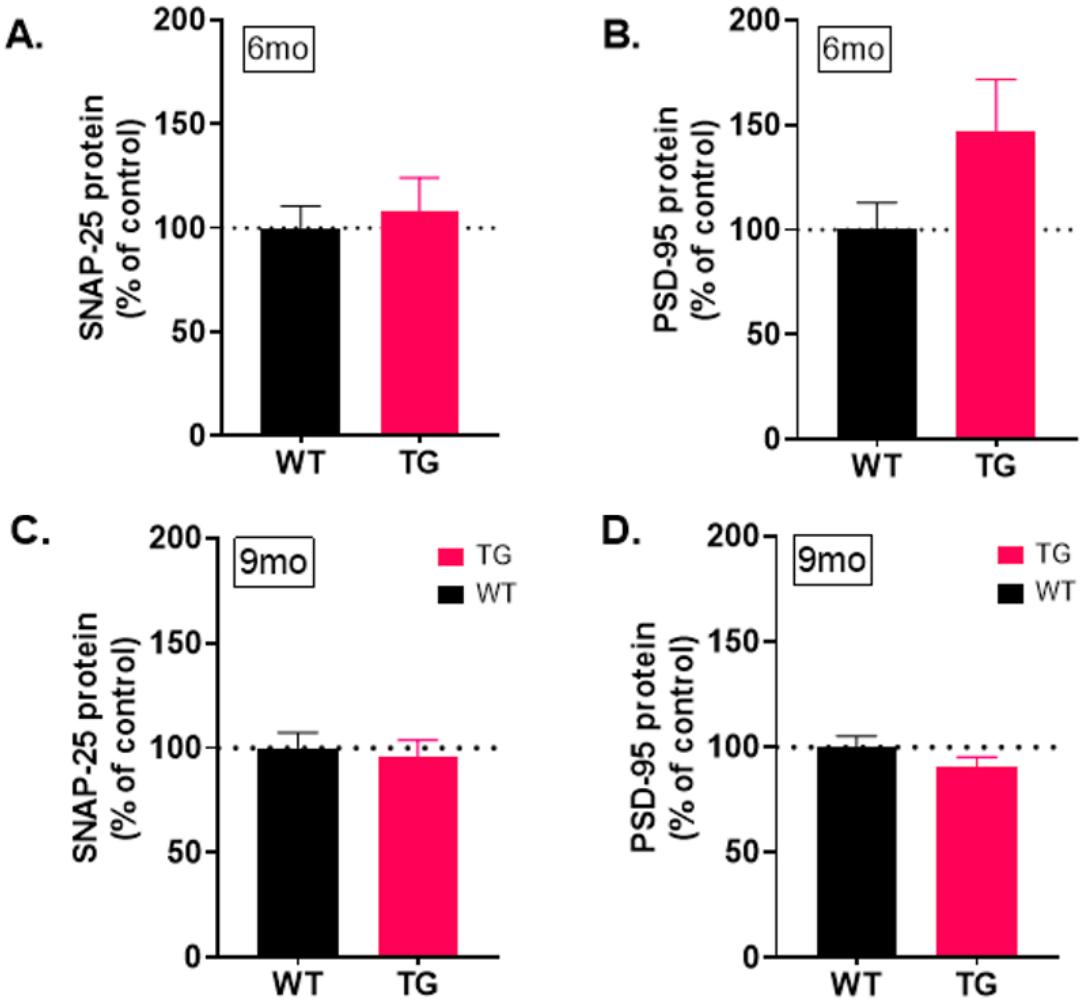

***Figure 4.10. Levels of synaptic markers SNAP-25, PSD-95 in the 6- and 9-month-old animals in the dorsal hippocampus.***

***(A)*** *6mo SNAP-25,* ***(B)*** *6mo PSD-95,* ***(C)*** *9mo SNAP-25, and* ***(D)*** *9mo PSD-95 levels in dorsal hippocampus was measured with Simple Wes. Levels of protein were normalised to total sample protein and expressed as the percentage increase of the control. Unpaired t-test was performed. Data presented as mean ± SEM. 6mo: WT: n=10, TG: n=11; 9mo: n=10 per group.*

### 4.3.2. Analysis of parvalbumin (PV) levels in dorsal hippocampus

#### *4.3.2.1. Simple Wes analysis of PV protein at 6 or 9 months old.*

Simple Wes analysis was used to compare the levels of PV proteins in the dorsal hippocampus of the TG and WT rats. The protein levels are presented as percentage of control (i.e., WT at each age). All data passed D'Agostino & Pearson test for normality. Unpaired t-test was performed to compare the statistical differences.

At 6 months of age, we found no significant difference in the levels of PV between WT and TG (96.36±12.47% of WT; P=0.7229, WT: n=10, TG: n=11) (**Figure 4.11.A)**.

At 9 months of age, we found a non-significant decrease in the levels of PV between WT and TG (84.68±7.44% of WT; P=0.2500, WT & TG, n=10 per group) (**Figure 4.11.B)**.

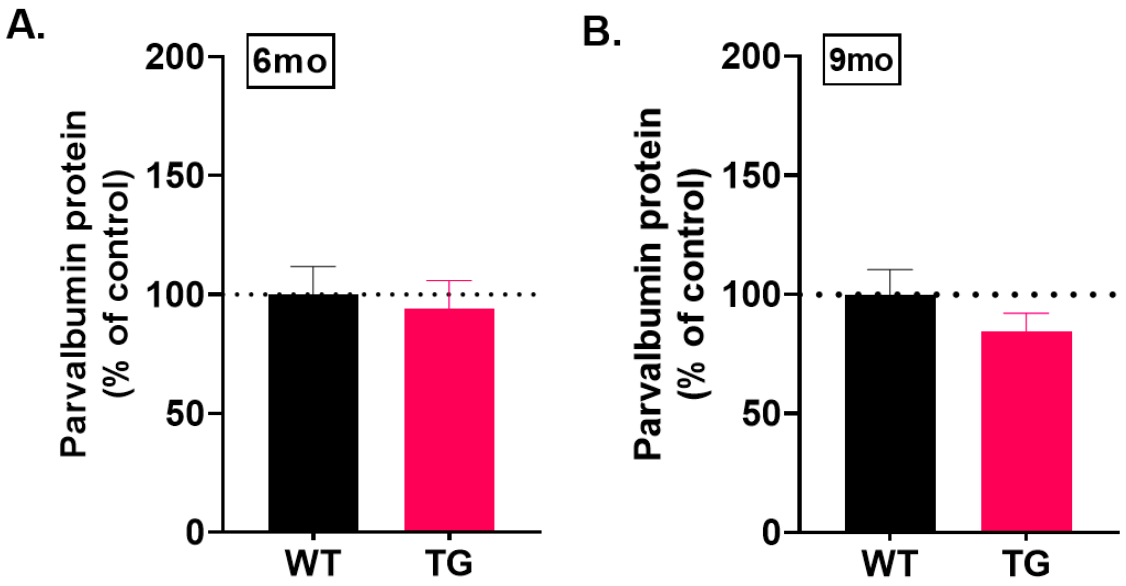


***Figure 4.11. Levels of PV in the 6- and 9-month-old animals in the dorsal hippocampus.***

***(A)*** *6mo and* ***(B)*** *9mo PV levels in dorsal hippocampus was measured with Simple Wes. Levels of protein were normalised to total sample protein and expressed as the percentage increase of the control. Unpaired t-test was performed. Data presented as mean ± SEM. 6mo: WT: n=10, TG: n=11; 9mo: n=10 per group.*

#### *4.3.2.2. Analysis of PV interneuron density in subregions of dorsal hippocampus.*

An immunohistochemistry (IHC) staining was conducted to compare the density of PV-immunoreactive interneurons in sub-regions of the DH at 6- and 9- months of age. A two-way ANOVA was performed to analyse the effect of genotype and DH sub-regions (CA1, CA2/3 or DG) on the density of PV-immunoreactive interneurons.

At 6 months old, we found a significant effect of subregion ($F(2, 30) = 134.2$, $P<0.0001$), but no genotype effect ($F(1, 15) = 0.5977$, $P=0.4515$) or interaction between subregions and genotypes ($F(2, 30) = 0.2270$, $P=0.7983$) (**Figure 4.12.A**).

However, in the 9-month-old animals, we found a statistically significant interaction effect ($F(2, 45)=11.49$; $P<0.0001$), a significant genotype effect ($F(1,45)=15.09$; $P<0.001$) and

significant subregion effect ($F(2,45)=167.8$; $P<0.0001$). *Post hoc* analysis of Šídák's multiple comparisons showed that there was a significant reduction in the mean cell density of PV-immunoreactive interneurons in the CA2/3 region of the DH in TG animals compared to WT ($P<0.0001$; WT: n=8, TG: n=9) **(Figure 4.12.B)**. There were no significant differences in PV-immunoreactive interneuron mean cell density in the CA1 ($P=0.9994$) and DG ($P=0.9534$) regions when comparing WT and TG animals.

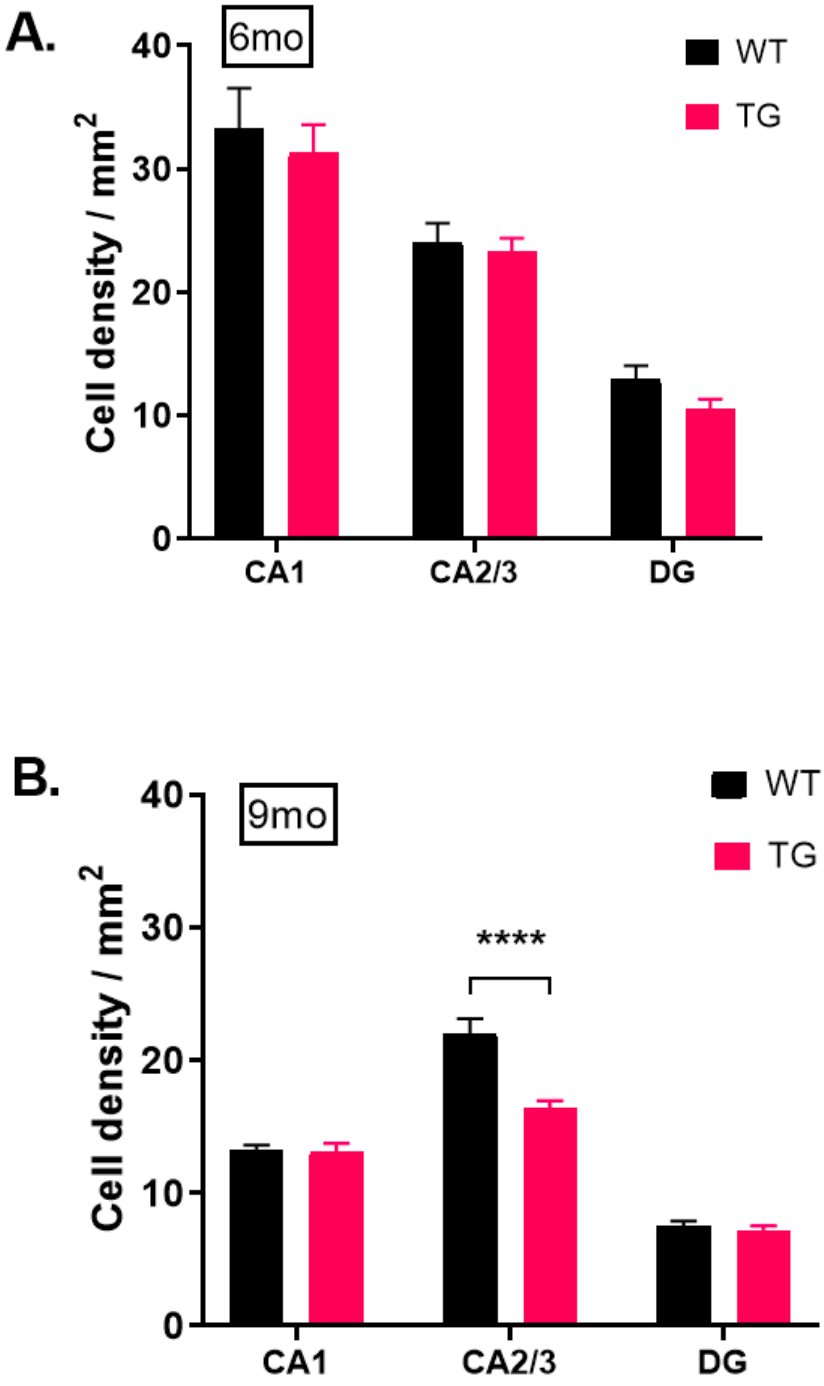


***Figure 4.12. Post-mortem analysis of PV interneuron density in dorsal hippocampal regions at 6mo & 9mo.***

*Density of PV-immunoreactive interneurons was calculated in hippocampal subregions (CA1, CA2/3 and DG) in **(A)** 6mo and **(B)** 9mo animals. Two-way ANOVA followed by Šídák's multiple comparisons test was performed. Data were presented as mean ± SEM. WT: n=8, TG: n=9 for both ages. ****p<0.0001.*

### 4.3.3. Simple Wes analysis for the levels of GABAerigc markers (GAD67 & GABA$\alpha_5$)

Simple Wes analysis was applied to compare the amount of GABAergic markers GAD67 and GABA$\alpha_5$ to assess GABAergic transmission in the DH. The levels of each protein were expressed as a percentage of control (i.e., WT). All data passed D'Agostino & Pearson test for normality. Unpaired t-test was performed to compare the statistical differences.

At 6 months of age, we found no significant difference in the levels of GAD67 between WT and TG (106.8±12.63% of WT; P=0.6731; WT: n=10, TG: n=11) (**Figure 4.13.A)**. At 6 months of age, we found no significant difference in the levels of GABA$\alpha_5$ between WT and TG (92.16±12.90% of WT; P=0.6165; WT&TG, n=9 per group) (**Figure 4.13.B)**.

At 9 months of age, we found no significant difference in the levels of GABA$\alpha_5$ between WT and TG (109.5±7.05% of WT; P=0.3172, WT & TG, n=10 per group) (**Figure 4.13.C)**. At 9 months of age, we found a non-significant increase in the levels of GABA$\alpha_5$ between WT and TG (96.27±9.24% of WT; P=0.7891, WT & TG, n=10 per group) (**Figure 4.13.D)**.

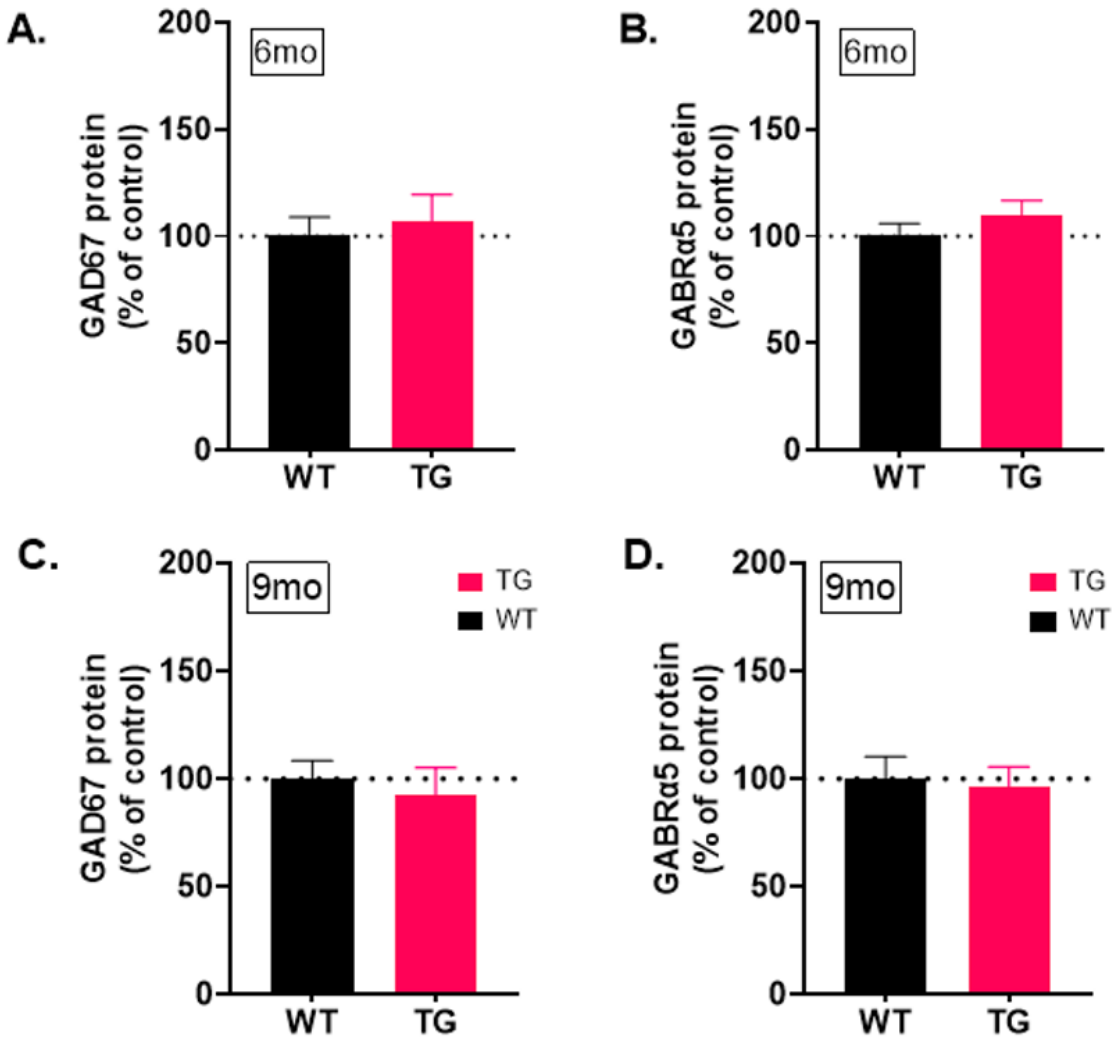


***Figure 4.13. Levels of GABAergic markers GAD67, GABAα$_5$ in the 6- and 9-month-old animals in the dorsal hippocampus.***

***(A)*** *6mo GAD67,* ***(B)*** *6mo GABAα$_5$,* ***(C)*** *9mo GAD67, and* ***(D)*** *9mo GABAα$_5$ levels in dorsal hippocampus was measured with Simple Wes. Levels of protein were normalised to total sample protein and expressed as the percentage increase of the control. Unpaired t-test was performed. Data presented as mean ± SEM. WT&TG n=10 per group.*

### 4.3.4. Simple Wes analysis for the levels of glutamatergic markers (NR2A & NR2B)

Simple Wes analysis was applied to compare the amount of NMDA receptor 2A (NR2A) and NMDA receptor 2B (NR2B) to compare changes in the amount of glutamatergic NMDA receptor subunit in the DH in the 6-month-old animals. The levels of each protein were

expressed as a percentage of control (i.e., WT). All data passed D'Agostino & Pearson test for normality. Unpaired t-test was performed to compare the statistical differences.

At 6 months of age, we found no significant difference in the levels of NR2A between WT and TG (112.2±7.46% of WT; P=0.2928; WT: n=10, TG: n=11) (**Figure 4.14.A)**. Similarly, we found no significant difference in the levels of NR2B between WT and TG (93.55±8.05% of WT; P=0.5321; WT: n=10, TG: n=11) (**Figure 4.14.B)**.

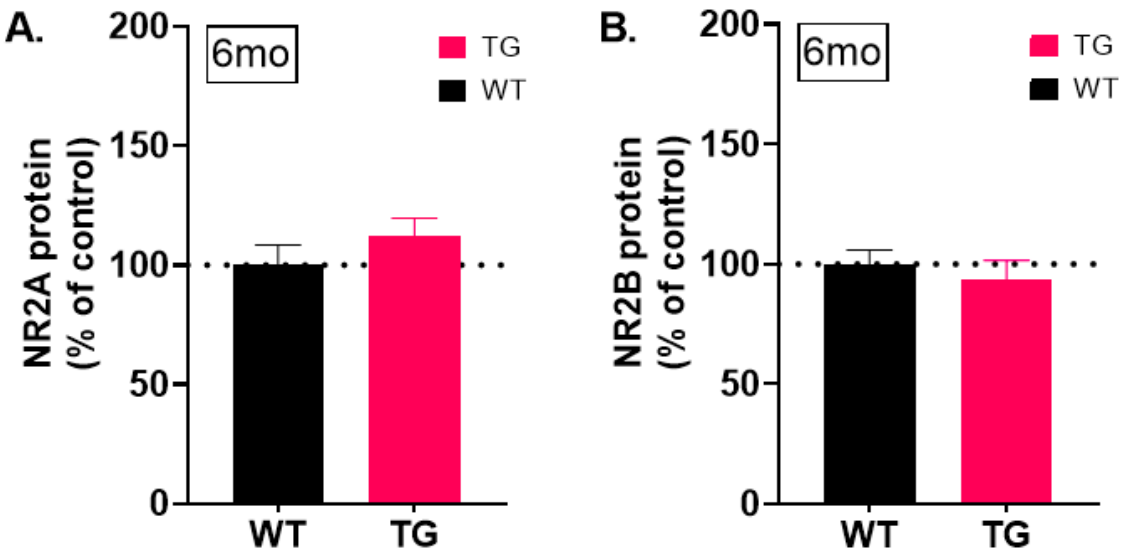


***Figure 4.14. Levels of NR2A and NR2B in the 6-month-old animals in the dorsal hippocampus.***

***(A)*** *6mo NR2A and* ***(B)*** *6mo NR2B levels in dorsal hippocampus was measured with Simple Wes. Levels of protein were normalised to total sample protein and expressed as the percentage increase of the control. Unpaired t-test was performed. Data presented as mean ± SEM. WT: n=10, TG: n=11.*

The ratio of NR2A to NR2B was calculated and compared between the genotypes at 6 months old. The data did not pass D'Agostino & Pearson test for normality, so Mann-Whitney U test was performed to compare the statistical differences. At 6 months of age, we found no

significant difference in the ratio of NR2A:NR2B between WT and TG (P=0.2512; WT: n=10, TG: n=11) (**Figure 4.15**).

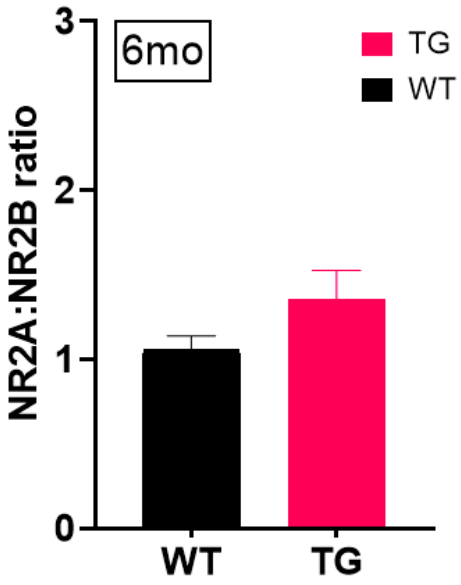


***Figure 4.15. Ratio of NR2A to NR2B in the 6-month-old animals in the dorsal hippocampus.***

*Levels of N2RA and NR2B in dorsal hippocampus of the 6mo animals was measured with Simple Wes, and the NR2A:NR2B ratio was calculated. Mann-Whitney U test was performed. Data presented as mean ± SEM. WT: n=10, TG: n=11.*

### 4.3.5. Analysis on the degree of neuroinflammation

#### 4.3.5.1. Microglia density in the dorsal hippocampus

An IHC staining was conducted to compare the density of microglia (Iba1+) in sub-regions of the DH at 6- and 9- months of age. A two-way ANOVA was performed to analyse the effect of genotype and DH sub-regions (CA1, CA2/3 or DG) on the density of Iba-1-immunoreactive cells.

At 6 months old, we found a significant effect of subregion ($F(2, 36) = 4.840$, $P=0.0137$), but no genotype effect ($F(1, 18) = 0.1346$, $P=0.7180$) or interaction between subregions and genotypes ($F(2, 36) = 1.439$, $P=0.2504$). *Post hoc* analysis of Šídák's multiple comparisons

showed that in TG animals, the microglia density in CA2/3 region was significantly higher than in DG (P=0.0341) (**Figure 4.16.A**).

However, in the 9-month-old animals, we found no statistical effect of subregion (F (2, 34) = 0.6147, P=0.5467), genotype (F (1, 17) = 0.09531, P=0.7613) or the interaction between two factors (F (2, 34) = 1.500, P=0.2376) using two-way ANOVA (**Figure 4.16.B**).

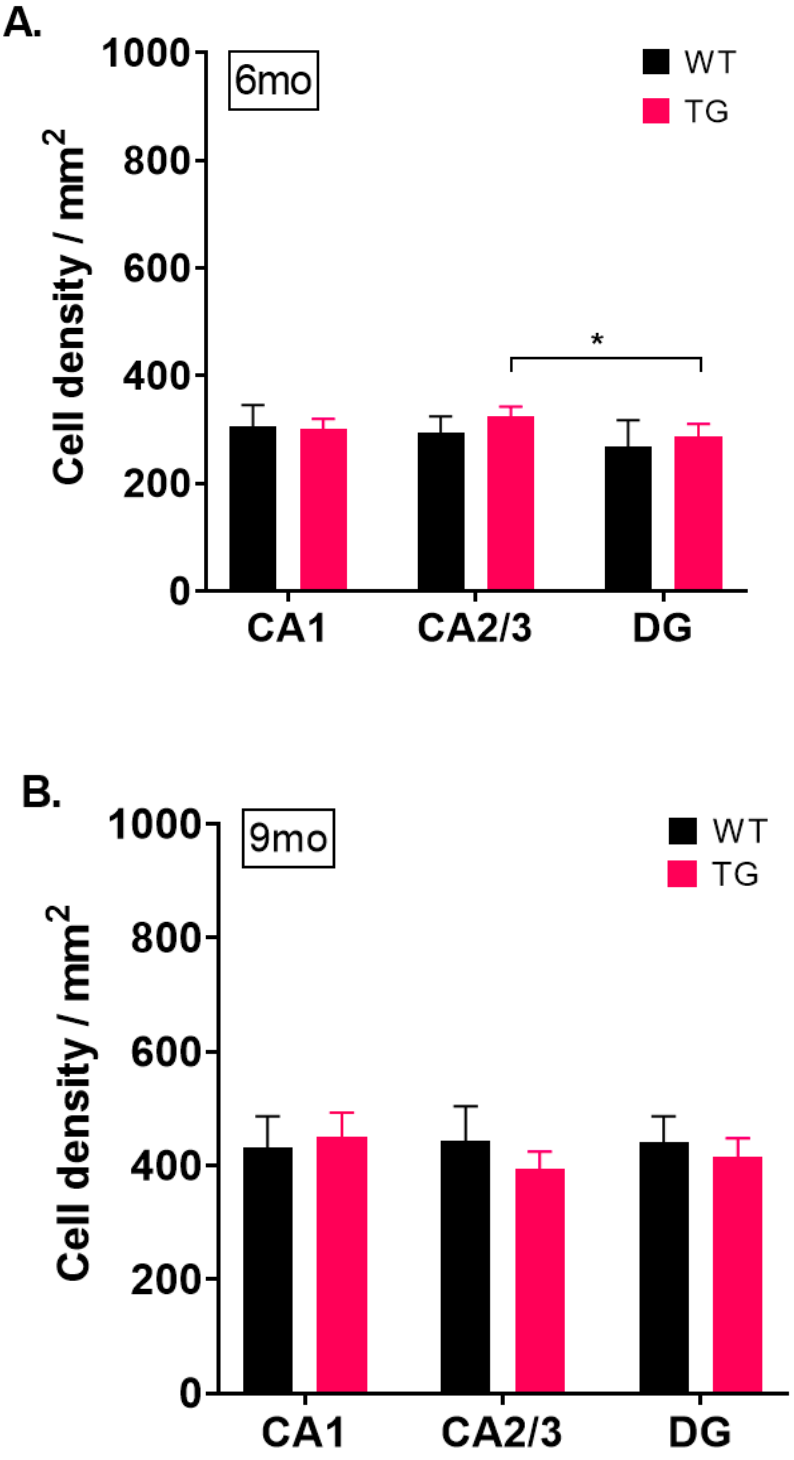


***Figure 4.16. Post-mortem analysis of microglia (Iba1+) density in dorsal hippocampal regions at 6mo & 9mo.***

*Density of microglia was calculated in hippocampal subregions (CA1, CA2/3 and DG) in* ***(A)*** *6mo and* ***(B)*** *9mo animals. Two-way ANOVA followed by Šídák's multiple comparisons test was performed. Data were presented as mean ± SEM. 6mo: WT: n=9, TG: n=11; 9mo: WT: n=10, TG: n=9. *p<0.05.*

Additionally, total microglia density was calculated for dorsal hippocampus (DH) in the 6- and 9-month-old animals. Two-way ANOVA was conducted to compare the effect of genotype and age. We found a significant effect of age ($F(1, 35) = 13.19$, $P=0.0009$), but no statistical effect of genotype ($F(1, 35) = 0.01177$, $P=0.9142$) or an interaction between these two factors ($F(1, 35) = 0.2496$, $P=0.6205$). *Post hoc* test of Šídák's multiple comparisons showed that in the WT group, total microglia density in DH was significantly higher in the 9-month-old animals compared to the 6-month ($P=0.0131$). The increase of total microglia density in the TG groups was not significantly different between age of 6mo and 9mo ($P=0.0621$) (**Figure 4.17**).

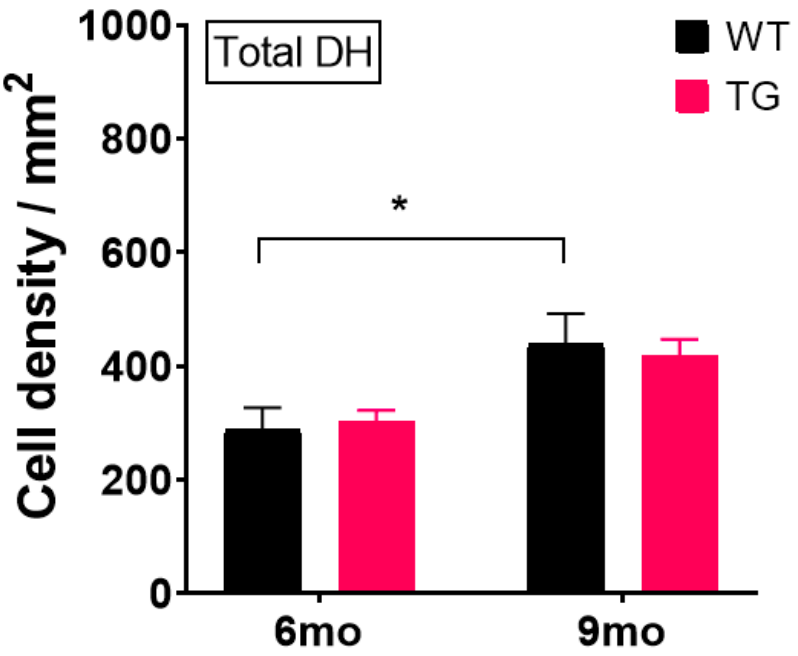


***Figure 4.17. Total microglia (Iba1+) density in dorsal hippocampal (DH) at 6mo & 9mo.***

*Two-way ANOVA followed by Šídák's multiple comparisons test was performed. Data were presented as mean ± SEM. 6mo: WT: n=9, TG: n=11; 9mo: WT: n=10, TG: n=9. *p<0.05.*

#### *4.3.5.2.* Measurements of microglia activation in dorsal hippocampal CA1

Using the immunofluorescence slides, a minimum of 100 microglia cells were identified and selected in the CA1 region of DH, and their activation state was assessed (i.e., resting, intermediate and activated; see **Figure 4.9**). The percentage of microglia at each activation state was calculated.

At the age of 6 months, two-way ANOVA showed that there was significantly different of percentage of microglia under different activation states ($F(2, 20) = 114.4$, $P<0.0001$), but there was no effect of genotype ($F(1, 10) = 0.3685$, $P=0.5574$). However, the interaction between activation state and genotype was significant ($F(2, 20) = 4.651$, $P=0.0219$). Tukey's multiple comparisons test showed that there were more microglia at resting or intermediate state compared to the activated state for both genotype ($P<0.0001$).

As shown by Tukey's test, there were more microglia at resting state than intermediate state in WT rats ($P=0.0114$); whereas in TG rats, no statistical difference was found between percentage of resting microglia and those at intermediate state ($P=0.7127$). Šídák's multiple comparisons test was used to compare differences between the genotype groups. As a result, TG rats had significantly lower percentage of resting microglia compared to the WT controls ($P=0.0197$), while no *post hoc* genotype difference was found for the percentage of microglia at other activation states (WT vs. TG: intermediate: $P=0.0976$; activated: $P=0.8706$) (**Figure 4.18**).

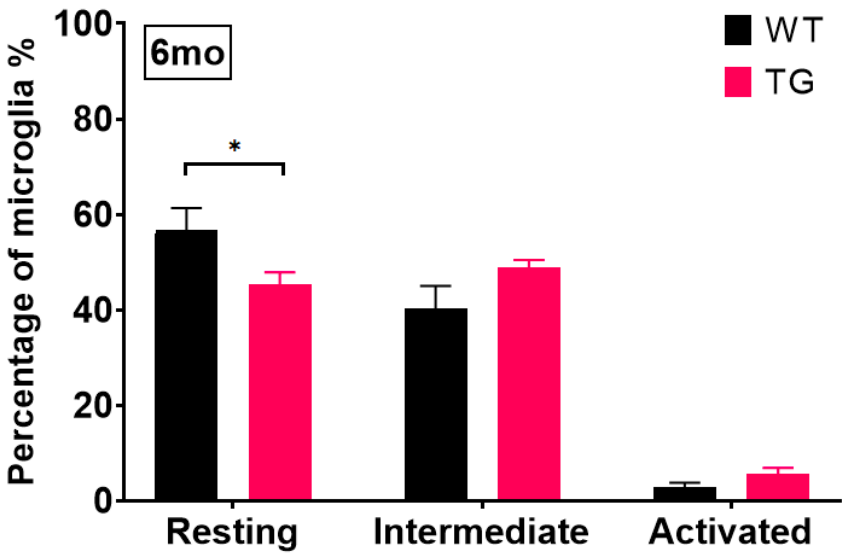


***Figure 4.18. Microglia activation states in dorsal hippocampal CA1 of 6-month-old animals.***

*Percentages of microglia at resting, intermediate or activated state in dorsal hippocampal CA1 region were plotted for animals at 6 months of age. Two-way repeated measure ANOVA was performed followed by Šídák's multiple comparisons test. Data presented as mean ± SEM. WT: n=5, TG: n=7. *P<0.05.*

In the 9-month-old animals as shown in **Figure 4.19**, two-way ANOVA showed significant changes in activation state ($F(2, 18) = 74.41$, $P<0.0001$) and the interaction of activation state and genotype ($F(2, 18) = 23.50$, $P<0.0001$), but there was no ANOVA difference for the genotype factor itself ($F(1, 9) = 0.07746$, $P=0.7871$). For WT rats, Tukey's multiple comparison showed that the percentage of resting microglia was significantly higher than that at the intermediate ($P<0.0001$) or activated state ($P<0.0001$). Also, there were more microglia at intermediate state compared to at the activated state in the WT controls ($P=0.0001$), as shown by Tukey's test. For TG rats, significantly more microglia were found to be at intermediate state compared to at resting ($P=0.0122$) or activated state ($P<0.0001$) using Tukey's test. However, the percentage of microglia at activated state was shown to be markedly less than that of resting microglia ($P=0.0005$). Interestingly, the *post hoc* of Šídák's

multiple comparisons test showed that in the TG rats, there were significantly more microglia at the intermediate state compared to the WT controls (P<0.0001), whereas the percentage of resting microglia in the TG animals were significantly lower than the WTs (P<0.0001) (**Figure 4.19**). No difference was found in terms of percentage of microglia under the activated state between genotype groups (P=0.5627).

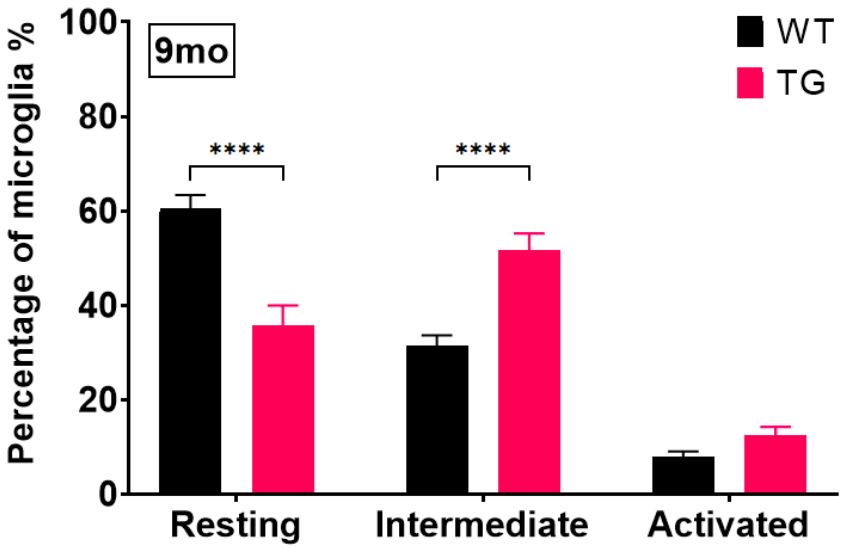


***Figure 4.19. Microglia activation states in dorsal hippocampal CA1 of 9-month-old animals.***

*Percentages of microglia at resting, intermediate or activated state in dorsal hippocampal CA1 region were plotted for animals at 9 months of age. Two-way repeated measure ANOVA was performed followed by Šídák's multiple comparisons test. Data presented as mean ± SEM. WT: n=6, TG: n=5. ****P<0.0001.*

For each genotype group at each age, the average activation score of the microglia in hippocampal CA1 region was calculated, as displayed in **Figure 4.20**. two-way ANOVA showed that there was significant effect of genotype (F (1, 19) = 26.06, P<0.0001) and age (F (1, 19) = 26.06, P=0.0494), but no significant interaction between these two factors was found (F (1, 19) = 3.272, P=0.0863). As suggested by Šídák's multiple comparisons test, the origin of the genotype effect came from the 9-month-old TG rats, who demonstrated significantly higher

scores and hence more inflammation than the age-matching WT controls (P=0.0002) (**Figure 4.20**). In contrast, the 6-month-old animals show statistical differences between genotypes (P=0.0562). Moreover, Šídák's multiple comparisons test showed that the significant age effect came from the TG rats, where they scored markedly higher at the age of 9 months than 6 months (P=0.0222) (**Figure 4.20**). However, in the WT controls, no difference of age was found for mean microglia activation score (P=0.9751).

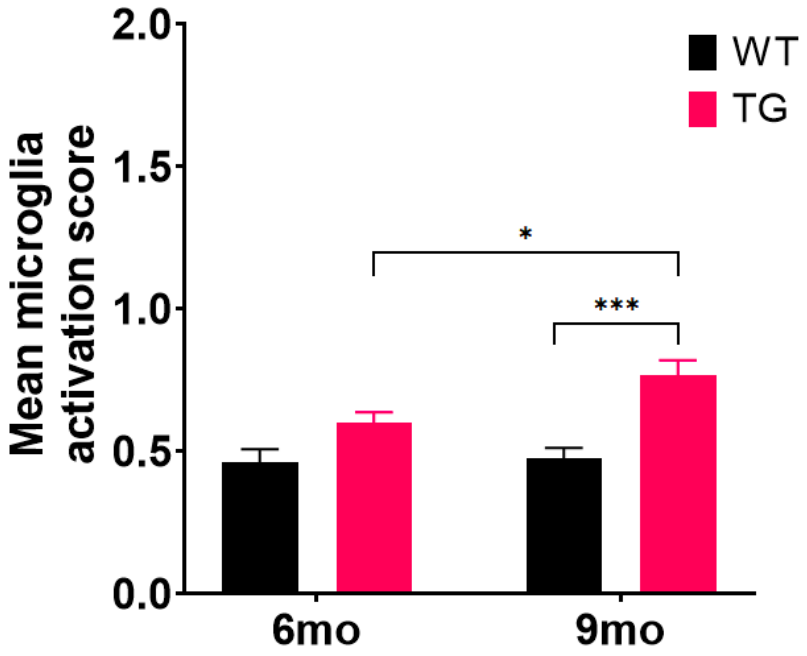


***Figure 4.20. Comparison of the average microglia activation score in dorsal CA1 in 6- and 9-month-old animals.***

*Two-way ANOVA was performed followed by Šídák's multiple comparisons test. Data presented as mean ± SEM. 6mo: WT: n=5, TG: n=7; 9mo: WT: n=6, TG: n=5. *P<0.05, ***P<0.001.*

#### *4.3.5.3.* Microglia expressing IL-1*β* in dorsal hippocampal CA1

The proinflammatory cytokine IL-1β was co-stained with microglia in dorsal hippocampus in the 6- and 9-month-old animals and analysed in the CA1 region for the percentage of IL-1β expressing microglia.

**Figure 4.21** shows the confocal images of the co-staining from four randomly selected animals. Notably, in 6 month and 9-month-old WT rats, the microglia had small cell bodies with long branches, indicating being at the resting state. However, in the 9-month-old TG rats, the microglia in CA1 region were more likely to have big spherical cell body with short and less projections, with IL-1β located inside of the cell body, suggested by the 3D confocal image in **Figure 4.21**.

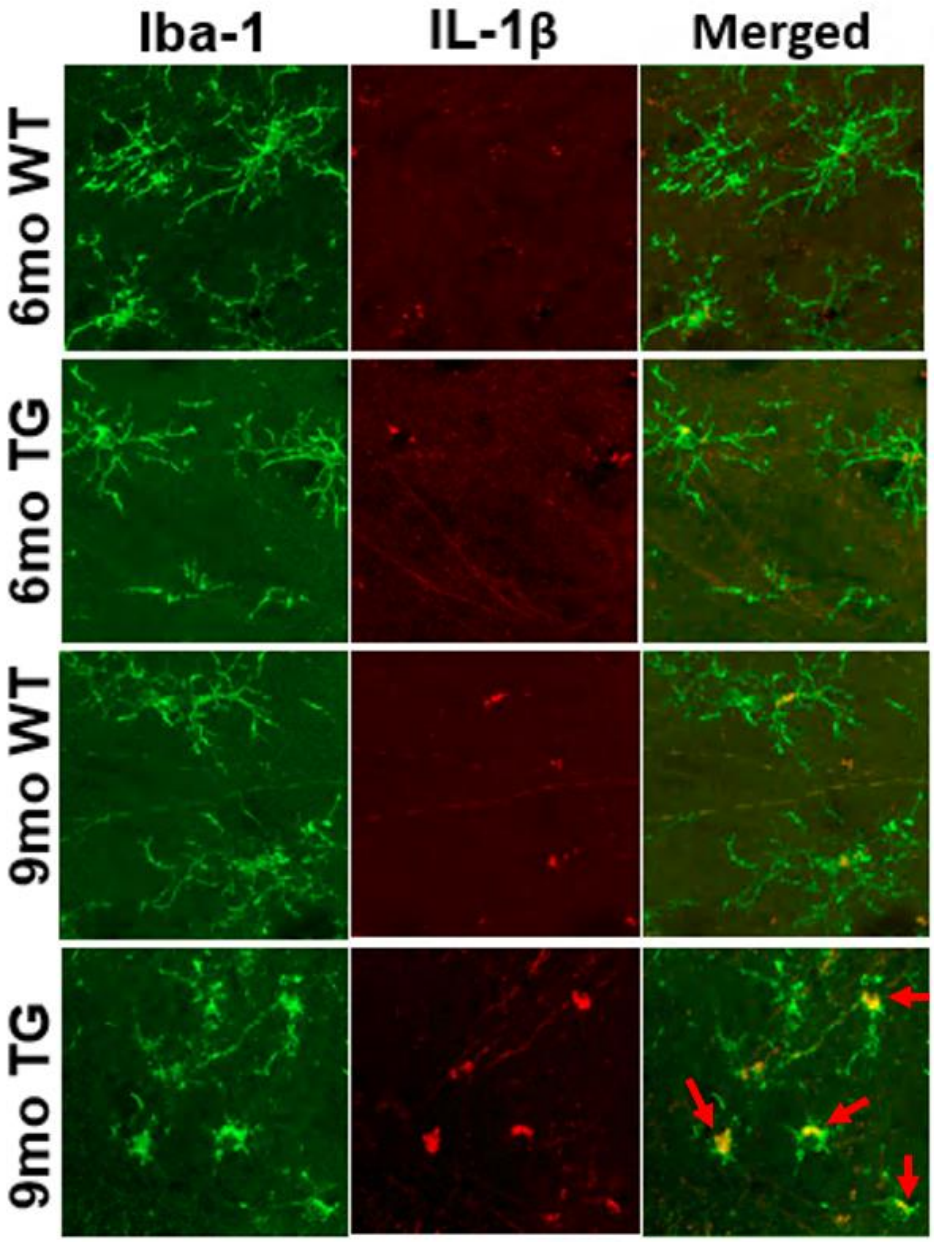


***Figure 4.21. Confocal images of microglia expressing interleukin-1β (IL-1β) in dorsal hippocampal CA1 in animals at both ages.***

*Iba1 antibody for microglia (green) co-stained with IL-1β (red) (63x confocal, 2x zoom-in). The co-expressions are shown in the merged pictures* (yellow).

The percentage of IL-1β-expressing microglia was counted in a minimum of 100 labelled microglia in the CA1 region of dorsal hippocampus. Statistical analysis was performed to investigate effects of genotype and age.

A two-way ANOVA revealed that both genotype (F (1, 19) = 11.34, P=0.0032) and age (F (1, 19) = 10.37, P=0.0045) significantly affected the number of IL-1β-expressing microglia in CA1, but there was no interaction of these two factors (F (1, 19) = 0.0006230, P=0.9803).

Further comparisons were made by Šídák's test, where there were statistically more microglia expressing IL-1β in the 6-month-old TG rats compared to the age-matching WT controls (P=0.0487).

9-month-old TG rats also displayed more IL-1β-expressing microglia in CA1 region than WT rats as shown in **Figure 4.22.A**, yet the statistical comparison was not significant by Šídák's test (P=0.0617). As for the *post hoc* comparison for the ageing effect, there was no age difference in either genotype group by Šídák's multiple comparison (WT: P=0.0706; TG: P=0.0650).

Overall, there was a shift of microglial activation from resting to the transition state and increase of expression of the proinflammatory cytokine IL-1β in the CA1 region with increasing age which is more obvious in the TG animals (**Figure 4.22.B**).

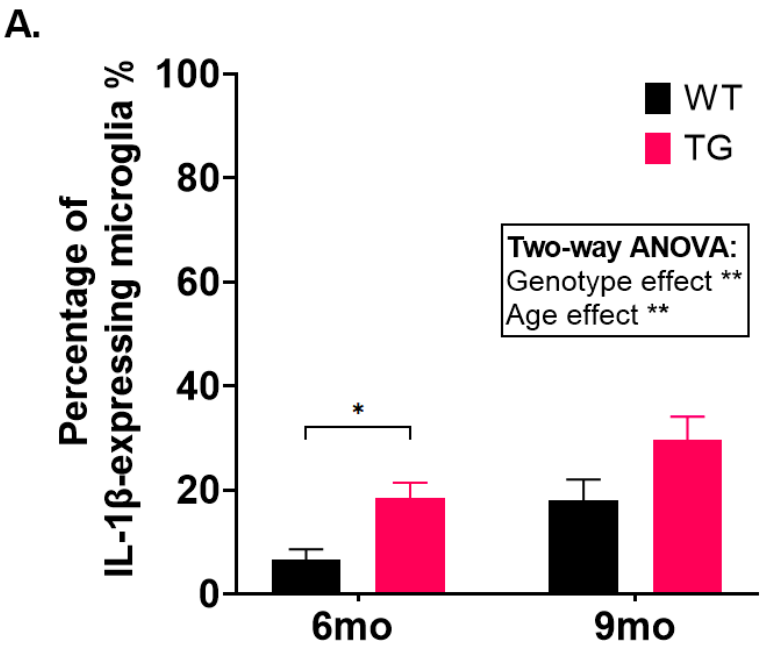

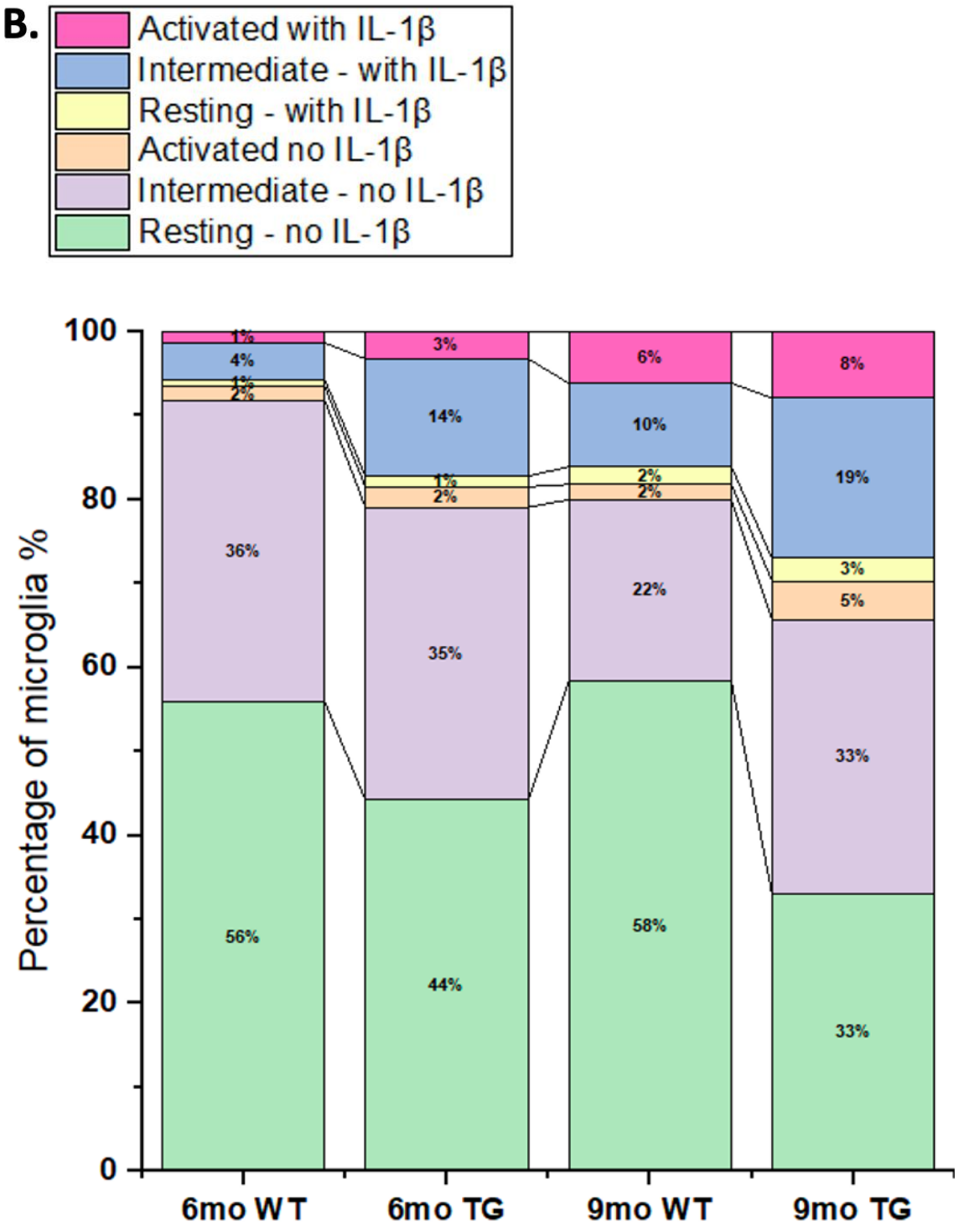


***Figure 4.22. Percentage of microglia expressing interleukin-1β (IL-1β) in dorsal hippocampal CA1.***

***(A)*** *Comparison of percentages of IL-1β-expressing microglia in CA1 region at 6mo and 9mo in WT and TG rats. Two-way ANOVA with Šídák's multiple comparisons test was performed.* ***(B)*** *A summary of percentage of IL-1β-expressing microglia under resting, intermediate and activated states at 6mo and 9mo in WT and TG rats. Data presented as mean ± SEM. 6mo: WT: n=5, TG: n=7; 9mo: WT: n=6, TG: n=5. *P<0.05, **P<0.01.*

### 4.3.6. Microglia clustered in hippocampus of 9-month-old TG rats

Clusters of Iba-1-positive microglia was found in the IHC sections (**Figure 4.23**) and IF sections of the 9mo TG rats in the dorsal hippocampus. The clusters were round shaped, with a darker colour compared to the non-clustered regions. Microglia were bundled together, and more densely contacted with one another compared to non-clustered regions. Microglia in the clusters were more activated at the intermediate and activated ameboid states. No resting microglia was observed in the clustered regions. On contrary, microglia clusters were not observed in the 6-month-old animals (WT & TG), or WT rats at 9 months of age.

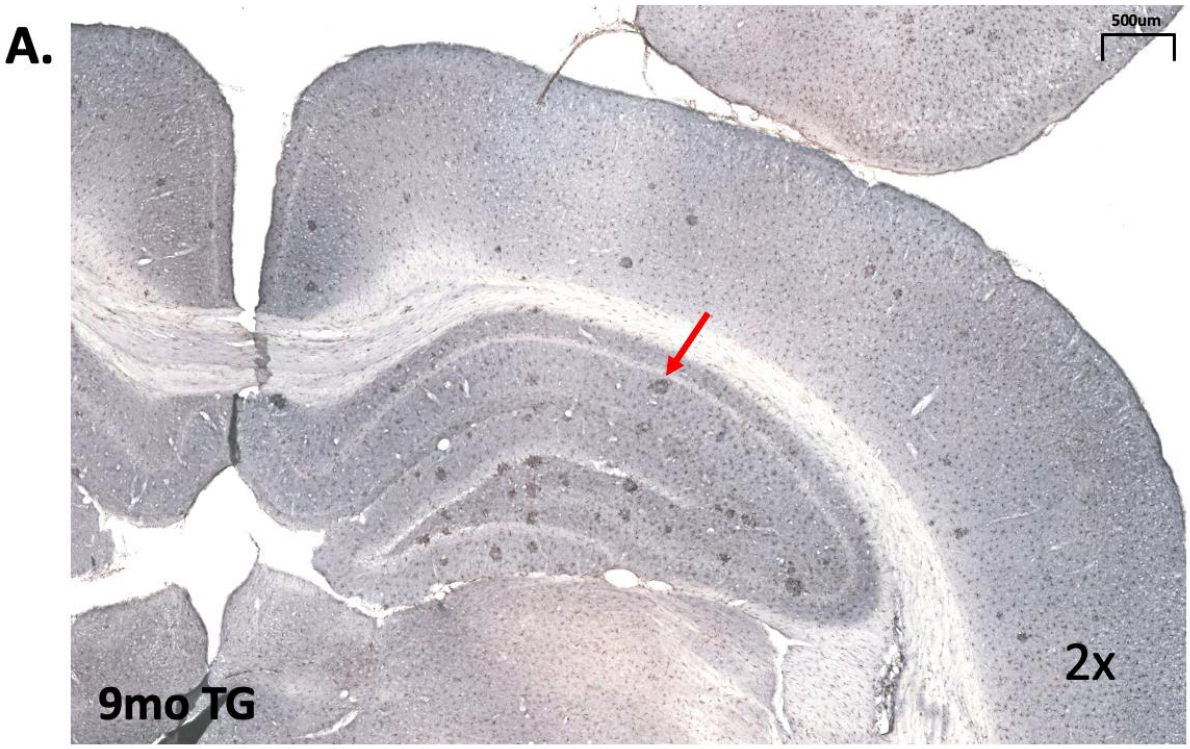

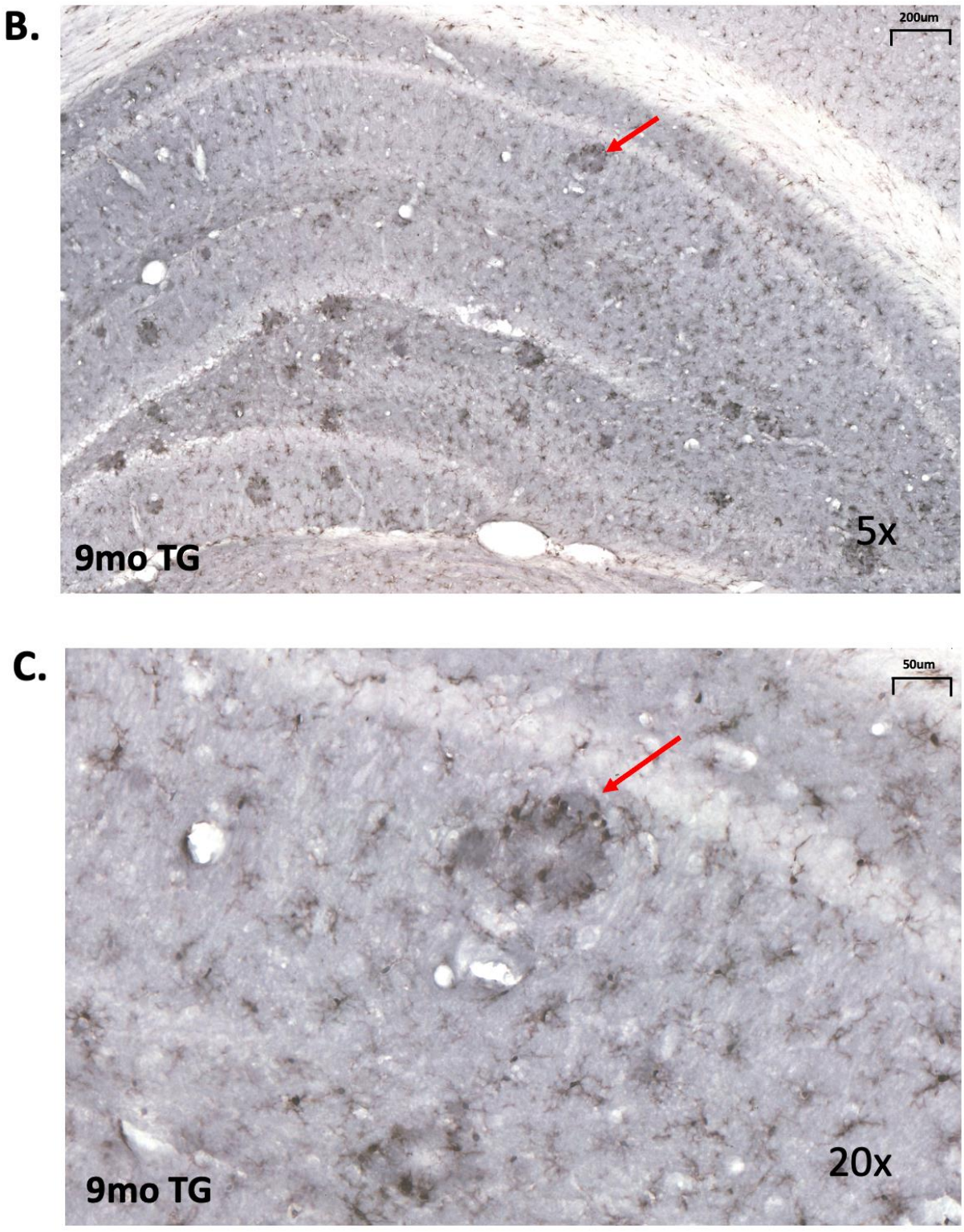


***Figure 4.23. 9-month-old TG showed microglia clustering in the dorsal hippocampus.***

*Iba-1 stain for microglia in dorsal hippocampus from a randomly selected 9-month-old TG animal at the magnification of* ***(A)*** *2x,* ***(B)*** *5x, and* ***(C)*** *20x. This 9mo TG sections showed clusters of microglia at intermediate to activated states, and this phenomenon was also found in other 9mo TG rats. No cluster was observed at 6mo old or in WT animals.*

These microglia clusters were also found in the cortex above the hippocampus in the same anterior-posterior (A-P) plane where dorsal hippocampi locate, particularly in the perirhinal cortex, dorsolateral entorhinal cortex, piriform cortex, and basolateral amygdala (**Figure 4.24**). Again, no microglia cluster was found in the cortices of younger animals or in WT rats.

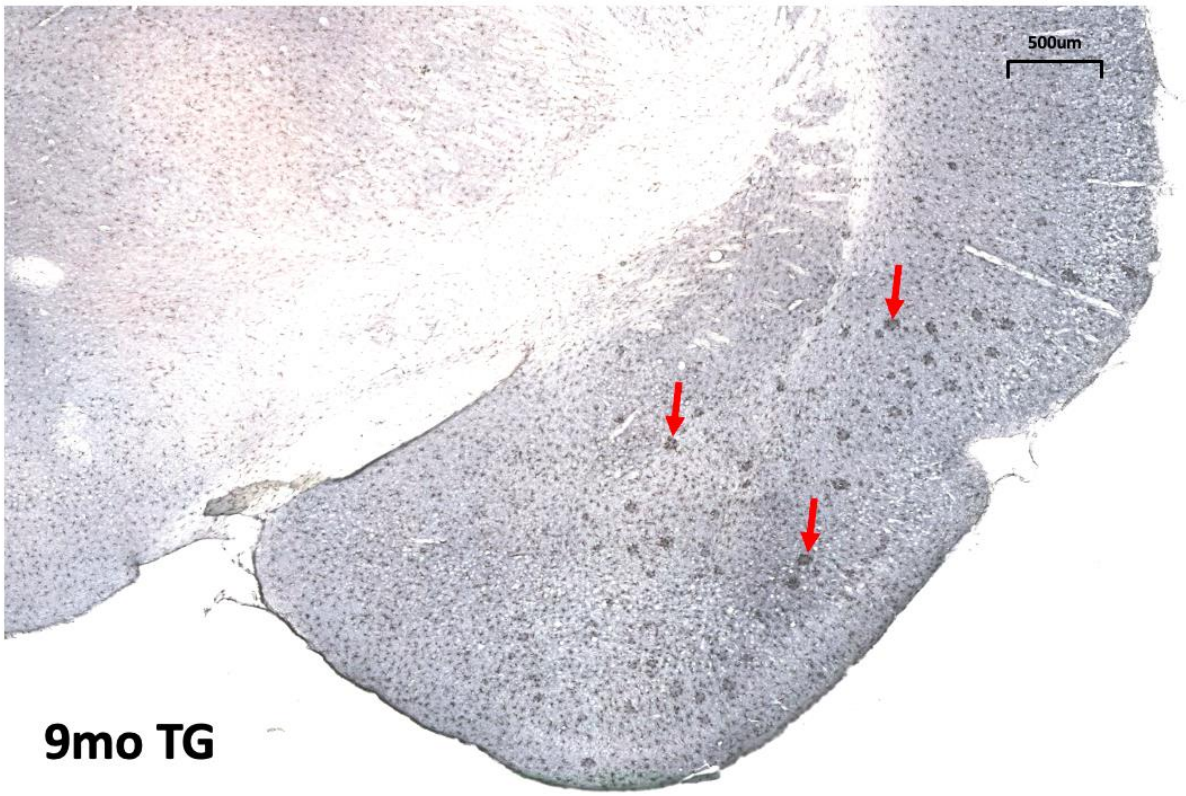


***Figure 4.24. 9-month-old TG showed microglia clustering in the cortex.***

*Iba-1 stain for microglia from a randomly selected TG animal. 9mo TG rats showed clusters of microglia at the cortex, especially concentrated at perirenal cortex, dorsolateral entorhinal cortex, piriform cortex, and basolateral amygdala. No cluster was observed at 6mo old or in WT animals.*

## 4.4. Discussion

To figure out the molecular mechanisms underlying the changes seen in the evoked responses, the dorsal hippocampus was taken out from the WT and TG rats at 6 and 9 months of age for post-mortem analysis. Pre- and post-synaptic proteins and markers involved in E/I balance were analysed using immunohistochemical methods. Since neuroinflammation has been recently recognised as another pathological hallmark for AD, the amount of neuroinflammation was also analysed with microglia activation as well as its co-expression with the proinflammatory cytokine IL-1β.

### 4.4.1. GABAergic disinhibition in hippocampal CA2/3 in 9-month-old TG rats.

In this study, simple Wes's analysis showed no statistical difference in PV protein levels in the dorsal hippocampal in either 6- or 9-months old TG animals. However, immunohistochemical staining showed that, in the 9-month-old TG rats, there was a reduction in the density of PV interneurons in the subregion of dorsal hippocampus, with no changes in the CA1 or DG. This result implies a reduction of GABAergic inhibition upstream of the CA1 region of the hippocampal Schaffer collateral in the 9-month-old TG rats. In contrast, PV interneuron density was unchanged in all subregions in 6-month-old TG animals.

A general reduction of PV interneuron density in the hippocampus is in line with a number of studies in AD mouse models. In Tg2576 mice expressing human Aβ, the hippocampal CA1-3 PV density was unchanged at the age of 6-7 months, but markedly reduced at 14-19 months (Huh et al., 2016). In addition, in APP/PS1 KI mice, there was a reduction of PV interneuron density in the CA1/2 region at 10 months old (Takahashi et al., 2010). Loss of PV interneuron density was also found in all hippocampal subregions in the 12-month-old 5xFAD mice with

Aβ plaques, but unchanged in the hippocampus of age-matching Tg4-42 mice without plaque, suggesting loss of PV interneuron could be associated with Aβ burden (Giesers and Wirths, 2020). Interestingly, a loss of PV interneurons was also observed in the CA1/2 and subiculum at 1-month in the TgCRND8 mouse model of AD (Mahar et al., 2016). These animals also had increased APP production (Mahar et al., 2016). However, the study of PV expression in AD models have also found other changes. For example, in a study in APPsw/PS1ΔE9 mice, there was an increase in PV cell density at 3 and 12 months in the hippocampal CA1 and CA3 regions and increased in DG at 12 months old (Verdaguer et al., 2015).

In the current study we found a reduction in the density of PV interneurons while PV protein levels were unchanged in the dorsal hippocampus. This could imply a compensatory increase of PV protein expression in individual interneurons in the dorsal hippocampus to balance out a potential reduction of PV interneuron function. However, in 9-month-old animals, although PV levels in TG rats were not significantly different from WT, there was a tendency of a reduction of PV protein in the TGs, which could link with the decrease in PV interneuron density in the dorsal hippocampus at this age. Also, the *in vivo* evoked response recordings (**Chapter 2, Section 2.3.2.1**) showed changes with an increased I/O, which could result from GABAergic disinhibition upstream of the CA3-CA1 circuit through a reduction of PV interneuron density in the CA2/3 region. To further clarify a direct role of PV interneurons in the hyperexcitability in the CA3-CA1 circuit, further investigations could be undertaken using pharmacological blockade or gain of functions, or selectively increase or decrease the activity of CA2/3 PV interneurons, by viral infection or optogenetic methods.

Albeit PV interneurons being an important class of GABAergic inhibitory interneurons that are also critical in generating gamma oscillations for cognitive processes, inhibitory interneurons

expressing other proteins are also resident in hippocampus and have been investigated in AD models. NYP- and SOM- expressing interneurons are generators of theta oscillation (4-10Hz) (Klausberger et al., 2003).The density NPY- and SOM- expressing interneurons were both decreased in CA1/2 and CA3 regions in 6-month-old TgCRND8 mice (Albuquerque et al., 2015). NYP-expressing interneurons were also reduced in the DG (Albuquerque et al., 2015). A study of 22 different pre- and post- synaptic, GABAergic and glutamatergic markers in 6-month-old PS1xAPP AD mice found a decrease in the expression of NPY and SOM interneurons with no changes in other markers including PV (Ramos et al., 2006). This also suggests a need to assess the changes in other types of GABAergic interneurons alongside PV.

### 4.4.2. Synaptic, glutamatergic and GABAergic markers were not found to be affected in the TG rats.

AD is characterised as a synaptic disease due to depression of synaptic plasticity that interferes with learning and memory. To study whether the pre-synaptic compartment or the post-synaptic compartment or both contribute to the synaptic deficits seen in the *in vivo* electrophysiology recordings, the levels of a pre-synaptic marker, SNAP-25, and a post-synaptic marker, PSD-95, were measured in the dorsal hippocampus. Using simple Wes analysis, there was no change of SNAP-25 or PSD-95 levels between TG and WT rats at either 6 or 9 months of age. This is contradictory to reports in other AD models, for example, in the hippocampus of APP/PS1 mice, the expression levels of SNAP-25, PSD-95, and NMDAR subunits were all reduced at age of 8 months, when Aβ deposits and cognitive deficits were developed (Xu et al., 2021).

Additionally, since LTP is related with NR2A-enriched NMDARs and LTD with NR2B-enriched NMDARs, the levels of NR2A and NR2B were measured in the 6-month-old animals using the P2 pellet. The results also turned out to be insignificant between genotypes for NR2A or NR2B levels. Also, no genotype difference for the NR2A to NR2B ratio was detected. These observations were in contrary to some literatures, where in the 8-month-old APP/PS1 mice, the NMDAR subunits were also found to reduce in the hippocampus (Xu et al., 2021).

Moreover, in an AD-like rat model expressing cognitive deficits in water maze, there was a significant increase of immunoreactivity intensity of NR2B-containing NMDARs in the hippocampus, with no change in the intensity of NR2A-containing NMDARs (Liu et al., 2012). These AD-like rats also showed significantly more neurodegeneration in hippocampus especially in the CA1 region using Terminal deoxynucleotidyl transferase dUTP nick end labelling (TUNEL) (Liu et al., 2012). Although this AD-like rat model was an acute model built by intracerebroventricular injection of $A\beta_{1\text{-}40}$ and continuous intraperitoneal injection of $AlCl_3$, making the results unconvincing, there is still a possibility that it is still early at 6-month-old in the TgF344-AD model as they don't have major neuronal loss at this age (Cohen et al., 2013). It is thus interesting to know the changes of LTD and levels of NR2B-containing NMDARs in the older animals, too. However, due to loss of the 9-month-old tissue, the analysis of NR2A and NR2B are not presented in this thesis.

Moreover, to investigate the deficit in GABAergic inhibition, there was no difference in $GABA\alpha_5$ or GAD67 levels between genotypes in ages tested here. This observation is consistent with another group using the same TgF344-AD model, where they found no change in $GABA_A$ receptor subunits $\alpha_1$, $\alpha_5$, and $\delta$, or the enzymes GAD65 and GAD67 in total hippocampus by western blot in 9-month-old animals (Bazzigaluppi et al., 2018). However,

very interestingly, 9-month-old TgF344-AD rats showed a significant reduction in the density of GAD67-postive cells in the CA1 region, and a non-significant reduced density in the CA3 region (Bazzigaluppi et al., 2018). These observations could suggest that at 9 months of age, the remaining GAD67-positive cells might produce more GAD67 protein than before to maintain its normal level in dorsal hippocampus. Studies also found that *in vivo* ripple oscillations in the TgF344-AD rats was irresponsive to $\alpha_5$IA, a selective negative allosteric modulator to $GABA_A$ receptors, by the age of 9 months (Ratner et al., 2021). This finding indicates that the changes of $GABA_A$ receptors could be functional instead of a change in the amount. Additionally, there might be a possibility of functional remodelling between subunits of $GABA_A$ receptors due to variants of subunits but might not be a change in the numbers of total GABA receptors. In a particular study using an *in vitro* model of AD, the $\alpha_1$ and $\gamma_1$ subunit were down-regulated whereas $\alpha_2$, $\beta_1$ and $\gamma_1$ transcripts were up-regulated (Limon et al., 2012).

The measurement of GABA and GAD levels in post-mortem tissue could be affected with factors like the post-mortem interval and the age of measurement. In patients with dementia (AD and other types of dementia), there was a reduction in GAD enzymatic activity in post-mortem homogenates from all cortices (Perry et al., 1978, Govindpani et al., 2017). However, it was only observed in the late stage of the disease, and it is doubted that it was likely the effect of the conditions at the perimortem agonal state instead of the AD pathologies (Bowen et al., 1977, Govindpani et al., 2017). Therefore, the post-mortem interval could affect to some extent the measurement of GAD activity, and levels of other biomarkers in the post-mortem tissues. Moreover, PV-, SOM- and NPY-expressing GABAergic interneurons were found to be lost in the hippocampus of AD models at 6 months of age that have increased production of APP, such as the TgCRND8 (Albuquerque et al., 2015) and PS1xAPP mice (Ramos et al., 2006). The 6-month-old TgCRND8 mice also showed reduced GAD67-expressing neuron

immunoreactivity (Krantic et al., 2012). However, in this mouse model, 6 months of age is already way after the overproduction of soluble Aβ, and the Aβ plaques load at this age was already enormous (Krantic et al., 2012), whereas our TG rats had more soluble forms of Aβ at 6 months old (Cohen et al., 2013). It is therefore possible that the loss of GAD67-expressing neurons would be found in the later stage of our TG rats here.

At the first glance, this result firstly indicates that these markers were not affected, at least at the ages tested here. However, as there were changes in the *in vivo* evoked responses, there should be changes of biomarkers where other molecular mechanism is involved. Firstly, to look at the hippocampus as a whole is insufficient especially using Wes analysis (Maruszak and Thuret, 2014). In these set of Wes analysis, the entire dorsal hippocampus was used. As seen with the PV results in this study, there could be changes in subregions whereas the protein levels in the whole area may not be necessarily altered. A decrease of protein levels in a particular subregion could be masked by an increase of the same protein in other subregions. Also, as the function of subregions might not necessarily be the same, it will be of interest to test these protein levels in other regions like the ventral hippocampus, frontal and prefrontal cortices, to figure out how the pathologies progress globally.

### 4.4.3. Factors that affect neuroinflammation measurements

Neuroinflammation is recognised as another critical biological hallmark for AD at the early stage (Heneka, 2017). To assess the degree of neuroinflammation, microglia activation and co-expression with the proinflammatory cytokine of IL-1β was studied. TG rats at both 6 and 9 months of age had fewer percentage of resting microglia in hippocampal CA1 region, whereas the 9-month-old TG rats showed significantly more microglia at the intermediate

state in transit to the activated ones. The activation score in the 9-month-old TG rats was significantly higher compared to the age-match WT controls, and higher than the younger TG rats. This result suggests that neuroinflammation appeared in the TG animals at the prodromal stage and became progressively more severe as animals aged. APP/PS1 mice and 3xTg mice at about 12 months of age showed more substantial degree of microglia activation than the age-matching and older wild-type controls (Cao et al., 2021, Daniels et al., 2016). Additionally, positron emission tomography (PET) using [$^{18}$F]DPA-714 for microglia activation showed increased neuroinflammation in the hippocampus of 12-month-old TgF344-AD rats compared to the controls (Chaney et al., 2021). [$^{18}$F]DPA-714 PET did not show genotype differences in the TgF344-AD model at 6 months of age (Chaney et al., 2021).

Also, in CA1 region, there was an increase of the percentage of IL-1β-expressing microglia in the TG animals, suggesting that there were more activated microglia detecting inflammatory responses, acting as a sign of increased neuroinflammation. Interestingly, in the current study, IL-1β were mostly in the amoeboid microglia that are fully activated, although this class of microglia comprised the lowest percentage among total microglia in the CA1 of hippocampus. This piece of finding is consistent with the observations of increased IL-1β in activated/amoeboid microglia in an acute A$\beta_{42}$-injection model as well as old 3xTg mice(13-14 months old) (Daniels et al., 2016).

Moreover, albeit the numerical amount was low, 6-month-old TG rats had a higher percentage of microglia with IL-1β. The 9-month-old TG rats had higher mean percentage of IL-1β-expressing microglia but was not statistically different from the WT rats. Firstly, these observations might suggest neuroinflammation could happen in the TG animals at the early stage of AD, but secondly, this could be possibly due to small sample size for ANOVA tests or

the fact that there was an increased amount of microglia expressing IL-1β in the WT animals at older age. As suggested by the ageing effect revealed by two-way ANOVA in this study, an age-dependent background increase of neuroinflammation in the WT animals might be possible.

Also, there are other factors associated with increased neuroinflammation. Albeit Aβ oligomers be one of the DAMPs, stress could also induce neuroinflammation (Grippo and Scotti, 2013). Therefore, it is arguable that whether the neuroinflammation is resulted from APP/PS1 transgenes or is it a result of ageing itself or the stress levels. In fact, at the age of 6 months old, both male and female TgF344-AD rats showed enhanced anxiety related behaviour in the elevate plus-maze without deficits in spatial memory (Pentkowski et al., 2018). Moreover, anxiety-like behaviour was observed in the 9-month-old TgF344-AD rats as seen with a reduced sniffing time and lower interaction with conspecific rats compared to the wildtype controls in social interaction test (Chaney et al., 2021). These findings suggest that anxiety could be a factor contributing to enhanced neuroinflammation.

For limitations of the neuroinflammation study, one of the limitations would be that scoring for activation states involves objective bias. Hence, markers to indicate phagocytosis such as CD68 could be used in combination to ensure counting of fully activated microglia (Waller et al., 2019). It is worth noticing that the amount of microglia in these animals' majority of them are at resting and intermediate state, where the fully activated ones or the ameboid one's percentage was very low compared to the other two states. Yet the co-expression of the proinflammatory cytokine is mostly in the ameboid ones, instead of the ones that are becoming activated (at the early phase of activation). Also, the coextension from the confocal

imaging showed clearly the IL-1β is inside the ameboid shape microglia, whereas at the other two states, IL-1β were at the adjacent space attaching to the microglia.

Another limitation could be resulted from the number of microglia being analysed for microglia activation and co-expression with IL-1β, in which about 100 microglia were counted and analysed in CA1. In this current study, about 100 microglia in a randomly fixed counting frame in the CA1 region were counted to represent the entire CA1 region, which might diminish some accuracy. However, Harte lab found that there was no difference between the analysis using 100 microglia and full microglia counting in the entire hippocampal region, making the analysis method in this study approvable (Rebecca Woods, unpublished).

Additionally, for a better understanding of the full amount of IL-1β in dorsal hippocampus, other methods could be used for measurement, such as enzyme-linked immunoassay (ELISA). However, due to a lack of tissue and the number of homogenates and high concentration of sample required, it was not feasible to the analysis of this study. Indeed, rat ELISA for IL-1β was tested, but the low amount of sample concentration brought about huge variability.

### 4.4.4. Amyloid load of TgF344-AD model

In this study, in order to investigate the load of soluble Aβ oligomers, we attempted to do IHC and IF staining with the conformational antibody for prefibrillar oligomers A11 (SPC-506, StressMarq Biosciences, Canada) (Kayed et al., 2007, Glabe, 2008). Also, a novel conformation-specific antibody DesAb-O was tried in combination with a novel ELISA method to detect and quantify early appearance of soluble Aβ oligomers in our animals (Aprile et al., 2020). However, none of them lead to successful assessment due to a lack inappropriate tissue preparation and antibody selection.

Nevertheless, from other literatures, it is known that at the age of 6 months, the soluble oligomers sensitive to A11 and OC antibodies are already detectable in the hippocampus of this AD model (Cohen et al., 2013). The TG rats already express excessive amount of soluble $A\beta_{40}$ at the age of 6 months, and the ratio of detergent soluble $A\beta_{42}$ to $A\beta_{40}$ oligomers progressively increase with age (Cohen et al., 2013). More importantly, direct measure of Aβ plaques comes from a study using the 6F3D antibody to label Aβ plaques. The 9-month-old TgF344-AD rats was shown to have 10.7±1.3 plaques/$mm^2$ in the whole hippocampus and 4.6±0.7 plaques/$mm^2$ in mPFC (Bazzigaluppi et al., 2018). However, there was no data related to the amount of soluble Aβ oligomers in 9-month-old animals.

Based on the original literature on the TgF344-AD model in terms of the age-dependent increase of soluble Aβ oligomers especially the $A\beta_{42}$ proportions, it could estimate that at 9 months old the TG animals should express more Aβ pathologies than at 6 months.

### 4.4.5. Microglia clusters in the dorsal hippocampus of 9-month-old TG rats

Interestingly, plaque-like clusters of microglia were found in the slices of the TG rats at 9 months of age in the dorsal hippocampus. The clusters were round shape, rich in microglia at the intermediate and activated states, with almost 100% of expression of IL-1β, suggesting this area could be highly inflamed. Not only in dorsal hippocampus had these clusters appeared, the clusters or plaque-like substance also appeared in the cortex on the same anterior-posterior plane where dorsal hippocampi locate, especially perirhinal cortex, dorsolateral entorhinal cortex, piriform cortex, and basolateral amygdala. Therefore, based on reasonable speculation, at 9 months old, the TG animals was possible to express more Aβ pathologies with the appearance of Aβ plaques. Also, Aβ plaques might not be present in the

TG animals at 6 months of age. In fact, direct measure of Aβ plaques from another study showed that plaque area was very low at the age of 4-6 months but increased 82-fold in hippocampus when they reached 24-25 months old (Saré et al., 2020). Huge augmentation of Aβ plaques area were also found in perirhinal cortex (63-fold), and piriform cortex (73-fold) at 24-25 months old (Saré et al., 2020). Taking consideration of measurements from the literature, soluble Aβ oligomers should be of dominance in the 6-month-old TG rats.

In addition, noted that the perirhinal and entorhinal cortices are important for olfactory processing (Li et al., 2010, Saiz-Sanchez et al., 2015). Olfaction seems to do nothing with memory and what we normally know about AD. However, it might be the first few signs of the disease (Saiz-Sanchez et al., 2015). Early-stage AD patients showed deficits in odour detection, frequently preceding cognitive impairment, and memory loss (Li et al., 2010). The observation of microglia clusters in these regions of the TG animals suggests that these regions could be vulnerable to Aβ pathologies as well as neuroinflammation. And neuroinflammation could be an important hallmark leading to memory loss.

## 4.5. Conclusion

In summary, there was a decrease in the density of PV interneurons in CA2/3 and hence GABAergic disinhibition upstream of the Schaffer collateral pathway in TG rats only when they were 9 months old. There was also no PV interneuron density change in other subregions of dorsal hippocampus, nor in the younger animals at 6 months old. There were no changes in synaptic (SNAP-25, PSD-95), or GABAergic ($GABA\alpha_5$, GAD67) transmission in the TG animals at either age, while no difference in the glutamatergic markers (NR2A, NR2B) that are associated with LTP and LTD synaptic plasticity, in the 6-month-old animals. However,

increased proinflammatory cytokine IL-1β was observed in TG rats in both ages compared to the age-match WT rats. There was also a progressing neuroinflammation as a measure of microglia activation in the TG animals in hippocampal CA1, from 6 months to 9 months of age. Although more studies need to be carried out to complete observations in the 9-month-old animals for NR2A and NR2B levels, and other potential transmission markers needs to be investigated, the current results suggest there were GABAergic disinhibition in the 9-month-old animals accompanied with increased neuroinflammation.

Although there is an urgent need to directly measure Aβ load for both soluble oligomers and insoluble plaques in these animals in the dorsal hippocampus, 9 months of age might be an important transition point for development of pathologies compared to 6 months of age in this animal model, thus being a valuable check point for future investigations on pharmacological interventions for early AD.

# Chapter 5. Discussion

In this thesis, hippocampal synaptic strength and plasticity as well as the putative pathologies involved in the early stages of AD were investigated at two different timepoints using the TgF344-AD rat model. Based on the outcomes from the experiments in this thesis a hypothesis underlying hippocampal hyperexcitability in early AD will be firstly discussed. This thesis focused on electrophysiological and pathological studies in this animal model, as no behavioural readouts were collected due to a number of issues related to the background strain and their ability to conduct consistent behavioural studies in different cohorts of animals. As such no behaviour is reported directly but this chapter will also include a summary of behavioural assessments in this animal model from other laboratories. Their qualities and implications will be discussed alongside my data in a discussion focusing on the validity of the TgF344 rat model for AD research. Outcomes, limitations and implications of these studies along with future direction will also be discussed.

## 5.1. Disease mechanisms at the early stage of Alzheimer's disease

AD progression is multifactorial involving the interplays of many pathways including Aβ-induced synaptic dysfunction and neuroinflammation. Hippocampal network abnormalities including hypersynchrony, changes in rhythmic oscillatory properties, synaptic depression, interneuron dysfunction, and hyperexcitability are all important factors contributing to the progressive cognitive impairment in AD (Kazim et al., 2021). Alongside these abnormalities and other mediators (e.g., soluble Aβ oligomers, NFTs), neuroinflammation is emerging as a key regulator driving disease progression. It is likely that these network abnormalities, changes in neuronal function and neuroinflammation will play a different role at certain stages of the disease and is a rationale as to why looking at disease progression in 6- and 9-

month-old TgF344-AD rats can help elucidate these changes and how they may relate to each other.

### 5.1.1. Hippocampal hyperexcitability in the TgF344-AD model

In the TgF344-AD rats at 9 months of age, there was an enhanced input strength to CA1 as for an upwardly shifted I/O curve, and also an increased output from CA1 as shown by the higher chance of having population spikes (**Chapter 2, Section 2.3.1.4** and **Section 2.3.2.4**). These observations suggest a potential hyperexcitability at the dorsal hippocampal CA1 region at the age of 9 months.

The increased fEPSP might be a consequence of presynaptic disinhibition, where the presynaptic neurons are less inhibited by the inhibitory interneurons (McGarrity et al., 2017). Indeed, the disinhibition of GABAergic interneurons has gradually become a popular explanation for synaptic dysfunction associated with Aβ-induced cognitive decline (McGarrity et al., 2017). PV positive interneurons are an important subset of GABAergic interneurons that are critical in maintaining the neuronal network balance in the brain and are vulnerable to AD-related pathologies (Ruden et al., 2021, Park et al., 2020, Hijazi et al., 2020a, Hijazi et al., 2020b). Notably, Huh et al. (2016) suggested that the aberrant LTP that re-emerged in aged Tg2576 mice was attributable to the loss of PV interneurons in hippocampal CA1-3 region, which prevent over-excitation of pyramidal cells by providing GABAergic inhibitory input in the CA1 region (Huh et al., 2016, Palop and Mucke, 2010). Hence, it is possible that synaptic hyperexcitability in this study was a result of PV interneuron loss.

In our study, we found 9-month-old TG rats tended to have less PV protein expression in the total dorsal hippocampus using simple Wes's analysis. Region specific changes investigated

using immunohistochemical techniques revealed that we have a significant reduction of PV cell density in CA2/3 region, but not CA1 or DG.

Firstly, our result is comparable to the reduction of PV-expressing interneurons in the hippocampus of 5xFAD mouse at 11 months of age (Seo et al., 2021), that GABAergic disinhibition might appear at the mid-adult age. In another study, direct application of $A\beta_{42}$ reduced the amplitude of inhibitory postsynaptic current mediated by monosynaptic $GABA_A$ receptor in the somatosensory cortex layer V *in vitro* (Ulrich, 2015). Intracerebroventricular injection of soluble Aβ oligomers in Lister hooded rats also showed a decrease of the PV-expressing interneurons in the frontal cortex (Watremez et al., 2018). In sum, these studies support the idea that presynaptic disinhibition could trigger synaptic hyperexcitability.

Secondly, it is interesting that CA2/3 is upstream of Schaffer collateral pathway where the stimulation was exerted on the presynaptic neuron. From these data, it seems very plausible that the loss of PV inhibition contributes to the increased baseline connectivity in this study. In the 9-month-old TG rats, a loss of PV inhibition, upstream of Schaffer collateral pathway, might lead to enhanced baseline fEPSPs recorded at CA1. Reduction of PV interneurons in the TgF344-AD model highlights them as a potential target for early stage-AD detection and treatment.

Furthermore, taking into consideration the $Ca^{2+}$ hypothesis of AD (**Chapter 1, Section 1.1.3.4**), hyperactivity could also emerge as a result of a disturbance with $Ca^{2+}$ homeostasis due to more intracellular $Ca^{2+}$. PV is a slow $Ca^{2+}$ buffer and can remove excessive intracellular $Ca^{2+}$, protecting the presynaptic cell from overflow of $Ca^{2+}$ (Caillard et al., 2000). PV can also maintain synaptic strength near its resting level by preventing collective facilitation, therefore information could process steadily to the postsynaptic neuron (Caillard et al., 2000). Thus,

besides contributing to synaptic disinhibition as seen by enhanced I/O, a lack of PV interneuron might also contribute to deficits in short-term synaptic plasticity.

However, there are over 20 different subsets of GABAergic interneurons in the CA1 region of the hippocampus, and the CCK- and SOM-expressing interneurons are also play a role in feedforward inhibition to prevent overexcitation of the hippocampal circuits (Klausberger and Somogyi, 2008). In fact, CCK-expressing interneurons are found to play a role in the feedforward inhibition in the CA1 region via projections from the EC to the CA1 circuit (Basu et al., 2013). Therefore, experiments looking beyond PV interneurons could also be conducted to investigate other contributing factors to the hyperactivity observed in the hippocampal CA1 region in 9-month-old TgF344-AD animals.

There is also an argument that hippocampal hyperexcitability will show increased LTP and decreased LTD, which is not what is reported in this study, where both short- and long-term synaptic plasticity seemed to be depressed (**Chapter 2, Section 2.3**). However, as evidenced by the finding that glutamate reuptake inhibitor threo-β-benzyloxyaspartate (TBOA) could induce LTD and epileptiform activities at the same time (Campbell et al., 2014), it is highly possible that the hippocampal network hyperexcitability and CA1 synaptic dysfunction could share a similar pathway that is mediated by an increased amount of soluble Aβ oligomers (Kazim et al., 2021). Previous studies have also demonstrated that chronic induction of LTD using chemical manipulations drives hyperphosphorylation of tau (Taylor et al., 2021), suggesting that the synaptic dysfunction in long-term plasticity could further exacerbate the AD pathologies.

### 5.1.2. Epilepsy and AD

Another piece of evidence to support the hypothesis of hippocampal hyperexcitability is from the observation in AD patients with genetic mutations that overproduce Aβ-related species. In AD patients who carried mutations of the APP, PS1 or PS2 genes, the chance of having seizures is 87-fold to those who do not carry the mutations (Amatniek et al., 2006); while in patients with sporadic AD, the seizure risk is only 3-fold higher (Cloyd et al., 2006, Kazim et al., 2021). Many of these patients experienced seizure and epileptic-like brain activities before the formation of Aβ plaques (Kazim et al., 2021). In our animal model, the hippocampal hyperactivity was observed as an increased chance of having population spikes in CA1 region in the 9-month-old TG rats, which is related to the mechanism of having epileptiform activities.

Seizure or epileptiform activities were found to cause cognitive decline and learning and memory impairment (Kazim et al., 2021). AD patients with comorbidities of seizure were found to be diagnosed with cognitive decline more than 5 years earlier compared to those who had not experienced seizures (Kazim et al., 2021, Vossel et al., 2017, Bakker et al., 2012).

In fact, treatment with low dose of the antiepileptic drug levetiracetam can reverse memory loss in MCI patients (Bakker et al., 2012). Levetiracetam modulate exocytosis by binding to SV2A, which is an abundant synaptic vesical protein at the presynaptic neuron (Lynch et al., 2004, Lam et al., 2017). Absence of SV2A leads to increased epileptic activities by increasing presynaptic accumulation of $Ca^{2+}$ and thus more release of neurotransmitters (Janz et al., 1999). Also interestingly, PV-immunoreactive cell density was reduced in the subiculum, DG and all CA fields especially the superficial aspect of hippocampal CA1 of epileptic patients, suggesting loss of GABAergic inhibition is associated with hyperactivity (Andrioli et al., 2007).

This evidence suggests that neuronal hyperexcitability could share a common pathway between epilepsy and progression of AD that leads to cognitive dysfunctions.

### 5.1.3. Association between neuroinflammation and Alzheimer's disease

Neuroinflammation is a crucial marker for AD that arouses increasingly more attention. Whether it is a result or has a causative role in the development of AD is a hotly debated topic (Weaver, 2021, Weaver, 2022). On one hand, patients with MCI and AD show increased activated microglia in brain regions important for cognition, including entorhinal, temporoparietal, and cingulate cortices (Kinney et al., 2018, Cagnin et al., 2001, Fan et al., 2017). On the other hand, including subjects with neuroinflammation as seen enhanced microglia activation are more prone to have cognitive impairment or loss of memory (Cherry et al., 2016, Aungst et al., 2014).

In fact, repetitive head impact (RHI) was found to cause prolonged activation of microglia with increased density of the CD68-positive cells in the dorsolateral frontal cortex. More interestingly, the activation of microglia was found to be partially mediated by an increased production of phosphor-tau (p-tau) induced by RHI (Cherry et al., 2016). Also, repetitive mild traumatic brain injury in rats caused significantly increased numbers of activated microglia in both hippocampi, corresponding with an attenuated response of *in vitro* NMDAR-mediated fEPSP and impaired cognitive function in both the Morris water maze and novel object recognition (NOR) paradigm (Aungst et al., 2014). Although it is unclear about the existence of Aβ species in these patients and animals, neuroinflammation itself could contribute to memory loss and cognitive impairment.

Enhanced neuroinflammation has been found to cause synaptic deficits by releasing glutamate and proinflammatory cytokines to create excitotoxicity and reduce the expression synaptic markers (Kivisakk et al., 2022, Rao et al., 2012). For example, in bacterial meningitis induced by *Streptococcus pneumoniae*, the neurotoxin pneumolysin was found to be sufficient to induce loss of PSD-95 immunoreactivity in the superficial layers of neocortex tissue via binding to astrocytes to initiate $Ca^{2+}$ influx and release of glutamate (Wippel et al., 2013). More relevantly, activated microglia can release nitric oxide which inhibits glutamate reuptake at the presynaptic site to induce activation of NMDA receptors (Rao et al., 2012). In fact, chronic activation of NMDA receptor would upregulate levels of proinflammatory cytokines IL-1β and TNF-α in the rat frontal cortex (Chang et al., 2008).

In this study, we found evidence of increased microglia activation in 9-month-old TG rats compared to age-matched WT and younger TG rats. 9-month-old TG animals also showed synaptic dysfunctions such as impaired short-term plasticity and enhanced I/O. However, it was difficult to statistically correlate the degree of neuroinflammation with *in vivo* changes in evoked synaptic responses, because of the employment of different tissues.

Another approach to examine this relationship would be to utilise animal models of neuroinflammation, such as injection of lipopolysaccharide into the brain, to investigate association with changes of *in vivo* synaptic plasticity, pathologies and behaviours. Levels of excitotoxicity, as measured by inducible nitric oxide synthase, could be measured in the TgF344-AD rats in this study tested for correlations with neuroinflammation and synaptic dysfunctions (Rao et al., 2012). In conclusion, neuroinflammation and synaptic dysfunction may exacerbate each other in a continuous feedback loop. Both neuroinflammation and

synaptic dysfunction are evident at the early stage of the disease where both play a role in progression of the disease and the resultant cognitive dysfunction.

## 5.2. Behavioural studies in the TgF344-AD model

Although no behavioural studies were reported in this thesis, other groups used the TgF344-AD model to investigate changes in cognitive and other behavioural phenotypes (Saré et al., 2020). For example, female TgF344-AD rats were found to be hypoactive in the open field test at 6 and 12 months of age, but not at 18 months old, whereas male TgF344-AD rats showed hyposmia regardless of age (Saré et al., 2020).

In the original study by Cohen et al., TgF344-AD rats showed cognitive deficits in reversal learning in the Morris water maze (MWM) at 6 months of age (Cohen et al., 2013). In another study, several spatial learning and memory tasks were performed to access working and reference memory in the female TgF344-AD model at 6, 9 and 12 months of age (Bernaud et al., 2022). The female TgF344-AD rats showed deficits in MWM with greater swim distance to the platform at all three age points (Bernaud et al., 2022). In the water radial-arm maze that requires both working and reference memory, the deficits were only observed in 6- and 12-month-old TgF344-AD rats, but not at 9 months of age (Bernaud et al., 2022). Another group also found deficits in spatial navigation emerged at 7-8 months old, and more profound at 10-11 months old using MWM task in the TgF344-AD rats counterbalanced for gender (Berkowitz et al., 2018). These data suggest that 6-9 months old might be an early start point of the cognitive deficits in the TgF344-AD model.

We tried to investigate cognitive function of the TgF344-AD model in the lab and in collaboration with collaborators at the University of Nottingham. Preliminary behaviour

studies were carried out for paired novel object recognition (pNOR) test. However, the exploration rate of the animals, even the WT rats, was too low compared to other strains of rats doing this experiment. Another example of the effect of low exploration in these animals was evident in the delayed match to place (DMP) water maze tested by our collaborators in the University of Nottingham (unpublished). This test is highly sensitive to hippocampal dysfunction, including hyperexcitability/GABA dysfunction (McGarrity et al., 2017). We found a reduction in both exploration and performance in behaviour in both WT and TG rats, with no clear genotype or gender difference found in the watermaze DMP tasks at different ages (unpublished).

## 5.3. Validity of the TgF344-AD model

Animal models are essential and necessary for understanding the disease symptoms, underlying mechanisms and for the identification of novel targets and testing of novel medications. An ideal animal model for AD should present with both behavioural and pathological features of AD patients (Goodarzi et al., 2019).

In general, the transgenic TgF344-AD rat model provides a better understanding of the fundamental biology of AD compared to an acute animal model injected with Aβ (Goodarzi et al., 2019). According to Willner's criteria, the face, construct and predictive validities are the three aspects to consider when validating an animal model for neuropsychiatric and neurodegenerative diseases (Goodarzi et al., 2019).

The predictive validity is to do with assessing the effects of therapeutic treatment (Belzung and Lemoine, 2011). The construct validity focused on the similarity of the animal model with human patients in relation to aetiology and pathology that are corresponding to the

mechanism of the disease (Belzung and Lemoine, 2011). The TgF344-AD model show good construct validity as they have the mutated genes commonly seen in familial cases of AD (Benilova et al., 2012). The face validity corresponds to the similarity of the behavioural symptoms and biomarkers of the model and patients (Belzung and Lemoine, 2011, Goodarzi et al., 2019). This section will focus on the face validity and discuss for electrophysiological, pathological and behavioural aspects.

For the TgF344-AD model, most of the changes in the TG rats comes from the *in vivo* electrophysiological recordings of evoked synaptic response. Indeed, the *in vivo* electrophysiology measurement is powerful to improve the translational validity of AD animal models for reliable biomarkers. Nevertheless, it is difficult to measure with human biomarkers at the synaptic level at the moment, and thus impossible to compare the changes in short- and long-term plasticity between the animal and human. Measuring change of rhythmic oscillations (theta and gamma power) and coherence (theta-gamma coupling) is feasible with human electroencephalogram (EEG), yet the spontaneous activity of this animal model needs to be analysed.

For pathological symptoms, a reduction of PV cell density was found in the subregion of hippocampus, which is comparable to reduction of PV levels in temporal cortex of AD patients and hippocampus in animal models when they are aged (Ruden et al., 2021, Ali et al., 2019). However, no changes were found in synaptic markers like SNAP-25 and PSD-95, or GABAergic neuronal markers like GAD67, as observed in patients with AD (Yuki et al., 2014, Sinclair et al., 2015). Nevertheless, the age of the animal must be considered, because this set of studies focused on the early changes in these markers before the abundant accumulation of Aβ plaques.

More importantly for the face validity, one of the advantages of using animal models for research is the benefit of doing behavioural tests. Although several groups have successfully measured deficits in spatial learning and memory in the TgF344-AD model (**Section 5.2**), the exploration rate of these animals reduced with age and 6-month-old animals were more active to the new environment (Saré et al., 2020). Moreover, we observed low exploration rate in these animals regardless of the gender at the ages tested here. Similar low exploration in novel object recognition was also found in the TgF344-AD and age-matched wildtype controls after age of 6 months, in which both genotypes were incapable of completing the NOR task (Chaney et al., 2021). Also, low locomotor activity was observed in both transgenic and wildtype animals of this model at 12 months of age (Chaney et al., 2021), and reduced locomotion was previously reported in male rats of the Fisher strain compared to other strains (Rex et al., 1999). The low exploration rate and reduced locomotor activity makes the TgF344-AD model incompetent for behavioural tests for preclinical studies compared to, for example, Wistar or Lister hooded rats (Chaney et al., 2021).

To conclude, a valid animal model should be similar to human in terms of aetiology, pathophysiology, symptoms and responses to treatment (Goodarzi et al., 2019). The TgF344-AD rat model has advantages in relation to construct validity and for understanding the underlying mechanism of AD progression, with 9-month-old being an interesting age here for assessing changes in AD pathologies. However, this model has poor face validity due to its cohort-to-cohort variability in relation to behavioural tests related to assessing cognitive function, a key feature of AD.

## 5.4. Future studies

### 5.4.1. Sexual dimorphism

One of the limitations of these sets of experiments is the observations were all from male animals. It is therefore difficult to conclude whether a sexual dimorphism exists in this AD model. Although no gender difference in levels of Aβ or tau were reported in the original study (Cohen et al., 2013), gender differences were observed in the open field behavioural test (Saré et al., 2020). Also, AD is known to be more prevalent in female patients than males where two-thirds of all AD patients are females according to US and European reports (Beam et al., 2018, Rajan et al., 2021). Moreover, the sexual dimorphism is indeed seen in pathologies like PV deficits, where it is more frequently seen in the males patients with schizophrenia who are more prone to the disease (Nahar et al., 2021). It is therefore important to also investigate the corresponding changes in female rats in this AD model. However, female TG rats especially at 9 months of age were vulnerable to the anaesthetic with more frequent deaths observed. The difficulty in experimental procedures must also be considered.

### 5.4.2. Future – theta gamma oscillation and coherence

In this study, the spontaneous oscillations in hippocampal CA1 and DG were recorded in the same animal simultaneously, creating an abundant resource to examine oscillatory activities and coherence between and within hippocampal subregions.

Both alpha and theta frequency were reduced in urethane-anaesthetised and freely moving TgF344-AD rats (Cope et al., 2022, Stoiljkovic et al., 2019). In the TgF344-AD model, evoked hippocampal theta activity was significantly decreased with reduced theta-gamma coupling

(TGC) when the animals were anaesthetised with urethane at age of 12 months (Stoiljkovic et al., 2019).

GABAergic interneurons in the hippocampus govern network synchronicity and oscillations (Buzsaki and Draguhn, 2004, Kazim et al., 2021). Because a reduction of PV interneuron density was found in the 9-month-old TG rats in this study, it will be interesting to check whether there is a change of rhythmic activities and TGC at the same age in the hippocampus.

# Chapter 6. Conclusion

In conclusion, as summarised in **Table 6.1** and **Figure 6.1**, this set of studies showed that the synaptic deficits in TG rats at 9 months were accompanied with CA1 hyperexcitability and a reduction of PV inhibition upstream of the CA3-CA1 circuity. The reduced inhibition upstream of this CA3→CA1 synapse could account for abnormal changes in synaptic plasticity at 9 months of age. Interestingly, the upwardly shifted I/O curve at baseline might indicate synaptic disinhibition, again potentially related to the reduction in PV interneuron density in the hippocampal CA2/3 region in the TG animals at this age. Although lacking pathological changes in general synaptic, glutamatergic, and other GABAergic markers, the TG rats at both ages showed hippocampal neuroinflammation, with 9-month-old TGs possessing more proinflammatory cytokine in microglia and a shift of microglial morphology towards the activated state. These results highlight mechanisms underlying progression of pathology in the TG model.

***Table 6.1. Summary of changes in electrophysiology and post-mortem tissue analysis of the 6- and 9-month-old male TgF344-AD rats.***

| TgF344-AD model | Dorsal hippocampus | Specific Area | 6mo TG | 9mo TG |
|---|---|---|---|---|
| *In vivo* electrophysiology CA3→CA1 | I/O | CA1 | — | ↑ |
| | PPF | | — | ↓ at baseline |
| | LTP | | ↓ | ↓ |
| | Depotentiation | | ↑ | x |
| *In vivo* electrophysiology CA3→DG | PPF | DG | — | x |
| | LTP | | — | — |
| | Depotentiation | | — | x |
| Wes | PV | DH | — | — |
| | SNAP-25 | | — | — |
| | PSD-95 | | — | — |
| | GABAα5 | | — | — |
| | GAD67 | | — | — |
| | NR2A, NR2B | | — | x |
| | NR2A:NR2B | | — | x |
| IHC | PV density | CA1, CA2/3, DG | — | Only CA2/3↓ |
| | Microglia density | | — | — |
| IF | Microglia activation | CA1 | — | ↑ |
| | IL-1β-expressed microglia | | ↑ | Non-significant increase |

Additionally, it is still interesting to understand how the local field potential changed in CA1 region since theta-gamma coupling and oscillations also affected in AD that is related to PV interneurons. Therefore, power of theta and gamma oscillations as well as their coherence will be investigated for the add-on analysis. Although poor cognitive performance in behavioural tasks may limit the suitability of the TgF344-AD model for testing clinically relevant memory deficits, the current study still showed significant electrophysiological and pathological changes in the early stage of AD, especially at 9 months of age, indicating that this might be a transition state for AD progression.

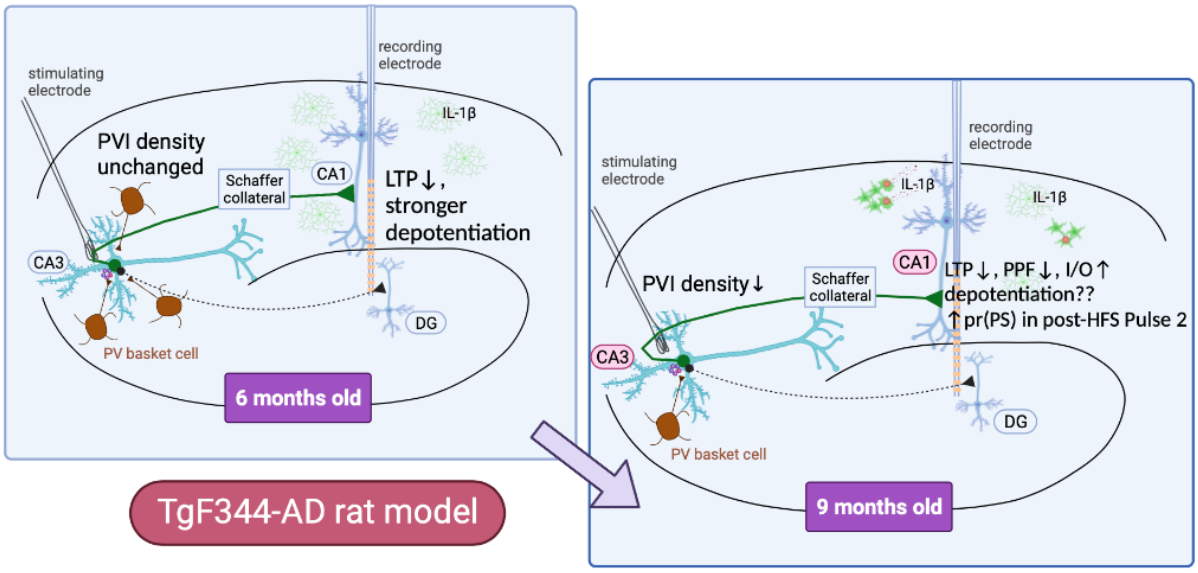


***Figure 6.1. Schematic summary of the findings in 6- and 9-month-old TgF344-AD model.***

*Briefly, PV density was only reduced in CA2/3 region that is upstream of the Schaffer collateral pathway in the 9-month-old TG rats that had enhanced CA1 activity measured with I/O, PPF and population spikes. These observations were not seen in the 6-month-old animals, suggesting synaptic disinhibition at 9 months of age. Also, 9-month-old TG rats exhibited more neuroinflammation in CA1 as measured with microglia activation and co-expression with IL-1β. Taken together, long-term synaptic plasticity was impaired at as early as 6 months old of the TG rats, but 9 months of age could be an important changing point as a result of Aβ pathologies in the TgF344-AD model at the early state of AD. Figure created with Biorender.*

## Acknowledgement

I would like to send my greatest thanks and appreciation to my supervisor, Professor Michael Harte, who generously provide critical and essential guidance to shape the direction of this project. An ocean of thanks and gratitude go to Dr John Gigg, my co-supervisor, for his expertise to train and help me on *in vivo* electrophysiology experiment and data analysis.

Many thanks to Lauren Rimmer, who contribute to the Simple Wes analysis and PV cell density analysis in the 9-month-old animals. I would also like to send my gratefulness to Jennifer Fletcher, who generously supported me with laboratory and data analysis skills. Thanks a lot, to student volunteers: Lysandra Fryer-Petridis and Mascha Von Der Lippe who contributed to the measurements and analysis of LTP/LTD in DG; Megan Taylor who helped with immunohistochemistry experiment and analysis of microglia density using QuPath; Niko Merlak-Radojcic who helped with the manual counting of microglia density; and Oana Puica, who contributed to the measurement of PPF responses in DG. Many thanks to Dr Tobias Bast and Marie-astrid Pezze, the collaborators in the University of Nottingham who did the behavioural tests in this animal model, providing some of the 9-month-old brain tissues and suggestion on analysis of PPF. Thanks to Dr Wenyang Xie for MATLAB code suggestions on measuring evoked responses of electrophysiological recordings. This project could not be done without your help and support. Appreciation also goes to the supportive lab manager Ben and lab members Anna, Katie, Jessica Brown, and Georgie, as well as the Biological Service Facility staff, Nathalie, Alison, Michael Simonsen-Jackson, Ian Miller and Mary Birch, for occasional laboratory inquires and technical suggestions. Thanks to my friends Anna, Amna, Ines, Georgie, Shuhui and Jingru for your support though my PhD years. Thank you so much to my partner Jeff for your scientific insights and emotional supports. Last but not least, all my thankfulness and gratitude belong to the invaluable supports from my mom and dad.

## References


ABRAMOV, E., DOLEV, I., FOGEL, H., CICCOTOSTO, G. D., RUFF, E. & SLUTSKY, I. 2009. Amyloid-beta as a positive endogenous regulator of release probability at hippocampal synapses. *Nat Neurosci,* 12**,** 1567-76.

ACKLEY, S. F., ZIMMERMAN, S. C., BRENOWITZ, W. D., TCHETGEN TCHETGEN, E. J., GOLD, A. L., MANLY, J. J., MAYEDA, E. R., FILSHTEIN, T. J., POWER, M. C., ELAHI, F. M., BRICKMAN, A. M. & GLYMOUR, M. M. 2021. Effect of reductions in amyloid levels on cognitive change in randomized trials: instrumental variable meta-analysis. *BMJ,* 372**,** n156.

ADEELA, K., ANGELS, A.-Q., JAMES, F. L., ELIZABETH, A. R. & LAWRENCE, S. B. G. 2001. Kinesin-mediated axonal transport of a membrane compartment containing β-secretase and presenilin-1 requires APP. *Nature,* 414**,** 643.

ALBUQUERQUE, M. S., MAHAR, I., DAVOLI, M. A., CHABOT, J. G., MECHAWAR, N., QUIRION, R. & KRANTIC, S. 2015. Regional and sub-regional differences in hippocampal GABAergic neuronal vulnerability in the TgCRND8 mouse model of Alzheimer's disease. *Front Aging Neurosci,* 7**,** 30.

ALI, F., BARINGER, S. L., NEAL, A., CHOI, E. Y. & KWAN, A. C. 2019. Parvalbumin-Positive Neuron Loss and Amyloid-beta Deposits in the Frontal Cortex of Alzheimer's Disease-Related Mice. *J Alzheimers Dis,* 72**,** 1323-1339.

ALZHEIMER'SASSOCIATION 2022. 2022 Alzheimer's disease facts and figures. *Alzheimers Dement.* 20220314 ed.

AMATNIEK, J. C., HAUSER, W. A., DELCASTILLO-CASTANEDA, C., JACOBS, D. M., MARDER, K., BELL, K., ALBERT, M., BRANDT, J. & STERN, Y. 2006. Incidence and predictors of seizures in patients with Alzheimer's disease. *Epilepsia,* 47**,** 867-72.

ANAND, K. S. & DHIKAV, V. 2012. Hippocampus in health and disease: An overview. *Ann Indian Acad Neurol,* 15**,** 239-46.

ANDORFER, C., KRESS, Y., ESPINOZA, M., DE SILVA, R., TUCKER, K. L., BARDE, Y. A., DUFF, K. & DAVIES, P. 2003. Hyperphosphorylation and aggregation of tau in mice expressing normal human tau isoforms. *Journal of Neurochemistry,* 86**,** 582-590.

ANDRIOLI, A., ALONSO-NANCLARES, L., ARELLANO, J. I. & DEFELIPE, J. 2007. Quantitative analysis of parvalbumin-immunoreactive cells in the human epileptic hippocampus. *Neuroscience,* 149**,** 131-43.

ANNETT, H., VEIT, H., GABOR, C. P., CAMERON, R. S., BRIAN, G. M., THOMAS, R., KATHERINE, A. F., EICKE, L., KATHRYN, J. M. & DOUGLAS, T. G. 2008. The NALP3 inflammasome is involved in the innate immune response to amyloid-β. *Nature Immunology,* 9**,** 857.

ANTONUCCI, F., CORRADINI, I., FOSSATI, G., TOMASONI, R., MENNA, E. & MATTEOLI, M. 2016. SNAP-25, a Known Presynaptic Protein with Emerging Postsynaptic Functions. *Front Synaptic Neurosci,* 8**,** 7.

APRILE, F. A., SORMANNI, P., PODPOLNY, M., CHHANGUR, S., NEEDHAM, L. M., RUGGERI, F. S., PERNI, M., LIMBOCKER, R., HELLER, G. T., SNEIDERIS, T., SCHEIDT, T., MANNINI, B., HABCHI, J., LEE, S. F., SALINAS, P. C., KNOWLES, T. P. J., DOBSON, C. M. & VENDRUSCOLO, M. 2020. Rational design of a conformation-specific antibody for the quantification of Abeta oligomers. *Proc Natl Acad Sci U S A,* 117**,** 13509-13518.

ASHOK, E. 2011. Long-term potentiation at CA3-CA1 hippocampal synapse with special emphasis on aging, disease, and stress. *Frontiers in aging neuroscience,* 3.

ATACK, J. R. 2010. Preclinical and clinical pharmacology of the GABAA receptor alpha5 subtype-selective inverse agonist alpha5IA. *Pharmacol Ther,* 125**,** 11-26.

AUNGST, S. L., KABADI, S. V., THOMPSON, S. M., STOICA, B. A. & FADEN, A. I. 2014. Repeated mild traumatic brain injury causes chronic neuroinflammation, changes in hippocampal synaptic plasticity, and associated cognitive deficits. *J Cereb Blood Flow Metab,* 34**,** 1223-32.

BAKKER, A., ALBERT, M. S., KRAUSS, G., SPECK, C. L. & GALLAGHER, M. 2015. Response of the medial temporal lobe network in amnestic mild cognitive impairment to therapeutic intervention assessed by fMRI and memory task performance. *Neuroimage Clin,* 7**,** 688-98.

BAKKER, A., KRAUSS, G. L., ALBERT, M. S., SPECK, C. L., JONES, L. R., STARK, C. E., YASSA, M. A., BASSETT, S. S., SHELTON, A. L. & GALLAGHER, M. 2012. Reduction of hippocampal hyperactivity improves cognition in amnestic mild cognitive impairment. *Neuron,* 74**,** 467-74.

BALLARD, C., GAUTHIER, S., CORBETT, A., BRAYNE, C., AARSLAND, D. & JONES, E. 2011. Alzheimer's disease. *Lancet (London, England),* 377**,** 1019.

BANKHEAD, P., LOUGHREY, M. B., FERNANDEZ, J. A., DOMBROWSKI, Y., MCART, D. G., DUNNE, P. D., MCQUAID, S., GRAY, R. T., MURRAY, L. J., COLEMAN, H. G., JAMES, J. A., SALTO-TELLEZ, M. & HAMILTON, P. W. 2017. QuPath: Open source software for digital pathology image analysis. *Sci Rep,* 7**,** 16878.

BAREGGI, S. R., FRANCESCHI, M., BONINI, L., ZECCA, L. & SMIRNE, S. 1982. Decreased CSF concentrations of homovanillic acid and gamma-aminobutyric acid in Alzheimer's disease. Age- or disease-related modifications? *Arch Neurol,* 39**,** 709-12.

BARTHOLOME, O., VAN DEN ACKERVEKEN, P., SÁNCHEZ GIL, J., DE LA BRASSINNE BONARDEAUX, O., LEPRINCE, P., FRANZEN, R. & ROGISTER, B. 2017. Puzzling Out Synaptic Vesicle 2 Family Members Functions. *Frontiers in molecular neuroscience,* 10**,** 148-148.

BASU, J., SRINIVAS, K. V., CHEUNG, S. K., TANIGUCHI, H., HUANG, Z. J. & SIEGELBAUM, S. A. 2013. A cortico-hippocampal learning rule shapes inhibitory microcircuit activity to enhance hippocampal information flow. *Neuron,* 79**,** 1208-21.

BAZZIGALUPPI, P., BECKETT, T. L., KOLETAR, M. M., LAI, A. Y., JOO, I. L., BROWN, M. E., CARLEN, P. L., MCLAURIN, J. & STEFANOVIC, B. 2018. Early-stage attenuation of phase-amplitude coupling in the hippocampus and medial prefrontal cortex in a transgenic rat model of Alzheimer's disease. *J Neurochem,* 144**,** 669-679.

BEAM, C. R., KANESHIRO, C., JANG, J. Y., REYNOLDS, C. A., PEDERSEN, N. L. & GATZ, M. 2018. Differences Between Women and Men in Incidence Rates of Dementia and Alzheimer's Disease. *J Alzheimers Dis,* 64**,** 1077-1083.

BEIQUE, J. C., LIN, D. T., KANG, M. G., AIZAWA, H., TAKAMIYA, K. & HUGANIR, R. L. 2006. Synapse-specific regulation of AMPA receptor function by PSD-95. *Proc Natl Acad Sci U S A,* 103**,** 19535-40.

BEKRIS, L. M., YU, C. E., BIRD, T. D. & TSUANG, D. 2010. *Genetics of Alzheimer's Disease*, John Wiley and Sons.

BELKHELFA, M., RAFA, H., MEDJEBER, O., ARROUL-LAMMALI, A., BEHAIRI, N., ABADA-BENDIB, M., MAKRELOUF, M., BELARBI, S., MASMOUDI, A. N., TAZIR, M. & TOUIL-BOUKOFFA, C. 2014. IFN-gamma and TNF-alpha are involved during Alzheimer disease progression and correlate with nitric oxide production: a study in Algerian patients. *J Interferon Cytokine Res,* 34**,** 839-47.

BELZUNG, C. & LEMOINE, M. 2011. Criteria of validity for animal models of psychiatric disorders: focus on anxiety disorders and depression. *Biol Mood Anxiety Disord,* 1**,** 9.

BENILOVA, I., KARRAN, E. & DE STROOPER, B. 2012. The toxic A beta oligomer and Alzheimer's disease: an emperor in need of clothes. *Nature Neuroscience,* 15**,** 349-357.

BERGSBAKEN, T., FINK, S. L. & COOKSON, B. T. 2009. Pyroptosis: host cell death and inflammation. *Nat Rev Microbiol,* 7**,** 99-109.

BERKOWITZ, L. E., HARVEY, R. E., DRAKE, E., THOMPSON, S. M. & CLARK, B. J. 2018. Progressive impairment of directional and spatially precise trajectories by TgF344-Alzheimer's disease rats in the Morris Water Task. *Sci Rep,* 8**,** 16153.

BERNAUD, V. E., BULEN, H. L., PENA, V. L., KOEBELE, S. V., NORTHUP-SMITH, S. N., MANZO, A. A., VALENZUELA SANCHEZ, M., OPACHICH, Z., RUHLAND, A. M. & BIMONTE-NELSON, H. A. 2022. Task-dependent learning and memory deficits in the TgF344-AD rat model of Alzheimer's disease: three key timepoints through middle-age in females. *Sci Rep,* 12**,** 14596.

BERRIDGE, M. J. 2010. Calcium hypothesis of Alzheimer's disease. *Pflugers Arch,* 459**,** 441-9.

BERRIDGE, M. J. 2011. Calcium signalling and Alzheimer's disease. *Neurochem Res,* 36**,** 1149-56.
BEZPROZVANNY, I. & MATTSON, M. P. 2008. Neuronal calcium mishandling and the pathogenesis of Alzheimer's disease. *Trends Neurosci,* 31**,** 454-63.
BI, D., WEN, L., WU, Z. & SHEN, Y. 2020. GABAergic dysfunction in excitatory and inhibitory (E/I) imbalance drives the pathogenesis of Alzheimer's disease. *Alzheimers Dement,* 16**,** 1312-1329.
BILKEI-GORZO, A. 2014. Genetic mouse models of brain ageing and Alzheimer's disease. *Pharmacology and Therapeutics,* 142**,** 244-257.
BILLINGS, L. M., ODDO, S., GREEN, K. N., MCGAUGH, J. L. & LAFERLA, F. M. 2005. Intraneuronal Aβ Causes the Onset of Early Alzheimer's Disease-Related Cognitive Deficits in Transgenic Mice. *Neuron,* 45**,** 675-688.
BLASKO, I., VEERHUIS, R., STAMPFER-KOUNTCHEV, M., SAURWEIN-TEISSL, M., EIKELENBOOM, P. & GRUBECK-LOEBENSTEIN, B. 2000. Costimulatory Effects of Interferon-γ and Interleukin-1β or Tumor Necrosis Factor α on the Synthesis of Aβ1-40 and Aβ1-42 by Human Astrocytes. *Neurobiology of Disease,* 7**,** 682-689.
BLISS, T. V. & COLLINGRIDGE, G. L. 2013. Expression of NMDA receptor-dependent LTP in the hippocampus: bridging the divide. *Mol Brain,* 6**,** 5.
BLISS, T. V. P. & COLLINGRIDGE, G. L. 1993. A synaptic model of memory: long-term potentiation in the hippocampus. *Nature,* 361**,** 31.
BOOKHEIMER, S. Y., STROJWAS, M. H., COHEN, M. S., SAUNDERS, A. M., PERICAK-VANCE, M. A., MAZZIOTTA, J. C. & SMALL, G. W. 2000. Patterns of brain activation in people at risk for Alzheimer's disease. *N Engl J Med,* 343**,** 450-6.
BOWEN, D. M., SMITH, C. B., WHITE, P., GOODHARDT, M. J., SPILLANE, J. A., FLACK, R. H. & DAVISON, A. N. 1977. Chemical pathology of organic dementias. I. Validity of biochemical measurements on human post-mortem brain specimens. *Brain,* 100**,** 397-426.
BRAAK, H. & BRAAK, E. 1991. Neuropathological stageing of Alzheimer-related changes. *Acta Neuropathol,* 82**,** 239-59.
BRAAK, H. & BRAAK, E. 1996. Evolution of the neuropathology of Alzheimer's disease. *Acta Neurol Scand Suppl,* 165**,** 3-12.
BRAAK, H., BRAAK, E. & BOHL, J. 1993. Staging of Alzheimer-related cortical destruction. *Eur Neurol,* 33**,** 403-8.
BRINKMALM, A., BRINKMALM, G., HONER, W. G., FROLICH, L., HAUSNER, L., MINTHON, L., HANSSON, O., WALLIN, A., ZETTERBERG, H., BLENNOW, K. & OHRFELT, A. 2014. SNAP-25 is a promising novel cerebrospinal fluid biomarker for synapse degeneration in Alzheimer's disease. *Mol Neurodegener,* 9**,** 53.
BROADHEAD, M. J., HORROCKS, M. H., ZHU, F., MURESAN, L., BENAVIDES-PICCIONE, R., DEFELIPE, J., FRICKER, D., KOPANITSA, M. V., DUNCAN, R. R., KLENERMAN, D., KOMIYAMA, N. H., LEE, S. F. & GRANT, S. G. 2016. PSD95 nanoclusters are postsynaptic building blocks in hippocampus circuits. *Sci Rep,* 6**,** 24626.
BRUNIG, I., SCOTTI, E., SIDLER, C. & FRITSCHY, J. M. 2002. Intact sorting, targeting, and clustering of gamma-aminobutyric acid A receptor subtypes in hippocampal neurons in vitro. *J Comp Neurol,* 443**,** 43-55.
BUSCHE, M. A., EICHHOFF, G., ADELSBERGER, H., ABRAMOWSKI, D., WIEDERHOLD, K. H., HAASS, C., STAUFENBIEL, M., KONNERTH, A. & GARASCHUK, O. 2008. Clusters of hyperactive neurons near amyloid plaques in a mouse model of Alzheimer's disease. *Science,* 321**,** 1686-9.
BUSCHE, M. A., KEKUS, M., ADELSBERGER, H., NODA, T., FORSTL, H., NELKEN, I. & KONNERTH, A. 2015. Rescue of long-range circuit dysfunction in Alzheimer's disease models. *Nat Neurosci,* 18**,** 1623-30.
BUZSAKI, G. 2002. Theta oscillations in the hippocampus. *Neuron,* 33**,** 325-40.
BUZSAKI, G. & DRAGUHN, A. 2004. Neuronal Oscillations in Cortical Networks. *Science (Washington),* 304**,** 1926-1929.

BUZSAKI, G. & WANG, X.-J. 2012. Mechanisms of Gamma Oscillations. *Annual Review of Neuroscience,* 35**,** 203-203.

BUZSÁKI, G. 1980. Long-term potentiation of the commissural path-CA1 pyramidal cell synapse in the hippocampus of the freely moving rat. *Neuroscience Letters,* 19**,** 293-296.

BUZSÁKI, G. 2005. Theta rhythm of navigation: Link between path integration and landmark navigation, episodic and semantic memory. *Hippocampus,* 15**,** 827-840.

CACCAVANO, A., BOZZELLI, P. L., FORCELLI, P. A., PAK, D. T. S., WU, J. Y., CONANT, K. & VICINI, S. 2020. Inhibitory Parvalbumin Basket Cell Activity is Selectively Reduced during Hippocampal Sharp Wave Ripples in a Mouse Model of Familial Alzheimer's Disease. *J Neurosci,* 40**,** 5116-5136.

CACQUEVEL, M., AESCHBACH, L., HOUACINE, J. & FRAERING, P. C. 2012. Alzheimer's disease-linked mutations in presenilin-1 result in a drastic loss of activity in purified gamma-secretase complexes. *PLoS One,* 7**,** e35133.

CAGNIN, A., BROOKS, D. J., KENNEDY, A. M., GUNN, R. N., MYERS, R., TURKHEIMER, F. E., JONES, T. & BANATI, R. B. 2001. In-vivo measurement of activated microglia in dementia. *Lancet,* 358**,** 461-7.

CAILLARD, O., MORENO, H., SCHWALLER, B., LLANO, I., CELIO, M. R. & MARTY, A. 2000. Role of the calcium-binding protein parvalbumin in short-term synaptic plasticity. *Proc Natl Acad Sci U S A,* 97**,** 13372-7.

CAMPBELL, S. L., HABLITZ, J. J. & OLSEN, M. L. 2014. Functional changes in glutamate transporters and astrocyte biophysical properties in a rodent model of focal cortical dysplasia. *Front Cell Neurosci,* 8**,** 425.

CAMPION, D., FLAMAN, J. M., BRICE, A., HANNEQUIN, D., DUBOIS, B., MARTIN, C., MOREAU, V., CHARBONNIER, F., DIDIERJEAN, O., TARDIEU, S. & ET AL. 1995. Mutations of the presenilin I gene in families with early-onset Alzheimer's disease. *Hum Mol Genet,* 4**,** 2373-7.

CAO, S., FISHER, D. W., RODRIGUEZ, G., YU, T. & DONG, H. 2021. Comparisons of neuroinflammation, microglial activation, and degeneration of the locus coeruleus-norepinephrine system in APP/PS1 and aging mice. *J Neuroinflammation,* 18**,** 10.

CHAKROBORTY, S., KIM, J., SCHNEIDER, C., JACOBSON, C., MOLGO, J. & STUTZMANN, G. E. 2012. Early presynaptic and postsynaptic calcium signaling abnormalities mask underlying synaptic depression in presymptomatic Alzheimer's disease mice. *J Neurosci,* 32**,** 8341-53.

CHAN ANTHONY, W., LEVEY ALLAN, I., WALKER LARY, C., FRITZ JASON, J., AGCA, C., LAH JAMES, J. & AGCA, Y. 2008. Development of transgenic rats producing human β-amyloid precursor protein as a model for Alzheimer's disease: Transgene and endogenous APP genes are regulated tissue-specifically. *BMC Neuroscience,* 9**,** 28.

CHANEY, A. M., LOPEZ-PICON, F. R., SERRIERE, S., WANG, R., BOCHICCHIO, D., WEBB, S. D., VANDESQUILLE, M., HARTE, M. K., GEORGIADOU, C., LAWRENCE, C., BUSSON, J., VERCOUILLIE, J., TAUBER, C., BURON, F., ROUTIER, S., REEKIE, T., SNELLMAN, A., KASSIOU, M., ROKKA, J., DAVIES, K. E., RINNE, J. O., SALIH, D. A., EDWARDS, F. A., ORTON, L. D., WILLIAMS, S. R., CHALON, S. & BOUTIN, H. 2021. Prodromal neuroinflammatory, cholinergic and metabolite dysfunction detected by PET and MRS in the TgF344-AD transgenic rat model of AD: a collaborative multi-modal study. *Theranostics,* 11**,** 6644-6667.

CHANG, Y. C., KIM, H. W., RAPOPORT, S. I. & RAO, J. S. 2008. Chronic NMDA administration increases neuroinflammatory markers in rat frontal cortex: cross-talk between excitotoxicity and neuroinflammation. *Neurochem Res,* 33**,** 2318-23.

CHAPMAN, P. F., WHITE, G. L., JONES, M. W., COOPER-BLACKETER, D., MARSHALL, V. J., IRIZARRY, M., YOUNKIN, L., GOOD, M. A., BLISS, T. V., HYMAN, B. T., YOUNKIN, S. G. & HSIAO, K. K. 1999. Impaired synaptic plasticity and learning in aged amyloid precursor protein transgenic mice. *Nat Neurosci,* 2**,** 271-6.

CHEN, K. H., REESE, E. A., KIM, H. W., RAPOPORT, S. I. & RAO, J. S. 2011. Disturbed neurotransmitter transporter expression in Alzheimer's disease brain. *J Alzheimers Dis,* 26**,** 755-66.

CHERRY, J. D., TRIPODIS, Y., ALVAREZ, V. E., HUBER, B., KIERNAN, P. T., DANESHVAR, D. H., MEZ, J., MONTENIGRO, P. H., SOLOMON, T. M., ALOSCO, M. L., STERN, R. A., MCKEE, A. C. & STEIN, T. D. 2016. Microglial neuroinflammation contributes to tau accumulation in chronic traumatic encephalopathy. *Acta Neuropathol Commun,* 4**,** 112.

CHERUBINI, E. & MILES, R. 2015. The CA3 region of the hippocampus: how is it? What is it for? How does it do it? *Front Cell Neurosci,* 9**,** 19.

CITRON, M., OLTERSDORF, T., HAASS, C., MCCONLOGUE, L., HUNG, A. Y., SEUBERT, P., VIGO-PELFREY, C., LIEBERBURG, I. & SELKOE, D. J. 1992. Mutation of the beta-amyloid precursor protein in familial Alzheimer's disease increases beta-protein production. *Nature,* 360**,** 672-4.

CITRON, M., VIGO-PELFREY, C., TEPLOW, D. B., MILLER, C., SCHENK, D., JOHNSTON, J., WINBLAD, B., VENIZELOS, N., LANNFELT, L. & SELKOE, D. J. 1994. Excessive production of amyloid beta-protein by peripheral cells of symptomatic and presymptomatic patients carrying the Swedish familial Alzheimer disease mutation. *Proc Natl Acad Sci U S A,* 91**,** 11993-7.

CLARK, R. E. & SQUIRE, L. R. 2013. Similarity in form and function of the hippocampus in rodents, monkeys, and humans. *Proc Natl Acad Sci U S A,* 110 Suppl 2**,** 10365-70.

CLAYTON, N. S. & DICKINSON, A. 1998. Episodic-like memory during cache recovery by scrub jays. *Nature,* 395**,** 272-4.

CLEARY, J., P., WALSH, D., M., HOFMEISTER, G., M., SHANKAR, G., M., KUSKOWSKI, M., A., SELKOE, D., J. & ASHE, K., H. 2004. Natural oligomers of the amyloid-β protein specifically disrupt cognitive function. *Nature Neuroscience,* 8**,** 79.

CLINTON, J., BLACKMAN, S. E., ROYSTON, M. C. & ROBERTS, G. W. 1994. Differential synaptic loss in the cortex in Alzheimer's disease: a study using archival material. *Neuroreport,* 5**,** 497-500.

CLOYD, J., HAUSER, W., TOWNE, A., RAMSAY, R., MATTSON, R., GILLIAM, F. & WALCZAK, T. 2006. Epidemiological and medical aspects of epilepsy in the elderly. *Epilepsy Res,* 68 Suppl 1**,** S39-48.

COHEN, N. J. 1993. *Memory, amnesia, and the hippocampal system,* Cambridge, Mass. ;, MIT.

COHEN, R. M., REZAI-ZADEH, K., WEITZ, T. M., RENTSENDORJ, A., GATE, D., SPIVAK, I., BHOLAT, Y., VASILEVKO, V., GLABE, C. G., BREUNIG, J. J., RAKIC, P., DAVTYAN, H., AGADJANYAN, M. G., KEPE, V., BARRIO, J. R., BANNYKH, S., SZEKELY, C. A., PECHNICK, R. N. & TOWN, T. 2013. A transgenic Alzheimer rat with plaques, tau pathology, behavioral impairment, oligomeric abeta, and frank neuronal loss. *J Neurosci,* 33**,** 6245-56.

COLGIN, L. L. & MOSER, E. I. 2010. Gamma oscillations in the hippocampus. *Physiology (Bethesda, Md.),* 25**,** 319-329.

COLLINSON, N., KUENZI, F. M., JAROLIMEK, W., MAUBACH, K. A., COTHLIFF, R., SUR, C., SMITH, A., OTU, F. M., HOWELL, O., ATACK, J. R., MCKERNAN, R. M., SEABROOK, G. R., DAWSON, G. R., WHITING, P. J. & ROSAHL, T. W. 2002. Enhanced learning and memory and altered GABAergic synaptic transmission in mice lacking the alpha 5 subunit of the GABAA receptor. *J Neurosci,* 22**,** 5572-80.

COLONNA, M. & BUTOVSKY, O. 2017. Microglia Function in the Central Nervous System During Health and Neurodegeneration. *Annu Rev Immunol,* 35**,** 441-468.

COMMINS, M. S., GIGG, M. J., ANDERSON, M. M. & O'MARA, M. S. 1998b. Interaction between paired-pulse facilitation and long-term potentiation in the projection from hippocampal area CA1 to the subiculum. *NeuroReport,* 9**,** 4109-4113.

COPE, Z. A., MURAI, T. & SUKOFF RIZZO, S. J. 2022. Emerging Electroencephalographic Biomarkers to Improve Preclinical to Clinical Translation in Alzheimer's Disease. *Front Aging Neurosci,* 14**,** 805063.

COTEL, M. C., LENARTOWICZ, E. M., NATESAN, S., MODO, M. M., COOPER, J. D., WILLIAMS, S. C., KAPUR, S. & VERNON, A. C. 2015. Microglial activation in the rat brain following chronic antipsychotic treatment at clinically relevant doses. *Eur Neuropsychopharmacol,* 25**,** 2098-107.

COUNTS, S. E., ALLDRED, M. J., CHE, S., GINSBERG, S. D. & MUFSON, E. J. 2014. Synaptic gene dysregulation within hippocampal CA1 pyramidal neurons in mild cognitive impairment. *Neuropharmacology,* 79**,** 172-9.

CRESTANI, F., KEIST, R., FRITSCHY, J. M., BENKE, D., VOGT, K., PRUT, L., BLUTHMANN, H., MOHLER, H. & RUDOLPH, U. 2002. Trace fear conditioning involves hippocampal alpha5 GABA(A) receptors. *Proc Natl Acad Sci U S A,* 99**,** 8980-5.

CROUZIN, N., BARANGER, K., CAVALIER, M., MARCHALANT, Y., COHEN-SOLAL, C., ROMAN, F. S., KHRESTCHATISKY, M., RIVERA, S., FERON, F. & VIGNES, M. 2013. Area-specific alterations of synaptic plasticity in the 5XFAD mouse model of Alzheimer's disease: dissociation between somatosensory cortex and hippocampus. *PLoS One,* 8**,** e74667.

CUESTA, P., OCHOA-URREA, M., FUNKE, M., HASAN, O., ZHU, P., MARCOS, A., LOPEZ, M. E., SCHULZ, P. E., LHATOO, S., PANTAZIS, D., MOSHER, J. C. & MAESTU, F. 2022. Gamma band functional connectivity reduction in patients with amnestic mild cognitive impairment and epileptiform activity. *Brain Commun,* 4**,** fcac012.

CURLEY, A. A., ARION, D., VOLK, D. W., ASAFU-ADJEI, J. K., SAMPSON, A. R., FISH, K. N. & LEWIS, D. A. 2011. Cortical deficits of glutamic acid decarboxylase 67 expression in schizophrenia: clinical, protein, and cell type-specific features. *Am J Psychiatry,* 168**,** 921-9.

DANIELS, M. J. D., RIVERS-AUTY, J., SCHILLING, T., SPENCER, N. G., WATREMEZ, W., FASOLINO, V., BOOTH, S. J., WHITE, C. S., BALDWIN, A. G., FREEMAN, S., WONG, R., LATTA, C., YU, S., JACKSON, J., FISCHER, N., KOZIEL, V., PILLOT, T., BAGNALL, J., ALLAN, S. M., PASZEK, P., GALEA, J., HARTE, M. K., EDER, C., LAWRENCE, C. B. & BROUGH, D. 2016. Fenamate NSAIDs inhibit the NLRP3 inflammasome and protect against Alzheimer's disease in rodent models. *Nature Communications,* 7.

DANSOKHO, C. & HENEKA, M. T. 2017. Neuroinflammatory responses in Alzheimer's disease. *Journal of neural transmission (Vienna, Austria : 1996)*.

DAS, M., MAO, W., SHAO, E., TAMHANKAR, S., YU, G. Q., YU, X., HO, K., WANG, X., WANG, J. & MUCKE, L. 2021. Interdependence of neural network dysfunction and microglial alterations in Alzheimer's disease-related models. *iScience,* 24**,** 103245.

DAVIS, K., FOX, S. & GIGG, J. 2014. Increased Hippocampal Excitability in the 3xTgAD Mouse Model for Alzheimer's Disease In Vivo. *PLoS One,* 9**,** e91203.

DAVIS, K. E., EASTON, A., EACOTT, M. J. & GIGG, J. 2013. Episodic-like memory for what-where-which occasion is selectively impaired in the 3xTgAD mouse model of Alzheimer's disease. *Journal of Alzheimer's disease : JAD,* 33**,** 681.

DE ERAUSQUIN, G. A., SNYDER, H., CARRILLO, M., HOSSEINI, A. A., BRUGHA, T. S., SESHADRI, S. & CONSORTIUM, C. S.-C.-. 2021. The chronic neuropsychiatric sequelae of COVID-19: The need for a prospective study of viral impact on brain functioning. *Alzheimers Dement,* 17**,** 1056-1065.

DE STROOPER, B., SAFTIG, P., CRAESSAERTS, K., VANDERSTICHELE, H., GUHDE, G., ANNAERT, W., VON FIGURA, K. & VAN LEUVEN, F. 1998. Deficiency of presenilin-1 inhibits the normal cleavage of amyloid precursor protein. *Nature,* 391**,** 387-90.

DESHPANDE, A., MINA, E., GLABE, C. & BUSCIGLIO, J. 2006. Different conformations of amyloid beta induce neurotoxicity by distinct mechanisms in human cortical neurons. *J Neurosci,* 26**,** 6011-8.

DICKERSON, B. C., SALAT, D. H., GREVE, D. N., CHUA, E. F., RAND-GIOVANNETTI, E., RENTZ, D. M., BERTRAM, L., MULLIN, K., TANZI, R. E., BLACKER, D., ALBERT, M. S. & SPERLING, R. A. 2005. Increased hippocampal activation in mild cognitive impairment compared to normal aging and AD. *Neurology,* 65**,** 404-11.

DIETRICH, K., BOUTER, Y., MULLER, M. & BAYER, T. A. 2018. Synaptic Alterations in Mouse Models for Alzheimer Disease-A Special Focus on N-Truncated Abeta 4-42. *Molecules,* 23.

DISABATO, D. J., QUAN, N. & GODBOUT, J. P. 2016. Neuroinflammation: the devil is in the details. *J Neurochem,* 139 Suppl 2**,** 136-153.

DOUCHAMPS, V., JEEWAJEE, A., BLUNDELL, P., BURGESS, N. & LEVER, C. 2013. Evidence for encoding versus retrieval scheduling in the hippocampus by theta phase and acetylcholine. *J Neurosci,* 33**,** 8689-704.

DRUMMOND, E. & WISNIEWSKI, T. 2017. Alzheimer's disease: experimental models and reality. *Acta Neuropathol,* 133**,** 155-175.

DUMANCHIN, C., TOURNIER, I., MARTIN, C., DIDIC, M., BELLIARD, S., CARLANDER, B., ROUHART, F., DUYCKAERTS, C., PELLISSIER, J. F., LATOUCHE, J. B., HANNEQUIN, D., FREBOURG, T., TOSI, M. & CAMPION, D. 2006. Biological effects of four PSEN1 gene mutations causing Alzheimer disease with spastic paraparesis and cotton wool plaques. *Hum Mutat,* 27**,** 1063.

EACOTT, M. J. & NORMAN, G. 2004. Integrated memory for object, place, and context in rats: a possible model of episodic-like memory? *The Journal of neuroscience : the official journal of the Society for Neuroscience,* 24**,** 1948.

EHRLICH, I. & MALINOW, R. 2004. Postsynaptic density 95 controls AMPA receptor incorporation during long-term potentiation and experience-driven synaptic plasticity. *J Neurosci,* 24**,** 916-27.

EICHENBAUM, H. 2000. A cortical-hippocampal system for declarative memory. *Nature Reviews: Neuroscience,* 1**,** 41-50.

EL-HUSSEINI, A. E., SCHNELL, E., CHETKOVICH, D. M., NICOLL, R. A. & BREDT, D. S. 2000. PSD-95 involvement in maturation of excitatory synapses. *Science,* 290**,** 1364-8.

ESCLAPEZ, M., TILLAKARATNE, N. J., KAUFMAN, D. L., TOBIN, A. J. & HOUSER, C. R. 1994. Comparative localization of two forms of glutamic acid decarboxylase and their mRNAs in rat brain supports the concept of functional differences between the forms. *J Neurosci,* 14**,** 1834-55.

FALDINI, E., AHMED, T., BUEE, L., BLUM, D. & BALSCHUN, D. 2019. Tau- but not Ass -pathology enhances NMDAR-dependent depotentiation in AD-mouse models. *Acta Neuropathol Commun,* 7**,** 202.

FAN, Z., BROOKS, D. J., OKELLO, A. & EDISON, P. 2017. An early and late peak in microglial activation in Alzheimer's disease trajectory. *Brain,* 140**,** 792-803.

FANSELOW, M. S. & DONG, H. W. 2010. Are the dorsal and ventral hippocampus functionally distinct structures? *Neuron,* 65**,** 7-19.

FARACO, G., HOCHRAINER, K., SEGARRA, S. G., SCHAEFFER, S., SANTISTEBAN, M. M., MENON, A., JIANG, H., HOLTZMAN, D. M., ANRATHER, J. & IADECOLA, C. 2019. Dietary salt promotes cognitive impairment through tau phosphorylation. *Nature*.

FERRANTE, M. & ASCOLI, G. A. 2015. Distinct and synergistic feedforward inhibition of pyramidal cells by basket and bistratified interneurons. *Front Cell Neurosci,* 9**,** 439.

FERREIRA, I. L., BAJOUCO, L. M., MOTA, S. I., AUBERSON, Y. P., OLIVEIRA, C. R. & REGO, A. C. 2012. Amyloid beta peptide 1-42 disturbs intracellular calcium homeostasis through activation of GluN2B-containing N-methyl-d-aspartate receptors in cortical cultures. *Cell Calcium,* 51**,** 95-106.

FILIPCIK, P., ZILKA, N., BUGOS, O., KUCERAK, J., KOSON, P., NOVAK, P. & NOVAK, M. 2012. First transgenic rat model developing progressive cortical neurofibrillary tangles. *Neurobiology of Aging,* 33**,** 1448-1456.

FOSSATI, G., MORINI, R., CORRADINI, I., ANTONUCCI, F., TREPTE, P., EDRY, E., SHARMA, V., PAPALE, A., POZZI, D., DEFILIPPI, P., MEIER, J. C., BRAMBILLA, R., TURCO, E., ROSENBLUM, K., WANKER, E. E., ZIV, N. E., MENNA, E. & MATTEOLI, M. 2015. Reduced SNAP-25 increases PSD-95 mobility and impairs spine morphogenesis. *Cell Death Differ,* 22**,** 1425-36.

FRANCIS, P. T., PALMER, A. M., SNAPE, M. & WILCOCK, G. K. 1999. The cholinergic hypothesis of Alzheimer's disease: a review of progress. *Journal of Neurology, Neurosurgery & Psychiatry,* 66**,** 137.

FRIEDMAN, D., HONIG, L. S. & SCARMEAS, N. 2012. Seizures and Epilepsy in Alzheimer's Disease. *CNS Neuroscience & Therapeutics,* 18**,** 285-294.

FRIEDMAN, E. M., SHIH, R. A., LANGA, K. M. & HURD, M. D. 2015. US Prevalence And Predictors Of Informal Caregiving For Dementia. *Health Aff (Millwood),* 34**,** 1637-41.

FUJIYAMA, F., STEPHENSON, F. A. & BOLAM, J. P. 2002. Synaptic localization of GABA(A) receptor subunits in the substantia nigra of the rat: effects of quinolinic acid lesions of the striatum. *Eur J Neurosci,* 15**,** 1961-75.

FURUYA, T. K., SILVA, P. N., PAYAO, S. L., BERTOLUCCI, P. H., RASMUSSEN, L. T., DE LABIO, R. W., BRAGA, I. L., CHEN, E. S., TURECKI, G., MECHAWAR, N., MILL, J. & SMITH, M. A. 2012. Analysis of SNAP25 mRNA expression and promoter DNA methylation in brain areas of Alzheimer's Disease patients. *Neuroscience,* 220**,** 41-6.

GABRIELLA, G. & GIOVANNA, C. 2010. gamma-Aminobutyric acid type A (GABA(A)) receptor subtype inverse agonists as therapeutic agents in cognition. *Methods Enzymol,* 485**,** 197-211.

GAIL CANTER, R., HUANG, W. C., CHOI, H., WANG, J., ASHLEY WATSON, L., YAO, C. G., ABDURROB, F., BOUSLEIMAN, S. M., YOUNG, J. Z., BENNETT, D. A., DELALLE, I., CHUNG, K. & TSAI, L. H. 2019. 3D mapping reveals network-specific amyloid progression and subcortical susceptibility in mice. *Commun Biol,* 2**,** 360.

GALVEZ, T., DUTHEY, B., KNIAZEFF, J., BLAHOS, J., ROVELLI, G., BETTLER, B., PREZEAU, L. & PIN, J. P. 2001. Allosteric interactions between GB1 and GB2 subunits are required for optimal GABA(B) receptor function. *EMBO J,* 20**,** 2152-9.

GANESH, M. S., SHAOMIN, L., TAPAN, H. M., AMAYA, G.-M., NINA, E. S., IMELDA, S., FRANCESCA, M. B., MICHAEL, A. F., MICHAEL, J. R., CYNTHIA, A. L., CIARAN, M. R., DOMINIC, M. W., BERNARDO, L. S. & DENNIS, J. S. 2008. Amyloid-β protein dimers isolated directly from Alzheimer's brains impair synaptic plasticity and memory. *Nature Medicine,* 14**,** 837.

GANGULI, M., DODGE, H. H., SHEN, C., PANDAV, R. S. & DEKOSKY, S. T. 2005. Alzheimer disease and mortality: a 15-year epidemiological study. *Arch Neurol,* 62**,** 779-84.

GENGLER, S., HAMILTON, A. & HOLSCHER, C. 2010. Synaptic plasticity in the hippocampus of a APP/PS1 mouse model of Alzheimer's disease is impaired in old but not young mice. *PLoS One,* 5**,** e9764.

GHATAK, S., DOLATABADI, N., TRUDLER, D., ZHANG, X., WU, Y., MOHATA, M., AMBASUDHAN, R., TALANTOVA, M. & LIPTON, S. A. 2019. Mechanisms of hyperexcitability in Alzheimer's disease hiPSC-derived neurons and cerebral organoids vs isogenic controls. *Elife,* 8.

GIESERS, N. K. & WIRTHS, O. 2020. Loss of Hippocampal Calretinin and Parvalbumin Interneurons in the 5XFAD Mouse Model of Alzheimer's Disease. *ASN Neuro,* 12**,** 1759091420925356.

GIUFFRIDA, M. L., CARACI, F., PIGNATARO, B., CATALDO, S., DE BONA, P., BRUNO, V., MOLINARO, G., PAPPALARDO, G., MESSINA, A., PALMIGIANO, A., GAROZZO, D., NICOLETTI, F., RIZZARELLI, E. & COPANI, A. 2009. Beta-amyloid monomers are neuroprotective. *The Journal of neuroscience : the official journal of the Society for Neuroscience,* 29**,** 10582-10587.

GLABE, C. G. 2008. Structural classification of toxic amyloid oligomers. *The Journal of biological chemistry,* 283**,** 29639-29643.

GLYKYS, J., MANN, E. O. & MODY, I. 2008. Which GABA(A) receptor subunits are necessary for tonic inhibition in the hippocampus? *J Neurosci,* 28**,** 1421-6.

GONZALEZ-REYES, R. E., NAVA-MESA, M. O., VARGAS-SANCHEZ, K., ARIZA-SALAMANCA, D. & MORA-MUNOZ, L. 2017. Involvement of Astrocytes in Alzheimer's Disease from a Neuroinflammatory and Oxidative Stress Perspective. *Front Mol Neurosci,* 10**,** 427.

GOODARZI, P., PAYAB, M., ALAVI-MOGHADAM, S., LARIJANI, B., RAHIM, F., BANA, N., SARVARI, M., ADIBI, H., FOROUGHI HERAVANI, N., HADAVANDKHANI, M. & ARJMAND, B. 2019. Development and validation of Alzheimer's Disease Animal Model for the Purpose of Regenerative Medicine. *Cell Tissue Bank,* 20**,** 141-151.

GOODMAN, M. S., KUMAR, S., ZOMORRODI, R., GHAZALA, Z., CHEAM, A. S. M., BARR, M. S., DASKALAKIS, Z. J., BLUMBERGER, D. M., FISCHER, C., FLINT, A., MAH, L., HERRMANN, N., BOWIE, C. R., MULSANT, B. H. & RAJJI, T. K. 2018. Theta-Gamma Coupling and Working Memory in Alzheimer's Dementia and Mild Cognitive Impairment. *Front Aging Neurosci,* 10**,** 101.

GORDON, B. A., BLAZEY, T. M., SU, Y., HARI-RAJ, A., DINCER, A., FLORES, S., CHRISTENSEN, J., MCDADE, E., WANG, G., XIONG, C., CAIRNS, N. J., HASSENSTAB, J., MARCUS, D. S., FAGAN, A. M., JACK, C. R., JR., HORNBECK, R. C., PAUMIER, K. L., ANCES, B. M., BERMAN, S. B., BRICKMAN, A. M., CASH, D. M., CHHATWAL, J. P., CORREIA, S., FORSTER, S., FOX, N. C., GRAFF-RADFORD, N. R., LA FOUGERE, C., LEVIN, J., MASTERS, C. L., ROSSOR, M. N., SALLOWAY, S., SAYKIN, A. J., SCHOFIELD, P. R., THOMPSON, P. M., WEINER, M. M., HOLTZMAN, D. M., RAICHLE, M. E., MORRIS, J. C., BATEMAN, R. J. & BENZINGER, T. L. S. 2018. Spatial patterns of neuroimaging biomarker change in individuals from families with autosomal dominant Alzheimer's disease: a longitudinal study. *Lancet Neurol,* 17**,** 241-250.

GOURE, W. F., KRAFFT, G. A., JERECIC, J. & HEFTI, F. 2014. Targeting the proper amyloid-beta neuronal toxins: a path forward for Alzheimer's disease immunotherapeutics. *Alzheimer's research & therapy,* 6**,** 42-42.

GOVINDPANI, K., CALVO-FLORES GUZMAN, B., VINNAKOTA, C., WALDVOGEL, H. J., FAULL, R. L. & KWAKOWSKY, A. 2017. Towards a Better Understanding of GABAergic Remodeling in Alzheimer's Disease. *Int J Mol Sci,* 18.

GRIFFIN, C. E., 3RD, KAYE, A. M., BUENO, F. R. & KAYE, A. D. 2013. Benzodiazepine pharmacology and central nervous system-mediated effects. *Ochsner J,* 13**,** 214-23.

GRIPPO, A. J. & SCOTTI, M. A. 2013. Stress and neuroinflammation. *Mod Trends Pharmacopsychiatry,* 28**,** 20-32.

GROVER, L. M. & TEYLER, T. J. 1990. Two components of long-term potentiation induced by different patterns of afferent activation. *Nature,* 347**,** 477-9.

GRUART, A., SÁNCHEZ-CAMPUSANO, R., FERNÁNDEZ-GUIZÁN, A. & DELGADO-GARCÍA, J. M. 2015. A Differential and Timed Contribution of Identified Hippocampal Synapses to Associative Learning in Mice. *Cerebral Cortex,* 25**,** 2542-2555.

GUELI, M. C. & TAIBI, G. 2013. Alzheimer's disease: amino acid levels and brain metabolic status. *Neurol Sci,* 34**,** 1575-9.

GUO, S., WANG, H. & YIN, Y. 2022. Microglia Polarization From M1 to M2 in Neurodegenerative Diseases. *Front Aging Neurosci,* 14**,** 815347.

GYLYS, K. H., FEIN, J. A., YANG, F., WILEY, D. J., MILLER, C. A. & COLE, G. M. 2004. Synaptic changes in Alzheimer's disease: increased amyloid-beta and gliosis in surviving terminals is accompanied by decreased PSD-95 fluorescence. *Am J Pathol,* 165**,** 1809-17.

HAMALAINEN, A., PIHLAJAMAKI, M., TANILA, H., HANNINEN, T., NISKANEN, E., TERVO, S., KARJALAINEN, P. A., VANNINEN, R. L. & SOININEN, H. 2007. Increased fMRI responses during encoding in mild cognitive impairment. *Neurobiol Aging,* 28**,** 1889-903.

HANSEN, D. V., HANSON, J. E. & SHENG, M. 2018. Microglia in Alzheimer's disease. *J Cell Biol,* 217**,** 459-472.

HARDY, J. A. & HIGGINS, G. A. 1992. Alzheimer's Disease: The Amyloid Cascade Hypothesis. *Science,* 256**,** 184-185.

HARRIS, E. W., GANONG, A. H. & COTMAN, C. W. 1984. Long-term potentiation in the hippocampus involves activation of N-methyl-D-aspartate receptors. *Brain Res,* 323**,** 132-7.

HASSELMO, M. E., BODELON, C. & WYBLE, B. P. 2002. A proposed function for hippocampal theta rhythm: separate phases of encoding and retrieval enhance reversal of prior learning. *Neural Comput,* 14**,** 793-817.

HECTOR, A. & BROUILLETTE, J. 2020. Hyperactivity Induced by Soluble Amyloid-beta Oligomers in the Early Stages of Alzheimer's Disease. *Front Mol Neurosci,* 13**,** 600084.

HENEKA, M. T. 2017. Inflammasome activation and innate immunity in Alzheimer's disease. *Brain Pathology,* 27**,** 220-222.

HENEKA, M. T., KUMMER, M. P., STUTZ, A., DELEKATE, A., SCHWARTZ, S., VIEIRA-SAECKER, A., GRIEP, A., AXT, D., REMUS, A., TZENG, T. C., GELPI, E., HALLE, A., KORTE, M., LATZ, E. & GOLENBOCK, D. T. 2013. NLRP3 is activated in Alzheimer's disease and contributes to pathology in APP/PS1 mice. *Nature,* 493**,** 674-8.

HEPPNER, F. L., RANSOHOFF, R. M. & BECHER, B. 2015. Immune attack: the role of inflammation in Alzheimer disease. *Nature Reviews Neuroscience,* 16**,** 358.

HIJAZI, S., HEISTEK, T. S., SCHELTENS, P., NEUMANN, U., SHIMSHEK, D. R., MANSVELDER, H. D., SMIT, A. B. & VAN KESTEREN, R. E. 2020a. Early restoration of parvalbumin interneuron activity prevents memory loss and network hyperexcitability in a mouse model of Alzheimer's disease. *Mol Psychiatry,* 25**,** 3380-3398.

HIJAZI, S., HEISTEK, T. S., VAN DER LOO, R., MANSVELDER, H. D., SMIT, A. B. & VAN KESTEREN, R. E. 2020b. Hyperexcitable Parvalbumin Interneurons Render Hippocampal Circuitry Vulnerable to Amyloid Beta. *iScience,* 23**,** 101271.

HINES, R. M., HINES, D. J., HOUSTON, C. M., MUKHERJEE, J., HAYDON, P. G., TRETTER, V., SMART, T. G. & MOSS, S. J. 2013. Disrupting the clustering of GABAA receptor alpha2 subunits in the frontal cortex leads to reduced gamma-power and cognitive deficits. *Proc Natl Acad Sci U S A,* 110**,** 16628-33.

HIPP, J. F., KNOFLACH, F., COMLEY, R., BALLARD, T. M., HONER, M., TRUBE, G., GASSER, R., PRINSSEN, E., WALLACE, T. L., ROTHFUSS, A., KNUST, H., LENNON-CHRIMES, S., DERKS, M., BENTLEY, D., SQUASSANTE, L., NAVE, S., NOLDEKE, J., WANDEL, C., THOMAS, A. W. & HERNANDEZ, M. C. 2021. Basmisanil, a highly selective GABA(A)-alpha5 negative allosteric modulator: preclinical pharmacology and demonstration of functional target engagement in man. *Sci Rep,* 11**,** 7700.

HO, R., ORTIZ, D. & SHEA, T. B. 2001. Amyloid-beta promotes calcium influx and neurodegeneration via stimulation of L voltage-sensitive calcium channels rather than NMDA channels in cultured neurons. *J Alzheimers Dis,* 3**,** 479-483.

HONARNEJAD, K., JUNG, C. K., LAMMICH, S., ARZBERGER, T., KRETZSCHMAR, H. & HERMS, J. 2013. Involvement of presenilin holoprotein upregulation in calcium dyshomeostasis of Alzheimer's disease. *J Cell Mol Med,* 17**,** 293-302.

HRNKOVA, M., ZILKA, N., MINICHOVA, Z., KOSON, P. & NOVAK, M. 2007. Neurodegeneration caused by expression of human truncated tau leads to progressive neurobehavioural impairment in transgenic rats. *Brain Research,* 1130**,** 206-213.

HSIEH, H., BOEHM, J., SATO, C., IWATSUBO, T., TOMITA, T., SISODIA, S. & MALINOW, R. 2006. AMPAR removal underlies Abeta-induced synaptic depression and dendritic spine loss. *Neuron,* 52**,** 831-43.

HU, Z., YU, P., ZHANG, Y., YANG, Y., ZHU, M., QIN, S., XU, J. T., DUAN, D., WU, Y., WANG, D., ROWAN, M. J. & HU, N. W. 2022. Inhibition of the ISR abrogates mGluR5-dependent long-term depression and spatial memory deficits in a rat model of Alzheimer's disease. *Transl Psychiatry,* 12**,** 96.

HUH, S., BAEK, S.-J., LEE, K.-H., WHITCOMB, D., J., JO, J., CHOI, S.-M., KIM, D. H., PARK, M.-S., LEE, K. H. & KIM, B. C. 2016. The reemergence of long-term potentiation in aged Alzheimer's disease mouse model. *Scientific Reports,* 6.

HYMAN, B. T. & GOMEZ-ISLA, T. 1994. Alzheimer's disease is a laminar, regional, and neural system specific disease, not a global brain disease. *Neurobiology of Aging,* 15**,** 353-354.

HYMAN, B. T., VAN HOESEN, G. W., DAMASIO, A. R. & BARNES, C. L. 1984. Alzheimer's disease: cell-specific pathology isolates the hippocampal formation. *Science,* 225**,** 1168-70.

IACCARINO, H. F., SINGER, A. C., MARTORELL, A. J., RUDENKO, A., GAO, F., GILLINGHAM, T. Z., MATHYS, H., SEO, J., KRITSKIY, O., ABDURROB, F., ADAIKKAN, C., CANTER, R. G., RUEDA, R., BROWN, E. N., BOYDEN, E. S. & TSAI, L. H. 2016. Gamma frequency entrainment attenuates amyloid load and modifies microglia. *Nature,* 540**,** 230-235.

IQBAL, K., ALONSO, A. D. C., CHEN, S., CHOHAN, M. O., EL-AKKAD, E., GONG, C.-X., KHATOON, S., LI, B., LIU, F., RAHMAN, A., TANIMUKAI, H. & GRUNDKE-IQBAL, I. 2005. Tau pathology in Alzheimer disease and other tauopathies. *Biochimica et biophysica acta,* 1739**,** 198-210.

JACK, C., KNOPMAN, D., JAGUST, W., PETERSEN, R., WEINER, M., AISEN, P., SHAW, L., VEMURI, P., WISTE, H., WEIGAND, S., LESNICK, T., PANKRATZ, V., DONOHUE, M. & TROJANOWSKI, J. 2013.

Update on hypothetical model of Alzheimer's disease biomarkers. *Alzheimer's & Dementia: The Journal of the Alzheimer's Association,* 9**,** P521-P522.

JACK, C. R., JR., KNOPMAN, D. S., JAGUST, W. J., SHAW, L. M., AISEN, P. S., WEINER, M. W., PETERSEN, R. C. & TROJANOWSKI, J. Q. 2010. Hypothetical model of dynamic biomarkers of the Alzheimer's pathological cascade. *Lancet Neurol,* 9**,** 119-28.

JACKMAN, S. L. & REGEHR, W. G. 2017. The Mechanisms and Functions of Synaptic Facilitation. *Neuron,* 94**,** 447-464.

JANZ, R., GODA, Y., GEPPERT, M., MISSLER, M. & SÜDHOF, T. C. 1999. SV2A and SV2B Function as Redundant Ca 2+ Regulators in Neurotransmitter Release. *Neuron,* 24**,** 1003-1016.

JAVANSHIRI, K., WALDO, M. L., FRIBERG, N., SJOVALL, F., WICKERSTROM, K., HAGLUND, M. & ENGLUND, E. 2018. Atherosclerosis, Hypertension, and Diabetes in Alzheimer's Disease, Vascular Dementia, and Mixed Dementia: Prevalence and Presentation. *J Alzheimers Dis,* 65**,** 1247-1258.

JAWORSKI, J., KAPITEIN, L. C., GOUVEIA, S. M., DORTLAND, B. R., WULF, P. S., GRIGORIEV, I., CAMERA, P., SPANGLER, S. A., DI STEFANO, P., DEMMERS, J., KRUGERS, H., DEFILIPPI, P., AKHMANOVA, A. & HOOGENRAAD, C. C. 2009. Dynamic microtubules regulate dendritic spine morphology and synaptic plasticity. *Neuron,* 61**,** 85-100.

JOHNSON, J. W. & KOTERMANSKI, S. E. 2006. Mechanism of action of memantine. *Curr Opin Pharmacol,* 6**,** 61-7.

JONSSON, T., STEFANSSON, H., STEINBERG, S., JONSDOTTIR, I., JONSSON, P. V., SNAEDAL, J., BJORNSSON, S., HUTTENLOCHER, J., LEVEY, A. I., LAH, J. J., RUJESCU, D., HAMPEL, H., GIEGLING, I., ANDREASSEN, O. A., ENGEDAL, K., ULSTEIN, I., DJUROVIC, S., IBRAHIM-VERBAAS, C., HOFMAN, A., IKRAM, M. A., VAN DUIJN, C. M., THORSTEINSDOTTIR, U., KONG, A. & STEFANSSON, K. 2013. Variant of TREM2 associated with the risk of Alzheimer's disease. *N Engl J Med,* 368**,** 107-16.

JOO, S. H., LIM, H. K. & LEE, C. U. 2016. Three Large-Scale Functional Brain Networks from Resting-State Functional MRI in Subjects with Different Levels of Cognitive Impairment. *Psychiatry Investig,* 13**,** 1-7.

JUNE, H. L., HARVEY, S. C., FOSTER, K. L., MCKAY, P. F., CUMMINGS, R., GARCIA, M., MASON, D., GREY, C., MCCANE, S., WILLIAMS, L. S., JOHNSON, T. B., HE, X., ROCK, S. & COOK, J. M. 2001. GABA(A) receptors containing (alpha)5 subunits in the CA1 and CA3 hippocampal fields regulate ethanol-motivated behaviors: an extended ethanol reward circuitry. *J Neurosci,* 21**,** 2166-77.

JUNG, J. H., AN, K., KWON, O. B., KIM, H. S. & KIM, J. H. 2011. Pathway-specific alteration of synaptic plasticity in Tg2576 mice. *Mol Cells,* 32**,** 197-201.

KARMAKAR, S., SHARMA, L. G., ROY, A., PATEL, A. & PANDEY, L. M. 2019. Neuronal SNARE complex: A protein folding system with intricate protein-protein interactions, and its common neuropathological hallmark, SNAP25. *Neurochem Int,* 122**,** 196-207.

KATZMAN, R. 2008. The prevalence and malignancy of Alzheimer disease: a major killer. *Alzheimers Dement,* 4**,** 378-80.

KAYED, R., HEAD, E., SARSOZA, F., SAING, T., COTMAN, C. W., NECULA, M., MARGOL, L., WU, J., BREYDO, L., THOMPSON, J. L., RASOOL, S., GURLO, T., BUTLER, P. & GLABE, C. G. 2007. Fibril specific, conformation dependent antibodies recognize a generic epitope common to amyloid fibrils and fibrillar oligomers that is absent in prefibrillar oligomers. *Molecular neurodegeneration,* 2**,** 18-18.

KAYED, R., HEAD, E., THOMPSON, J., MCINTIRE, T., MILTON, S., COTMAN, C. & GLABE, C. 2003. Common Structure of Soluble Amyloid Oligomers Implies Common Mechanism of Pathogenesis. *Science (Washington),* 300**,** 486-489.

KAZIM, S. F., CHUANG, S.-C., ZHAO, W., WONG, R. K. S., BIANCHI, R. & IQBAL, K. 2017. Early-Onset Network Hyperexcitability in Presymptomatic Alzheimer's Disease Transgenic Mice Is Suppressed by Passive Immunization with Anti-Human APP/Aβ Antibody and by mGluR5 Blockade. *Frontiers in aging neuroscience,* 9**,** 71-71.

KAZIM, S. F., SEO, J. H., BIANCHI, R., LARSON, C. S., SHARMA, A., WONG, R. K. S., GORBACHEV, K. Y. & PEREIRA, A. C. 2021. Neuronal Network Excitability in Alzheimer's Disease: The Puzzle of Similar versus Divergent Roles of Amyloid beta and Tau. *eNeuro,* 8.

KEITH, D. & EL-HUSSEINI, A. 2008. Excitation Control: Balancing PSD-95 Function at the Synapse. *Front Mol Neurosci,* 1**,** 4.

KEREN-SHAUL, H., SPINRAD, A., WEINER, A., MATCOVITCH-NATAN, O., DVIR-SZTERNFELD, R., ULLAND, T. K., DAVID, E., BARUCH, K., LARA-ASTAISO, D., TOTH, B., ITZKOVITZ, S., COLONNA, M., SCHWARTZ, M. & AMIT, I. 2017. A Unique Microglia Type Associated with Restricting Development of Alzheimer's Disease. *Cell,* 169**,** 1276-1290 e17.

KERTI, K., LORINCZ, A. & NUSSER, Z. 2012. Unique somato-dendritic distribution pattern of Kv4.2 channels on hippocampal CA1 pyramidal cells. *Eur J Neurosci,* 35**,** 66-75.

KESNER, R. P. & ROLLS, E. T. 2015. A computational theory of hippocampal function, and tests of the theory: new developments. *Neurosci Biobehav Rev,* 48**,** 92-147.

KINNEY, J. W., BEMILLER, S. M., MURTISHAW, A. S., LEISGANG, A. M., SALAZAR, A. M. & LAMB, B. T. 2018. Inflammation as a central mechanism in Alzheimer's disease. *Alzheimers Dement (N Y),* 4**,** 575-590.

KITCHIGINA, V. F. 2018. Alterations of Coherent Theta and Gamma Network Oscillations as an Early Biomarker of Temporal Lobe Epilepsy and Alzheimer's Disease. *Front Integr Neurosci,* 12**,** 36.

KIVISAKK, P., CARLYLE, B. C., SWEENEY, T., QUINN, J. P., RAMIREZ, C. E., TROMBETTA, B. A., MENDES, M., BROCK, M., RUBEL, C., CZERKOWICZ, J., GRAHAM, D. & ARNOLD, S. E. 2022. Increased levels of the synaptic proteins PSD-95, SNAP-25, and neurogranin in the cerebrospinal fluid of patients with Alzheimer's disease. *Alzheimers Res Ther,* 14**,** 58.

KLAUSBERGER, T., MAGILL, P. J., MARTON, L. F., ROBERTS, J. D., COBDEN, P. M., BUZSAKI, G. & SOMOGYI, P. 2003. Brain-state- and cell-type-specific firing of hippocampal interneurons in vivo. *Nature,* 421**,** 844-8.

KLAUSBERGER, T. & SOMOGYI, P. 2008. Neuronal diversity and temporal dynamics: the unity of hippocampal circuit operations. *Science,* 321**,** 53-7.

KLYUBIN, I., WALSH, D. M., LEMERE, C., CULLEN, W., SHANKAR, G., BETTS, V., SPOONER, E., JIANG, L., ANWYL, R., SELKOE, D. & ROWAN, M. 2005. Amyloid beta protein immunotherapy neutralizes A beta oligomers that disrupt synaptic plasticity in vivo. *Nature Medicine,* 11**,** 556-561.

KNOTT, G. W., QUAIRIAUX, C., GENOUD, C. & WELKER, E. 2002. Formation of dendritic spines with GABAergic synapses induced by whisker stimulation in adult mice. *Neuron,* 34**,** 265-73.

KOH, M. T., BRANCH, A., HABERMAN, R. & GALLAGHER, M. 2020. Significance of inhibitory recruitment in aging with preserved cognition: limiting gamma-aminobutyric acid type A alpha5 function produces memory impairment. *Neurobiol Aging,* 91**,** 1-4.

KOH, M. T., ROSENZWEIG-LIPSON, S. & GALLAGHER, M. 2013. Selective GABA(A) alpha5 positive allosteric modulators improve cognitive function in aged rats with memory impairment. *Neuropharmacology,* 64**,** 145-52.

KOHARA, K., PIGNATELLI, M., RIVEST, A. J., JUNG, H. Y., KITAMURA, T., SUH, J., FRANK, D., KAJIKAWA, K., MISE, N., OBATA, Y., WICKERSHAM, I. R. & TONEGAWA, S. 2014. Cell type-specific genetic and optogenetic tools reveal hippocampal CA2 circuits. *Nat Neurosci,* 17**,** 269-79.

KONG, Y., HUANG, L., LI, W., LIU, X., ZHOU, Y., LIU, C., ZHANG, S., XIE, F., ZHANG, Z., JIANG, D., ZHOU, W., NI, R., ZHANG, C., SUN, B., WANG, J. & GUAN, Y. 2021. The Synaptic Vesicle Protein 2A Interacts With Key Pathogenic Factors in Alzheimer's Disease: Implications for Treatment. *Front Cell Dev Biol,* 9**,** 609908.

KOSON, P., ZILKA, N., KOVAC, A., KOVACECH, B., KORENOVA, M., FILIPCIK, P. & NOVAK, M. 2008. Truncated tau expression levels determine life span of a rat model of tauopathy without causing neuronal loss or correlating with terminal neurofibrillary tangle load. *European Journal of Neuroscience,* 28**,** 239-246.

KRANTIC, S., ISORCE, N., MECHAWAR, N., DAVOLI, M. A., VIGNAULT, E., ALBUQUERQUE, M., CHABOT, J. G., MOYSE, E., CHAUVIN, J. P., AUBERT, I., MCLAURIN, J. & QUIRION, R. 2012. Hippocampal

GABAergic neurons are susceptible to amyloid-beta toxicity in vitro and are decreased in number in the Alzheimer's disease TgCRND8 mouse model. *J Alzheimers Dis,* 29**,** 293-308.

KUCHIBHOTLA, K. V., GOLDMAN, S. T., LATTARULO, C. R., WU, H. Y., HYMAN, B. T. & BACSKAI, B. J. 2008. Abeta plaques lead to aberrant regulation of calcium homeostasis in vivo resulting in structural and functional disruption of neuronal networks. *Neuron,* 59**,** 214-25.

KUWABARA, Y., ISHIZEKI, M., WATAMURA, N., TOBA, J., YOSHII, A., INOUE, T. & OHSHIMA, T. 2014. Impairments of long-term depression induction and motor coordination precede Abeta accumulation in the cerebellum of APPswe/PS1dE9 double transgenic mice. *J Neurochem,* 130**,** 432-43.

LAM, A. D., DECK, G., GOLDMAN, A., ESKANDAR, E. N., NOEBELS, J. & COLE, A. J. 2017. Silent hippocampal seizures and spikes identified by foramen ovale electrodes in Alzheimer's disease. *Nat Med,* 23**,** 678-680.

LAMBERT, M. P., BARLOW, A. K., CHROMY, B. A., EDWARDS, C., FREED, R., LIOSATOS, M., MORGAN, T. E., ROZOVSKY, I., TROMMER, B., VIOLA, K. L., WALS, P., ZHANG, C., FINCH, C. E., KRAFFT, G. A. & KLEIN, W. L. 1998. Diffusible, Nonfibrillar Ligands Derived from Aβ 1-42 are Potent Central Nervous System Neurotoxins. *Proceedings of the National Academy of Sciences of the United States of America,* 95**,** 6448-6453.

LAUTERBORN, J. C., SCADUTO, P., COX, C. D., SCHULMANN, A., LYNCH, G., GALL, C. M., KEENE, C. D. & LIMON, A. 2021. Increased excitatory to inhibitory synaptic ratio in parietal cortex samples from individuals with Alzheimer's disease. *Nat Commun,* 12**,** 2603.

LECLERC, B. & ABULROB, A. 2013. Perspectives in Molecular Imaging Using Staging Biomarkers and Immunotherapies in Alzheimer's Disease. *The Scientific World Journal,* 2013.

LEE, H.-G., PERRY, G., MOREIRA, P. I., GARRETT, M. R., LIU, Q., ZHU, X., TAKEDA, A., NUNOMURA, A. & SMITH, M. A. 2005. Tau phosphorylation in Alzheimer's disease: pathogen or protector? *Trends in Molecular Medicine,* 11**,** 164-169.

LEE, S. L. T., LEW, D., WICKENHEISSER, V. & MARKUS, E. J. 2019. Interdependence between dorsal and ventral hippocampus during spatial navigation. *Brain Behav,* 9**,** e01410.

LENART, N., BROUGH, D. & DENES, A. 2016. Inflammasomes link vascular disease with neuroinflammation and brain disorders. *Journal of Cerebral Blood Flow and Metabolism,* 36**,** 1668-1685.

LEON, W. C., CANNEVA, F., PARTRIDGE, V., ALLARD, S., FERRETTI, M. T., DEWILDE, A., VERCAUTEREN, F., ATIFEH, R., DUCATENZEILER, A., KLEIN, W., SZYF, M., ALHONEN, L. & CUELLO, A. C. 2010. A novel transgenic rat model with a full Alzheimer's-like amyloid pathology displays pre-plaque intracellular amyloid-beta-associated cognitive impairment. *Journal of Alzheimer's disease : JAD,* 20**,** 113-126.

LESNÉ, S., KOH, M. T., KOTILINEK, L., KAYED, R., GLABE, C. G., YANG, A., GALLAGHER, M. & ASHE, K. H. 2006. A specific amyloid-beta protein assembly in the brain impairs memory. *Nature,* 440**,** 352.

LEUNG, L. S. & PÉLOQUIN, P. 2010. Cholinergic Modulation Differs between Basal and Apical Dendritic Excitation of Hippocampal CA1 Pyramidal Cells. *Cerebral Cortex,* 20**,** 1865-1877.

LEWIS, D. A., CHO, R. Y., CARTER, C. S., EKLUND, K., FORSTER, S., KELLY, M. A. & MONTROSE, D. 2008. Subunit-selective modulation of GABA type A receptor neurotransmission and cognition in schizophrenia. *Am J Psychiatry,* 165**,** 1585-93.

LEYH, J., PAESCHKE, S., MAGES, B., MICHALSKI, D., NOWICKI, M., BECHMANN, I. & WINTER, K. 2021. Classification of Microglial Morphological Phenotypes Using Machine Learning. *Front Cell Neurosci,* 15**,** 701673.

LI, S., HONG, S., SHEPARDSON, N. E., WALSH, D. M., SHANKAR, G. M. & SELKOE, D. 2009. Soluble oligomers of amyloid Beta protein facilitate hippocampal long-term depression by disrupting neuronal glutamate uptake. *Neuron,* 62**,** 788-801.

LI, S., JIN, M., KOEGLSPERGER, T., SHEPARDSON, N. E., SHANKAR, G. M. & SELKOE, D. J. 2011. Soluble Abeta oligomers inhibit long-term potentiation through a mechanism involving excessive activation of extrasynaptic NR2B-containing NMDA receptors. *J Neurosci,* 31**,** 6627-38.

LI, W., HOWARD, J. D. & GOTTFRIED, J. A. 2010. Disruption of odour quality coding in piriform cortex mediates olfactory deficits in Alzheimer's disease. *Brain,* 133**,** 2714-26.

LI, X. L., HU, N., TAN, M. S., YU, J. T. & TAN, L. 2014. Behavioral and psychological symptoms in Alzheimer's disease. *Biomed Res Int,* 2014**,** 927804.

LI, Y., SUN, H., CHEN, Z., XU, H., BU, G. & ZHENG, H. 2016. Implications of GABAergic Neurotransmission in Alzheimer's Disease. *Front Aging Neurosci,* 8**,** 31.

LIMON, A., REYES-RUIZ, J. M. & MILEDI, R. 2012. Loss of functional GABA(A) receptors in the Alzheimer diseased brain. *Proc Natl Acad Sci U S A,* 109**,** 10071-6.

LISMAN, J. 2010. Working memory: the importance of theta and gamma oscillations. *Curr Biol,* 20**,** R490-2.

LIU, C.-C., LIU, C.-C., KANEKIYO, T., XU, H. & BU, G. 2013. Apolipoprotein E and Alzheimer disease: risk, mechanisms and therapy. *Nature reviews. Neurology,* 9**,** 106-118.

LIU, L., GRIFFIN, W. S. T., LI, Y., MRAK ROBERT, E. & BARGER STEVEN, W. 2006. Interleukin-1 mediates Alzheimer and Lewy body pathologies. *Journal of Neuroinflammation,* 3**,** 5.

LIU, L., WONG, T. P., POZZA, M. F., LINGENHOEHL, K., WANG, Y., SHENG, M., AUBERSON, Y. P. & WANG, Y. T. 2004. Role of NMDA receptor subtypes in governing the direction of hippocampal synaptic plasticity. *Science,* 304**,** 1021-4.

LIU, Z., LV, C., ZHAO, W., SONG, Y., PEI, D. & XU, T. 2012. NR2B-containing NMDA receptors expression and their relationship to apoptosis in hippocampus of Alzheimer's disease-like rats. *Neurochem Res,* 37**,** 1420-7.

LOPEZ, J. R., LYCKMAN, A., ODDO, S., LAFERLA, F. M., QUERFURTH, H. W. & SHTIFMAN, A. 2008. Increased intraneuronal resting [Ca2+] in adult Alzheimer's disease mice. *J Neurochem,* 105**,** 262-71.

LOPEZ-MADRONA, V. J., PEREZ-MONTOYO, E., ALVAREZ-SALVADO, E., MORATAL, D., HERRERAS, O., PEREDA, E., MIRASSO, C. R. & CANALS, S. 2020. Different theta frameworks coexist in the rat hippocampus and are coordinated during memory-guided and novelty tasks. *Elife,* 9.

LOWE, S. L., FRANCIS, P. T., PROCTER, A. W., PALMER, A. M., DAVISON, A. N. & BOWEN, D. M. 1988. Gamma-aminobutyric acid concentration in brain tissue at two stages of Alzheimer's disease. *Brain,* 111 ( Pt 4)**,** 785-99.

LYNCH, B. A., LAMBENG, N., NOCKA, K., KENSEL-HAMMES, P., BAJJALIEH, S. M., MATAGNE, A. & FUKS, B. 2004. The synaptic vesicle protein SV2A is the binding site for the antiepileptic drug levetiracetam. *Proc Natl Acad Sci U S A,* 101**,** 9861-6.

LYNCH, G., LARSON, J., KELSO, S., BARRIONUEVO, G. & SCHOTTLER, F. 1983. Intracellular injections of EGTA block induction of hippocampal long-term potentiation. *Nature,* 305**,** 719-21.

LYTHGOE, M. P., JENEI, K. & PRASAD, V. 2022. Regulatory decisions diverge over aducanumab for Alzheimer's disease. *BMJ,* 376**,** e069780.

MAHAR, I., ALBUQUERQUE, M. S., MONDRAGON-RODRIGUEZ, S., CAVANAGH, C., DAVOLI, M. A., CHABOT, J. G., WILLIAMS, S., MECHAWAR, N., QUIRION, R. & KRANTIC, S. 2016. Phenotypic Alterations in Hippocampal NPY- and PV-Expressing Interneurons in a Presymptomatic Transgenic Mouse Model of Alzheimer's Disease. *Front Aging Neurosci,* 8**,** 327.

MAJUMDAR, A., CAPETILLO-ZARATE, E., CRUZ, D., GOURAS, G. K. & MAXFIELD, F. R. 2011. Degradation of Alzheimer's amyloid fibrils by microglia requires delivery of ClC-7 to lysosomes. *Mol Biol Cell,* 22**,** 1664-76.

MALENKA, R. C. & BEAR, M. F. 2004. LTP and LTD: an embarrassment of riches. *Neuron,* 44**,** 5-21.

MANGO, D., SAIDI, A., CISALE, G. Y., FELIGIONI, M., CORBO, M. & NISTICO, R. 2019. Targeting Synaptic Plasticity in Experimental Models of Alzheimer's Disease. *Front Pharmacol,* 10**,** 778.

MARC AUREL, B., XIAOWEI, C., HORST, A. H., JULIA, R., MATTHIAS, S., BERT, S. & ARTHUR, K. 2012. Critical role of soluble amyloid-β for early hippocampal hyperactivity in a mouse model of Alzheimer's disease. *Proceedings of the National Academy of Sciences - PNAS,* 109**,** 8740-8745.

MARTIN, D. L., MARTIN, S. B., WU, S. J. & ESPINA, N. 1991. Regulatory properties of brain glutamate decarboxylase (GAD): the apoenzyme of GAD is present principally as the smaller of two molecular forms of GAD in brain. *J Neurosci,* 11**,** 2725-31.

MARTIN, J. 2003. *Neuroanatomy: text and atlas* McGraw-Hill Companies.

MARUSZAK, A. & THURET, S. 2014. Why looking at the whole hippocampus is not enough-a critical role for anteroposterior axis, subfield and activation analyses to enhance predictive value of hippocampal changes for Alzheimer's disease diagnosis. *Front Cell Neurosci,* 8**,** 95.

MASTRANGELO, M. A. & BOWERS, W. J. 2008. Detailed immunohistochemical characterization of temporal and spatial progression of Alzheimer's disease-related pathologies in male triple-transgenic mice. *BMC Neurosci,* 9**,** 81.

MATOS, M., AUGUSTO, E., OLIVEIRA, C. R. & AGOSTINHO, P. 2008. Amyloid-beta peptide decreases glutamate uptake in cultured astrocytes: involvement of oxidative stress and mitogen-activated protein kinase cascades. *Neuroscience,* 156**,** 898-910.

MATSUZAKI, M., HONKURA, N., ELLIS-DAVIES, G. C. & KASAI, H. 2004. Structural basis of long-term potentiation in single dendritic spines. *Nature,* 429**,** 761-6.

MATTHEWS, F. E., STEPHAN, B. C., ROBINSON, L., JAGGER, C., BARNES, L. E., ARTHUR, A., BRAYNE, C., COGNITIVE, F. & AGEING STUDIES, C. 2016. A two decade dementia incidence comparison from the Cognitive Function and Ageing Studies I and II. *Nat Commun,* 7**,** 11398.

MCBRAYER, M. & NIXON, R. A. 2013. Lysosome and calcium dysregulation in Alzheimer's disease: partners in crime. *Biochem Soc Trans,* 41**,** 1495-502.

MCDADE, E., CUMMINGS, J. L., DHADDA, S., SWANSON, C. J., REYDERMAN, L., KANEKIYO, M., KOYAMA, A., IRIZARRY, M., KRAMER, L. D. & BATEMAN, R. J. 2022. Lecanemab in patients with early Alzheimer's disease: detailed results on biomarker, cognitive, and clinical effects from the randomized and open-label extension of the phase 2 proof-of-concept study. *Alzheimers Res Ther,* 14**,** 191.

MCGARRITY, S., MASON, R., FONE, K. C., PEZZE, M. & BAST, T. 2017. Hippocampal Neural Disinhibition Causes Attentional and Memory Deficits. *Cerebral cortex (New York, N.Y. 1991),* 27**,** 4447-4462.

MCNAUGHTON, B. L. 1982. Long-term synaptic enhancement and short-term potentiation in rat fascia dentata act through different mechanisms. *J Physiol,* 324**,** 249-62.

MEGHDADI, A. H., STEVANOVIC KARIC, M., MCCONNELL, M., RUPP, G., RICHARD, C., HAMILTON, J., SALAT, D. & BERKA, C. 2021. Resting state EEG biomarkers of cognitive decline associated with Alzheimer's disease and mild cognitive impairment. *PLoS One,* 16**,** e0244180.

MEIER-STEPHENSON, F. S., MEIER-STEPHENSON, V. C., CARTER, M. D., MEEK, A. R., WANG, Y., PAN, L., CHEN, Q., JACOBO, S., WU, F., LU, E., SIMMS, G. A., FISHER, L., MCGRATH, A. J., FERMO, V., BARDEN, C. J., CLAIR, H. D. S., GALLOWAY, T. N., YADAV, A., CAMPAGNA-SLATER, V., HADDEN, M., REED, M., TAYLOR, M., KELLY, B., DIEZ-CECILIA, E., KOLAJ, I., SANTOS, C., LIYANAGE, I., SWEETING, B., STAFFORD, P., BOUDREAU, R., REID, G. A., NOYCE, R. S., STEVENS, L., STANISZEWSKI, A., ZHANG, H., MURTY, M., LEMAIRE, P., CHARDONNET, S., RICHARDSON, C. D., GABELICA, V., DEPAUW, E., BROWN, R., DARVESH, S., ARANCIO, O. & WEAVER, D. F. 2022. Alzheimer's disease as an autoimmune disorder of innate immunity endogenously modulated by tryptophan metabolites. *Alzheimers Dement (N Y),* 8**,** e12283.

MINGER, S. L., HONER, W. G., ESIRI, M. M., MCDONALD, B., KEENE, J., NICOLL, J. A., CARTER, J., HOPE, T. & FRANCIS, P. T. 2001. Synaptic pathology in prefrontal cortex is present only with severe dementia in Alzheimer disease. *J Neuropathol Exp Neurol,* 60**,** 929-36.

MINKEVICIENE, R., RHEIMS, S., DOBSZAY, M. B., ZILBERTER, M., HARTIKAINEN, J., FULOP, L., PENKE, B., ZILBERTER, Y., HARKANY, T., PITKANEN, A. & TANILA, H. 2009. Amyloid beta-induced neuronal hyperexcitability triggers progressive epilepsy. *J Neurosci,* 29**,** 3453-62.

MOHRMANN, R., DE WIT, H., CONNELL, E., PINHEIRO, P. S., LEESE, C., BRUNS, D., DAVLETOV, B., VERHAGE, M. & SORENSEN, J. B. 2013. Synaptotagmin interaction with SNAP-25 governs vesicle docking, priming, and fusion triggering. *J Neurosci,* 33**,** 14417-30.

MORRIS, G. P., CLARK, I. & VISSEL, B. 2014. Inconsistencies and Controversies Surrounding the Amyloid Hypothesis of Alzheimer's Disease. *Acta Neuropathol. Commun.*: BMC.

MOSER, M. B., ROWLAND, D. C. & MOSER, E. I. 2015. Place cells, grid cells, and memory. *Cold Spring Harb Perspect Biol,* 7**,** a021808.

MUCKE, L., MASLIAH, E., YU, G. Q., MALLORY, M., ROCKENSTEIN, E. M., TATSUNO, G., HU, K., KHOLODENKO, D., JOHNSON-WOOD, K. & MCCONLOGUE, L. 2000. High-level neuronal expression of abeta 1-42 in wild-type human amyloid protein precursor transgenic mice: synaptotoxicity without plaque formation. *J Neurosci,* 20**,** 4050-8.

MULKEY, R. M. & MALENKA, R. C. 1992. Mechanisms underlying induction of homosynaptic long-term depression in area CA1 of the hippocampus. *Neuron,* 9**,** 967-75.

NAHAR, L., DELACROIX, B. M. & NAM, H. W. 2021. The Role of Parvalbumin Interneurons in Neurotransmitter Balance and Neurological Disease. *Front Psychiatry,* 12**,** 679960.

NAYEEM, N., GREEN, T. P., MARTIN, I. L. & BARNARD, E. A. 1994. Quaternary structure of the native GABAA receptor determined by electron microscopic image analysis. *J Neurochem,* 62**,** 815-8.

NELSON, O., TU, H., LEI, T., BENTAHIR, M., DE STROOPER, B. & BEZPROZVANNY, I. 2007. Familial Alzheimer disease-linked mutations specifically disrupt Ca2+ leak function of presenilin 1. *J Clin Invest,* 117**,** 1230-9.

NEWMAN, E. L., GUPTA, K., CLIMER, J. R., MONAGHAN, C. K. & HASSELMO, M. E. 2012. Cholinergic modulation of cognitive processing: insights drawn from computational models. *Frontiers in Behavioral Neuroscience,* 6.

NOOR, A. & ZAHID, S. 2017. A review of the role of synaptosomal-associated protein 25 (SNAP-25) in neurological disorders. *Int J Neurosci,* 127**,** 805-811.

O'HARE, E., SCOPES, D. I. C., KIM, E.-M., PALMER, P., JONES, M., WHYMENT, A. D., SPANSWICK, D., AMIJEE, H., NEROU, E., MCMAHON, B., TREHERNE, J. M. & JEGGO, R. 2013. Orally bioavailable small molecule drug protects memory in Alzheimer's disease models. *Neurobiology of Aging,* 34**,** 1116-1125.

O'HARE, E., WELDON, D. T., MANTYH, P. W., GHILARDI, J. R., FINKE, M. P., KUSKOWSKI, M. A., MAGGIO, J. E., SHEPHARD, R. A. & CLEARY, J. 1999. Delayed behavioral effects following intrahippocampal injection of aggregated A beta (1-42). *Brain research,* 815**,** 1-10.

OAKLEY, H., COLE, S. L., LOGAN, S., MAUS, E., SHAO, P., CRAFT, J., GUILLOZET-BONGAARTS, A., OHNO, M., DISTERHOFT, J., VAN ELDIK, L., BERRY, R. & VASSAR, R. 2006. Intraneuronal beta-amyloid aggregates, neurodegeneration, and neuron loss in transgenic mice with five familial Alzheimer's disease mutations: potential factors in amyloid plaque formation. *The Journal of neuroscience : the official journal of the Society for Neuroscience,* 26**,** 10129.

ODDO, S., CACCAMO, A., SHEPHERD, J. D., MURPHY, M. P., GOLDE, T. E., KAYED, R., METHERATE, R., MATTSON, M. P., AKBARI, Y. & LAFERLA, F. M. 2003. Triple-Transgenic Model of Alzheimer's Disease with Plaques and Tangles: Intracellular Aβ and Synaptic Dysfunction. *Neuron,* 39**,** 409-421.

OKSANEN, M., HYOTYLAINEN, I., TRONTTI, K., ROLOVA, T., WOJCIECHOWSKI, S., KOSKUVI, M., VIITANEN, M., LEVONEN, A. L., HOVATTA, I., ROYBON, L., LEHTONEN, S., KANNINEN, K. M., HAMALAINEN, R. H. & KOISTINAHO, J. 2020. NF-E2-related factor 2 activation boosts antioxidant defenses and ameliorates inflammatory and amyloid properties in human Presenilin-1 mutated Alzheimer's disease astrocytes. *Glia,* 68**,** 589-599.

OLAH, V. J., GOETTEMOELLER, A. M., RAYAPROLU, S., DAMMER, E. B., SEYFRIED, N. T., RANGARAJU, S., DIMIDSCHSTEIN, J. & ROWAN, M. J. M. 2022. Biophysical Kv3 channel alterations dampen excitability of cortical PV interneurons and contribute to network hyperexcitability in early Alzheimer's. *Elife,* 11.

OLSSON, B., LAUTNER, R., ANDREASSON, U., OHRFELT, A., PORTELIUS, E., BJERKE, M., HOLTTA, M., ROSEN, C., OLSSON, C., STROBEL, G., WU, E., DAKIN, K., PETZOLD, M., BLENNOW, K. & ZETTERBERG, H. 2016. CSF and blood biomarkers for the diagnosis of Alzheimer's disease: a systematic review and meta-analysis. *Lancet Neurol,* 15**,** 673-684.

OREN, I. & KULLMANN, D. M. 2012. Mapping out hippocampal inhibition. *Nat Neurosci,* 15**,** 346-7.
OUDIN, A. 2020. Short review: Air pollution, noise and lack of greenness as risk factors for Alzheimer's disease- epidemiologic and experimental evidence. *Neurochem Int,* 134**,** 104646.
PALOP & MUCKE 2010. Amyloid-beta-induced neuronal dysfunction in Alzheimer's disease: from synapses toward neural networks. *Nature neuroscience,* 13**,** 812-818.
PALOP, J. J., CHIN, J., ROBERSON, E. D., WANG, J., THWIN, M. T., BIEN-LY, N., YOO, J., HO, K. O., YU, G. Q., KREITZER, A., FINKBEINER, S., NOEBELS, J. L. & MUCKE, L. 2007. Aberrant excitatory neuronal activity and compensatory remodeling of inhibitory hippocampal circuits in mouse models of Alzheimer's disease. *Neuron,* 55**,** 697-711.
PALOP, J. J. & MUCKE, L. 2016. Network abnormalities and interneuron dysfunction in Alzheimer disease. *Nat Rev Neurosci,* 17**,** 777-792.
PAN, E., PURANAM, R. S. & MCNAMARA, J. O. 2022. Long-Term Potentiation of Mossy Fiber Feedforward Inhibition of CA3 Pyramidal Cells Maintains E/I Balance in Epilepsy Model. *eNeuro,* 9.
PANDIS, D. & SCARMEAS, N. 2012. Seizures in Alzheimer Disease: Clinical and Epidemiological Data: Seizures in Alzheimer Disease. Los Angeles, CA: SAGE Publications.
PANG, K., JIANG, R., ZHANG, W., YANG, Z., LI, L. L., SHIMOZAWA, M., TAMBARO, S., MAYER, J., ZHANG, B., LI, M., WANG, J., LIU, H., YANG, A., CHEN, X., LIU, J., WINBLAD, B., HAN, H., JIANG, T., WANG, W., NILSSON, P., GUO, W. & LU, B. 2022. An App knock-in rat model for Alzheimer's disease exhibiting Abeta and tau pathologies, neuronal death and cognitive impairments. *Cell Res,* 32**,** 157-175.
PAPOUIN, T., LADEPECHE, L., RUEL, J., SACCHI, S., LABASQUE, M., HANINI, M., GROC, L., POLLEGIONI, L., MOTHET, J. P. & OLIET, S. H. 2012. Synaptic and extrasynaptic NMDA receptors are gated by different endogenous coagonists. *Cell,* 150**,** 633-46.
PARADISE, M., COOPER, C. & LIVINGSTON, G. 2009. Systematic review of the effect of education on survival in Alzheimer's disease. *Int Psychogeriatr,* 21**,** 25-32.
PARK, K., LEE, J., JANG, H. J., RICHARDS, B. A., KOHL, M. M. & KWAG, J. 2020. Optogenetic activation of parvalbumin and somatostatin interneurons selectively restores theta-nested gamma oscillations and oscillation-induced spike timing-dependent long-term potentiation impaired by amyloid beta oligomers. *BMC Biol,* 18**,** 7.
PASSINGHAM, R. E. 1979. The hippocampus as a cognitive map. *Neuroscience.,* 4**,** 863.
PASTALKOVA, E., ITSKOV, V., AMARASINGHAM, A. & BUZSAKI, G. 2008. Internally generated cell assembly sequences in the rat hippocampus. *Science,* 321**,** 1322-7.
PAXINOS, G. & WATSON, C. 2007. *The rat brain in stereotaxic coordinates,* Sydney, Academic Press.
PELKEY, K. A., CHITTAJALLU, R., CRAIG, M. T., TRICOIRE, L., WESTER, J. C. & MCBAIN, C. J. 2017. Hippocampal GABAergic Inhibitory Interneurons. *Physiol Rev,* 97**,** 1619-1747.
PENTKOWSKI, N. S., BERKOWITZ, L. E., THOMPSON, S. M., DRAKE, E. N., OLGUIN, C. R. & CLARK, B. J. 2018. Anxiety-like behavior as an early endophenotype in the TgF344-AD rat model of Alzheimer's disease. *Neurobiol Aging,* 61**,** 169-176.
PENTTONEN, M., KAMONDI, A., ACSÁDY, L. & BUZSÁKI, G. 1998. Gamma frequency oscillation in the hippocampus of the rat: intracellular analysis in vivo. *European Journal of Neuroscience,* 10**,** 718-728.
PERRY, E. K., TOMLINSON, B. E., BLESSED, G., BERGMANN, K., GIBSON, P. H. & PERRY, R. H. 1978. Correlation of cholinergic abnormalities with senile plaques and mental test scores in senile dementia. *Br Med J,* 2**,** 1457-9.
PETRACHE, A. L., KHAN, A. A., NICHOLSON, M. W., MONACO, A., KUTA-SIEJKOWSKA, M., HAIDER, S., HILTON, S., JOVANOVIC, J. N. & ALI, A. B. 2020. Selective Modulation of alpha5 GABA(A) Receptors Exacerbates Aberrant Inhibition at Key Hippocampal Neuronal Circuits in APP Mouse Model of Alzheimer's Disease. *Front Cell Neurosci,* 14**,** 568194.

PODLISNY, M. B., OSTASZEWSKI, B., SQUAZZO, S., KOO, E., RYDELL, R., TEPLOW, D. & SELKOE, D. 1995. AGGREGATION OF SECRETED AMYLOID BETA-PROTEIN INTO SODIUM DODECYL SULFATE-STABLE OLIGOMERS IN CELL-CULTURE. *Journal Of Biological Chemistry,* 270**,** 9564-9570.

POLINSKY, R. J. 1998. Clinical pharmacology of rivastigmine: a new-generation acetylcholinesterase inhibitor for the treatment of Alzheimer's disease. *Clin Ther,* 20**,** 634-47.

POZUETA, J., LEFORT, R. & SHELANSKI, M. L. 2013. Synaptic changes in Alzheimer's disease and its models. *Neuroscience,* 251**,** 51-65.

QUERFURTH, H. W. & LAFERLA, F. M. 2010. Alzheimer's Disease. *The New England Journal of Medicine,* 362**,** 1844-5.

RAJAN, K. B., WEUVE, J., BARNES, L. L., MCANINCH, E. A., WILSON, R. S. & EVANS, D. A. 2021. Population estimate of people with clinical Alzheimer's disease and mild cognitive impairment in the United States (2020-2060). *Alzheimers Dement,* 17**,** 1966-1975.

RAMMES, G., HASENJAGER, A., SROKA-SAIDI, K., DEUSSING, J. M. & PARSONS, C. G. 2011. Therapeutic significance of NR2B-containing NMDA receptors and mGluR5 metabotropic glutamate receptors in mediating the synaptotoxic effects of beta-amyloid oligomers on long-term potentiation (LTP) in murine hippocampal slices. *Neuropharmacology,* 60**,** 982-90.

RAMOS, B., BAGLIETTO-VARGAS, D., DEL RIO, J. C., MORENO-GONZALEZ, I., SANTA-MARIA, C., JIMENEZ, S., CABALLERO, C., LOPEZ-TELLEZ, J. F., KHAN, Z. U., RUANO, D., GUTIERREZ, A. & VITORICA, J. 2006. Early neuropathology of somatostatin/NPY GABAergic cells in the hippocampus of a PS1xAPP transgenic model of Alzheimer's disease. *Neurobiol Aging,* 27**,** 1658-72.

RAO, J. S., KELLOM, M., KIM, H. W., RAPOPORT, S. I. & REESE, E. A. 2012. Neuroinflammation and synaptic loss. *Neurochem Res,* 37**,** 903-10.

RAO, M. V., MOHAN, P. S., PETERHOFF, C. M., YANG, D. S., SCHMIDT, S. D., STAVRIDES, P. H., CAMPBELL, J., CHEN, Y., JIANG, Y., PASKEVICH, P. A., CATALDO, A. M., HAROUTUNIAN, V. & NIXON, R. A. 2008. Marked calpastatin (CAST) depletion in Alzheimer's disease accelerates cytoskeleton disruption and neurodegeneration: neuroprotection by CAST overexpression. *J Neurosci,* 28**,** 12241-54.

RATNER, M. H., DOWNING, S. S., GUO, O., ODAMAH, K. E., STEWART, T. M., KUMARESAN, V., ROBITSEK, R. J., XIA, W. & FARB, D. H. 2021. Prodromal dysfunction of alpha5GABA-A receptor modulated hippocampal ripples occurs prior to neurodegeneration in the TgF344-AD rat model of Alzheimer's disease. *Heliyon,* 7**,** e07895.

RAYMOND, C. R., IRELAND, D. R. & ABRAHAM, W. C. 2003. NMDA receptor regulation by amyloid-beta does not account for its inhibition of LTP in rat hippocampus. *Brain Res,* 968**,** 263-72.

RAZAY, G. & WILCOCK, G. K. 2008. Galantamine in Alzheimer's disease. *Expert Rev Neurother,* 8**,** 9-17.

REILLY, J. F., GAMES, D., RYDEL, R. E., FREEDMAN, S., SCHENK, D., YOUNG, W. G., MORRISON, J. H. & BLOOM, F. E. 2003. Amyloid deposition in the hippocampus and entorhinal cortex: quantitative analysis of a transgenic mouse model. *Proc Natl Acad Sci U S A,* 100**,** 4837-42.

REX, A., VOIGT, J. P. & FINK, H. 1999. Behavioral and neurochemical differences between Fischer 344 and Harlan-Wistar rats raised identically. *Behav Genet,* 29**,** 187-92.

RICHARDS, J. G., HIGGINS, G. A., OUAGAZZAL, A. M., OZMEN, L., KEW, J. N., BOHRMANN, B., MALHERBE, P., BROCKHAUS, M., LOETSCHER, H., CZECH, C., HUBER, G., BLUETHMANN, H., JACOBSEN, H. & KEMP, J. A. 2003. PS2APP transgenic mice, coexpressing hPS2mut and hAPPswe, show age-related cognitive deficits associated with discrete brain amyloid deposition and inflammation. *J Neurosci,* 23**,** 8989-9003.

RIZZI, L., ROSSET, I. & RORIZ-CRUZ, M. 2014. Global epidemiology of dementia: Alzheimer's and vascular types. *Biomed Res Int,* 2014**,** 908915.

ROBERT, N., DALILA, M., GEORGIA, M., SONIA, P., NICOLA, B., MARCO, P., MARCO, F., ALESSANDRA, M., ANTONIETTA, G., FRANCESCO, M., GIORGIO, B., FERDINANDO, N., NICOLA, B. M. & DIEGO, C. 2013. Inflammation subverts hippocampal synaptic plasticity in experimental multiple sclerosis. *PLoS ONE,* 8**,** e54666.

ROJAS-CHARRY, L., CALERO-MARTINEZ, S., MORGANTI, C., MORCIANO, G., PARK, K., HAGEL, C., MARCINIAK, S. J., GLATZEL, M., PINTON, P. & SEPULVEDA-FALLA, D. 2020. Susceptibility to cellular stress in PS1 mutant N2a cells is associated with mitochondrial defects and altered calcium homeostasis. *Sci Rep,* 10**,** 6455.

ROLLS, E. T. 2013. The mechanisms for pattern completion and pattern separation in the hippocampus. *Front Syst Neurosci,* 7**,** 74.

ROSSOR, M. N., IVERSEN, L. L., REYNOLDS, G. P., MOUNTJOY, C. Q. & ROTH, M. 1984. Neurochemical characteristics of early and late onset types of Alzheimer's disease. *Br Med J (Clin Res Ed),* 288**,** 961-4.

RUAN, Z., PATHAK, D., VENKATESAN KALAVAI, S., YOSHII-KITAHARA, A., MURAOKA, S., BHATT, N., TAKAMATSU-YUKAWA, K., HU, J., WANG, Y., HERSH, S., ERICSSON, M., GORANTLA, S., GENDELMAN, H. E., KAYED, R., IKEZU, S., LUEBKE, J. I. & IKEZU, T. 2021. Alzheimer's disease brain-derived extracellular vesicles spread tau pathology in interneurons. *Brain,* 144**,** 288-309.

RUDEN, J. B., DUGAN, L. L. & KONRADI, C. 2021. Parvalbumin interneuron vulnerability and brain disorders. *Neuropsychopharmacology,* 46**,** 279-287.

RYAN, N. S. & ROSSOR, M. N. 2010. Correlating familial Alzheimer's disease gene mutations with clinical phenotype. *Biomark Med,* 4**,** 99-112.

SAIZ-SANCHEZ, D., DE LA ROSA-PRIETO, C., UBEDA-BANON, I. & MARTINEZ-MARCOS, A. 2015. Interneurons, tau and amyloid-beta in the piriform cortex in Alzheimer's disease. *Brain Struct Funct,* 220**,** 2011-25.

SANTACRUZ, K., LEWIS, J., SPIRES, T., PAULSON, J., KOTILINEK, L., INGELSSON, M., GUIMARAES, A., DETURE, M., RAMSDEN, M., MCGOWAN, E., FORSTER, C., YUE, M., ORNE, J., JANUS, C., MARIASH, A., KUSKOWSKI, M., HYMAN, B., HUTTON, M. & ASHE, K. H. 2005. Tau suppression in a neurodegenerative mouse model improves memory function. *Science (New York, N.Y.),* 309**,** 476-481.

SARÉ, R. M., COOKE, S. K., KRYCH, L., ZERFAS, P. M., COHEN, R. M. & SMITH, C. B. 2020. Behavioral Phenotype in the TgF344-AD Rat Model of Alzheimer's Disease. *Front Neurosci,* 14**,** 601.

SCHARFMAN, H. E. 2007. The CA3 "backprojection" to the dentate gyrus. *Progress in brain research,* 163**,** 627.

SCHEFF, S. W., PRICE, D. A., SCHMITT, F. A. & MUFSON, E. J. 2006. Hippocampal synaptic loss in early Alzheimer's disease and mild cognitive impairment. *Neurobiology of Aging,* 27**,** 1372-1384.

SCHNELL, E., SIZEMORE, M., KARIMZADEGAN, S., CHEN, L., BREDT, D. S. & NICOLL, R. A. 2002. Direct interactions between PSD-95 and stargazin control synaptic AMPA receptor number. *Proc Natl Acad Sci U S A,* 99**,** 13902-7.

SCHWAB, C., YU, S., WONG, W., MCGEER, E. G. & MCGEER, P. L. 2013. GAD65, GAD67, and GABAT immunostaining in human brain and apparent GAD65 loss in Alzheimer's disease. *J Alzheimers Dis,* 33**,** 1073-88.

SEAB, J. P., JAGUST, W. J., WONG, S. T., ROOS, M. S., REED, B. R. & BUDINGER, T. F. 1988. Quantitative NMR measurements of hippocampal atrophy in Alzheimer's disease. *Magnetic resonance in medicine,* 8**,** 200-208.

SELKOE, D. 2001. Alzheimer's disease: Genes, proteins, and therapy. *Physiological Reviews***,** 741-766.

SELKOE, D. J. 1991. The molecular pathology of Alzheimer's disease. *Neuron,* 6**,** 487-498.

SEO, H. J., PARK, J. E., CHOI, S. M., KIM, T., CHO, S. H., LEE, K. H., SONG, W. K., SONG, J., JEONG, H. S., KIM, D. H. & KIM, B. C. 2021. Inhibitory Neural Network's Impairments at Hippocampal CA1 LTP in an Aged Transgenic Mouse Model of Alzheimer's Disease. *Int J Mol Sci,* 22.

SERNEELS, L., T'SYEN, D., PEREZ-BENITO, L., THEYS, T., HOLT, M. G. & DE STROOPER, B. 2020. Modeling the beta-secretase cleavage site and humanizing amyloid-beta precursor protein in rat and mouse to study Alzheimer's disease. *Mol Neurodegener,* 15**,** 60.

SERRANO-POZO, A., MIELKE, M. L., GOMEZ-ISLA, T., BETENSKY, R. A., GROWDON, J. H., FROSCH, M. P. & HYMAN, B. T. 2011. Reactive glia not only associates with plaques but also parallels tangles in Alzheimer's disease. *Am J Pathol,* 179**,** 1373-84.

SETTI, S. E., HUNSBERGER, H. C. & REED, M. N. 2017. Alterations in Hippocampal Activity and Alzheimer's Disease. *Translational issues in psychological science,* 3**,** 348-356.

SHAO, C., MIRRA, S., SAIT, H., SACKTOR, T. & SIGURDSSON, E. 2011. Postsynaptic degeneration as revealed by PSD-95 reduction occurs after advanced Aβ and tau pathology in transgenic mouse models of Alzheimer's disease. *Acta Neuropathologica,* 122**,** 285-292.

SHEN, J. & KELLEHER, R. J. 2007. The presenilin hypothesis of Alzheimer's disease: evidence for a loss-of-function pathogenic mechanism. *Proceedings of the National Academy of Sciences of the United States of America,* 104**,** 403-409.

SIEGHART, W. & SPERK, G. 2002. Subunit composition, distribution and function of GABA(A) receptor subtypes. *Curr Top Med Chem,* 2**,** 795-816.

SIEGLE, J. H. & WILSON, M. A. 2014. Enhancement of encoding and retrieval functions through theta phase-specific manipulation of hippocampus. *Elife,* 3**,** e03061.

SINCLAIR, L. I., TAYLER, H. M. & LOVE, S. 2015. Synaptic protein levels altered in vascular dementia. *Neuropathol Appl Neurobiol,* 41**,** 533-43.

SISODIA, S. S. & ST GEORGE-HYSLOP, P. H. 2002. gamma-Secretase, Notch, Abeta and Alzheimer's disease: where do the presenilins fit in? *Nature reviews. Neuroscience,* 3**,** 281-290.

SLOVITER, R. 1987. Decreased hippocampal inhibition and a selective loss of interneurons in experimental epilepsy. *Science (American Association for the Advancement of Science),* 235**,** 73-76.

SMITH, L. A. & MCMAHON, L. L. 2018. Deficits in synaptic function occur at medial perforant path-dentate granule cell synapses prior to Schaffer collateral-CA1 pyramidal cell synapses in the novel TgF344-Alzheimer's Disease Rat Model. *Neurobiology of Disease,* 110**,** 166-179.

SNYDER, E. M., NONG, Y., ALMEIDA, C. G., PAUL, S., MORAN, T., CHOI, E. Y., NAIRN, A. C., SALTER, M. W., LOMBROSO, P. J., GOURAS, G. K. & GREENGARD, P. 2005. Regulation of NMDA receptor trafficking by amyloid-beta. *Nat Neurosci,* 8**,** 1051-8.

SOLAS, M., PUERTA, E. & RAMIREZ, M. J. 2015. Treatment Options in Alzheimer s Disease: The GABA Story. *Curr Pharm Des,* 21**,** 4960-71.

SOSULINA, L., MITTAG, M., GEIS, H. R., HOFFMANN, K., KLYUBIN, I., QI, Y., STEFFEN, J., FRIEDRICHS, D., HENNEBERG, N., FUHRMANN, F., JUSTUS, D., KEPPLER, K., CUELLO, A. C., ROWAN, M. J., FUHRMANN, M. & REMY, S. 2021. Hippocampal hyperactivity in a rat model of Alzheimer's disease. *J Neurochem,* 157**,** 2128-2144.

SPERLING, R. A., DONOHUE, M. C., RAMAN, R., SUN, C. K., YAARI, R., HOLDRIDGE, K., SIEMERS, E., JOHNSON, K. A., AISEN, P. S. & TEAM, A. S. 2020. Association of Factors With Elevated Amyloid Burden in Clinically Normal Older Individuals. *JAMA Neurol,* 77**,** 735-745.

SQUIRE, L. R. 1992. Memory and the Hippocampuss: A Synthesis From Findings With Rats, Monkeys, and Humans. *Psychological Review,* 99**,** 195-231.

SQUIRE, L. R. & ZOLA-MORGAN, S. 1991. The medial temporal lobe memory system. *Science,* 253**,** 1380-6.

STEIN, V., HOUSE, D. R., BREDT, D. S. & NICOLL, R. A. 2003. Postsynaptic density-95 mimics and occludes hippocampal long-term potentiation and enhances long-term depression. *J Neurosci,* 23**,** 5503-6.

STOILJKOVIC, M., KELLEY, C., STUTZ, B., HORVATH, T. L. & HAJOS, M. 2019. Altered Cortical and Hippocampal Excitability in TgF344-AD Rats Modeling Alzheimer's Disease Pathology. *Cereb Cortex,* 29**,** 2716-2727.

STUTZMANN, G. E., SMITH, I., CACCAMO, A., ODDO, S., LAFERLA, F. M. & PARKER, I. 2006. Enhanced ryanodine receptor recruitment contributes to Ca2+ disruptions in young, adult, and aged Alzheimer's disease mice. *J Neurosci,* 26**,** 5180-9.

SULTANA, R., BANKS, W. A. & BUTTERFIELD, D. A. 2010. Decreased levels of PSD95 and two associated proteins and increased levels of BCl2 and caspase 3 in hippocampus from subjects with amnestic mild cognitive impairment: Insights into their potential roles for loss of synapses and

memory, accumulation of Abeta, and neurodegeneration in a prodromal stage of Alzheimer's disease. *J Neurosci Res,* 88**,** 469-77.

TAHAMI MONFARED, A. A., TAFAZZOLI, A., YE, W., CHAVAN, A. & ZHANG, Q. 2022. Long-Term Health Outcomes of Lecanemab in Patients with Early Alzheimer's Disease Using Simulation Modeling. *Neurol Ther,* 11**,** 863-880.

TAKAHASHI, H., BRASNJEVIC, I., RUTTEN, B. P., VAN DER KOLK, N., PERL, D. P., BOURAS, C., STEINBUSCH, H. W., SCHMITZ, C., HOF, P. R. & DICKSTEIN, D. L. 2010. Hippocampal interneuron loss in an APP/PS1 double mutant mouse and in Alzheimer's disease. *Brain Struct Funct,* 214**,** 145-60.

TAKAHASHI, K., ROCHFORD, C. D. & NEUMANN, H. 2005. Clearance of apoptotic neurons without inflammation by microglial triggering receptor expressed on myeloid cells-2. *J Exp Med,* 201**,** 647-57.

TALANTOVA, M., SANZ-BLASCO, S., ZHANG, X., XIA, P., AKHTAR, M. W., OKAMOTO, S., DZIEWCZAPOLSKI, G., NAKAMURA, T., CAO, G., PRATT, A. E., KANG, Y. J., TU, S., MOLOKANOVA, E., MCKERCHER, S. R., HIRES, S. A., SASON, H., STOUFFER, D. G., BUCZYNSKI, M. W., SOLOMON, J. P., MICHAEL, S., POWERS, E. T., KELLY, J. W., ROBERTS, A., TONG, G., FANG-NEWMEYER, T., PARKER, J., HOLLAND, E. A., ZHANG, D., NAKANISHI, N., CHEN, H. S., WOLOSKER, H., WANG, Y., PARSONS, L. H., AMBASUDHAN, R., MASLIAH, E., HEINEMANN, S. F., PINA-CRESPO, J. C. & LIPTON, S. A. 2013. Abeta induces astrocytic glutamate release, extrasynaptic NMDA receptor activation, and synaptic loss. *Proc Natl Acad Sci U S A,* 110**,** E2518-27.

TAN, M. S., TAN, L., JIANG, T., ZHU, X. C., WANG, H. F., JIA, C. D. & YU, J. T. 2014. Amyloid-β induces NLRP1-dependent neuronal pyroptosis in models of Alzheimer's disease. *Cell Death and Disease,* 5**,** e1382.

TARGA DIAS ANASTACIO, H., MATOSIN, N. & OOI, L. 2022. Neuronal hyperexcitability in Alzheimer's disease: what are the drivers behind this aberrant phenotype? *Transl Psychiatry,* 12**,** 257.

TAVAZZANI, E., TRITTO, S., SPAIARDI, P., BOTTA, L., MANCA, M., PRIGIONI, I., MASETTO, S. & RUSSO, G. 2014. Glutamic acid decarboxylase 67 expression by a distinct population of mouse vestibular supporting cells. *Front Cell Neurosci,* 8**,** 428.

TAYLOR, H. B. C., EMPTAGE, N. J. & JEANS, A. F. 2021. Long-term depression links amyloid-beta to the pathological hyperphosphorylation of tau. *Cell Rep,* 36**,** 109638.

TENNANT, S. A., FISCHER, L., GARDEN, D. L. F., GERLEI, K. Z., MARTINEZ-GONZALEZ, C., MCCLURE, C., WOOD, E. R. & NOLAN, M. F. 2018. Stellate Cells in the Medial Entorhinal Cortex Are Required for Spatial Learning. *Cell Rep,* 22**,** 1313-1324.

TERUNUMA, M. 2018. Diversity of structure and function of GABA(B) receptors: a complexity of GABA(B)-mediated signaling. *Proc Jpn Acad Ser B Phys Biol Sci,* 94**,** 390-411.

TERUNUMA, M., REVILLA-SANCHEZ, R., QUADROS, I. M., DENG, Q., DEEB, T. Z., LUMB, M., SICINSKI, P., HAYDON, P. G., PANGALOS, M. N. & MOSS, S. J. 2014. Postsynaptic GABAB receptor activity regulates excitatory neuronal architecture and spatial memory. *J Neurosci,* 34**,** 804-16.

THOMPSON, P. M., EGBUFOAMA, S. & VAWTER, M. P. 2003. SNAP-25 reduction in the hippocampus of patients with schizophrenia. *Prog Neuropsychopharmacol Biol Psychiatry,* 27**,** 411-7.

TOMASONI, R., REPETTO, D., MORINI, R., ELIA, C., GARDONI, F., DI LUCA, M., TURCO, E., DEFILIPPI, P. & MATTEOLI, M. 2013. SNAP-25 regulates spine formation through postsynaptic binding to p140Cap. *Nat Commun,* 4**,** 2136.

TOWNSEND, M., CLEARY, J. P., MEHTA, T., HOFMEISTER, J., LESNE, S., O' HARE, E., WALSH, D. M. & SELKOE, D. J. 2006. Orally available compound prevents deficits in memory caused by the Alzheimer amyloid-β oligomers. *Annals of Neurology,* 60**,** 668-676.

TOWNSEND, M., QU, Y., GRAY, A., WU, Z., SETO, T., HUTTON, M., SHEARMAN, M. S. & MIDDLETON, R. E. 2010. Oral treatment with a γ-secretase inhibitor improves long-term potentiation in a mouse model of Alzheimer's disease. *Journal of Pharmacology and Experimental Therapeutics,* 333**,** 110-119.

TUKKER, J. J., FUENTEALBA, P., HARTWICH, K., SOMOGYI, P. & KLAUSBERGER, T. 2007. Cell type-specific tuning of hippocampal interneuron firing during gamma oscillations in vivo. *The Journal of neuroscience : the official journal of the Society for Neuroscience,* 27**,** 8184-8189.

TULVING, E. 2002. EPISODIC MEMORY: From Mind to Brain. *Annual Review of Psychology,* 53**,** 1-25.

UHLHAAS, P. J. & SINGER, W. 2006. Neural Synchrony in Brain Disorders: Relevance for Cognitive Dysfunctions and Pathophysiology. *Neuron,* 52**,** 155-168.

ULRICH, D. 2015. Amyloid-β Impairs Synaptic Inhibition via GABA(A) Receptor Endocytosis. *The Journal of neuroscience : the official journal of the Society for Neuroscience,* 35**,** 9205.

VALACHOVA, B., BREZOVAKOVA, V., BUGOS, O., JADHAV, S., SMOLEK, T., NOVAK, P. & ZILKA, N. 2018. A comparative study on pathological features of transgenic rat lines expressing either three or four repeat misfolded tau. *Journal of Comparative Neurology,* 526**,** 1777-1789.

VAN DUIJN, C. M. & HOFMAN, A. 1991. Relation between nicotine intake and Alzheimer's disease. *British Medical Journal,* 302**,** 1491.

VAN DYCK, C. H., SWANSON, C. J., AISEN, P., BATEMAN, R. J., CHEN, C., GEE, M., KANEKIYO, M., LI, D., REYDERMAN, L., COHEN, S., FROELICH, L., KATAYAMA, S., SABBAGH, M., VELLAS, B., WATSON, D., DHADDA, S., IRIZARRY, M., KRAMER, L. D. & IWATSUBO, T. 2023. Lecanemab in Early Alzheimer's Disease. *N Engl J Med,* 388**,** 9-21.

VARGA, E., JUHASZ, G., BOZSO, Z., PENKE, B., FULOP, L. & SZEGEDI, V. 2014. Abeta(1-42) enhances neuronal excitability in the CA1 via NR2B subunit-containing NMDA receptors. *Neural Plast,* 2014**,** 584314.

VERDAGUER, E., BROX, S., PETROV, D., OLLOQUEQUI, J., ROMERO, R., DE LEMOS, M. L., CAMINS, A. & AULADELL, C. 2015. Vulnerability of calbindin, calretinin and parvalbumin in a transgenic/knock-in APPswe/PS1dE9 mouse model of Alzheimer disease together with disruption of hippocampal neurogenesis. *Exp Gerontol,* 69**,** 176-88.

VICKERS, C. A., STEPHENS, B., BOWEN, J., ARBUTHNOTT, G. W., GRANT, S. G. & INGHAM, C. A. 2006. Neurone specific regulation of dendritic spines in vivo by post synaptic density 95 protein (PSD-95). *Brain Res,* 1090**,** 89-98.

VINNAKOTA, C., GOVINDPANI, K., TATE, W. P., PEPPERCORN, K., ANEKAL, P. V., WALDVOGEL, H. J., FAULL, R. L. M. & KWAKOWSKY, A. 2020. An 5 GABAA Receptor Inverse Agonist, 5IA, Attenuates Amyloid Beta-Induced Neuronal Death in Mouse Hippocampal Cultures. *Int J Mol Sci,* 21.

VOSSEL, K. A., TARTAGLIA, M. C., NYGAARD, H. B., ZEMAN, A. Z. & MILLER, B. L. 2017. Epileptic activity in Alzheimer's disease: causes and clinical relevance. *The Lancet Neurology,* 16**,** 311-322.

WALLER, R., BAXTER, L., FILLINGHAM, D. J., COELHO, S., POZO, J. M., MOZUMDER, M., FRANGI, A. F., INCE, P. G., SIMPSON, J. E. & HIGHLEY, J. R. 2019. Iba-1-/CD68+ microglia are a prominent feature of age-associated deep subcortical white matter lesions. *PLoS One,* 14**,** e0210888.

WALLIN, Å., BLENNOW, K., ANDREASEN, N. & MINTHON, L. 2006. CSF Biomarkers for Alzheimer's Disease: Levels of [beta]-Amyloid, Tau, Phosphorylated Tau Relate to Clinical Symptoms and Survival. *Dementia and Geriatric Cognitive Disorders,* 21**,** 131-8.

WALSH, D., M., KLYUBIN, I., FADEEVA, J., V., CULLEN, W., K., ANWYL, R., WOLFE, M., S., ROWAN, M., J. & SELKOE, D., J. 2002. Naturally secreted oligomers of amyloid β protein potently inhibit hippocampal long-term potentiation in vivo. *Nature,* 416**,** 535.

WALSH, D. M., TOWNSEND, M., PODLISNY, M. B., SHANKAR, G. M., FADEEVA, J. V., EL AGNAF, O., HARTLEY, D. M. & SELKOE, D. J. 2005. Certain inhibitors of synthetic amyloid beta-peptide (Abeta) fibrillogenesis block oligomerization of natural Abeta and thereby rescue long-term potentiation. *The Journal of neuroscience : the official journal of the Society for Neuroscience,* 25**,** 2455-2462.

WANG, S., ZHANG, J., PAN, T. & FOR ALZHEIMER'S DISEASE NEUROIMAGING, I. 2018. APOE epsilon4 is associated with higher levels of CSF SNAP-25 in prodromal Alzheimer's disease. *Neurosci Lett,* 685**,** 109-113.

WATREMEZ, W., JACKSON, J., ALMARI, B., MCLEAN, S., GRAYSON, B., NEILL, J., FISCHER, N., ALLOUCHE, A., KOZIEL, V., PILLOT, T. & HARTE, M. 2018. Stabilized Low-n Amyloid-β Oligomers Induce Robust Novel Object Recognition Deficits Associated with Inflammatory, Synaptic, and GABAergic Dysfunction in the Rat. *Journal of Alzheimer's Disease,* 62**,** 213-226.

WEAVER, D. F. 2021. beta-Amyloid is an Immunopeptide and Alzheimer's is an Autoimmune Disease. *Curr Alzheimer Res,* 18**,** 849-857.

WEAVER, D. F. 2022. Alzheimer's disease as an innate autoimmune disease (AD(2) ): A new molecular paradigm. *Alzheimers Dement*.

WHITE, C. S., LAWRENCE, C. B., BROUGH, D. & RIVERS‐AUTY, J. 2017. Inflammasomes as therapeutic targets for Alzheimer's disease. *Brain Pathology,* 27**,** 223-234.

WIEGAND, J. P., GRAY, D. T., SCHIMANSKI, L. A., LIPA, P., BARNES, C. A. & COWEN, S. L. 2016. Age Is Associated with Reduced Sharp-Wave Ripple Frequency and Altered Patterns of Neuronal Variability. *J Neurosci,* 36**,** 5650-60.

WILKINSON, D. G. 1999. The pharmacology of donepezil: a new treatment of Alzheimer's disease. *Expert Opin Pharmacother,* 1**,** 121-35.

WIPPEL, C., MAURER, J., FORTSCH, C., HUPP, S., BOHL, A., MA, J., MITCHELL, T. J., BUNKOWSKI, S., BRUCK, W., NAU, R. & ILIEV, A. I. 2013. Bacterial cytolysin during meningitis disrupts the regulation of glutamate in the brain, leading to synaptic damage. *PLoS Pathog,* 9**,** e1003380.

WOJCIK, S. M., RHEE, J. S., HERZOG, E., SIGLER, A., JAHN, R., TAKAMORI, S., BROSE, N. & ROSENMUND, C. 2004. An essential role for vesicular glutamate transporter 1 (VGLUT1) in postnatal development and control of quantal size. *Proc Natl Acad Sci U S A,* 101**,** 7158-63.

WOOD, S. J. & TATTERSALL, J. E. 2001. An improved brain slice model of nerve agent-induced seizure activity. *J Appl Toxicol,* 21 Suppl 1**,** S83-6.

WOODRUFF, G., YOUNG, J. E., MARTINEZ, F. J., BUEN, F., GORE, A., KINAGA, J., LI, Z., YUAN, S. H., ZHANG, K. & GOLDSTEIN, L. S. 2013. The presenilin-1 DeltaE9 mutation results in reduced gamma-secretase activity, but not total loss of PS1 function, in isogenic human stem cells. *Cell Rep,* 5**,** 974-85.

WU, S. Z., BODLES, A. M., PORTER, M. M., GRIFFIN, W. S., BASILE, A. S. & BARGER, S. W. 2004. Induction of serine racemase expression and D-serine release from microglia by amyloid beta-peptide. *J Neuroinflammation,* 1**,** 2.

XU, L., ZHOU, Y., HU, L., JIANG, H., DONG, Y., SHEN, H., LOU, Z., YANG, S., JI, Y., RUAN, L. & ZHANG, X. 2021. Deficits in N-Methyl-D-Aspartate Receptor Function and Synaptic Plasticity in Hippocampal CA1 in APP/PS1 Mouse Model of Alzheimer's Disease. *Front Aging Neurosci,* 13**,** 772980.

XU, M. Y. & WONG, A. H. C. 2018. GABAergic inhibitory neurons as therapeutic targets for cognitive impairment in schizophrenia. *Acta Pharmacol Sin,* 39**,** 733-753.

YANG, P. & SUN, F. 2021. Aducanumab: The first targeted Alzheimer's therapy. *Drug Discov Ther,* 15**,** 166-168.

YANG, Q., ZHU, G., LIU, D., JU, J. G., LIAO, Z. H., XIAO, Y. X., ZHANG, Y., CHAO, N., WANG, J., LI, W., LUO, J. H. & LI, S. T. 2017. Extrasynaptic NMDA receptor dependent long-term potentiation of hippocampal CA1 pyramidal neurons. *Sci Rep,* 7**,** 3045.

YANG, S., SMIT, A. F., SCHWARTZ, S., CHIAROMONTE, F., ROSKIN, K. M., HAUSSLER, D., MILLER, W. & HARDISON, R. C. 2004. Patterns of insertions and their covariation with substitutions in the rat, mouse, and human genomes. *Genome research,* 14**,** 517-527.

YAO, Y., WU, M., WANG, L., LIN, L. & XU, J. 2020. Phase Coupled Firing of Prefrontal Parvalbumin Interneuron With High Frequency Oscillations. *Front Cell Neurosci,* 14**,** 610741.

YASHIRO, K. & PHILPOT, B. D. 2008. Regulation of NMDA receptor subunit expression and its implications for LTD, LTP, and metaplasticity. *Neuropharmacology,* 55**,** 1081-94.

YASSA, M. A., STARK, S. M., BAKKER, A., ALBERT, M. S., GALLAGHER, M. & STARK, C. E. 2010. High-resolution structural and functional MRI of hippocampal CA3 and dentate gyrus in patients with amnestic Mild Cognitive Impairment. *Neuroimage,* 51**,** 1242-52.

YASUNO, F., KOSAKA, J., OTA, M., HIGUCHI, M., ITO, H., FUJIMURA, Y., NOZAKI, S., TAKAHASHI, S., MIZUKAMI, K., ASADA, T. & SUHARA, T. 2012. Increased binding of peripheral benzodiazepine receptor in mild cognitive impairment–dementia converters measured by positron emission tomography with [11C]DAA1106. *Psychiatry Research: Neuroimaging,* 203**,** 67-74.

YIANNOPOULOU, K. G. & PAPAGEORGIOU, S. G. 2013. Current and future treatments for Alzheimer's disease. *Ther Adv Neurol Disord,* 6**,** 19-33.

YING, Z., BINGAMAN, W. & NAJM, I. M. 2004. Increased numbers of coassembled PSD-95 to NMDA-receptor subunits NR2B and NR1 in human epileptic cortical dysplasia. *Epilepsia,* 45**,** 314-21.

YUKI, D., SUGIURA, Y., ZAIMA, N., AKATSU, H., TAKEI, S., YAO, I., MAESAKO, M., KINOSHITA, A., YAMAMOTO, T., KON, R., SUGIYAMA, K. & SETOU, M. 2014. DHA-PC and PSD-95 decrease after loss of synaptophysin and before neuronal loss in patients with Alzheimer's disease. *Sci Rep,* 4**,** 7130.

ZALLO, F., GARDENAL, E., VERKHRATSKY, A. & RODRIGUEZ, J. J. 2018. Loss of calretinin and parvalbumin positive interneurones in the hippocampal CA1 of aged Alzheimer's disease mice. *Neurosci Lett,* 681**,** 19-25.

ZHANG, J. M. & AN, J. 2007. Cytokines, inflammation, and pain. *Int Anesthesiol Clin,* 45**,** 27-37.

ZHANG, Y., LI, P., FENG, J. & WU, M. 2016. Dysfunction of NMDA receptors in Alzheimer's disease. *Neurol Sci,* 37**,** 1039-47.

ZHU, B. 2019. *Synaptic Excitability Changes Within the Hippocampal Formation of 3xTgAD Mice.* Doctor of Philosophy, The University of Manchester.

ZHU, X. C., TAN, L., WANG, H. F., JIANG, T., CAO, L., WANG, C., WANG, J., TAN, C. C., MENG, X. F. & YU, J. T. 2015. Rate of early onset Alzheimer's disease: a systematic review and meta-analysis. *Ann Transl Med,* 3**,** 38.

ZOTT, B., BUSCHE, M. A., SPERLING, R. A. & KONNERTH, A. 2018. What Happens with the Circuit in Alzheimer's Disease in Mice and Humans? *Annu Rev Neurosci,* 41**,** 277-297.

ZOTT, B., SIMON, M. M., HONG, W., UNGER, F., CHEN-ENGERER, H.-J., FROSCH, M. P., SAKMANN, B., WALSH, D. M. & KONNERTH, A. 2019. A vicious cycle of amyloid β-dependent neuronal hyperactivation. *Science (American Association for the Advancement of Science),* 365**,** 559-565.

ZUCCA, S., GRIGUOLI, M., MALEZIEUX, M., GROSJEAN, N., CARTA, M. & MULLE, C. 2017. Control of Spike Transfer at Hippocampal Mossy Fiber Synapses In Vivo by GABAA and GABAB Receptor-Mediated Inhibition. *J Neurosci,* 37**,** 587-598.

ZUCKER, R. S. & REGEHR, W. G. 2002. Short-term synaptic plasticity. *Annu Rev Physiol,* 64**,** 355-405.

Online source:

Alzforum (2023): https://www.alzforum.org/research-models (Accessed on 9 March 2023)